University of Zagreb

Faculty of Veterinary Medicine

Nikolina Škvorc

CHARACTERIZATION OF ANTLER BONE FORMATION AND OSTEOCYTE VIABILITY FROM VELVET PHASE TILL ANTLER CASTING IN RED DEER (*CERVUS ELAPHUS* L.)

DOCTORAL THESIS

Zagreb, 2025

Sveučilište u Zagrebu

Veterinarski fakultet

Nikolina Škvorc

FORMIRANJE KOSTI I PREŽIVLJENJE OSTEOCITA U RAZDOBLJU OD RASTA DO ODBACIVANJA ROGOVLJA JELENA OBIČNOGA (*CERVUS ELAPHUS* L.)

DOKTORSKI RAD

Zagreb, 2025.

University of Zagreb

Faculty of Veterinary Medicine

Nikolina Škvorc

CHARACTERIZATION OF ANTLER BONE FORMATION AND OSTEOCYTE VIABILITY FROM VELVET PHASE TILL ANTLER CASTING IN RED DEER (*CERVUS ELAPHUS* L.)

DOCTORAL THESIS

Mentors:
Full Professor Snježana Kužir, PhD
Full Professor Dean Konjević, PhD, Dipl. ECZM

Zagreb, 2025

Sveučilište u Zagrebu

Veterinarski fakultet

Nikolina Škvorc

FORMIRANJE KOSTI I PREŽIVLJENJE OSTEOCITA U RAZDOBLJU OD RASTA DO ODBACIVANJA ROGOVLJA JELENA OBIČNOGA (*CERVUS ELAPHUS* L.)

DOKTORSKI RAD

Mentori:
prof. dr. sc. Snježana Kužir
prof. dr. sc. Dean Konjević, Dipl. ECZM

Zagreb, 2025.

University of Zagreb

FACULTY OF VETERINARY MEDICINE

I Z J A V A

Ja, Nikolina Škvorc, potvrđujem da je moj doktorski rad izvorni rezultat mojega rada te da se u njegovoj izradi nisam koristila drugim izvorima do onih navedenih u radu.

_____

(potpis studenta)

Zagreb, 2025.

This doctoral thesis was conducted in the Laboratory for Histology, Histochemistry and Immunohistochemistry of the Department of Anatomy, Histology and Embryology, Faculty of Veterinary Medicine, University of Zagreb, and at the Department of Biology (Hard Tissue and Bioarcheology Research Group), University of Hildesheim, Germany.

Mentors:

Full Professor Snježana Kužir, PhD

Full Professor Dean Konjević, PhD, Dipl. ECZM

Department Head:

Assistant Professor Mirela Pavić Vulinović, PhD

Doctoral thesis contains:

199 pages,

78 figures,

10 tables.

About mentors:

Professor Snježana Kužir:

Professor Snježana Kužir was born on April 9, 1969 in Zagreb, Croatia. She earned her degree in Veterinary Medicine in 1996 from the Faculty of Veterinary Medicine, University of Zagreb. In 1997, she was appointed to the position of Junior Assistant – Research Fellow at the Department of Anatomy, Histology and Embryology, where she also enrolled in a postgraduate scientific program in the same field. She obtained her Master of Science degree in the field of Biomedicine and Health Sciences in 2002, followed by a Doctorate (PhD) in the same field in 2006. She was appointed to the rank of Research Associate in April 2007, Senior Research Associate in November 2008, Research Advisor in June 2012, and in 2019 attained the permanent title of Research Advisor in the scientific field of Biomedicine and Health Sciences, with a specialization in Veterinary Medicine. In February 2010, she was appointed Assistant Professor, in September 2015 Associate Professor, and in December 2020 Full Professor at the Faculty of Veterinary Medicine. Professor Kužir has been actively engaged in teaching and curriculum development for several courses within the Integrated Undergraduate and Graduate University Study Program in Veterinary Medicine. She initiated the course *Histology with General Embryology* for the first generation of students enrolled in the English language program. Additionally, she is involved in the delivery of the Postgraduate Specialist Program in Forensic Veterinary Medicine and the Doctoral Program in Veterinary Sciences.

She has participated in research activities related to three scientific projects funded by the Ministry of Science, Education and Sports (MZOŠ) and three projects supported by the Croatian Science Foundation. Furthermore, she collaborated on the project Enhancing Collaboration between Fishermen and Scientists in the Introduction of Advanced Fishing Gear Tagging Technologies, Fish Health Protection and Environmental Conservation (co-funded by the European Maritime and Fisheries Fund and the Republic of Croatia). She has also been a collaborator on three projects relating to teaching development and has served as principal investigator or collaborator on six Research Support Grants. She has twice held the position of Head of the Laboratory for Histology, Histochemistry, and Immunohistochemistry at the Department. She serves as a reviewer for several scientific journals and is a member of the editorial board of the journal Veterinar, as well as Associate Editor of the journal

Veterinarski arhiv. Professor Kužir actively participates in the work of the Faculty Council at the Faculty of Veterinary Medicine. She is a member of the Croatian Veterinary Chamber and the Croatian Morphological Society. Internationally, she is an active member of the European Association of Veterinary Anatomists and the International Society of Education in Animal Sciences. She co-authored the first Croatian electronic manual, 3D Atlas of Horse Appendicular Skeleton, and contributed to the Croatian translation of the textbook Veterinary Embryology (2014), originally authored by T. A. McGeady, P. J. Quinn, E. S. FitzPatrick, and M. T. Ryan, published by Naklada Slap.

Her scientific interests focus on the morphology of domestic and wild animals, with a particular emphasis on histology.

A complete list of her published works is available at: https://www.croris.hr/osobe/profil/2792.

1. DEVČIĆ, L., D. VALIĆ, M. LOVRIĆ, I. VLAHEK, V. BENKO, **S. KUŽIR** (2025): Comprehensive study of the digestive tract in the European hake (*Merluccius merluccius*) Slov. Vet. Res., 62, 37-48. doi: 10.26873/SVR-2093-2024

2. ŠKVORC, N., M. BUJANIĆ, K. SEVERIN, L. ŠERIĆ JELASKA, M. PALIĆ, A. GUDAN KURILJ, **S. KUŽIR**, D. KONJEVIĆ (2024): Red deer (*Cervus elaphus*) antler myiasis caused by *Prochyliza nigrimanus* (Meigen 1826). Parasitol. Res., 123, 1-7. doi: 10.1007/s00436-024-08421-9

3. DRAGUN, Z., D. IVANKOVIĆ, N. TEPIĆ, V. FILIPOVIĆ MARIJIĆ, S. ŠARIRI, T. MIJOŠEK PAVIN, S. DRK, E. GJURČEVIĆ, K. MATANOVIĆ, **S. KUŽIR**, F. BARAC, Z. KIRALJ, T. KRALJ, D. VALIĆ (2024): Metal bioaccumulation in the muscle of the northern pike (*Esox lucius*) from historically contaminated river and the estimation of the human health risk. Fishes 9:364. doi:10.3390/fishes9090364

4. BASTIANČIĆ, L., I. VLAHEK, V. BENKO, M. LOVRIĆ, D. VALIĆ, **S. KUŽIR** (2024): Histochemical research of enzymes involved in cellular digestion in the digestive tract of tub gurnard, *Chelidonichthys lucerna*. Fish Physiol. Biochem., 50, 157-170. doi: 10.1007/s10695-023-01188-3

5. SAVOCA, S., K. MATANOVIĆ, G. D'ANGELO, V. VETRI, S. ANSELMO, T. BOTTARI, M. MANCUSO, **S. KUŽIR**, N. SPANÒ, G. CAPILLO, D. DI PAOLA, D. VALIĆ, E. GJURČEVIĆ (2021): Ingestion of plastic and non-plastic microfibers by farmed gilthead sea bream (*Sparus aurata*) and common carp (*Cyprinus carpio*) at different life stages. Sci. Total Environ. 782, 146851. doi: 10.1016/j.scitotenv.2021.146851

Professor Dean Konjević, Dipl. ECZM:

Dean Konjević was born on October 26, 1974 in Zagreb. In 1993 he enrolled at the Faculty of Veterinary Medicine, University of Zagreb, where he graduated in 2000. During the study he was awarded a prize for the best 5th year student. After graduation, he was employed as a scientific novice at the Department for Game Biology, Pathology and Breeding. He received his PhD in 2009 from the Faculty of Veterinary Medicine, University of Zagreb, with the topic "Non-invasive monitoring of adrenocortical gland in fallow deer". During that period, he spent 4 months at University of Veterinary Medicine Košice (Slovakia) and 2 months at Ontario Veterinary College University of Guelph (Canada). In 2010, he was board certified by the European College of Zoological Medicine and awarded the title European Veterinary Specialist in Zoological Medicine (Wildlife Population Health). In 2013, he was appointed to the rank of Assistant Professor at the Department of Veterinary Economics and Epidemiology. In 2023, he was appointed to the rank of Full Professor. He was appointed to the rank of a scientific advisor in 2011. His research area currently includes wildlife diseases, management and conservation, with special emphasis on pathology, epidemiology and public health. In addition to the aforementioned, he is actively involved in the research in the field of comparative odontology and dental pathology. Prof. Konjević has published more than 100 scientific and professional articles and three books as author and co-author. He has also presented more than 70 conference papers and has been an invited lecturer several times. He is an assistant editor of BMC Veterinary Research and European Journal of Wildlife Research.

A complete list of his published works is available at: https://www.croris.hr/osobe/profil/26771.

1. BUET, A. F. N. R., M. BUJANIĆ, K. KRAPINEC, I. BOŠKOVIĆ, A. GAŠPAR, **D. KONJEVIĆ** (2025): Development of the Roe Deer–*Fascioloides magna* Association over Time. Pathogens 14, 516. doi: 10.3390/pathogens14060516

2. DE JONG, MENNO J., G. ANAYA, A. NIAMIR, J. PÉREZ-GONZÁLEZ, C. BROGGINI, A. M. DEL POZO, M. NEBENFUEHR, E. DE LA PEÑA, J. RUIZ-OLMO, J. M. SEOANE, G. VEDEL, A. BARBOIRON, L. BARTOŠ, E. BUŽAN, R. F. CARDEN, G. DARCHIASHVILI, A. C. FRANTZ, D. GAČIĆ, A. GÉRARD, A. GORT-ESTEVE, E. GUILLAUMAT, A. HANTSCHMANN, M.-R. HEMAMI, J. HÖGLUND, F. DE JONG, JOOST, N. KARAISKOU, V. KERDIKOSHVILI, C. KERN, **D. KONJEVIĆ**, P. KOUBEK, J. KROJEROVÁ-PROKEŠOVÁ, A. D. MCDEVITT, S. MERKER, M. PELLERIN, M. PFENNINGER, K. H. RØED, C. SAINT-ANDRIEUX, F. SARIGOL, M. SYKUT, A. TRIANTAFYLLIDIS, J. PEMBERTON, U. SAARMA, L. IACOLINA, M. NIEDZIAŁKOWSKA, F. E. ZACHOS, J. CARRANZA, A. JANKE (2025): Red Deer Resequencing Reveals the Importance of Sex Chromosomes for Reconstructing Late Quaternary Events. Mol. Biol. Evol. 42, msaf031. doi: 10.1093/molbev/msaf031

3. **KONJEVIĆ, D.**, E. KLARIĆ, M. BUJANIĆ, N. ŠKVORC, Z. JANICKI, V. JUMIĆ, K. KRAPINEC (2025): The impact of *Fascioloides magna* infection on characteristics of red deer antlers. Book of Abstracts 60th Croatian & 20th International Symposium on Agriculture, 1-6 June, Brač, Croatia, p. 96.

4. KULEŠ, J., M. BUJANIĆ, I. RUBIĆ, K., ŠIMONJI, **D. KONJEVIĆ** (2024): A Comprehensive Multi-Omics Study of Serum Alterations in Red Deer Infected by the Liver Fluke *Fascioloides magna*. Pathogens 13, 922. doi: 10.3390/pathogens13110922

5. ŠKVORC, N., M. BUJANIĆ, K. SEVERIN, L. ŠERIĆ JELASKA, M. PALIĆ, A. GUDAN KURILJ, S. KUŽIR, **D. KONJEVIĆ** (2024): Red deer (*Cervus elaphus*) antler myiasis caused by *Prochyliza nigrimanus* (Meigen 1826). Parasitol. Res. 123, 1-7. doi: 10.1007/s00436-024-08421-9

Acknowledgements

I sincerely extend my deepest gratitude to Professor Uwe Kierdorf, PhD and Professor Horst Kierdorf, PhD for generously sharing their profound knowledge, offering invaluable guidance, and providing unwavering, multifaceted support throughout the course of my doctoral research. Furthermore, I am deeply grateful for the warm hospitality and kindness extended to me during my stay in Hildesheim, and for every moment of your valuable time that you so generously devoted to me.

I express my sincere gratitude to my mentors, Professor Snježana Kužir and Professor Dean Konjević for their invaluable guidance in developing the research topic, securing the essential resources required for conducting the study, and facilitating the successful completion of my doctoral degree.

I would like to sincerely thank O. G. LETEC for their invaluable support in facilitating the execution of the research and the collection of samples.

I wish to express my sincere gratitude to the Department of Biology at the University of Hildesheim, and to Sabrina Kohne and Dr. Carsten Witzel for their invaluable assistance with the preparation and processing of samples.

I would like to express my sincere gratitude to the University of Split School of Medicine, and in particular to Professor Natalija Filipović for her generous hospitality, the valuable knowledge she shared, and her kind assistance with the processing of part of the samples.

I wish to extend my sincere gratitude to the University of Zagreb School of Medicine, and especially to Assistant Professor Ivan Alić for his valuable advice, his support in finding solutions, and his contribution to the realization of the sample analysis.

I would like to express my sincere gratitude to Professor Krešimir Krapinec for his selfless assistance with the statistical analysis of the results.

I am sincerely grateful to University Hospital Dubrava for making the densitometry analysis possible.

I would like to extend my sincere gratitude to the staff of the Faculty of Veterinary Medicine, University of Zagreb — Professor Ivan-Conrado Šoštarić-Zuckermann, Professor Andrea Gudan Kurilj, Professor Krešimir Severin and Professor Zrinka Štritof — as well as to the Laboratory of Cytology and Histopathology (Department of Veterinary Pathology), and the Laboratory for Histology, Histochemistry, and Immunohistochemistry (Department of Anatomy, Histology and Embryology). My special gratitude goes to Nada Crnogaj for her kind assistance with sample processing.

And last, but most importantly, my heartfelt gratitude goes to my closest colleague, friend, and fiancé Miljenko Bujanić for all his help during the sampling and processing of materials, his support during the writing of this dissertation, and his constant positive spirit throughout the entire process. I also sincerely thank my parents, Irena and Siniša, for their unwavering support, help, and endless patience during the preparation of this doctoral thesis.

ABSTRACT

Characterization of antler bone formation and osteocyte viability from velvet phase till antler casting in red deer (*Cervus elaphus* L.)

The red deer (*Cervus elaphus* L.) is a member of the mammalian family Cervidae (deer). One of the main characteristics of this family are special type of cranial bony appendages, called antlers, which are the only organ in mammals that undergo complete annual regeneration. Anatomically, deer cranial appendages are composed of a perennial part (pedicle) and a deciduous part (antler). The primary cranial appendages (i.e., pedicles and first antlers) are growing from mesenchymal stem cells located in the antlerogenic periosteum. Antlers are initially formed of cartilage that is subsequently replaced by bone. There is still debate whether hard antlers are dead or living structures, and whether they have a regular blood supply. The hypothesis of this study is that hard antlers are dead structures and that remaining blood plays no role in preserving osteocyte vitality. Velvet antlers (n = 2), antlers at velvet shedding (n = 2), hard antlers (n = 14) and cast antlers (n = 2) of red deer were collected and subjected to histological analysis (hematoxylin-eosin, Alcian Blue + Alizarin Red S, modified staining to show the ossification process, Villanueva's tetrachrome bone staining, von Kossa, TUNEL fluorescence assay, scanning electron microscopy with backscatter electron detector [SEM-BSE], circularly polarized light, normal transmitted light with phase contrast) and densitometry, according to three segments (proximal, middle and distal). The results of this study present the detailed antler histological structure at different stages of the antler cycle and different parts, examined at monthly intervals from velvet to cast phase. It is evident that there are no significant structural differences after the velvet is shed. Densitometry revealed no differences in mineral density of the hard antlers. Morphological analysis of osteocytes showed the presence of living cells only in the velvet antlers, while the cells were dead or missing in the later stages. Additionally, after the velvet is shed, the remaining red fluid in antler cavities does not contain blood elements, but the presence of bacteria was detected. Minor micropetrosis was observed in chondrocyte and osteocyte lacunae across all analyzed antlers. Obtained results confirm that mineralized antlers are already dead structures at the time of velvet shedding.

Key words: red deer, antlers, velvet shedding, osteocyte, histological structure

PROŠIRENI SAŽETAK

Značajke formiranja kosti i vitalnost osteocita u razdoblju od rasta do odbacivanja rogovlja jelena običnoga (*Cervus elaphus* L.)

UVOD

Jelensko rogovlje parni su kranijalni koštani izdanci i jedini organ sisavaca sposoban za potpunu regeneraciju svake godine. Rogovlje raste umnažanjem i diferencijacijom matičnih stanica smještenih u posebnom periostu rožišta iz kojih nastaje hrskavični model kojeg će postupno zamijeniti koštano tkivo. Rogovlje je tijekom rasta prekriveno specifičnom kožom (bast, runje, liko, velvet). U široj znanstvenoj zajednici još uvijek nije u potpunosti prihvaćeno je li tzv. tvrdo (mineralizirano) rogovlje nakon skidanja basta mrtva ili živa struktura, kao niti postoji li i dalje opskrba krvlju takvog rogovlja. Jedan dio znanstvenika tvrdi da je rogovlje živa struktura sve do oko tri tjedna prije odbacivanja te da ima očuvanu opskrbu krvlju i žive osteocite, odnosno da čak redovito prolazi kroz procese koštane pregradnje. Prekid opskrbe rogovlja krvlju doveo je drugi dio znanstvenika do zaključka da je mineralizirano rogovlje mrtvo. Nadalje, osim što rogovlje nakon skidanja basta nema aktivni krvotok, nema niti živce, zbog čega postaje neosjetljivo na bol. Isto tako, skidanjem basta dolazi do isušivanja rogovlja čija vlažnost nakon toga ostvaruje takozvani ekvilibrij s vlagom u okolišu. Pokazano je da se koštana pregradnja u rogovlju događa u slučajevima pokusnog antiandrogenog tretiranja, čime se faza rasta produljuje na umjetan način. Pretpostavka ovoga istraživanja je da je tvrdo rogovlje mrtva struktura i da krv koja zaostaje u njemu nema ulogu u očuvanju i preživljenju osteocita. Kako bi se potvrdila ili odbacila ova pretpostavka, postavljeno je nekoliko ciljeva: i) utvrditi prisutnost krvi, ii) utvrditi preživljenje osteocita, iii) utvrditi intenzitet lakunarne mikropetroze te iv) analizirati histološke značajke rogovlja mjesečno u razdoblju od prije skidanja basta pa sve do odbacivanja rogovlja.

PREGLED DOSADAŠNJIH SPOZNAJA

Jelen obični (*Cervus elaphus* L.) sisavac je iz porodice jelena (Cervidae). Najupečatljivija oznaka jelena su kranijalni izdanci zvani rogovlje. S iznimkom soba ili karibua (*Rangifer tarandus* L.), kod kojeg oba spola imaju rogovlje, te vodenog jelena (*Hydropotes inermis* L.), koji uobičajeno nema ni rožišta ni rogovlje, kod svih ostalih vrsta jelena rogovlje nose isključivo mužjaci. Oblik rogovlja izrazito je specifičan za svaku vrstu te

se čak koristi i u taksonomske svrhe. Anatomski gledano, rogovlje se sastoji od trajnog dijela (rožišta – koštani nastavci čeonih kostiju) i promjenjivog dijela (grana roga s paroščima). Ova podjela razlikuje se od autora do autora, pa tako u lovačkoj terminologiji rogovlje u smislu trofeja predstavljaju obje grane roga s paroščima i dijelom ili cijelom lubanjom. Nasuprot tome, u užem smislu rogovlje su samo grane roga s paroščima. Rogovlje kao sekundarno spolno obilježje vizualni je znak društvene hijerarhije i služi u pokaznim i borbenim interakcijama u sezoni parenja. Društvenu hijerarhiju mužjaci postižu međusobno uspoređujući veličinu i izgled rogovlja, isprva bez fizičkog kontakta. Ako na taj način ne uspostave hijerarhiju, dolazi do međusobne borbe u kojoj rogovlje koriste kao oružje, početno u udarcima, a nakon toga u naguravanju. Tijekom borbi ponekad dolazi do lomljenja vrhova parožaka ili čak većih dijelova rogovlja. Također, jeleni se rogovljem koriste i za označavanje teritorija trljajući se njime o grmlje, lišće i koru drveća. U jelenske teladi rožište počinje rasti u dobi od oko osam mjeseci, dok prvo rogovlje raste u dobi od približno jedne godine. Odbacivanjem prvog rogovlja, mužjak ulazi u redoviti ciklus rasta i odbacivanja rogovlja. U prosjeku su potrebna oko četiri mjeseca za dovršetak rasta, što rogovlje čini jednim od najbrže rastućih organa sisavaca. U prirodnim okolnostima, u odraslih mužjaka jelena običnoga rogovlje počinje rasti u proljeće (kraj veljače – početak ožujka), dok u srpnju/kolovozu, neposredno pred riku, dolazi do skidanja basta. Rast rožišta (i prvog rogovlja) iz čeonih kostiju započinje putem specifičnog periosta (*engl.* antlerogenic periost [AP]) koji sadrži matične stanice, značajno je deblji od periosta na drugim dijelovima lubanje te nosi receptore za testosteron. Regeneracija rogovlja izravno je ovisna o AP, odnosno o matičnim stanicama periosta rožišta. Tijekom rasta rogovlja razina testosterona u krvi je niska, dok njen porast neposredno pred riku dovodi do mineralizacije rogovlja i posljedičnog skidanja basta. Ponovni pad razine testosterona nakon rike stimulira aktivnost osteoklasta u rožištu, što dovodi do slabljenja veze rožište-grana roga i odbacivanja rogovlja. Rastuće rogovlje može se podijeliti u nekoliko zona. Ispod dermalnog dijela basta nalazi se proliferativna zona (hiperplastični perihondrij) podijeljena u tri podzone: pričuvni mezenhim, predhrskavični i hrskavični sloj. Proksimalno od proliferativne zone nalazi se zona hrskavice. Nakon navedene zone slijedi primarna spongioza u kojoj simultano teku procesi hondroklazije, osteoklazije i osteoblastične aktivnosti, što rezultira zamjenom mineralizirane hrskavice koštanim trabekulama. Proksimalno na primarnu spongiozu nalazi se sekundarna u kojoj se između koštanih trabekula nalazi lamelarna kost. Odlaganje fibrolamelarne kosti na perifernom dijelu rogovlja dovodi do formiranja kortikalne kosti. Do izduživanja rogovlja dolazi u njegovom distalnom dijelu kroz proliferaciju matičnih stanica i njihovu

diferencijaciju u hondroblaste i hondrocite. Nastala hrskavica postupno se mineralizira i nastaje kost. Mineralizirano rogovlje sastoji se od središnje spužvaste kosti okružene kompaktnom kosti. Spužvasta kost sadrži kanaliće koji teku paralelno sa središnjom osi grane roga. Kompakta je izgrađena od osteona lamelarne strukture te sadrži kolagena vlakna tipa I i kalcijev fosfat (hidroksiapatit). Najveći dio kompakte sastoji se od primarnih osteona različitog oblika koji često sadrže više krvnih kanalića, dok su sekundarni osteoni mali i rijetki. Sekundarni osteoni nastaju prilikom kontinuirane pregradnje kosti kao odgovor na mehanički stres. Nedostatak sekundarnih osteona u rogovlju također se može pripisati kratkom životnom vijeku rogovlja zbog kojega nije moguća njegova znatnija pregradnja. Ostaci mineralizirane hrskavice (intenzivnija mineralizacija hrskavičnog matriksa u usporedbi s koštanim matriksom) unutar kompakte, posebice distalnih dijelova rogovlja, ukazuju na nepotpunu zamjenu hrskavice najvjerojatnije uslijed kratkog života rogovlja. Osteociti se nalaze u lakunama i čine oko 90 % svih stanica kosti. Kompaktna i spužvasta kost razlikuju se u poroznosti i koštanoj masi. U dobro oblikovanom rogovlju kompakta ima manju poroznost (manje od 5 %) od spužvaste kosti (preko 60 %). Kompakta čini većinu mineraliziranog područja rogovlja, a njezina debljina smanjuje se od proksimalnog dijela rogovlja prema njegovu distalnom dijelu. Uloge osteocita su mnogobrojne (transport iona i hranjivih tvari putem citoplazmatskih izdanaka, unos kalcija, regulacija aktivnosti osteoklasta, mehanotransdukcija). Općenito, životni vijek osteocita je različit, ali u određenim okolnostima mogu preživjeti i nekoliko desetljeća. Živi osteociti mogu održavati nemineralizirani prostor oko sebe izlučivanjem različitih enzima te inhibitora kristalizacije i mineralizacije. S druge strane, ukoliko su osteociti mrtvi, izostaje pregradnja kosti te se u lakune odlažu minerali. Postoje i određeni dokazi da pored pasivne mineralizacije dolazi i do aktivnog odlaganja minerala potaknutoga otpuštanjem vezikula matriksa od strane osteocita. Promjena kod koje su lakune i koštani kanalići ispunjeni mineralima naziva se mikropetroza. Mineralizacija lakuna blokira protok tekućina i hranjivih tvari do osteocita, narušava funkcionalnost lakuna i kanalića te dovodi do smrti stanica. Iz toga razloga mikropetroza se dovodi u svezu s apoptozom osteocita. Takve mineralne naslage utvrđene su u lakunama hondrocita i osteocita u rogovlju različitih vrsta jelena. I danas se u znanstvenoj javnosti vodi rasprava o tome je li rogovlje jelena mrtva kost ili može preživjeti skidanje basta kroz dulje vrijeme. Prekid opskrbe rogovlja krvlju doveo je većinu znanstvenika do zaključka kako je mineralizirano rogovlje mrtvo. U razmatranju rogova šupljorožaca i rogovlja punorožaca, zaključeno je kako rogovlje nakon skidanja basta nema aktivni krvotok niti živce te je neosjetljivo na bol. S druge strane, dio znanstvenika je analizirajući rogovlje jelena lopatara

(*Dama dama* L.) došao do zaključka kako je tvrdo rogovlje živo tkivo sve do oko tri tjedna prije odbacivanja. Prema ovome istraživanju, mineralizirano rogovlje ima očuvanu opskrbu krvlju i žive osteocite te čak redovito prolazi kroz procese koštane pregradnje. S druge strane, na primjeru muntjaka opisani su očuvani Volkmanovi kanali neposredno nakon skidanja basta, ali ne i linije zastoja u rastu ili drugi znakovi koji bi ukazivali na produljeni život rogovlja. Novije istraživanje na rogovlju jelena običnoga pokazalo je da nakon skidanja basta dolazi do isušivanja rogovlja čija vlažnost nakon toga ostvaruje ekvilibrij s vlagom u okolišu. Također je dokazano da nakon skidanja basta prestaje mineralizacija te da su sekundarni osteoni nastali istodobno kada i primarni. Na primjeru jelena lopatara dokazano je da se koštana pregradnja u rogovlju događa u slučajevima pokusnog antiandrogenog tretiranja, čime se faza rasta produljuje na umjetan način. Sukladno navedenome, sve je više dokaza koji podupiru tvrdnju da je tvrdo rogovlje mrtva struktura te da je vjerojatni razlog godišnje regeneracije rogovlja upravo činjenica da je mineralizirano rogovlje mrtva koštana struktura.

Hipoteza i ciljevi istraživanja

Hipoteza ovog istraživanja je da je tvrdo rogovlje mrtva struktura i da preostala krv nema ulogu u očuvanju vitalnosti osteocita.

Ciljevi istraživanja su:

1. Odrediti prisustvo krvi u rogovlju na mjesečnom nivou, od perioda prije skidanja basta do odbacivanja rogovlja.
2. Odrediti vitalnost osteocita na mjesečnom nivou, od perioda prije skidanja basta do odbacivanja rogovlja.
3. Odrediti intenzitet lakunarne mikropetroze na mjesečnom nivou, od perioda prije skidanja basta do odbacivanja rogovlja.
4. Analizirati histološke karakteristike rogovlja na mjesečnom nivou, od perioda prije skidanja basta do odbacivanja rogovlja.

MATERIJAL I METODE

Dizajn istraživanja uključivao je uzorkovanje rogovlja jelena običnih u dobi od dvije godine (uzorkovanje s nevjerojatnošću), mjesečno od rogovlja u bastu do odbacivanja rogovlja. U istraživanju je sudjelovalo 10 mužjaka (20 rogova: rogovlje u bastu [n = 2]; rogovlje pred skidanje basta [n = 2]; tvrdo rogovlje [n = 14]; odbačeno rogovlje [n = 2]) jelena običnoga, držanih u otvorenom odjeljku, na paši i s vodom *ad libitum*. Jeleni koji su sudjelovali u istraživanju potječu iz farmskog uzgoja OG Letec te su nakon istraživanja ostali u uzgoju. Rogovlje u bastu uzorkovalo se u potpunoj kemijskoj imobilizaciji izazvanoj sredstvima tiletamin-zolazepam i ksilazin (1,2 mg/kg tiletamina + 1,2 mg/kg zolazepama i 2,3 mg/kg ksilazina) u dozama preporučenim za jelene, a sukladno tjelesnoj masi. Tvrdo rogovlje uklanjano je sitnozubom pilom u *crush* sustavu na oko 5 cm iznad vijenca roga. Nakon dopreme na Veterinarski fakultet, uzorkovane grane rogovlja podijeljene su na tri segmenta te su se od svakog segmenta rezali manji isječci mikromotorom (NSK Ultimate 500) pomoću flex dijamantne separirke, 45 mm (Flex Diamond Disc, Edenta) i dijamantne pile (Mecatome T180 [Presi, Eybens, Francuska]), ovisno o daljnjoj histološkoj obradi i denzitometriji. Mineralizirani neuklopljeni uzorci pripremljeni su za denzitometriju i bojenja (Alcijan plava + Alizarin crvena S, Villanuevino tetrakromno bojenje za kost). Mineralizirani uzorci uklopljeni su u plastiku (BIODUR®, BIODUR® Products GmbH, Njemačka) te analizirani sljedećim metodama: von Kossa bojenjem, skenirajućim elektronskim mikroskopiranjem s detektorom povratno raspršenih elektrona (SEM-BSE), kružno polariziranom svjetlošću i normalnom propuštenom svjetlošću s faznim kontrastom. Dio uzoraka podvrgnut je procesu demineralizacije te nakon toga uklopljen u parafin. Dobiveni parafinski blokovi rezani su na debljinu 6 µm te podvrgnuti nekoj od metoda (hematoksilin eosin, Alcijan plava + Alizarin crvena S, modificirano bojenje za prikaz procesa okoštavanja, TUNEL fluorescencijski test). Za svaki uzorak roga, koji je bio podijeljen u tri segmenta, proučavani su uzdužni i poprečni presjeci na preparatima bojenima hematoksilin-eozinom (HE) (tvrdo rogovlje) ili modificiranom metodom bojenja za prikaz procesa okoštavanja (rogovlje u bastu). Osteociti su podijeljeni u pet različitih skupina (tip A, tip B, tip C, tip D, tip E) na temelju položaja i oblika jezgre, stupnja ispunjenosti lakune jezgrom te stupnja kondenzacije kromatina. U svakoj zoni (korteks, prijelazna zona i spongioza) ispitano je i razvrstano po 100 osteocita u ranije definirane skupine. Statistička obrada podataka odrađena je u programskom paketu Statistica 14.0.0.15. Raspodjele podataka testirane su Shapiro-Wilk testom. Izračun povezanosti (korelacije) istraživanih značajki proveden je Kendall-Tau

korelacijskim koeficijentom. Analiza podataka nadalje je obavljena testovima ANOVA, Leveneovim testom i Shefféovim post hoc testom.

REZULTATI

Ovim istraživanjem prikazana je detaljna histološka struktura rogovlja u različitim razvojnim fazama, proučavana u mjesečnim razmacima – od rogovlja u bastu do odbacivanja rogovlja. U svim prikupljenim uzorcima prisutni su ostaci kalcificirane hrskavice (s većom količinom u distalnim dijelovima rogovlja). Osteoblasti, osteoklasti i osteociti prisutni su u rogovlju u bastu gdje je morfološka analiza osteocita pokazala prisutnost živih stanica i stanica u odumiranju. Vaskularni kanali rogovlja u bastu sadrže krvne elemente (crvena krvna tjelešca, eozinofile, limfocite, krvne pločice). Nakon skidanja basta, u strukturi tvrdog rogovlja nisu uočene značajne razlike među uzorcima prikupljenima tijekom različitih mjeseci. U svim uzorcima tvrdog rogovlja preostala crvena tekućina („zaostala krv“) u šupljinama ne sadrži krvne elemente, ali je utvrđena prisutnost bakterija. Morfološkom analizom osteocita u tvrdom rogovlju utvrđeni su avitalni (mrtvi) osteociti te brojne prazne lakune. Analizom dobivenih rezultata utvrđeno je statistički znakovito opadanje udjela osteocita tipa C (mrtvi osteociti) u tvrdom rogovlju kroz vremenski period nakon faze skidanja basta. Istovremeno, udio osteocita tipa E (prazne lakune) statistički znakovito raste. Slabija mikropetroza osteocitnih i hondrocitnih lakuna uočena je u svim uzorcima rogovlja od razdoblja prije skidanja basta do odbacivanja rogovlja, bez promjene u intenzitetu. Denzitometrijom je utvrđeno da je mineralna gustoća kosti najniža u rogovlju u bastu. Razlika u mineralnoj gustoći kosti nije statistički znakovita u rogovlju uzorkovanom mjesečno od skidanja basta do odbacivanja rogovlja. Statistički znakovita razlika utvrđena je u srednjoj mineralnoj gustoći kosti između različitih segmenata grane roga.

ZAKLJUČAK

Histološka analiza provedena u ovom istraživanju pokazuje da rogovlje jelena nakon odbacivanja basta ne sadrži krvne žile i vitalne stanice, što potvrđuje da je „mrtvo“, odnosno metabolički neaktivno. Također je potvrđeno da zaostala crvena tekućina nije krv te da kao takva ne može podržavati život mineraliziranog rogovlja. Konačno, podjednaka gustoća rogovlja tijekom svih faza nakon skidanja basta demantira prethodna nagađanja o postupnom

povratu minerala iz rogovlja u kosti tijela. Ovo saznanje ima izravnu primjenu u uzgoju jelena, osobito tijekom različitih postupaka rukovanja. U fazi basta, bilo kakva intervencija na rogovlju dopuštena je isključivo veterinarima koja se mora obaviti pod anestezijom i analgezijom. S druge strane, manipulacija tvrdim rogovljem znatno je češća, osobito kada je riječ o njihovom odstranjivanju prije rike kod farmskog uzgoja jelena. Ova praksa provodi se kako bi se spriječile moguće ozljede mužjaka uslijed međusobnih sukoba, ozljede ženki ili pak oštećenja infrastrukture farme. Ovo istraživanje potvrđuje da takvi zahvati ne uzrokuju bol ni krvarenje (osim prisutnosti ostataka crvene tekućine – zaostale krvi koja više nije funkcionalna).

Ključne riječi: jelen obični, rogovlje, skidanje basta, osteociti, histološka struktura

LIST OF SYMBOLS AND ABBREVIATIONS

AB-ARS	Alcian Blue-Alizarin Red S
AV	antlers in velvet
AVS	antlers at velvet shedding
BMD	bone mineral density
bv	blood vessel
↟	calcified cartilage
CA	cast antlers
CL	chondrocyte lacuna
CPL	circularly polarized light
CPL+1 λ	circularly polarized light and 1λ-plate
cf	collagen fibers
C	cortex
d	dermis
dCA	distal segment of cast antler
dHA	distal segment of hard antler
dVA	distal segment of velvet antler
dVS	distal segment of antler at velvet shedding
⇳	distoproximal antler axis
ed	epidermis
hf	hair follicles
HA	hard antlers
HE	hematoxylin-eosin
◗	Howship's lacunae
⇪	hypermineralized seams
lb	lamellar bone
▲	lamellar infilling
mCA	middle segment of cast antler
mHA	middle segment of hard antler
mVA	middle segment of velvet antler
mVS	middle segment of antler at velvet shedding
MSOP	modified staining to show the ossification process
◯	multicanaled osteon

TL	normal transmitted light (bright field microscopy)
PHACO	normal transmitted light with phase contrast
ob	osteoblast
ocl	osteoclast
★	osteocyte
OL	osteocyte lacuna
↑	osteoid seam
o	osteon
P	periosteum
pfl	periosteal fibrous layer
pol	periosteal osteogenic layer
pCA	proximal segment of cast antler
pHA	proximal segment of hard antler
pVA	proximal segment of velvet antler
pVS	proximal segment of antler at velvet shedding
RBC	red blood corpuscles
rb	residual blood
R	resorption cavity
▸	resorption line
SEM-BSE	scanning electron microscopy using a backscattered electron detector
sg	sebaceous gland
⁂	soft tissue
S	trabecular zone
TZ	transitional zone
✖	tubular structures
TUNEL	TUNEL fluorescence assay
✱	vascular canal
V	velvet
VTBS	Villanueva´s tetrachrome bone staining
VK	von Kossa
wb	woven bone

CONTENTS

LIST OF FIGURES AND TABLES

FIGURES

Figure 11. Schematic view of antler development; bottom left – after velvet shedding, the antler is dead bone; bottom right – the antler is living bone.

Figure 12. a) One of the enclosures of the red deer farm with a mixed red deer herd of stags and hinds; **b)** Red deer stag after cutting of hard antlers.

Figure 13. Timeline overview of the antler sampling. The samples were collected over two consecutive years. Sample 7 was collected in the second year of sampling, but at an earlier developmental stage than Sample 2.

Figure 14. a) Sampled red deer (spiker) antler beams (a and b) in velvet; **b)** Sampled red deer (spiker) hard antler beams (a and b); **c)** Sampled antler beams divided into three equal segments (1 – proximal [part of the antler close to the head], 2 – middle, 3 – distal [top of the antler]); **d)** Transverse section of a segment of antler in the velvet; **e)** Transverse section of a segment of hard antler; **f)** Transversely sampled antler fragment cut with micromotor using a flex diamond separator with water cooling; **g)** Longitudinally sampled antler fragments cut with micromotor using a flex diamond separator with water cooling; **h)** Fragment cut with rotary saw with a water-cooled diamond-edged blade.

Figure 15. a) Transverse antler fragments from each segment; **b)** Device for testing bone mineral density.

Figure 16. a) Closed vacuum system with desiccator and pressure regulator; **b)** Bubbles in the plastic visible due to pressure drop; **c)** Fragment of antler segment in the hardened plastic; **d)** Cutting the excess plastic; **(e, f)** Cube-shape finished antler samples in the plastic ready for further analysis.

Figure 17. a) Cut surfaces of plastic-embedded antler fragment smoothed and polished by hand using a series of silicon carbide papers; **b)** Specimens were checked for scratches during polishing; **c)** Samples in the ultrasonic cleaner for removing adherent particles from the polishing process; **d)** Polished surface of plastic-embedded antler fragment; **e)** Copper foil attached to the edge of the plastic.

Figure 18. a) Mounted sample on a glass attached to a holder using vacuum and sectioned using a rotary saw with a water-cooled diamond-edged blade; **b)** Sample grinding (with cup wheel); **c)** Final polishing step with deer leather cloth and a polishing compound; **d)** The thickness of the glass and glass/plastic/antler fragment checked with a micrometer screw; **e)** Ground section of hard antler fragment.

Figure 19. a) Process of demineralization. Antler fragments wrapped in gauze and immersed in the solution; **b)** Cups with antler fragments on a digital orbital shaker; **c)** Paraffin blocks cut with rotary microtome with a standard knife.

Figure 20. Overview of the methods used in the research.

Figure 21. Summary of the average value of antler BMD by segments during the antler development cycle.

Figure 22. Transverse section of red deer antler segments in velvet: **a)** Segment 1, **b)** Segment 2, **c)** Segment 3. Mineralized, epoxy-resin embedded, unstained samples, Keyence VHX 500 (reflected light images of polished block surfaces).

Figure 23. Transverse section of red deer antler samples in velvet: **a)** Segment 1, **b)** Segment 2. Mineralized, epoxy-resin embedded, unstained samples, Keyence VHX 7000 (reflected light images of polished block surfaces).

Figure 24. Section of red deer antlers in velvet, segment 3, longitudinal section, demineralized, paraffin embedded sample, (**a**, **b** – HE; **c**, **d** – MSOP), NanoZoomer 2.0RS.

Figure 25. Longitudinal section of red deer antlers in velvet, segment 3, demineralized, paraffin embedded sample, MSOP, Axio Imager M2.

Figure 26. Polished block surfaces of the red deer antlers in velvet, segment 3, transverse sections, mineralized, epoxy-resin embedded, unstained sample, SEM-BSE.

Figure 27. Red deer antlers in velvet, segment 2, transverse sections, mineralized, epoxy-resin embedded, unstained sample: **a), b)** Polished surface, SEM-BSE; **c), d)** Ground section, Axio Imager M2 (**c** – TL, **d** – PHACO).

Figure 28. Red deer antlers in velvet, segment 2, transverse sections: **a)**, **b)** Demineralized, paraffin embedded samples, HE, ABARS, NanoZoomer 2.0RS; **c)**, **d)** Mineralized, ground sections, epoxy-resin embedded, unstained samples, Axio Imager M2 (PHACO); **e)**, **f)** Mineralized, polished surfaces, epoxy-resin embedded, VK, Keyence VHX 7000.

Figure 29. Polished surfaces of red deer antlers in velvet, segment 2, transverse sections, mineralized, epoxy-resin embedded, unstained sample, SEM-BSE.

Figure 30. Polished surfaces of red deer antlers in velvet, segment 1, transverse sections, mineralized, epoxy-resin embedded, unstained samples, SEM-BSE.

Figure 31. Red deer antlers in velvet, segment 1, transverse section, mineralized, epoxy-resin embedded, unstained samples: **a)**, **b)** Polished surface, SEM-BSE; **c)**, **d)**, **e)**, **f)** Ground section, Axio Imager M2 (**c, e** – PHACO; **d, f** – CPL).

Figure 32. Transverse section of red deer antlers at velvet shedding: **a)** Segment 1, **b)** Segment 2, **c)** Segment 3. Mineralized, epoxy-resin embedded, unstained samples, Keyence VHX 500 (reflected light images of polished block surfaces).

Figure 33. Red deer antlers at velvet shedding, segment 3, transverse and longitudinal sections, mineralized, unembedded samples, VTBS, Digicyte DX50, NanoZoomer 2.0RS.

Figure 34. Red deer antlers at velvet shedding, segment 3, transverse (**a**, **c**, **e**, **f**) and longitudinal (**b**, **d**) sections, demineralized, paraffin embedded samples, NanoZoomer 2.0RS, (**a**, **b**, **c**, **d** – MSOP; **e**, **f** – ABARS).

Figure 35. Red deer antlers at velvet shedding, segment 3, transverse section: **a)**, **b)**, **d)**, **e)**, **f)** Ground section, mineralized, epoxy-resin embedded, unstained samples, Axio Imager M2 (**a**, **b** – TL; **d** – CPL; **e**, **f** – PHACO); **c)** Demineralized, paraffin embedded, HE, Keyence, VHX 7000.

Figure 36. Polished surfaces of red deer antlers at velvet shedding, segment 3, transverse section, mineralized, epoxy-resin embedded, unstained sample, SEM-BSE.

Figure 37. Ground section of red deer antler at velvet shedding, segment 3, transverse section, mineralized, epoxy-resin embedded, unstained sample, Axio Imager M2 (**a**, **b**, **c**, **d**, **e** – PHACO; **f** – CPL).

Figure 38. Red deer antlers at velvet shedding, segment 2: **a)**, **b)**, **c), d)** Ground section, transverse section, mineralized, epoxy-resin embedded, unstained sample, Axio Imager M2 (TL); **e)**, **f)** Longitudinal section, demineralized, paraffin embedded, HE, Keyence VHX 7000.

Figure 39. Ground section of red deer antler at velvet shedding, segment 2, transverse section, mineralized, epoxy-resin embedded, unstained sample, Axio Imager M2 (**a**, **c** – CPL; **b**, **d**, **e**, **f** – PHACO).

Figure 40. Polished surfaces of red deer antlers at velvet shedding, segment 2, transverse section, mineralized, epoxy-resin embedded, unstained sample, SEM-BSE.

Figure 41. Ground section of red deer antler at velvet shedding, segment 2, transverse section, mineralized, epoxy-resin embedded, unstained sample, Axio Imager M2 (PHACO).

Figure 42. Ground section of red deer antlers at velvet shedding, segment 2, transverse section, mineralized, epoxy-resin embedded, unstained sample, Axio Imager M2 (**a** – TL; **b**, **c**, **d** – CPL).

Figure 43. Red deer antlers at velvet shedding, segment 1: **a)**, **b)** Transverse section, mineralized, unembedded samples, VTBS, Digicyte DX50; **c)**, **d)**, **e)**, **f)** Transverse and longitudinal sections, demineralized, paraffin embedded samples (**c** – MSOP, NanoZoomer 2.0RS; **d** – ABARS, NanoZoomer 2.0RS; **e**, **f** – HE, Keyence VHX 7000).

Figure 44. Polished surfaces of red deer antlers at velvet shedding, segment 1, transverse section, mineralized, epoxy-resin embedded, unstained sample (**a**, **b** – SEM-BSE; **c** – PHACO, **d** – CPL – Axio Imager M2).

Figure 45. Ground section of red deer antler at velvet shedding, segment 1, transverse section, mineralized, epoxy-resin embedded, unstained sample, Axio Imager M2 (CPL).

Figure 46. Ground section of red deer antlers at velvet shedding, segment 1, transverse section, mineralized, epoxy-resin embedded, unstained sample, Axio Imager M2 (**a** – PHACO; **b**, **c**, **d** – CPL).

Figure 47. Polished surfaces of red deer antlers at velvet shedding, segment 1, transverse section, mineralized, epoxy-resin embedded, unstained sample, SEM-BSE.

Figure 48. Transverse section of red deer hard antlers: **a)** Segment 1, **b)** Segment 2, **c)** Segment 3. Mineralized, epoxy-resin embedded samples, Keyence VHX 500 (reflected light images of polished block surfaces).

Figure 49. Red deer hard antlers, segment 3: **a)** Longitudinal section, mineralized, unembedded sample, ABARS; **b)**, **c)** Longitudinal section, demineralized, paraffin embedded samples, MSOP, NanoZoomer 2.0RS; **d)**, **e)**, **f)**, **g)** Polished surfaces, transverse section, mineralized, epoxy-resin embedded, unstained sample, SEM-BSE.

Figure 50. Polished surfaces of red deer hard antlers, segment 3, transverse section, mineralized, epoxy-resin embedded, unstained sample, SEM-BSE.

Figure 51. Red deer hard antlers, segment 2: **a)** Transverse section, mineralized, unembedded sample, ABARS; **b)** Longitudinal section, demineralized, paraffin embedded samples, MSOP, NanoZoomer 2.0RS; **c)**, **d)**, **e)** Transverse sections, mineralized, epoxy-resin embedded, VK, (Keyence VHX 7000).

Figure 52. Polished surfaces of red deer hard antlers, segment 2, transverse section, mineralized, epoxy-resin embedded, unstained sample, SEM-BSE.

Figure 53. Red deer hard antlers, segment 1: Transverse (**a**, **d**, **e**, **f**) and longitudinal (**b**, **c**) sections, mineralized, unembedded samples, VTBS, (**a**, **b** – NanoZoomer 2.0RS; **c** – Digicyte DX50; **d**, **e**, **f** – Olympus BX41).

Figure 54. Ground section of red deer hard antlers, segment 1, transverse section, mineralized, epoxy-resin embedded, unstained sample, Axio Imager M2 (**a** – TL; **b**, **c** – PHACO; **d** – CPL + 1λ).

Figure 55. Ground section of red deer hard antlers, segment 1, transverse section, mineralized, epoxy-resin embedded, unstained sample, Axio Imager M2 (**a**, **b**, **e** – PHACO; **c**, **d**, **f** – CPL + 1λ).

Figure 56. Polished surfaces of red deer hard antlers, segment 1, transverse section, mineralized, epoxy-resin embedded, unstained sample, SEM-BSE.

Figure 57. Transverse section of red deer cast antlers: **a)** Segment 1, **b)** Segment 2, **c)** Segment 3. Mineralized, epoxy-resin embedded, unstained samples, Keyence VHX 500 (reflected light images of polished block surfaces).

Figure 58. Polished surfaces of red deer cast antlers, segment 3, transverse section, mineralized, epoxy-resin embedded, unstained sample, SEM-BSE.

Figure 59. Ground section of red deer cast antlers, segment 3, transverse section, mineralized, epoxy-resin embedded, unstained sample, Axio Imager M2 (**a** – bright field; **b**, **d**, **e**, **h** – PHACO; **c**, **f**, **g** – CPL + 1λ).

Figure 60. Red deer cast antlers, segment 2: **a)** Transverse section, demineralized, paraffin embedded samples, HE, NanoZoomer 2.0RS; **b)**, **c)**, **d)**, Transverse sections, mineralized, epoxy-resin embedded, VK, (**b**, **c** – Axioskop, 2Plus; **d** – Keyence VHX 7000).

Figure 61. Polished surfaces of red deer cast antlers, segment 2, transverse section, mineralized, epoxy-resin embedded, unstained sample, SEM-BSE.

Figure 62. Polished surfaces of red deer cast antlers, segment 2, transverse section, mineralized, epoxy-resin embedded, unstained sample, SEM-BSE.

Figure 63. Red deer cast antlers, segment 1: **a)**, **d)** Transverse sections; **b)**, **c)** Longitudinal sections. Demineralized, paraffin embedded samples, HE, NanoZoomer 2.0RS.

Figure 64. Ground section of red deer cast antlers, segment 1, transverse section, mineralized, epoxy-resin embedded, unstained sample, Axio Imager M2 (**a**, **c** – TL; **d**, **e** – PHACO; **b**, **f**, **g –** CPL + 1λ; **h** – CPL).

Figure 65. Polished surfaces of red deer cast antlers, segment 1, transverse section, mineralized, epoxy-resin embedded, unstained sample, SEM-BSE.

Figure 66. Polished surfaces of red deer cast antlers, segment 1, transverse section, mineralized, epoxy-resin embedded, unstained sample, SEM-BSE.

Figure 67. Pseudo-color SEM-BSE image of polished section surface of antler segments: **a)**, **c)**, **e)** Antlers in velvet; **b)**, **d)**, **f)** Antlers at velvet shedding. The 16 grey-level bands spanning the grey value range from 0 (black) to 255 (peak white) as indicated by the color bar below the figure.

Figure 68. Pseudo-color SEM-BSE image of polished section surface of antler segments: **a)**, **c)**, **e)** Hard antlers; **b)**, **d)**, **f)** Cast antlers. The 16 grey-level bands spanning the grey value range from 0 (black) to 255 (peak white) as indicated by the color bar below the figure.

Figure 69. Osteocyte classification in five different types (alive [A], dying [B], dead [C, D, E]); (**a**, **b**, **c** – antlers in velvet, MSOP, Keyence VHX 7000/Axio Imager M2); (**d** – antlers at velvet shedding, HE, Keyence VHX 7000; **e** – hard antlers, HE, Olympus; **f** – cast antlers, HE, NanoZoomer 2.0RS).

Figure 70. The proportion of certain types of osteocytes in different developmental stages of antlers (according to Table 3. Classification of osteocytes).

Figure 71. Dependence of the proportion of osteocytes type C (y-axis, [%]) over the sampling timeline (x-axis), across different antler zones and segments.

Figure 72. Dependence of the proportion of osteocytes type E (y-axis, [%]) over the sampling timeline (x-axis), across different antler zones and segments.

Figure 73. Red deer antlers in velvet, longitudinal section, demineralized, paraffin embedded samples, TUNEL, Axio Imager M2.

Figure 74. Red deer antlers in velvet, longitudinal section, demineralized, paraffin embedded samples, TUNEL, Axio Imager M2.

Figure 75. Red deer antlers: antlers at velvet shedding (**a**-**c**), hard antlers (**d**-**i)**, longitudinal section, demineralized, paraffin embedded samples, TUNEL, Olympus BX51.

Figure 76. Smear from the antler liquid material (**a**, **b** – antlers in velvet; **c** – hard antlers (ID 8), larvae; **d** – hard antlers (ID 9)), MGG, Digicyte DX50.

Figure 77. Section of antlers in different developmental phases, IBG, NanoZoomer 2.0RS.

Figure 78. Red deer antlers (ID 8): **a**, **b** – macroscopic views; **c**, **e** – HE; **d**, **f** – MSOP, NanoZoomer 2.0RS.

TABLES

1. INTRODUCTION

The red deer (*Cervus elaphus* L.) belongs to the family Cervidae (deer). The most characteristic trait of deer family members is a special type of paired cranial bony appendages, i.e. antlers. They are the only organs in mammals that undergo complete annual regeneration. Anatomically, the cranial appendages of deer are composed of a perennial part (pedicle) and a deciduous part (antler). Antlers are initially made of cartilage that is later replaced with bone. Mineralized antler consists of peripheral compact bone and central trabecular bone. It takes approximately four months to complete the growth, making antlers one of the fastest growing organs in mammals. During their growth, antlers are covered with skin (velvet) that is shed just before mating season. The lack of secondary osteons in antlers, as well as the presence of remnants of mineralized cartilage within the compact bone (especially in the distal portions), can be attributed to their short lifespan.

In the wider scientific community, there is no consensus whether hard antlers are dead or living structures after velvet shedding, nor whether they have a blood supply. Some scientists claim that antlers remain living structures until approximately three weeks before casting, maintaining a functional blood supply and viable osteocytes, and even undergo regular bone remodeling processes after velvet shedding. However, the interruption of blood supply to antlers has led most scientists to conclude that mineralized antlers are dead. Furthermore, in addition to the fact that antlers have no active blood supply after velvet shedding, they also have no nerves and are insensitive to pain. In addition, velvet shedding causes antlers to dry out, the moisture content of which then reaches equilibrium with the environment. More extensive bone remodeling in antlers has been shown to occur in cases of experimental antiandrogen treatment, which artificially prolongs the velvet antler phase.

Considering the above, the hypothesis of this study is that hard antlers are dead structures and that remaining blood plays no role in preserving osteocyte vitality. The main goals of the thesis are to determine the presence of blood, osteocyte survival, the intensity of lacunar micropetrosis, and analyze the histological characteristics of antlers monthly in the period from before velvet shedding to antler casting.

2. OVERVIEW OF PREVIOUS FINDINGS

2.1. Red deer

The red deer (*Cervus elaphus* L.) is a member of the mammalian order Artiodactyla, suborder Ruminantia and family Cervidae (deer). The group of deer represents the second most diverse group of ruminants. They are originally widespread in the Americas, Europe and Asia and mostly inhabit the Northern Hemisphere (SCOTT and JANIS, 1987; GEIST, 1998; GENTRY, 2000; WEBB, 2000). In Croatia, red deer are mostly distributed in lowland habitats in forests along the Danube, Drava and Sava rivers, in mountain habitats in Gorski Kotar, Velika and Mala Kapela. The species is somewhat less present on Velebit and Lička Plješivica, and in Mediterranean habitats (TROHAR, 2004).

Based on morphological characteristics, deer were historically taxonomically divided into two subfamilies: Telemetacarpi and Plesometacarpi (YOUNG, 1962; HARRINGTON, 1985). A more recent classification, supported by morphological and molecular evidence, divides deer into two subfamilies: Cervinae (consisting of Muntiacini and Cervini) and Capreolinae (consisting of Alceini, Capreolini, Odocoileini and Rangiferini) (GROVES and GRUBB, 1990; MIYAMOTO et al., 1990; CRONIN et al., 1996; RANDI et al., 1998, 2001; HASSANIN and DOUZERY, 2003; KUZNETSOVA et al., 2005; PRICE et al., 2005; GILBERT et al., 2006; HUGHES et al., 2006; OUITHAVON et al., 2009; HASSANIN et al., 2012; HECKEBERG et al., 2016; GUTIÉRREZ et al., 2017).

2.2. Cranial appendages in ruminants

Members of the Artiodactyla, especially the suborder Ruminantia, have the most diverse cranial appendages. Two ruminant families Tragulidae and Moschidae do not have cranial appendages, while the other four of the six living ruminant families do. These appendages are known as (pedicles and) antlers (family Cervidae), pronghorns (family Antilocapridae), ossicones (family Giraffidae), and horns (family Bovidae). They are located entirely on the frontal bones or in the frontoparietal region (DAVIS et al., 2011; DEMIGUEL et al., 2014).

The ancestors of Artiodactyls possessed tusk-like upper canines (CABRERA and STANKOWICH, 2020), which were lost with the evolution of antlers, horns, ossicones and pronghorns. In the Chinese water deer (Cervidae: *Hydropotes*) and musk deer (Moschidae: *Moschus*) they constitute the only fighting/display weapon (AITCHISON, 1946; FENNESSY, 1984; CABRERA and STANKOWICH, 2020). Presently, the musk deer is no longer classified as a deer, it has been placed into a separate family, the Moschidae (HALL, 2015). Tusks and short, deciduous antlers on long bony pedicles are characteristics of primitive deer, the muntiacines (muntjacs: *Muntiacus*) and tufted deer: *Elaphodus* (GROVES and GRUBB, 1990).

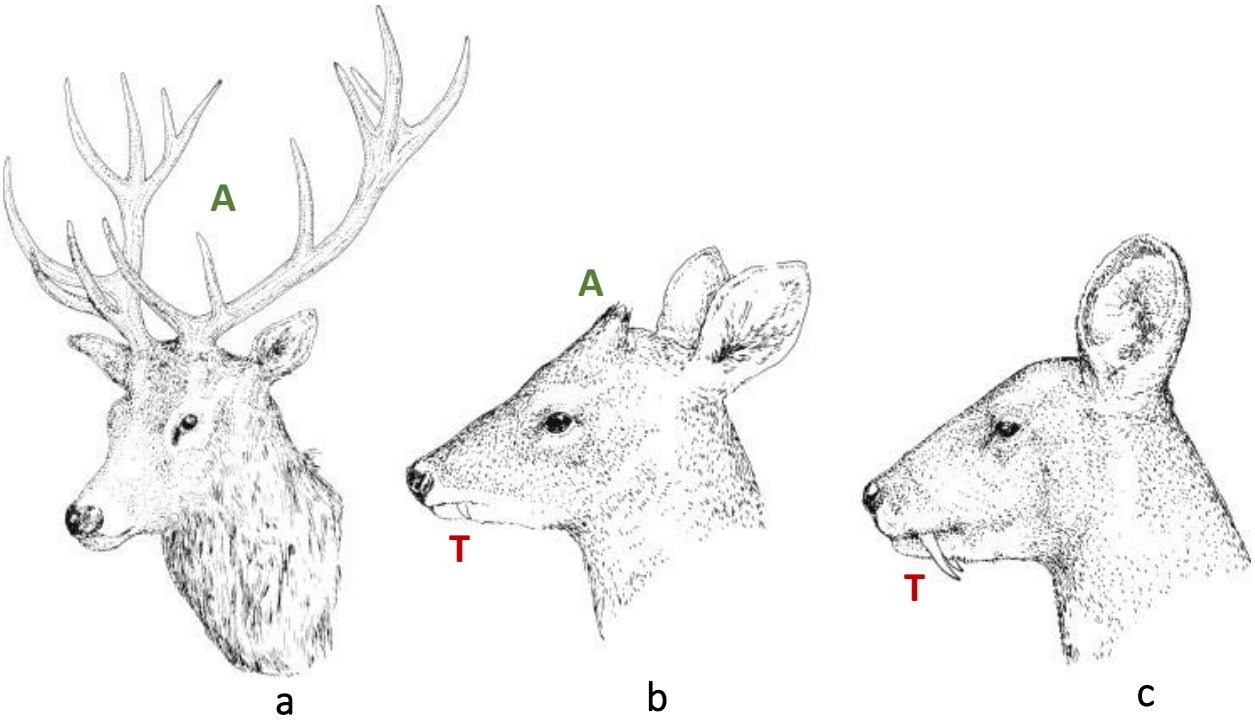

Figure 1. Antlers **(A)** and tusk-like upper canine teeth **(T)** in different species: **a)** The red deer (*Cervus elaphus*) possesses antlers and no tusks, **b)** Tufted deer (*Elaphodus cephalophus*) small tusks and short antlers and **c)** Siberian musk deer (*Moschus moschiferus*) with prominent tusks and absence of antlers (modified from GOSS, 1983; HALL, 2015).

The bony core that is present in all types of ruminant cranial appendages is formed in two ways. First, like in the case of red deer pedicles/antlers, as a direct outgrowth (apophysis) from the cranium (GOSS, 1983), or, as in the case of the giraffid, ossicone as an independent element (epiphysis) that secondarily fuses to the cranium (CHURCHER, 1990).

The simplest type of cranial appendages are the ossicones of giraffids. In adult giraffes, they are located in the frontoparietal region, while in okapis they are located on the frontal bones. Ossicones are made of a bony core covered by hairy skin which in giraffes permanently covers the entire bony core, while in older okapis the skin is lost from the ossicone tip (CHURCHER, 1990; DAVIS et al., 2011). Pronghorns are located on the frontal bones. They are unbranched projections permanently covered by hairy skin, whose epidermis produces an annually replaced keratinous sheath. The horns of bovids are also located on the frontal bones. They consist of a permanent bony horncore that is permanently covered with skin. The bony horncore increases in length by apical growth and in diameter by periosteal apposition. The epidermis produces the keratinous horn sheath, a permanent structure, which increases in size by the production of successive cone-shaped keratin layers (DAVIS et al., 2011). The periodic production of new keratin layers leads to the formation of growth rings in the horn sheath that are used for age evaluation (HABERMEHL, 1985). Members of the family Cervidae have different cranial appendages from other ruminants because they consist of a perennial proximal portion – pedicle, and a deciduous distal portion – antler (GEIST, 1998). Pedicles are permanently covered with skin, while antlers are covered only during their growth (GOSS, 1983). Antler skin (velvet) is different from the skin in other head regions. Velvet epidermis is thicker than that of scalp skin, the hair follicles in the velvet lack arrector pili muscles, and velvet is rich in large sebaceous glands (BUBENIK, 1993; LI and SUTTIE, 2000).

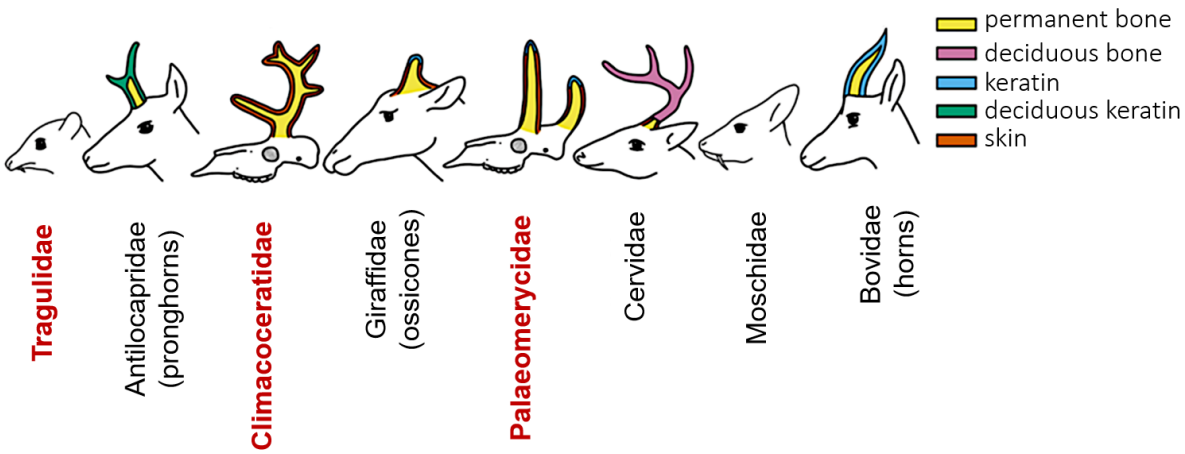

Figure 2. Tissue composition of cranial appendage of living and **extinct** ruminants (modified from CALAMARI and FLYNN, 2024).

2.3. Antlers

The most characteristic trait of deer is a special type of cranial appendage, antlers. Antlers are paired bony structures and the only organ in mammals that undergoes complete annual regeneration (CHEN et al., 2009; GOSS, 1984, 1992). With the exception of reindeer/caribou (*Rangifer tarandus* L.) where both sexes carry antlers and water deer (*Hydropotes inermis* L.) that normally lack both pedicles and antlers, antlers are present only in males, and their shape is characteristic and even used for taxonomic purposes (BUBENIK and BUBENIK, 1990; HALL, 2015; LANDETE-CASTILLEJOS et al., 2019; HECKEBERG et al., 2023). Hard bony antlers have many grooves, in which blood vessels were positioned. Special bumps called "pearls" are formed, most commonly on the beam and distal tines, but not on the tips (JIN and SHIPMAN, 2010).

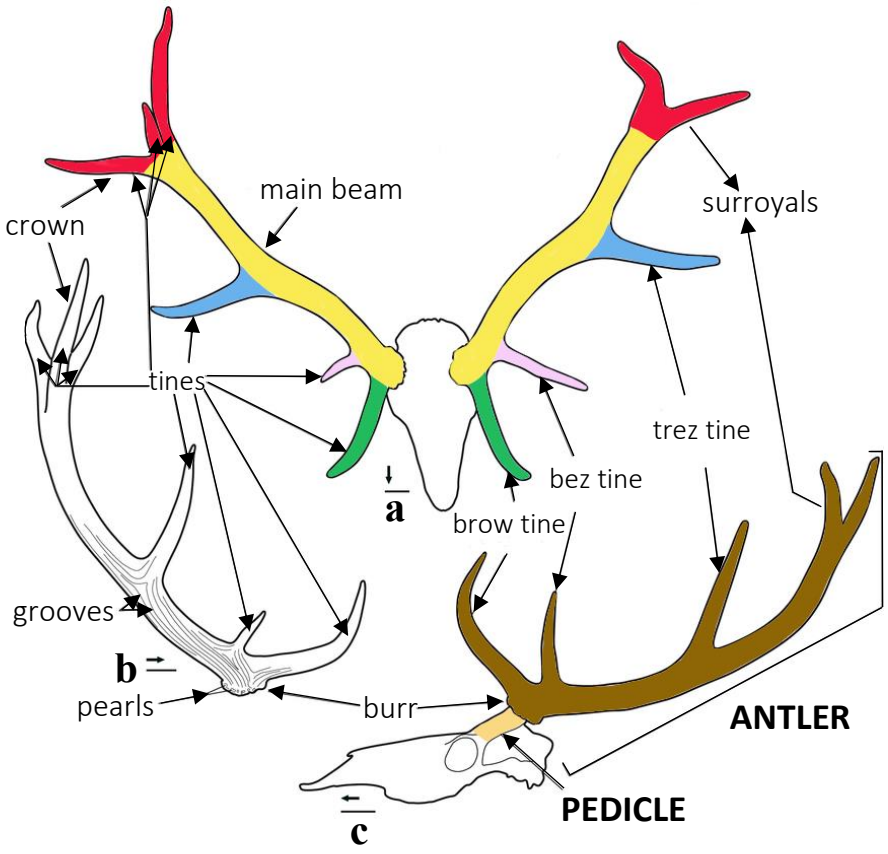

Figure 3. a) Dorsal view of the skull and antlers, **b)** Lateral view of the right antler, **c)** Lateral view of the skull and left antler of red deer. Terms for different antler parts, structures, and ornamentation (modified from HECKEBERG et al., 2023).

2.3.1. Antler size and complexity

Antler shape and size show interspecific variations, they can range from small spike antlers 5 to 9 cm in length (*Pudu pudu*) up to more than 140 cm multibranched antlers in wapiti (*Cervus canadensis*) (GEIST, 1998), or huge palmated forms in the moose (*Alces alces*) (GOULD, 1973; CLUTTON-BROCK et al., 1980; LINCOLN, 1992). The extinct giant deer *Megaloceros giganteus* had the largest antlers, with an antler span of 3.5 m in large stags and an antler mass of up to 40 to 45 kg (GEIST, 1998). Antler size and complexity vary greatly with an animal's age. In comparison, antlers of a red deer yearling are spikes, while antlers of a prime-aged stag usually form an impressive multitined rack. Nutrition is the most important extrinsic factor affecting antler size and shape (VOGT, 1936; BARTOŠ, 1990; BROWN, 1990; DEMARAIS and STRICKLAND, 2011). Antler size in deer is related to body size and mating group size. A positive allometric relationship exist between antler size and body size (GOULD, 1973), which means that smaller species have small and simple antlers, while large species have large multibranched antlers. It is also speculated that there is an ecologically functional influence on antler size and complexity in different mating systems. Therefore, in order to successfully compete for females, males from larger breeding groups have relatively larger and more complex antlers than males from smaller groups, whose antlers are smaller and simpler (CLUTTON-BROCK et al., 1980; KITCHENER, 1985; ROBERTS, 1996; CARO et al., 2003). Antler size and complexity are influenced by the choice of females as females prefer males with relatively larger antlers because of their "superior" genetic quality (CLUTTON-BROCK, 1982). Species living in open habitats have larger and more complex antlers, while antlers of species from closed habitats are shorter and simpler, which allows them to move quickly through dense vegetation (SIMPSON, 1949; COLBERT, 1955; CARO et al., 2003). The size and shape of the regenerating antlers are influenced by regeneration tissue forming on the pedicle stump after casting of the previous antlers as well as the amount of blood supplied to the growth zones (GOSS, 1961).

2.3.2. Antler composition

Macroscopically, on transverse sections of mature (hard) antlers, different zones have been distinguished. From the periphery towards the center, the outermost portion is the antler cortex, subdivided into a thin outer cortex (subvelvet zone) (ROLF and ENDERLE, 1999; CHEN et al.,

2009), and a much broader main cortex composed of lamellar compact bone. The following parts are a transition zone where the porosity increases markedly in centripetal direction, and a core zone composed of trabecular (cancellous) bone with a high porosity (DAVISON et al., 2006). Porosity and bone mass are different in the cortical and trabecular parts. Cortical bone has a low porosity (< 5% in well-formed antlers), while trabecular bone has high porosity (over 60%). The cortex constitutes the majority of the mineralized area in red deer antlers and cortical thickness decreases from proximal to distal portions (LANDETE-CASTILLEJOS et al., 2019). The compact bone is composed of osteons that have a laminated structure of concentric circles (lamellae) containing type I collagen fibers and calcium phosphate (hydroxyapatite) (CURREY, 2002). Antler bone present in a young or old animal is always a developmentally young bone, composed largely of primary bone tissue with only a few secondary osteons (LANDETE-CASTILLEJOS et al., 2019). The majority of the antler cortex consists of primary osteons, which are variable in shape and often contain more than one vascular canal (KIERDORF et al., 2013), which is called "osteon conglomerates" (SKEDROS et al., 2014). The few secondary osteons are small and surrounded by a reversal line resulting from the patchy resorption of primary bone tissue. The short lifespan of antlers does not allow significant remodeling and that is the reason for the small number of secondary osteons, termed modelling osteons, which indicates the fact that they are formed at the same time as primary osteons in other locations (while bone modelling is still ongoing) (GOMEZ et al., 2013). Furthermore, during antler development, they are subjected to only minor mechanical loading, and, because of that, secondary osteons will not develop (CHEN et al., 2009). Along the periphery of many primary osteons in the antler cortex are bright lines or hypermineralized seams which resemble the reversal lines present around secondary osteons (KRAUSS et al., 2011; SKEDROS et al., 2014). These hypermineralized seams represent cement lines that have been interpreted as either resting lines (KRAUSS et al., 2011) or reversal lines (KIERDORF et al., 2013). Tertiary Haversian systems (i.e., secondary osteons replacing earlier formed secondary osteons) and interstitial lamellae in antler are not present. Antler tissue has been deposited across its entire width from the onset of growth and basic, i.e. circumferential, lamellae are not formed (WISLOCKI, 1942; WALDO et al., 1949). One more consequence of their short lifespan are remnants of calcified cartilage inside the antler cortex, especially in the distal antler portions, which indicates an incomplete replacement of cartilage by bone (GOMEZ et al., 2013; KIERDORF et al., 2013, 2022).

The cancellous bone contains canals that run parallel to the long axis of the beam (CURREY, 2002). The ratio between compact and cancellous bone depends on the deer species (CHAPMAN, 1975) and antler size (LAUNEY et al., 2010). Chemically, antlers are, like other bones, composed of hydroxyapatite, collagen, noncollagenous proteins and water (CURREY, 2002; LANDETE-CASTILLEJOS et al., 2007a, 2007b; GOMEZ et al., 2013; PICAVET and BALLIGAND, 2016). Compared to other bones, antlers contain more organic matrix and less mineral. Because of that they are more resistant to fractures (CURREY, 2002). The antler mineral contains various macro and trace elements in different concentrations (KIERDORF et al., 2014; CAPPELLI et al., 2017).

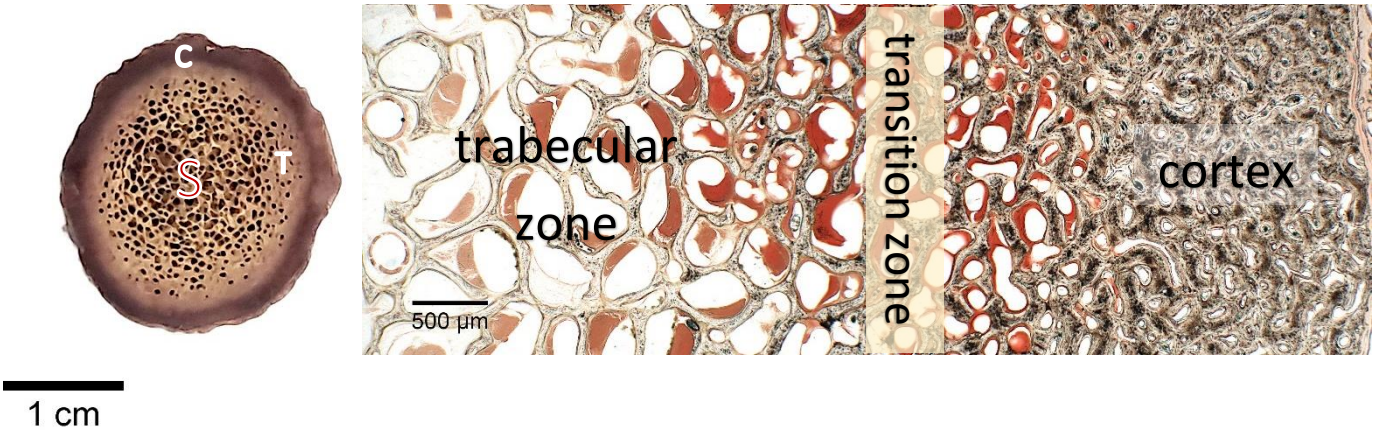

Figure 4. a) Macroscopical transversal section of red deer hard antler (segment 2); **b)** Microscopical transversal section of red deer antler at velvet shedding (segment 2), (Axio Imager M2). Different zones are visible: cortex (C), transition zone (T), trabecular/cancellous, spongy zone (S).

2.3.3. Antler functions

Antlers are functional during the hard antler phase (LINCOLN, 1992). Deer protect their antlers from blows and avoid physical fighting when their antlers are covered with velvet because of the extensive innervation of the growing antlers. They confront each other with front legs, by standing upright on their hindlegs (JIN and SHIPMAN, 2010). There are several functions of antlers. The most important function is that they are weapons in intra-specific combat when males compete during the rutting season for social dominance and access to females. They also serve as organs of display (visual importance for dominance determination amongst males or to attract

females) (CLUTTON-BROCK, 1982; LINCOLN, 1992). The display is the first stage during an encounter. Antlers of mature European red deer stags are characterized by the presence of a crown, a complex of three or more distal tines, which serve mostly in display (BENINDE, 1937; LISTER, 1987). In the case of fighting, the use of antlers is a two-step process consisting of an initial clash (animals lock antlers) followed by a phase of pushing and twisting in an attempt to break the opponent's balance and cause injuries. These injuries are caused by the sharp tips of antler tines and can be serious (LINCOLN, 1992). In the first step of combat, antlers need a high resistance to impact loading, while in the second step they need resistance to torsional forces (KLINKHAMER et al., 2019; LANDETE-CASTILLEJOS et al., 2019). Antler tines also have a protective role. The lowermost tine (brow tine) protects the eyes and the facial region (GOSS, 1983; CROITOR, 2021). Trez tine provides additional protection in larger cervines (CROITOR, 2021). Change in fighting behavior relates to the evolution of antlers. For example, muntjacs have small antlers and large canine teeth, and utilize both types of weapons in aggressive encounters (BARRETTE, 1977). During cervid evolution, larger antlers become the primary weapons, while the canines underwent regression (LINCOLN, 1992). Red deer antlers are visually important for expressing dominance (BUBENIK, 1968; LINCOLN, 1972). To emphasize their appearance, rutting males of larger deer species carry vegetation on antlers and wallow in mud (SCHALLER, 1967; LINCOLN, 1972). Some other functions of antlers are defense against predators, thermoregulation during the growth phase (CLUTTON-BROCK, 1982) and territory marking by rubbing them against bushes, leaves and tree bark (JIN and SHIPMAN, 2010). In non-aggressive situations, deer occasionally chew on each other's antlers, thus utilizing them as a mineral resource (BOWYER, 1983; BARRETTE, 1985).

2.3.4. Mechanical properties of antlers

The mechanical properties of bones are largely determined by their contents of organic matrix, mineral, and water (CURREY, 1999; CURREY et al., 2009a), and they vary from base to the tip (CURREY, 1999), which is related to the combined effects of bone microarchitecture and mineralization. The mechanical properties of antlers are extremely important in order to be able to function as a weapon. The parameters used to characterize the mechanical properties of the bone are: Young's modulus of elasticity (a measure of material stiffness), bending strength (the

maximum stress tolerated or minimum load per unit of volume required to break a specimen), work of fracture (the work necessary to break a specimen) and impact energy absorption (the energy required to break a specimen in impact) (CURREY, 1979a; LAUNEY et al., 2010). When they are used in fights, antlers are in a dry state (they have very small amount of moisture, which is result of antlers being in equilibrium with the atmosphere). Several comparisons are made between dry antlers and wet bovine bone. For example, Young's modulus of red deer antlers is 22% lower than wet bovine bone. This moisture content in antlers is increased only shortly after velvet shedding, but then in a short period of time they get dried out (CURREY et al., 2009b). Dry antlers also have 25% higher static bending strength than wet bone. Dry antler energy absorption is nearly 2.5 times greater than that of wet bone. Impact energy absorption of dry antler is on average 6.6 times greater than that of wet bone (CURREY et al., 2009a). More proximal portion of antlers in Young's modulus had a somewhat higher value of elasticity and of bending strength than the distal ones (CURREY et al., 2009b). KRAUSS et al. (2009) state that possible reason for this is its deformation behavior at the nanoscale, which is different from "ordinary" cortical bone. Dry and wet bones have different mechanical properties. Dry bone has higher modulus of elasticity (stiffness), but undergoes much less post-yield strain (EVANS and LEBOW, 1951). During the fights, high energy absorption is good for initial clashing, while high stiffness is important for the second phase, the pushing match (CURREY et al., 2009b).

The mechanical properties of antler and other bones are determined by the cortex (DAVISON et al., 2006). Decisive parameters are cortical thickness, porosity, microarchitecture, and material properties, namely the degree of mineralization (DAVISON et al., 2006; LANDETE-CASTILLEJOS et al., 2007c, 2012a). The mechanical properties of antlers are related to their histological parameters (bone porosity, osteocyte lacuna number, primary and secondary osteon populations, collagen fiber orientation). The most important parameter is collagen fiber orientation (SKEDROS et al., 2006). Antler's mechanical properties (bending strength, impact resistance) improve primary osteons, whose collagen fibers are mainly oriented along the pores. Antler bending strength is improved by collagen orientation in osteons over tens of centimeters. Furthermore, this architecture is essential for the fast-unidirectional bone growth needed for the annual antler regrowth and for improving the mechanical properties of the whole antler regarding bending strength and impact resistance (KRAUSS et al., 2011).

On the antler transverse sections viewed with polarized light, the largest part of the wall of the primary osteons appears dark, which indicates a longitudinal orientation of the collagen fibers. Along the osteons periphery bright seams are visible, which indicates that collagen fibers are oriented more perpendicularly to the path of the light (KRAUSS et al., 2011; SKEDROS et al., 2014). Brightness of the osteon periphery in transverse and longitudinal antler sections suggests an oblique orientation of the collagen fibers in this area (SKEDROS et al., 2014).

Bone porosity is related to material stiffness (CURREY, 1988), and a small increase in porosity leads to a disproportionately large loss in bone strength (TURNER, 2002; DAVISON et al., 2006). The degree of cortical porosity is one of the main features of hard antlers that may affect the frequency of breakage (LANDETE-CASTILLEJOS et al., 2019). Also, there is a relationship between mechanical properties of antlers, antler porosity, quantity and quality of their diet in red deer (LANDETE-CASTILLEJOS et al., 2007b, 2007c, 2012b). Bone mechanical properties are also influenced by some other factors such as cement (reversal) lines around secondary osteons (YENI and NORMAN, 2000; SKEDROS et al., 2005) or the possible equivalent function of the hypermineralized seams around primary osteons in the case of antlers, which may lead to a toughening of the antler bone (SKEDROS et al., 2014).

Another important parameter is mineral density of the antler cortex. Measurements of areal bone mineral density (aBMD) of the cortex in transverse antler sections showed that antler bones have low values compared to non-antler bone cortices. In addition, aBMD in a series of intact antlers was significantly higher than in broken antlers from a different year and varied between different positions within a single antler as well as between different antlers. There was also a decline from proximal to distal positions (LANDETE-CASTILLEJOS et al., 2010).

Of all studied bones, antlers had the greatest impact energy absorption, which relates to lower mineral content of antler bones (CURREY, 1979b).

2.3.5. Antler cycle

In deer, the development of primary cranial appendages and the subsequent regrowth of antlers are different processes. The primary cranial appendages are newly-formed bony structures, while the development of subsequent antlers is a regenerative process (KIERDORF et al., 1994). The formation of primary cranial appendages includes the development of pedicles and the subsequent growth of the first antler set (GOSS, 1983, 1990; KIERDORF and KIERDORF, 1992).

Antlers develop from the pedicles, which are permanent bony protuberances on the frontal bone. Pedicle growth in red deer starts at about 5-7 months of age, and first antlers start to form at approximately 1 year (JANICKI et al., 2007).

With the detachment (casting) of the first antlers, the stag enters into a regular cycle of antler regrowth and casting. On average it takes approximately four to five months for the growth phase to be completed, which makes antlers one of the fastest growing organs in mammals (CHAPMAN, 1975; GOSS, 1983; GOMEZ et al., 2013; WANG et al., 2019a). According to the assessment based on data from wild deer antlers that grow in 137-153 days, the rate of antler growth can be as high as 6-7 mm per day (TZALKIN, 1945). In wapiti (*Cervus canadensis*), a peak growth rate of 2.75 cm per day has been reported (GOSS, 1970). Under natural conditions, antler growth in adult red deer stags starts in late winter or early spring (late February – early March), and velvet is shed (antler cleaning), revealing the hard antlers in July/August, prior to the mating season (GÓMEZ et al., 2022).

Pedicle and primary antler growth from the frontal bones (distal parts of the *cristae externae*) is initiated by a special periosteum called antlerogenic periosteum (AP) (HARTWIG and SCHRUDDE, 1974; GOSS and POWEL, 1985; KIERDORF and KIERDORF, 2000). Formation of primary antlers can start only after full pedicle development (GOSS, 1983; LINCOLN, 1984). The AP, which has mesenchymal stem cells (WANG et al., 2019b) is considerably thicker than the periosteum of other parts of the skull (LI and SUTTIE, 1994) and contains specific binding sites for testosterone (LI et al., 1998). Cells of the AP's cambial layer are rich in glycogen, which is an energy source for rapid proliferation (LI and SUTTIE, 1998). Antler regeneration is dependent on pedicle periosteal stem cells that are derivatives of the AP (KIERDORF and KIERDORF, 2012; LI, 2012; WANG et al., 2019b).

The antler cycle is linked to seasonal fluctuations of testosterone (WISLOCKI et al., 1947; GOSS, 1968; SUTTIE et al., 1995). Cells from AP become activated by rising testosterone levels in the blood (GOSS and POWEL, 1985). During antler growth, circulating testosterone levels are low, while an increase in blood testosterone prior to the mating season (in late summer) results in intense antler ossification and subsequent velvet shedding (SUTTIE et al., 1995). This is followed by a hard antler phase that lasts as long as testosterone concentration is above a certain threshold (through the autumn and winter) (LINCOLN, 1989). Decreased testosterone levels in the blood following the mating season (late winter) stimulate osteoclastic activity in the pedicle, leading to a weakening of the pedicle-antler connection and casting of antlers (WALDO et al., 1949; KIERDORF et al., 2013). Normally, antlers are cast within a day or so of each other (GOSS et al., 1992). After antler casting, osteoclasts continue to resorb bone in the distal pedicle, creating a smooth surface. The portion of the pedicle that was lost with the cast antler is then partially restored by bone formation (KIERDORF et al., 2003). Wound healing mechanisms, leading to the initial formation of a scab and the migration of a newly-formed hairless skin over the pedicle, starts after antler casting (LI et al., 2004, 2005), followed by a short period of partial pedicle restoration by intramembranous (direct) ossification, and finally new antler growth (WISLOCKI, 1942; KIERDORF et al., 2003; LI et al., 2005). Early in the summer, the concentration of testosterone is low, which leads to a rapid antler regeneration (LINCOLN, 1989). In most species from highly seasonal climates, antler casting and regeneration occur every 12 months, while in the tropical species that period lasts between 10 and 15 months (LINCOLN, 1992). So far, only Père David's deer (*Elaphurus davidianus*) normally produces two sets of antlers each year. In reindeer and moose, antlers are cast in late autumn. In these species the wound does not heal over the pedicle and regeneration is stopped until environmental conditions are appropriate, even several months later (PRICE et al., 2005). In addition, annual reproductive cycle in cervid species that live in higher latitudes is strictly controlled by the photoperiod (GOSS, 1983; LINCOLN, 1992; ROLF and FISCHER, 1996).

Furthermore, in antler regeneration, a non-gonadal factor called 'antler growth stimulus' is involved (WISLOCKI, 1943). This has been identified as insulin-like growth factor I (IGF-I) whose concentrations are high during the period of rapid antler growth (SUTTIE et al., 1985). The IGF receptors are present on an antler's growing tip (ELLIOTT et al., 1992, 1993) and IGFs promote proliferation of antler cells (PRICE et al., 1994; SADIGHI et al., 1994). Antler growth

cycle is also dependent on the changes in concentrations of other hormones such as calcitriol (VAN DER EEMS et al., 1988; SEMPERE et al., 1989), thyroid hormones (SHI and BARRELL, 1994), cortisol (BUBENIK et al., 1975; SUTTIE et al., 1995) and prolactin (SEMPERE et al., 1983; SUTTIE et al., 1984).

WANG et al. (2019a) state that different proto-oncogenes are involved in antler formation making their expression profile more similar to that of osteosarcomas than to that of physiological bone, but that several tumor suppressor genes are also highly expressed in growing antlers. According to these authors, antler growth, therefore, involves the unique combination of oncogenic and tumor-suppression pathways that enables rapid growth and simultaneously prevent oncogenesis.

Several hypotheses have been put forward to explain the periodical casting and regeneration of antlers: an obligatory feature of their evolution in relation to periodic damage (COOPE, 1968), their replacement in case of breakage (SPINAGE, 1970), the adjustment of their size during the life cycle to allow antler size to keep pace with body size (GOSS, 1983), to mimic females after casting and thereby avoid predation (GEIST, 1981), could have evolved as a measure to ensure that complete antlers were available as display organs each year. According to LANDETE-CASTILLEJOS et al. (2019), the main reason for their annual regeneration is most likely the fact that hard (polished) antlers are dead bony structures and thus incapable of undergoing repair.

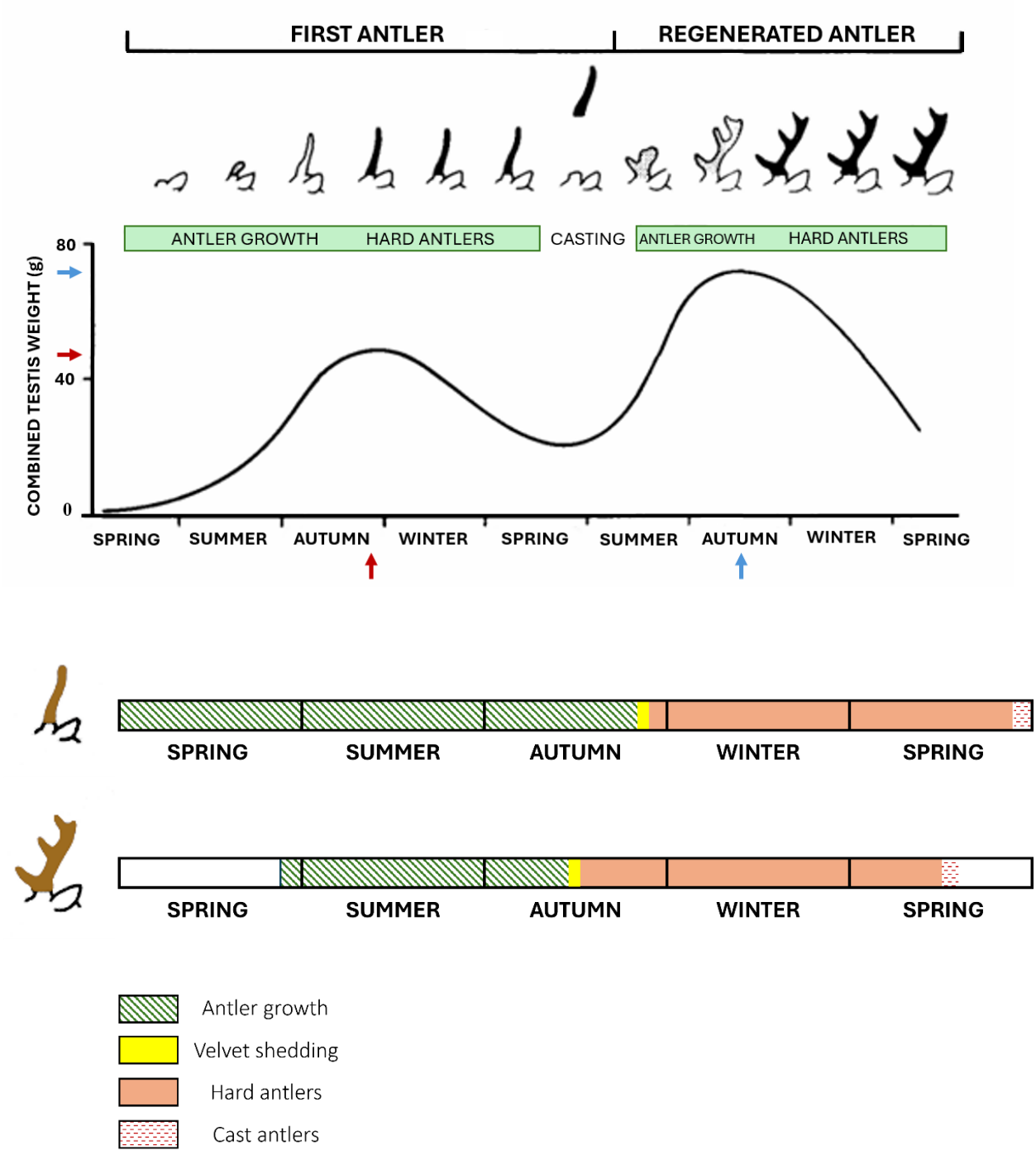

Figure 5. Cycle of antler regrowth and casting: difference between spikers (first antlers) and older animals (modified from LINCOLN, 1984).

2.3.6. Histology of growing antler

Growing antlers are surrounded by the velvet, which is formed of epidermis and dermis. The inner portion of the dermis is fused with the fibrous layer of the shaft periosteum. The cellular layer of the periosteum is hyperplastic with numerous osteoprogenitor cells and osteoblasts. The periosteum is continuous with the perichondrium of the actively elongating distal portion of antler. Growing antler can be divided into different zones (BANKS, 1974).

Below the dermal part of the velvet is the **1) hyperplastic perichondrium**, a proliferative zone that can be divided into 3 subzones: the *reserve mesenchyme*, a *prechondroblastic zone* and a *chondroblastic zone*. The *reserve mesenchyme* forms the antler tip and contains numerous mitotic cells in different phases that are divided into two layers. The superficial layer is fused with the fibrous part of the perichondrium, containing numerous spindle-shaped basophilic cells that have a centrally located oval nucleus with 1 or 2 nucleoli. Cells are tightly packed, and oriented perpendicular to the antler long axis. The intercellular spaces contain collagen, while the ground substance is slightly metachromatic and alcianophilic. The inner layer contains spindle-shaped, basophilic cells that have oval or round nuclei with 1 or 2 nucleoli. Cells are hypertrophied, irregularly oriented and separated from each other by more intercellular material that contains collagen fibers and is slightly metachromatic. Small, thin-walled sinuses (vascular channels) can be present and are continuous with large vessels located in the inner portion of the dermis. Around the vessels is an adventitial sheath with a thickness of 1 to 3 cells that are spindle-shaped, and oriented parallel to the long axis of the vessels. Other cells in this zone have no orientation to the vascular channels, which distinctly marks the beginning of the columns more clearly defined in deeper (proximal) antler portions. The *prechondroblastic zone* is organized in a distal to proximal orientation with more progressive changes located proximally. This zone contains a heterogeneous cell population in different stages. Cells in the distal portion are spindle-shaped, some of them slightly polarized and without processes, while other cells are hypertrophic and oriented in a swirl-like fashion, and they swirl between the vascular channels. Collagen fibers are thicker and denser than in the mesenchymal zone. The proximal portion contains spindle-shaped to oval cells that are irregularly oriented, show cellular hypertrophy and have a more pronounced polarity. The round polarized cells contain a distinct and extensive juxtanuclear pale-staining area within the basophilic granular cytoplasm which is finely reticulated. Orientation of collagen fibers is

irregular. Progressing from distal to proximal, an increase in collagen fibers and in the metachromatic properties of the ground substance is present. The *chondroblastic zone* contains round, polarized cells with progressive increase in the metachromatic properties of the ground substance and the lacunar borders. The endothelial lining around vascular channels is weakened, and the sinus spaces are slightly enlarged. Perivascular cells are longitudinally oriented (BANKS, 1974).

Proximal to the proliferative zone is the **2) chondrocytic zone** that is divided into 2 subzones: the *mature cartilage zone* and *mineralizing cartilage zone*. **Chondrocytic zone** is cartilaginous with visible hypercellularity of hypertrophic chondrocytes which are a heterogeneous mixture of cell types. In the central part of the cartilaginous columns the cells are rounded and polarized with a juxtanuclear pale region within the finely reticulated cytoplasm, some of them have processes. All cells contain highly metachromatic and alcianophilic capsules. Necrosis is visible in some of the cells. The peripheral chondrocytes are spindle-shaped to oval cells, with irregular orientation. Cellular hypertrophy and polarity are more pronounced. Round polarized cells contain a distinct and extensive juxtanuclear pale-staining area within the basophilic granular finely reticulated cytoplasm. The cytoplasm of hypertrophic chondrocytes is shrunken, while nuclear integrity is maintained. Within each column there is a longitudinal and a latitudinal gradient of differentiation. The interterritorial matrix is reduced and possesses less intense staining properties. The vascular channels, lined with an attenuated endothelium, are large and accompanied by an enlarged perivascular compartment that contain collagen fibers and numerous stellate and spindle-shaped cells. Cartilaginous columns are not covered by an ordered arrangement of perivascular cells, instead, these cells and accompanying matrix components gradually blend with the cartilage of the columns. Chondroclasts are visible on the surfaces of the chondrocytic columns. Progressive mineralization from distal to proximal is visible. Mineralization begins in the central portions of the columns and corresponds to those regions which are metachromatic, alcianophilic and strongly PAS-positive. It is pronounced initially in the perilacunar regions and spread throughout the matrix proximally (BANKS, 1974).

Next is the **3) primary spongiosa**, where the processes of chondroclasia, osteoclasia, and osteoblastic activity occur simultaneously, which leads to the replacement of the mineralized cartilage network by bony trabeculae. Changes in the cartilaginous columns are present in the

chondrocytes, which are placed in the peripheral portions of the columns. Some cells are stellate, while others are fusiform. Many of the chondrocytes are retracted from their lacunar margins, and vacuoles are present in many of them that are not fully retracted. Some nuclei are pyknotic, while some lacunae are empty. Numerous chondroclasts are visible (many are present on the cartilaginous columns prior to osteoblasts, others accompany osteoblasts, while some of them are visible within the depths of the cartilaginous columns). Woven bone is deposited, and osteoclasia is visible upon cartilaginous columns. Remodeling of woven bone and mineralized cartilage occurs. The mineralized cartilage and woven bone are gradually removed. Peripherally, woven and lamellar bone are deposited intramembranously as a sleeve of periosteal bone (BANKS, 1974).

Proximally, the primary spongiosa is followed by the **4) secondary spongiosa** in which the spaces between the bony trabeculae are filled with lamellar bone. Secondary spongiosa contain lamellar bone in a compact and cancellous configuration. In the early stages of development, the compact bone is in the peripheral part, while the cancellous bone is in the medullary cavity. In this zone numerous osteons in various stages of filling are present, while there is no osteoclasia (BANKS, 1974). Regarding circular lamellar systems, these are predominantly primary osteons.

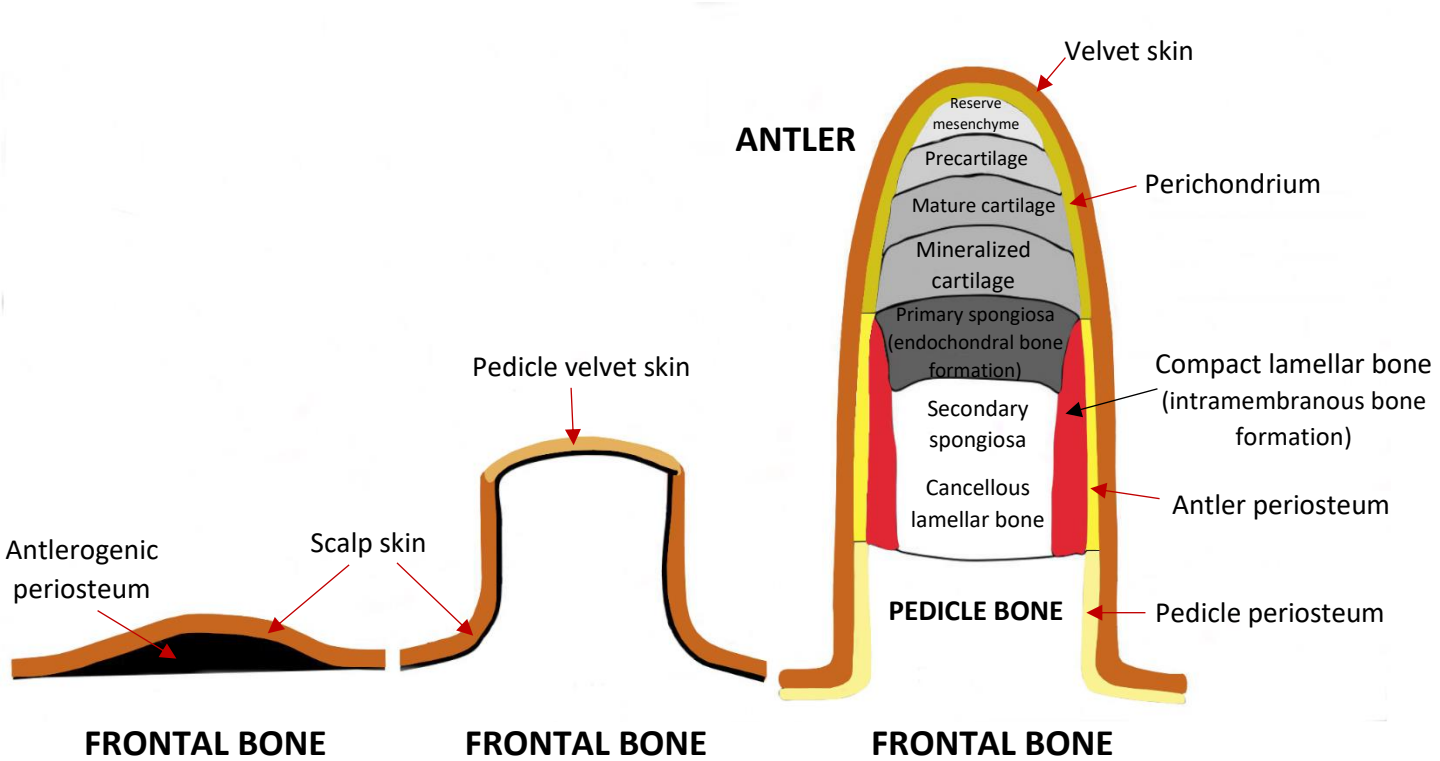

Figure 6. Primary antler development (modified from PRICE et al., 2005).

2.3.7. Antler histodifferentiation

There have been many disagreements about the process of antler histodifferentiation. Different authors have come to different conclusions and have accordingly supported different processes involved in antler development. Certain authors support the hypothesis that antlers develop by intramembranous (direct) ossification (MACEWEN, 1920; MODELL and NOBACK, 1931; WISLOCKI, 1942; JUDKINS, 1958; DAVIS, 1962; KUHLMAN et al., 1963; HARTWIG, 1967), others support the idea of endochondral (indirect) ossification (MACEWEN, 1920; LOJDA, 1956; JUDKINS, 1958; DAVIS, 1962), while some support the process of metaplastic conversion of cartilage to bone (MACEWEN, 1920; NOBACK, 1929; GRUBER, 1937; WISLOCKI et al., 1947; LOJDA, 1956; GOSS, 1970).

MACEWEN (1920) states that intramembranous and endochondral ossification occur in antler histodifferentiation, but that it is predominantly endochondral process that was characterized as a direct conversion of cartilage to bone (metaplasia). NOBACK (1929) agreed with metaplastic conversion, while MODELL and NOBACK (1931) supported intramembranous ossification and state that the true cartilage does not exist. GRUBER (1937) compared antler growth with the process occurring at the epiphyseal plate. He highlighted the importance of periosteal and perichondral involvement and gave the evidence for the occurrence of metaplasia. WISLOCKI (1942) considered that intramembranous ossification occurs, but with difference because of the existence of preosseous columns. WISLOCKI et al. (1947) said that the primary way of antler ossification is “chondroidal bone formation”, which means that cartilage cells convert into osteocytes and that this process is an intermediate between intramembranous and endochondral ossification. LOJDA (1956) supported endochondral ossification, but also metaplastic conversion of mineralized cartilage to woven bone. JUDKINS (1958) had evidence that both endochondral and intramembranous ossification occurred in antler development, which was supported by DAVIS (1962). KUHLMAN et al. (1963) did not support endochondral ossification, but they claim that antler formation was mediated through a modified type of intramembranous ossification involving the initial differentiation of preosseous fibrocellular columns. HARTWIG (1967) supported the mechanism of intramembranous ossification, while GOSS (1970) believed that the cartilaginous trabeculae were converted directly into bony tissue by deposition of mineralized

material within the matrix. FRASIER and BANKS (1973) confirmed with histochemical and enzyme digestion studies that the preosseous tissue of antler is cartilage.

Pedicle formation occurs by process which is comparable to endochondral ossification in fallow deer (KIERDORF et al., 1994; SZUWART et al., 1994) and red deer (LI and SUTTIE, 1994).

There is now a principal consensus that antler formation occurs by endochondral and intramembranous ossification (GRUBER, 1937; BANKS, 1974; BANKS and NEWBREY, 1983a, b; PRICE et al., 1996). There is a growth zone at the tip (distal portion) of the main beam and each tine beneath the velvet dermis that contains numerous undifferentiated mesenchymal stem cells (WISLOCKI, 1942; BANKS, 1974; KIERDORF et al., 2003; LI et al., 2005). Proliferation of these cells leads to antler growth and elongation, which is appositional (KIERDORF et al., 2003, 2022). Mesenchymal cells differentiate into chondroblasts and chondrocytes, which make cartilaginous columns longitudinally oriented and separated by a vascular tissue (WISLOCKI et al., 1947; BANKS, 1974; KIERDORF et al., 2003; LI et al., 2005). During this phase, antler cartilage is highly vascularized. In the next step, cartilage becomes mineralized, eroded by chondroclasts/osteoclasts, and replaced with bone. At the antler periphery, a bone sleeve is formed by osteoblasts derived from the osteogenic (cambium) layer of the periosteum in the process of intramembranous (direct) ossification (KIERDORF et al., 2003). Distal to proximal zonation is visible along the antler vertical axis, which means that at the antler tips (distal part) are the youngest portions and at the antler base (proximal part) the oldest portions (GOMEZ et al., 2013; KIERDORF et al., 2022). In growing antlers, growth plates and secondary ossification centers are not present (LI and SUTTIE, 1994; PRICE et al., 2005; KIERDORF et al., 2007).

In the process of antler cortex formation, a network of mineralized cartilage (longitudinally oriented tubular structure) with cylindrical pores oriented along the antler's long axis is formed first (KRAUSS et al., 2011). Following this, the cartilaginous network proximally undergoes resorption by chondroclasts and is replaced with framework of trabecular (cancellous) bone with the same orientation (VON KORFF, 1914; BANKS, 1974; BANKS and NEWBREY, 1983a; LI and SUTTIE, 1994; KIERDORF et al., 1995a; SZUWART et al., 1998, 2002; FAUCHEUX et al., 2001; KRAUSS et al., 2011; LANDETE-CASTILLEJOS et al., 2019). The trabecular bony framework is largely formed of woven bone, which is later replaced with lamellar bone (GOMEZ

et al., 2013) with a low degree of collagen orientation over longer distances (micro-lamellar bone) (KRAUS et al., 2011). Micro-lamellar bone is a sub-type of a woven bone (KERSCHNITZKI et al., 2011). According to GOMEZ et al. (2013) and KIERDORF et al. (2013), both woven and lamellar bone can be present in the trabecular scaffold depending on the location.

The intertrabecular cavities lined with the osseous framework (scaffold) in the future cortical region are filled with primary osteons that are likewise oriented along the antler's long axis (KRAUSS et al., 2011; GOMEZ et al., 2013; KIERDORF et al., 2013; SKEDROS et al., 2014; LANDETE-CASTILLEJOS et al., 2019). Resorption at the trabecular scaffold occurs before infilling the intertrabecular cavities with primary osteons (GOMEZ et al., 2013; KIERDORF et al., 2013).

2.3.8. Velvet

The velvet epidermis is deeply pigmented, covered with fine soft hairs and rests upon the dermis which have two parts: outer – papillary layer and inner – reticular layer. In the papillary layer are numerous papillae that project into the epidermis, hair follicles and their attendant sebaceous glands, while sweat glands are absent. The reticular layer contains hair follicles and sebaceous glands. Beneath the reticular layer is a loose connective tissue, often containing fat. It is in loose continuity with the dermis. A typical subcutaneous layer does not exist. In addition, beneath the reticular layer is the tunic consisting of dense parallel bundles of collagenous tissue with the main blood vessels that supply an antler (vascular layer). This layer is adnexa of the skin, not the outer layer of the periosteum because it is continuous with the skin and cannot be properly separated from it. The layer of fibrocellular tissue that is adherent to the bone represents the true periosteum and it is composed of superficial and deeper layers. The superficial layer consists of parallel collagen fibers with spindle-shaped cells between they, while the deeper layer is more loosely organized and contains more cells. Fibrocellular periosteal layer at the growing tips of the antlers is in the form of hypertrophied caps of periosteal cells embedded in a network of collagen fibers. The cap-like structures resembling the mesenchyme (young connective tissue) and represent germinal areas at the tips of the tines from which the entire antler has been gradually laid down. Dermis and the periosteum are fused in areas where caps are visible. Antler tips are covered with fewer and more delicate hairs than in other locations on the velvet (WISLOCKI, 1942).

2.3.8.1. Velvet shedding

When the velvet is shed, the blood supply of antlers ends, bone formation and mineralization cease, and the antler bone undergoes necrosis (GOMEZ et al., 2013). Within a few days, the velvet is removed from antlers by rubbing them on vegetation (JIN and SHIPMAN, 2010). It has been suggested that the color of the antler external surface is caused by dried blood (WISLOCKI, 1942) or by dried blood mixed with soil or dust (VON KORFF, 1914). However, it is more likely that impregnation of plant juices plays the dominant role.

In a growing antler, the trabecular bone contains a large amount of blood, and some of this blood is trapped in antlers at velvet shedding (CHAPMAN, 1981). According to CHAPMAN (1981), there is no fluid in cast antlers, which were examined a few days after casting. The author concluded that in the red deer antlers spongy bone retains the fluid, which keeps them wet and highly impact resistant (work of fracture) during the fight. Fluid evaporates gradually and sometimes diminishes before antler casting. As antler dries out, the impact of resistance declines simultaneously as the frequency of fighting declines. Antlers in deer species that do not fight with antlers in the same way and extent as red deer do not need to have high impact resistance, also it is not necessary that they are wet and have a core of spongy bone. This old view claimed that wet antlers were better adapted to fighting than dry ones, but this has been refuted by new research (CURREY et al., 2009a, b; LANDETE-CASTILLEJOS et al., 2019).

2.3.9. Calcified cartilage

Cores of calcified cartilage in mammals are first present during endochondral ossification and they are completely replaced with bone tissue during remodeling (PRITCHARD, 1972; ALLEN and BURR, 2014). In mammals, calcified cartilage persist in some areas, such as articular calcified cartilage present in diarthrodial joints of the adult skeleton (FERGUSON et al., 2003; BOYDE, 2021), calcified cartilage islands in long bones of rats and mice (BACH-GANSMO et al., 2013; JING et al., 2017), larger amounts of calcified cartilage in large mammals in the ribs of extant and fossil sirenians (FAWCETT, 1942; DE BUFFRÉNIL et al., 2008) and fossil cetaceans (DE BUFFRÉNIL et al., 1990).

The antler cartilage has been classified as secondary cartilage, a type of cartilage that occurs in rapidly forming intramembranous bones. Deer antlers, which go through a cartilaginous phase during their growth, develop from periosteal cells of an intramembranous bone (frontal bone). Antlers are a type of secondary cartilage since they are produced after development of other skeletal bones and their growth is predominantly endochondral from an intramembranous bone (GALEA et al., 2021).

In order to adapt to the rapidity of antler growth and its associated high metabolic demands, antler cartilage is richly vascularized (GOSS, 1983). Antler chondrocytes are not hypoxic in contrast to chondrocytes in the avascular growth plate (GALEA et al., 2021).

In the growing antlers, a zone of calcified cartilage was below a zone composed of precartilage zone and mature cartilage. During cartilage maturation, the antler chondrocytes undergo hypertrophy and the cartilage matrix becomes mineralized. Proximally, chondroclasts resorb calcified cartilage. Simultaneously, woven bone is deposited by newly-differentiated osteoblasts on the partially eroded cartilaginous trabeculae (zone of primary spongiosa). The woven bone is first deposited directly on the calcified cartilage, and lamellar bone is later deposited on this initial woven bone. Hypertrophic chondrocytes or their remnants are found in the larger cores of calcified cartilage within mature (hard) antlers (KIERDORF et al., 2022).

Calcified cartilage in hard antlers indicates that the antler bone had not undergone any significant remodeling. In the hard antlers, remnants of calcified cartilage were not distributed isotropically. No or only few patches of remnants of calcified cartilage are present in the proximal antler portion (KIERDORF et al., 2022), while in the distal portions they are regularly found (LANDETE-CASTILLEJOS et al., 2012b; KIERDORF et al., 2013, 2021, 2022). The distal antler portion is late-formed, and resorption of the calcified cartilage framework is typically incomplete, while more proximally the cartilage is largely or entirely replaced with bone (KIERDORF et al., 2022). In the peripheral cortex of the proximal antler portions calcified cartilage is always absent because these zones are formed by intramembranous (direct) ossification. In larger areas of calcified cartilage, remnants of hypertrophic chondrocytes are found whose lacunae are larger and more roundish than osteocyte lacunae. Compared to bone, the calcified cartilage matrix in antlers and other types of mammalian bone has a higher degree of mineralization. Due to the presence of Howship's lacunae, the surface of the calcified cartilage remnants is scalloped and along these

scalloped borders are hypermineralized seams. These are cement (reversal) lines deposited during the initial phase, subsequent to the end of cartilage resorption. Primary osteons sometimes directly border on the calcified cartilage in the antler tip (distal portion), which means that in places resorption of the calcified cartilage scaffold had been directly followed by formation of primary osteons, without a replacement of the cartilaginous by an osseous trabecular framework (entire step is skipped). The reason for this is a shortened duration of the successive histogenetic phases in the distal portions compared to the more proximal antler portions. Occasionally, the entire step (replacement of the cartilaginous by an osseous scaffold) is skipped (KIERDORF et al., 2022). Because of the short antler lifespan in the distal antler, calcified cartilage is particularly prominent in this region (KIERDORF et al., 2021).

KIERDORF et al. (2022) for the first time showed mineralized deposits in some chondrocyte lacunae of the calcified cartilage remnants. Mineralized deposits have granular to globular texture and partly or completely fill the lacunae. In partly filled lacunae, they sometimes show a ring-like shape, which suggests a centripetal infilling process because of a shrinking of the dying chondrocyte and the expansion of the pericellular space within a lacuna. Sometimes, mineralized deposits were also observed in osteocyte lacunae adjacent to calcified cartilage remnants (KIERDORF et al., 2022).

Higher Ca and P concentrations were found in mineralized cartilage matrix and mineralized chondrocyte lacunae than in the surrounding mineralized bone matrix of hard antlers. Furthermore, hypermineralized cement (reversal) lines had an increased Zn content compared to the surrounding mineralized matrix (KIERDORF et al., 2022).

2.3.10. Antler regeneration

WISCLOCKI (1942) collected antlers from white-tailed deer (*Odocoileus virginianus borealis*) at intervals throughout an entire year and described changes in their structure and differences by months. As previously mentioned, in the antler histogenesis, WISLOCKI (1942) does not describe an endochondral process.

After casting in January, the concave apex of each pedicle is covered with newly-formed hairless skin and a small superficial central black scab of clotted blood. The concavity is partially filled with a fibrocellular tissue, and between were few newly-formed delicate spongy osseous trabeculae. The newly-formed epidermis lacks hair follicles and covers portion of the original defect. In March the pedicle is surrounded by whitish fibrocellular tissue which adheres to the bone, and beneath the fibrocellular layer there is a more reddish narrow zone of spongy bone. The fibrocellular layer then decreases in thickness, while the spongy bony trabeculae increase and fill the original shallow concavity at the distal end of the pedicle. In May, antler regrowth has not yet started. The skin covering the pedicles consists of a pigmented epidermis and well-developed dermis with two layers. The outer layer contains hair follicles and sebaceous glands, while the deeper layer is extremely vascular and composed of parallel bundles of collagen fibers. A layer of subcutaneous fatty tissue is missing. The dermis and the fibrocellular layer are firmly fused at the tip of the pedicle. The fibrocellular layer initiates ossification and because of that reminds on periosteum, which begins to deposit spongy bone in the shape of irregular delicate parallel osseous columns. Beneath this is a narrow zone of irregular, spongy bone (from the bone growth in the concave defect of the pedicle). Osseous columns become denser and interwoven which represent antler base at the antler pedicle junction (future area of detachment) (WISLOCKI, 1942). WALDO et al. (1949) found that when antlers first develop in May they are composed of delicate spongy bone. In June, antlers are covered by black epidermis and delicate sparse hairs, while corona/burr is not present. Antlers are soft because they are slightly mineralized, with unmineralized tip. They consist of a red bony core, surrounded by a sheath of white periosteum and skin. Frontal bone and pedicle are yellow because of the presence of fatty marrow. Mineralization progresses from the base (proximal portion) of an antler toward the tip (distal portion) of an antler. Histologically, June and July antlers differ very little. Antlers in July are covered by a coat of delicate short hair, and mineralization is progressing slowly from the base to the tip. In August, antlers are visible in their

almost final form. They are very hard (better mineralized) and covered with velvet (WISLOCKI, 1942). In July and August, according to WISLOCKI (1942), or in June, July and August, according to WALDO et al. (1949), internal reconstruction is happening. The peripheral cortical part of the spongy antler becomes replaced with dense compact bone with primary Haversian system, while the center becomes reorganized into spongy lamellae with wider marrow spaces (WISLOCKI, 1942; WALDO et al., 1949). Osteoblasts laid down layers of concentric bone lamellae and created primary Haversian systems, central cancellous part is under the reorganization, osteoclasts and osteoblasts activity lead to destruction and new formation of bony lamellae (the interior part is composed of relatively few, coarse spicules of spongy bone that enclose wide marrow spaces). These spaces in antlers in June, which are growing, are filled with blood vessels and young connective tissue. This marrow spaces are not real bone marrow cavity, and "marrow" is not a hematopoietic tissue. As a result of weakened circulation and focal necrosis, detritus is present in some parts of marrow without distinguishable cells or recognizable structure (WISLOCKI, 1942). Reorganization of the bone is different at the base of antler-pedicle junction compared to the rest of the antler. It becomes hard and dense, grooves are visible externally on the antler longitudinal, while they are not present inside central cancellous structure. In the zone of antler-pedicle junction, the Haversian systems interweave irregularly at oblique angles, which gives strength and hardness to the antler base, while in the cortex of the rest of an antler, they run parallel to one another (WISLOCKI, 1942; WALDO et al., 1949). After velvet shedding in October, the antler surface of the lower parts was brownish (desiccated blood in the crevices of the bone surface and in the porous part). The marrow spaces of the lower parts were reddish (relatively fresh blood). A small amount of blood may come to the interior of the antler base after the velvet shedding through small connections directly with the frontal bone. In antlers from December, interior of the antler base is brown (blood desiccated progressively). The pedicle is well vascularized and on its concave apical border is in contact with the avascular antler base (WISLOCKI, 1942).

2.3.11. Antler blood supply

Antler is supplied by branches of the superficial temporal artery (*a. temporalis superficialis*) (WISLOCKI, 1942; WALDO et al., 1949). The walls of these branches are thick and composed of interlacing elastic, muscular and collagen elements with no distinct internal elastic membrane (*lamina elastica interna*) or external elastic membrane (*lamina elastica externa*) (WISLOCKI and SINGER, 1946). The blood from antler returns by veins that are less numerous, larger than the arteries and located near the antler base. The veins and arteries are not in pairs; they are placed independently in velvet connective tissue. Comparing arteries and veins, arteries are round and have well-developed muscular part, while veins are extremely delicate, situated more superficially and have oval lumina (WISLOCKI, 1942). At the antler base, the majority of blood vessels curve around the outer surfaces of the burrs, just some of them pass through tunnels (grooves) between the bony nodules of the coronet (WISLOCKI, 1942; WALDO et al., 1949). The antler veins receive branches from the velvet and antler bony part (WALDO et al., 1949), collect beneath the coronet (burr) into a single large vein which accompanies the lateral coronal artery, and into a much smaller vein associated with the medial coronal artery (WISLOCKI, 1942). These veins drain into superficial temporal vein (*v. temporalis superficialis*) on the side of the head (WISLOCKI, 1942; WALDO et al., 1949).

As antlers grow, venous and arterial drainage becomes modified. Changes in venous drainage are even greater than in the arterial supply since in the early growth stages drainage takes place almost entirely through internal channels. The initial drainage system using vessels connecting pedicle and antler is replaced with an extensive venous collecting systems that return the blood directly from the antler core to the vascular layer of the velvet. Extensive venous collecting systems are formed at intervals when antler increases in length. The early disappearance of nearly all vascular connections between the base of the antler and the interior of the pedicle is caused by progressive ossification, which gradually affects the veins exits. As peripheral mineralization increases, the large venous collecting systems always become occluded, which interrupts the blood circulation through the major portion of the antler substance. Constriction of the thick-walled velvet afferent arteries are induced by venous stasis in the antler core, which leads to ischemia of the entire antler. These vessels are extremely sensitive to mechanical stimuli and respond by constricting, which is the reason why this process is happening (WALDO et al., 1949).

During growth, antlers are supplied primarily by arteries from the overlying velvet whose innermost part constitutes is a vascular layer with large afferent and efferent blood vessels (WALDO et al., 1949). Small amounts of blood come to antler through small collaterals located in Haversian canals, which connect the pedicle and antler (WISLOCKI, 1942). Direct arterial communications exist between antler and the pedicle in the early stages of growth (April, May and June). As the bone across the antler base increases in density, these communications diminish rapidly in diameter and during later growth stages, antler is supplied exclusively via the vessels in the vascular layer of the velvet (WALDO et al., 1949). Sizable arteries are not present in the marrow spaces of the bony antler (WISLOCKI, 1942).

The superficial temporal artery gives off branch that goes posteriorly across the lateral surface of the pedicle below its base. After that, superficial temporal artery continues upward on the skull anterior to the antler pedicle. It divides just above the level of the eye into a large supraorbital branch (*a. supraorbitalis*) that runs forward, and into a lesser posterior branch that supplies the medial surface of the pedicle. The pedicle is supplied by two arteries, a larger lateral coronal artery (*a. coronalis lateralis*) and a lesser medial coronal artery (*a. coronalis medialis*), and by small collaterals internally through the marrow spaces or Haversian canals of the frontal bone. The lateral coronal artery is more sizable and supplies a larger area. The medial coronal artery encircles the antler pedicle, giving rise to several arteries that ascend an antler. The anterior, lateral and posterior antler surfaces are supplied by lateral coronal artery, while the medial surface is supplied by medial coronal artery. These arteries branch from the antler base to the tips (Fig. 7) (WISLOCKI, 1942).

Toward the antler tips, arteries of the vascular layer branch and anastomose with one another, giving rise to an arterial plexus surrounding the growing tips. At the center of the growing antler tip, capillary retia are newly-formed and penetrate the germinal cap. The capillary retia are located at the growing tip between the capillary plexus and the efferent arterioles representing sites at which vasculogenesis takes place. In the proximal part, the capillary retia are transformed into the efferent arterioles which pass into the medullary sinuses. At the antler base, some of them communicate with pedicle venous channels during the initial phase of the growth. The external and internal capillary plexuses are located on the surface of the periosteal layer, except over the growing tip where the internal plexus is lacking. The newly-formed capillary retia become curved

and shift toward the antler sides. The capillary retia at the center of the antler tip are least affected by these changes, while those toward the circumference are gradually transformed into recurrent arterioles (WALDO et al., 1949). Capillaries unite in the marrow spaces to form venules; they further unite to form larger venules that pass outward through the cortex and periosteum of the bony antler to enter the veins of the velvet vascular layer. The blood from the skin is returned by venules that enter the larger veins of the vascular layer (WISLOCKI, 1942).

Recurrent arterioles branch off from the main arteries, traverse the periosteal layer and penetrate the antler shaft. Peripheral portions of the antler bone along the surface of the entire bony shaft, and at the circumference of the growing tip are supplied by small superficial recurrent arterioles. The central antler core is supplied by deep recurrent arterioles that empty into the medullary sinuses (system of thin-walled, anastomosing, longitudinal channels located in the antler interior). Superficial and deep recurrent arterioles form loops consisting of ascending and descending limbs connected by a curved portion that spans the periosteal layer (WALDO et al., 1949).

Mineralization of the antler shaft leads to the fixation of the terminal portions of these vessels at the points where they enter the bone. The origins of the recurrent arterioles, which lie in the velvet, tend to be constant since velvet growth takes place at the antler tip. The periosteal layer grows interstitially throughout its length, slower near the antler base than at the tip. Because of that, the recurrent arterioles that cross the periosteal layer are drawn out into loops, which become constantly longer as one approaches the base of an antler (WALDO et al., 1949).

Only traces of the capillary retia and the efferent arterioles are visible as the growing tips approaches completion. The germinal cap has disappeared, leaving a periosteal layer that is connected to that at the sides of antler. An inner capillary plexus has differentiated over the bony tip. The bone has become compact and vascularized by superficial recurrent arterioles and venules crossing the periosteal layer to communicate with vessels of the Haversian systems. With the progress of ossification, the peripheral part of the bony shaft becomes reorganized and densely mineralized. Therefore, capillaries lose most of their connections with the medullary sinuses and are drained to the velvet veins instead by the superficial venules that cross the periosteal layer. The superficial recurrent arterioles and venules connect with the capillary beds of the Haversian canals along the shaft and at the growing antler base and provide blood supply and drainage for the

compact peripheral bone. There are numerous minute arterioles and venules in the Haversian systems of antler compact part (Haversian arterioles and venules). Sometime, minute arterioles are present between the sinuses in the deep antler interior. After the bone has become compact at the antler base, minute arterioles and venules persist, which communicate locally through the pedicle (external and internal arterioles and venules of the pedicle). The recurrent venules and veins that cross the periosteal layer possess very short loops because they differentiate later than the recurrent arterioles. A significant number of small vessels that connect the velvet arteries with antler substance at all stages of growth is important (WALDO et al., 1949). They are also found by RHUMBLER (1929) and WISLOCKI (1942). When antler is completed, the core with marrow spaces is surrounded by compact bone (antler base, at the tips of the tines). Because of that, the afferent and efferent blood vessels supplying the medullary sinuses have been reduced and the blood flow in the core has diminished nearly to the point of stagnation (complete necrosis of the contents in the medullary spaces is visible in antler sections from August) (WALDO et al., 1949).

Efferent veins are large and numerous in the antler distal portion below the growing tips, while they diminish in size and number in the compact bone near the antler base. Numerous small superficial venules drain the peripheral compact bone, passing outward to enter the velvet veins. The superficial venules and the trunks of the venous collecting systems cross the periosteal layer in a straight course or with very short loops, in contrast to the recurrent arterioles. In antlers, venous channels lack valves (WALDO et al., 1949).

By mid-July, most of the efferent flow is external, through the vessels of the velvet. External vessels have become the only significant ones by late July, and their closure resulted in antler death. There are sufficient internal vascular channels in June, but these internal channels are no longer available or adequate by July (WALDO et al., 1949).

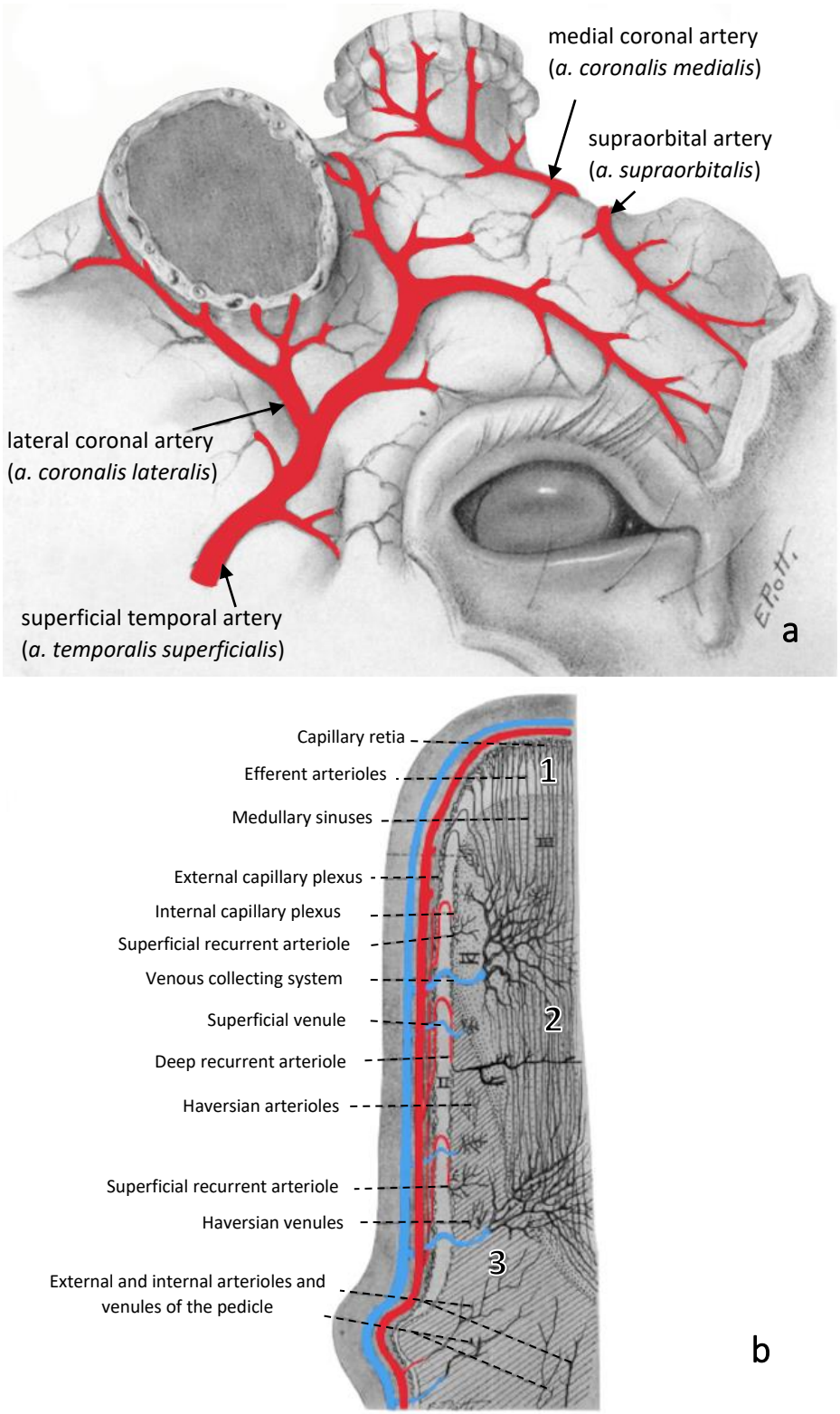

Figure 7. a) The blood supply of June antlers of a white-tailed deer (modified from WISLOCKI, 1942); **b)** The vascular elements of a growing antler: 1 – germinal cap, 2 – medullary spaces, 3 – compact bone (modified from WALDO et al., 1949).

When the velvet is partially shed, the antler surface is rough and dull with a lot of small depressions and elevations. Along the beam and at the bases of the tines, there are few small apertures. Many minute pores containing broken-off blood vessels (small superficial recurrent arterioles and venules) are visible at the antler surface. Mature antlers have a polished, smooth, shiny surface, and absence of apertures large enough to transmit the vessels of the numerous venous collecting systems present in earlier stages of development. These paths for venous blood from the antler interior have been eliminated by the time when mineralization is completed, and their disappearance coincides with the gradual cessation of blood flow and stagnation in the medullary sinuses (during August). There is no significant number of apertures of sufficient size to transmit vessels other than small arterioles or venules after velvet shedding (WALDO et al., 1949).

2.3.12. Antler innervation

Antlers are innervated by two branches of the trigeminal nerve (*n. trigeminus*), the supraorbital (*n. supraorbitalis*) and temporal nerves (*n. temporalis*). The supraorbital nerve exits beneath the upper edge of the orbit and branches in several nerves backward over the skull toward the base of the antler where small branches are given off to the anterior and medial surface of the pedicle and the antler. The temporal nerve exits on the scalp near the zygomatic arch and divides into branches that run toward the base of an antler and others that run behind the antler to the ear region. The temporal nerve, which reaches the base of the antler passes outward onto the lateral and posterior surfaces of the antler pedicle and then on an antler (WISLOCKI and SINGER, 1946). The innervation of this nerve coincides with the distributions of the lateral and medial coronary branches of the superficial temporal artery (WISLOCKI, 1942). The nerve fibers, placed in the vascular layer of the velvet, lie between the individual arteries and veins in the relatively loose connective tissue. A relatively distinct perineurium is around the bundles of myelinated and nonmyelinated nerve fibers. The nerves die as far back as the antler pedicle when the velvet is shed, so the innervation of an antler is renewed annually (WISLOCKI and SINGER, 1946).

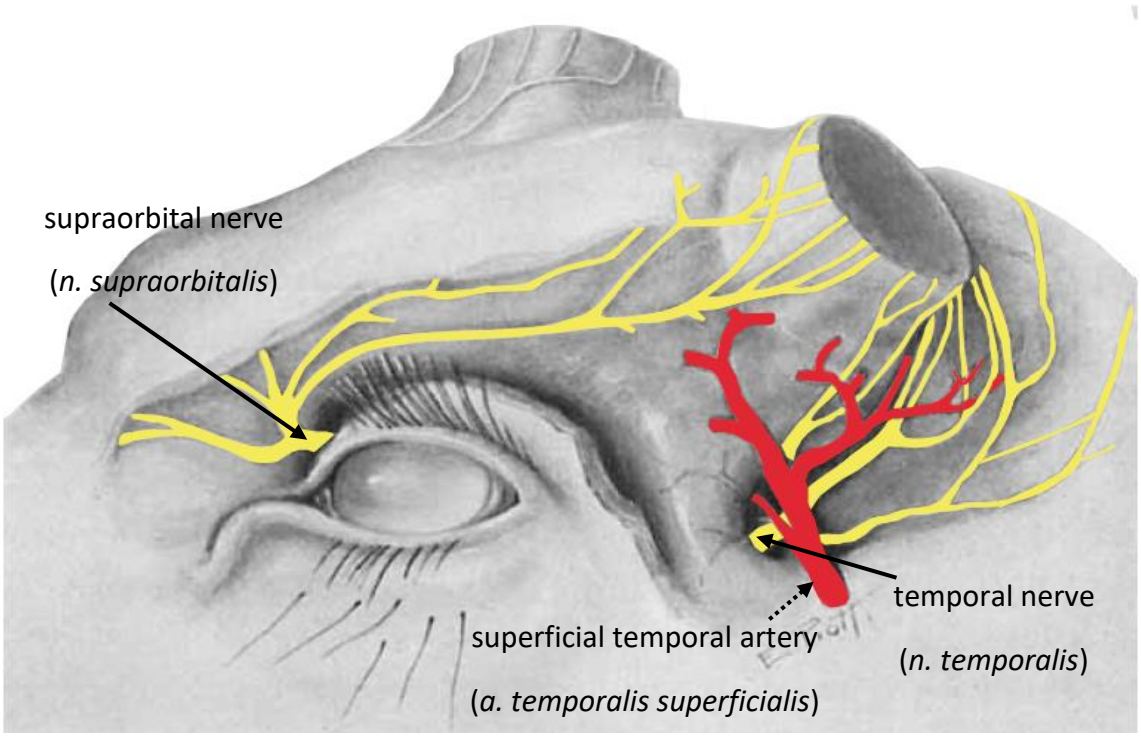

Figure 8. Antler innervation with the branches of the trigeminal nerve: the supraorbital nerve innervates the anterior and medial antler surfaces, the temporal nerve innervates the lateral and posterior antler surfaces (modified from WISLOCKI and SINGER, 1946).

2.4. Annual physiological osteoporosis

The formation of new antlers every year within a period of few months is a significant physiological effort and challenging process for mineral metabolism, especially regarding calcium and phosphorus (LANDETE-CASTILLEJOS et al., 2019). Since the digestive system is unable to absorb the necessary amount of minerals in the relatively short period of time of antler growth, the necessary minerals cannot be fully provided via dietary uptake (HILLMAN et al., 1973; MUIR et al., 1987; BAXTER et al., 1999). For meeting this demand during antler growth, bone resorption therefore occurs in different locations of the postcranial skeleton (MEISTER, 1956; TAFT et al., 1956; BANKS et al., 1968; MUIR et al., 1987). Even in cases where the diet is sufficient in minerals, such demineralization of bones takes place (BANKS et al., 1968), which means that the resorption is genetically programmed (evolutionarily acquired) and is not an immediate reaction to an acute shortage. Most of the skeletal minerals transferred to an antler originates from the ribs and sternum, rather than from the long bones (COWAN et al., 1968). After the antler growth is stopped (BANKS et al., 1968), or even before completion of this process (BAXTER et al., 1999),

new bone refills the resorption spaces caused by mineral mobilization process. The seasonal change between bone resorption and remodeling in the postcranial skeleton that is associated with the antler cycle has been termed “cyclic physiological osteoporosis” (BANKS et al., 1968), “cyclic bone remodeling” (HILLMAN et al., 1973) or “reversible osteoporosis” (BAXTER et al., 1999).

BROCKSTEDT-RASMUSSEN et al. (1987) examined metacarpal bones and antlers of Danish roe bucks (*Capreolus capreolus*) to determine the relationship between their porosity during the antler cycle. They investigated porosity at two different antler locations (immediately above the coronet and 5 cm above the coronet), and the porosity of metacarpal bones. Porosity of antlers immediately above the coronet varied between 16.2% (in March) and 3.5% (in November). The earliest antlers they studied were still in velvet. Early in the antler cycle, the porosity of the antlers was high (from March to April), and the highest values were observed in antlers still in velvet. Antler porosity decreased from May to October, and the lowest values were found late in the antler cycle (November). The porosity of antlers 5 cm above the coronet varied from 15.2% to 3.3%. The porosity of the metacarpal bones varied from 2.1% to 6.1% and showed a significant increase when analyzed in relation to the months of the year. The minimum levels of porosity (2.4% and 2.6%) were found in deer who had cast their antlers (December). From February to November, porosity increased (from 2.1% to 6.1%), with peak values in November just before antler casting. The highest porosity of antlers occurred together with the lowest porosity of the bones, and the lowest porosity of antlers occurred together with the highest porosity of the bones.

The porosity of the metacarpal bones continuously increased from February to November, indicating that calcium is mobilized through rapid remodeling. The porosity of the bones returns rapidly to its original level after antler casting, because formation in the cortical remodeling is compensated (BROCKSTEDT-RASMUSSEN et al., 1987). According to these findings, the authors interpret that hard antlers are living structures, stating that they do not die after velvet shedding and that bone formation continues within an antler until it is cast.

2.5. Bone cells

Bone contains different types of cells: osteoprogenitor cells, osteoblasts, bone-lining cells, osteocytes and osteoclasts. Osteoprogenitor cells develop from mesenchymal stem cells. They are flattened, pale cells with an oval nucleus present in the endosteum and periosteum. Osteoprogenitor cells are mitotically active and differentiate into osteoblasts (LIEBICH, 2019). Osteoblasts produce the organic components of the bone matrix (type I collagen fibers, non-collagenous proteins, proteoglycans, glycosaminoglycans, glycoproteins), and also deposit the bone inorganic components (MESCHER, 2018; LIEBICH, 2019). They regulate the process of mineralization (the nucleation and subsequent growth of hydroxyapatite crystals from calcium and phosphate between the collagen fibrils in the bone matrix). Non-collagenous proteins, such as osteocalcin, osteonectin and osteopontin, regulate the process of mineralization. Furthermore, osteoblasts modulate osteoclast function by releasing neutral proteases and collagenases in preparation for resorption. The regulatory function of osteoblasts is influenced by parathyroid hormone, calcitonin, steroid hormones and numerous cytokines (IL-1, IL-6, TNF-α, TNF-β, BDGF [bone-derived growth factor] and EGF [epidermal growth factor]) (LIEBICH, 2019).

Active osteoblasts are located at the surfaces of bone matrix, typically forming a single layer of cuboidal cells (an epithelium-like sheet) (MESCHER, 2018; LIEBICH, 2019). They are basophilic, with round nucleus, and have numerous cell processes extending from the osteoid-facing surface of the cell that serves for contact (LIEBICH, 2019). Osteoblasts are polarized cells during the processes of matrix synthesis and mineralization. Matrix components are secreted that are in contact with existing bone matrix (MESCHER, 2018). This layer of irregularly arranged collagen fibers and ground substance forms the organic, unmineralized bone matrix (osteoid), which is placed between the osteoblast layer and the preexisting mineralized bone (MESCHER, 2018; LIEBICH, 2019). Approximately, osteoblasts produce 1 μm of unmineralized osteoid per day, up to an average total thickness of 6 μm. Within 3 to 4 days (initial rapid mineralization), bone reaches 70% of its final mineral content, while the final 30% are added over a period of 6 weeks (later phase of mineralization) (LIEBICH, 2019). When osteoblast activity stops, some of them will differentiate in osteocytes that become entrapped within the mineralized matrix. Some of osteoblasts will elongate, flatten and cover the matrix surface as bone lining cells, and the majority will undergo apoptosis (MESCHER, 2018). Bone lining cells are also called inactive or

resting osteoblasts, which are in direct contact with peripheral osteocytes via bone canals (*canaliculi ossei*) (LIEBICH, 2019). Canaliculi extend throughout the entire bone, with osteocyte processes inside them interlinking the osteocyte–osteoblast network. The fluid within the canaliculi produces hydrodynamic pressure, which has an important functional role.

Osteoclasts are derived from pluripotent hemopoietic stem cells of the granulocyte-monocyte line. These are multinuclear giant cells with 10 to 20, or even up to 100, nuclei per cell (LIEBICH, 2019). Active osteoclasts lie directly on the surface of bone tissue within etched cavities – resorption lacunae (Howship's lacunae) that they form by secreting acids for mineral resorption and lytic enzyme for matrix degradation (MESCHER, 2018; LIEBICH, 2019). Osteoclasts are structurally similar to chondroclasts and it has been proposed that these terms refer to the same cell type (LIEBICH, 2019).

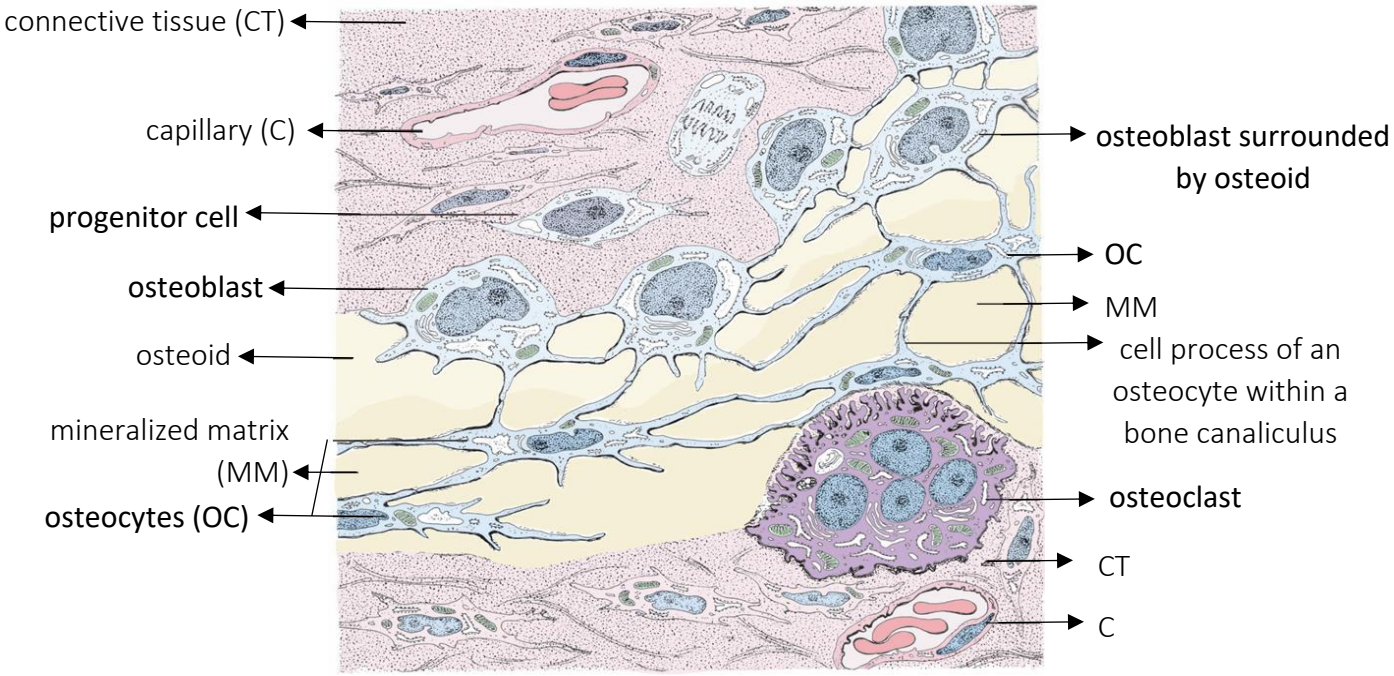

Figure 9. Bone cells and matrix (modified from LIEBICH, 2019).

2.5.1. Osteocytes

Osteocytes are mature bone cells that develop from osteoblasts (LIEBICH, 2019). The size of the cell decreases by up to 70% and the number of organelles diminishes in transition process from osteoblast to osteocyte. Osteocytes possess less rough endoplasmic reticulum, smaller Golgi

complexes, and more condensed nuclear chromatin than osteoblasts (MESCHER, 2018; LIEBICH, 2019). Osteocytes are flattened cells (with oval nucleus) located in lacunae and surrounded by mineralized bone matrix. Cells within the lacunas, which are partially or completely surrounded by matrix that has not yet mineralized, located close to the surface of the bone, between the osteoblast layer and the mineralized bone matrix are immature osteocytes. As the process of maturation advances, the osteocytes become incorporated into mineralized bone and surrounded by a mineralized matrix (mature osteocytes). They have numerous long, finger-like cytoplasmic processes extended into canals (*canaliculi ossei*) within the bone matrix, which establish a direct contact with nearby cells, mainly other osteocytes (LIEBICH, 2019). Osteocytes, situated in their lacunae, constitute approximately 90% of all bone cells (PARFITT, 1977).

Osteocytes have many functions, such as ion or nutrient transport via cytoplasmic processes, calcium uptake, regulation of osteoclastic activity, and mechanotransduction (YELLOWLEY et al., 2000). Furthermore, they participate in intercellular transport of low-molecular weight substances and waste products (LIEBICH, 2019). Besides communicating with each other, they are also in contact with nearby osteoblasts and bone lining cells. Osteocytes make connections with nearly all other bone cells via the lacunar-canalicular network, which allows them to be mechanosensors. They express different proteins (factors with paracrine and endocrine effects that help regulate bone remodeling) (MESCHER, 2018) and stimulate osteoblasts to undergo differentiation. Osteocytes are important components of bone even though their metabolic activity is reduced due to reduced nutrient diffusion and gas exchange when they are fully embedded in the matrix (LIEBICH, 2019). Osteocytes maintain the mineralized matrix that becomes resorbed rapidly when they degenerate and die (MESCHNER, 2018; LIEBICH, 2019).

The lifespan of osteocytes is variable, but unlike other bone cells, in certain circumstances they can survive for several decades (MANOLAGAS and PARFITT, 2010). When alive, osteocytes can maintain an unmineralized space around them by producing enzymes (digest their immediate surroundings) and inhibitors of crystallization and mineralization (MILOVANOVIC and BUSSE, 2020). However, if osteocytes die off, the lacunae will become occluded by mineral deposition, which represents passive (spontaneous) mineral deposition (BUSSE et al., 2010; MILOVANOVIC and BUSSE, 2020). However, dying osteocytes can release matrix vesicles as part of active lacunar mineralization (MILOVANOVIC et al., 2017; MILOVANOVIC and

BUSSE, 2020). The filling of lacunae and canaliculi with minerals is called micropetrosis (FROST, 1960a; BOYDE, 2003; BELL et al., 2008; MILOVANOVIC and BUSSE, 2020). The process involves the production of spherical bodies termed nanospherites, which represent mineralized apoptotic cell debris (BOYDE, 2003; BELL et al., 2008; MILOVANOVIC et al., 2017; MILOVANOVIC and BUSSE, 2020). The bone mineral deposited in the osteocyte lacunae during micropetrosis is a hydroxyapatite. Mineralized lacunae cause local dysfunction of the lacunocanalicular network of osteocytes (MILOVANOVIC et al., 2017) that block nutrient supply and fluid flow to other osteocytes, leading to cell death. Micropetrosis is thus associated with osteocyte apoptosis (BUSSE et al., 2010; MILOVANOVIC and BUSSE, 2020) and is evidence of osteocyte death (BOYDE, 2003). Mineralization of canaliculi may precede occlusion of osteocyte lacunae with mineral. Sometimes, the dying osteocyte "cell mummy" itself can become mineralized (BOYDE, 2003; BELL et al., 2008). The mineralization of chondrocyte lacunae is associated with the apoptosis of hypertrophic chondrocytes that has been observed to occur during antler growth (SZUWART et al., 1998). Such mineralized deposits have been observed in antler chondrocyte and osteocyte lacunae from different deer species (KIERDORF et al., 2022).

2.5.2. Cell death in bone

Cell death includes necrosis and programmed cell death (controlled form of cell death in response to various physiological or developmental signals) (KANDUC et al., 2002). One type of programmed cell death is apoptosis (ELMORE, 2007).

Necrosis is an uncontrolled form of cell death that is caused by irreversible external stimuli and occurs in response to injury, trauma, or infection (GOLSTEIN and KROEMER, 2007; CHEN et al., 2018). The cellular mechanisms that lead to necrosis involve different events that result in cell membrane rupture and the release of cell contents into the extracellular space (CHEN et al., 2018; KHALID and AZIMPOURAN, 2020). The content released by the dying cells can activate the immune system and damage neighboring cells. Because of that, necrosis is frequently associated with inflammation and damage to the surrounding tissues (BERGHE et al., 2014). Microscopically necrosis is recognizable by changes in the nucleus (swelling, pyknosis, karyorrhexis, karyolysis) and in the cytoplasm, which becomes eosinophilic. There are different terms for bone death, such as osteonecrosis, avascular necrosis, ischemic necrosis, subchondral

avascular necrosis, and aseptic necrosis of bone (MCCARTHY, 1982). It has long been accepted that empty osteocytic lacunae are histologic sign indicative of osteonecrosis. However, empty osteocytic lacunae can also be an artefact due to the suboptimal tissue fixation. In addition, according to studies conducted on human material and experimental bone infarction in animals, osteocyte loss is not complete until two to four weeks after the beginning of ischemia (BONFIGLIO, 1954; CATTO, 1965; YOUNG, 1966). Patchily distributed empty lacunae are occasionally present in the cortical bone in the interstitial lamellae between osteons. With age, their number increases because of diminished blood supply. In severe ischemic events, there is a complete loss of osteocytes (FROST, 1960b). In the marrow spaces, earliest microscopic signs indicative of bone ischemia are present from day two after cessation of blood supply onward (CATTO, 1976). Osteocyte lacunae are empty after 15 days, while are absent on the trabecular surface cells. The necrotic zone is bordered by a zone showing proliferation of capillaries accompanied by fibroblasts and histiocytes. Osteoclasts partly removed dead bone, which becomes replaced with newly-formed trabeculae or, alternatively, woven bone is laid down on the surface of dead trabeculae (PHEMISTER, 1915, 1930).

Apoptosis is a form of individual cell death in which cells undergo controlled self-destruction (genetically regulated) (KERR et al., 1972; CHEN et al., 2018). This is an important regulatory mechanism that controls cell numbers during embryonic development, allows removal of excess tissue (soft tissue between developing fingers) and is responsible for some of the cell loss from regenerating epithelial surfaces in adult tissues (skin, alimentary tract) (BOYCE et al., 2002). It is characterized by morphological changes in nuclear chromatin and cytoplasm (KERR et al., 1972; WYLLIE et al., 1980; ELMORE, 2007). Certain changes are visible within the apoptotic cells: they contract, lose attachment to nearby cells and break up into fragments (apoptotic bodies) which are phagocytosed by surrounding cells. The most remarkable changes are visible in the nucleus, starting with chromatin clumping into dense aggregates around the nuclear membrane. After that, chromatin condensation, disintegration of the nucleus, and the formation of numerous aggregates of condensed chromatin within the cytoplasm occur. This is accompanied by cell shrinkage due to fluid movement out of the cell and loss of contact with the neighboring cells or matrix. As apoptosis progresses, numerous cell surface convolutions are formed, and a cell disintegrates into multiple membrane-bound, condensed apoptotic bodies (KERR et al., 1972; BOYCE et al., 2002; ELMORE, 2007; CHEN et al., 2018). The apoptotic bodies are phagocytosed

by neighboring cells (BOYCE et al., 2002; ELMORE, 2007; CHEN et al., 2018). In some cells, apoptosis can last from few minutes to several hours, while in others DNA fragmentation can begin 2 days before cellular disintegration (POMPEIANO et al., 1998).

Apoptosis activation runs through two main pathways, extrinsic and intrinsic (BOYCE et al., 2002; GHOBRIAL et al., 2005). Both are activated by proteolytic enzymes (caspases) (BOYCE et al., 2002).

The extrinsic pathway is activated by extracellular ligands that binds to death receptors on the cell surface (LOCKSLEY et al., 2001; WAJANT, 2002) after which death-inducing signaling complexes are formed. They activate initiator caspases (ASHKENAZI, 2002), which cleave and activate effector caspases leading to the degradation of intracellular components and the induction of apoptosis (RIEDL and SHI, 2004).

The intrinsic pathway is activated by intracellular stressors (DNA damage, oxidative stress, and loss of survival signaling), which lead to permeabilization of the outer mitochondrial membrane (REDZA-DUTORDOIR and AVERILL-BATES, 2016). This pathway is regulated by anti- and pro-apoptotic proteins (CZABOTAR et al., 2014). Activation of proapoptotic proteins inhibits antiapoptotic proteins. Proapoptotic proteins lead to the formation of mitochondrial pores, releasing of cytochrome c into the cytoplasm (KLUCK et al., 1997), and formation of apoptosomes. They contain apoptotic protease activating factor-1 and activates caspases (OW et al., 2008).

Early during apoptosis, caspase-activated DNases are activated (NAGATA, 2000) which split genomic DNA at nucleosomes into fragments of varying sizes, giving rise to characteristic “ladders” that are seen on gel electrophoresis (WYLLIE et al., 1980; ARENDS et al., 1990; KAUFMANN et al., 2000). Fragmentation and condensation of the nucleus can be visualized using acridine orange, Hoechst dyes, and propidium iodide by their bright fluorescence upon binding to DNA (ARNDT-JOVIN and JOVIN, 1977; ARENDS et al., 1990). A useful tool for studying apoptosis in cells co-transfected with genes of interest are cells transfected with green fluorescent protein containing a nuclear localization sequence (BELLIDO et al., 2000; KOUSTENI et al., 2001). Degraded DNA can be detected enzymatically and quantified (STADELMANN and LASSMANN, 2000) using TUNEL (TdT-mediated dUTP-biotin nick end labelling) (GAVRIELI et al., 1992), ISNT (in situ nick translation) (GOLD et al., 1993) and ISEL methods (in situ nick

end labelling) (ANSARI et al., 1993; WIJSMAN et al., 1993). ISEL is 10 times more sensitive than TUNEL and can even detect cells undergoing DNA repair (can be less specific) (GOLD et al., 1994). These DNA labelling methods can also identify cells undergoing necrosis (GRASL-KRAUPP et al., 1995).

There is a difference between apoptosis and ischemic necrosis. Apoptosis affects single cells, apoptotic cells and their nuclei do not swell, and their destruction does not attract inflammatory cells. Ischemic necrosis affects group of cells, their nuclei swell, and their destruction attract inflammatory cells (Fig. 10) (BOYCE et al., 2002).

Programmed cell death detection methods include few different groups: **membrane permeability/damage detection methods** (annexin V binding assay, lactate dehydrogenase assay, electrochemical methods); **mitochondrial damage/alteration detection methods** (MTT and XTT assay, mitochondrial membrane potential detection, mitochondrial activity of streptolysin O permeabilized cells assay, cytochrome c release detection); **caspase activity detection methods** (ELISA, fluorometric and colorimetric assays, immunohistochemical methods, laser and mass spectroscopic methods); **p53 activity detection methods** (FASAY, p53 protein analysis methods); **DNA fragmentation/denaturation/condensation detection methods** (APO ssDNA assay, TUNEL assay, ISEL, ELISA, gel electrophoresis-based methods, DNA-specific fluorochrome based methods) (KARI et al., 2022).

The **Annexin V binding assay** detects apoptosis while the cell membrane is partially intact in comparation to the other impermeable dyes which fail to detect onset of apoptosis and indicates the loss of cell viability (VERMES et al., 2000). This assay demonstrates a false-positive result and is therefore less reliable, making the use of additional staining mandatory (SARASTE and PULKKI, 2000). In the **lactate dehydrogenase assay**, released LDH in the extracellular space is a biomarker of cell membrane damage, which indicates apoptosis or necrosis (the release of LDH occurs at the early stage of necrosis but at a late stage of apoptosis). However, LDH is a good parameter to measure the percentage of damaged cells in the sample. This method can detect low-level damage to the cell membrane, which cannot be detected by other methods (PARHAMIFAR et al., 2019). **Electrochemical methods** are unable to measure apoptosis on a single-cell level or give cell-specific information in a large cell population (MARTINEZ et al., 2010). M30 (**caspase** cleaved CK18) is a specific antibody which appears at the early stage of apoptosis. It is a reliable

indicator of apoptosis because it does not react with intact or necrotic cells. Immunological staining with M30 antibody has shown correlation with other apoptosis assays like TUNEL and ISEL (CUMMINGS et al., 2008). A quantitative method that allows the counting of apoptotic bodies is the immunohistochemical detection of caspase activity. The problem with this method is that pre-apoptotic cells are very difficult to detect (ECKLE et al., 2004). For tissues or cell cultures with a high density of apoptotic cells, DNA ladder assay is a suitable method (WATANABE et al., 2002). TUNEL assay is the most popular and more sensitive (in comparation with ISEL) method for detecting fragmented DNA. It can be used to identify the onset of apoptosis because it detects DNA breaks that occur at an early stage of apoptosis, which cannot be detected morphologically (ARCHANA et al., 2013). It also detects necrotic cells and can thereby provide false-positive results of apoptosis. The TUNEL assay sometimes identifies cells in the process of DNA replication and active gene transcription providing false-positive results (KOCKX et al., 1998). The ISEL technique (a modified form of TUNEL assay) identifies apoptotic cells and labelled cells prior to DNA fragmentation (ASSAD et al., 1997). A method with higher sensitivity than the TUNEL assay and the DNA ladder assay is the comet assay (single-cell gel electrophoresis). It provides specific information about the degree and heterogeneity of DNA damage. This assay somewhat damages the cell membrane and changes the respective frequencies of live, necrotic and apoptotic cells (ARCHANA et al., 2013). DNA-specific fluorochromes (dyes like PI, DAPI, Trypan blue, Hoechst, and AO) are also used to detect apoptosis (NICOLETTI et al., 1991). These are accurate and quantitative methods in both viable and fixed single cells, but in intact tissues, enzymatic pre-treatment is required to release individual cells for analysis (ARCHANA et al., 2013).

APOPTOSIS		NECROSIS
controlled form of cell death		uncontrolled and pathological form of cell death
one cell	CELL	group of cells
cell shrinkage, chromatin condensation, membrane blebbing, nuclear fragmentation, and apoptotic body formation		cell swelling, membrane rupture, intracellular content release
phagocytosys		inflammation and tissue damage

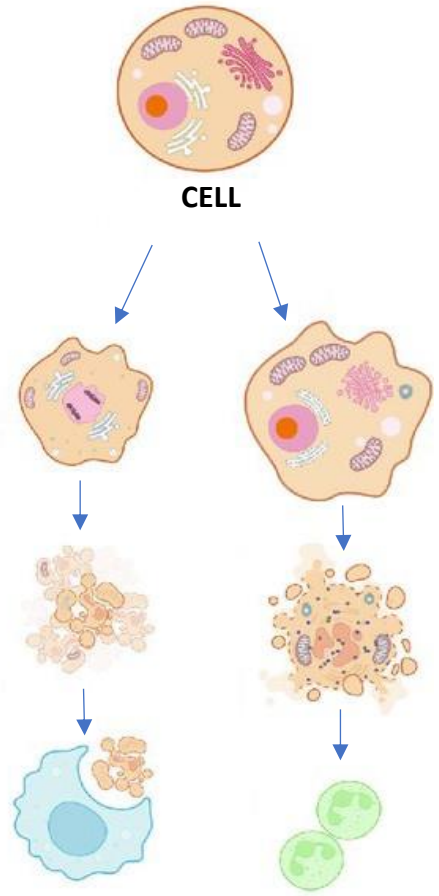

Figure 10. Morphological features of apoptosis and necrosis (modified from PARK et al., 2023).

2.6. TUNEL assay

The presence of multiple DNA strands breaks (DSBs) demonstrates DNA fragmentation, which is the gold standard for the identification of programmed cell death (HU et al., 2021). The TUNEL assay is used for detection of DSBs in situ by labelling them with fluorochromes. In different types of TUNEL assay, not only d-UTP, but a variety of deoxynucleotides, can be directly or indirectly tagged with fluorochromes. This method identifies and quantifies the apoptotic and necroptotic cells by fluorescence cytometry and microscopy (DARZYNKIEWICZ et al., 2008). Necroptosis represents a form of programmed cell death that shares characteristics of both apoptosis and necrosis (DHURIYA and SHARMA, 2018). In their study, KELLY et al. (2003)

observed apoptosis and necrosis through TUNEL assay where the cells were previously stained with propidium iodide to distinguish apoptotic and necrotic cells. TUNEL staining predominantly marked apoptotic cells, while necrotic cells showed no TUNEL signal. TUNEL assay showed 99% specificity and 64% sensitivity (35% of apoptotic cells were TUNEL negative).

COLITTI et al. (2005) conducted a study on red deer antlers sampled 25 to 50 days after the previous set had been cast (rapidly growing antlers). They identified sites of apoptosis in the growing antler tip using TUNEL. No TUNEL-positive cells were observed in the velvet epidermis and the dermis. TUNEL-positive cells were associated with some hair follicles, which can be the result of a continuous cycle of keratinocyte proliferation, differentiation, cell death, and quiescence that persists throughout the entire lifespan of the hair follicle (HARDY, 1992; PAUS et al., 1993; STENN and PAUS, 2001). In the fibrous perichondrium, the authors observed a significant number of TUNEL-positive cells and few proliferating cells. This suggests that expansion of a progenitor cell population in the perichondrium occurs at an early stage of regeneration. Furthermore, in the outer and inner mesenchyme, significant proportion of cells were TUNEL positive. The reason for that, according to GUO and HAY (1999), is that signaling between proliferation and cell death occurs. In this rapidly growing tissue, a high rate of apoptosis may be required to prevent neoplastic transformations (MEDH and THOMPSON, 2000). The apoptotic index was higher in non-mineralized than in mineralized cartilage. Apoptotic chondrocytes were often observed adjacent to cells that appeared morphologically normal or adjacent to empty lacunae. According to COLITTI et al. (2005), the apparently high level of apoptosis in cartilage is probably a consequence of the fact that antler cartilage is vascularized, and most chondrocytes maintain a close relationship with nearby vascular canals (BANKS and NEWBREY, 1983a). The TUNEL assay has been reported to produce false-positive results when applied to cartilage tissue (AIGNER et al., 2001). In the fibrous and cellular layers of the periosteum, a significant proportion of cells were TUNEL-positive (proliferation ratio was higher in the deeper cellular zone), significantly more than in the overlying skin. At sites of intramembranous bone formation, a proportion of osteocytes and osteoblasts were TUNEL positive, but no apoptotic osteoclasts were observed. COLITTI et al. (2005) provided evidence that apoptosis may play a significant role in the growth of regenerating antlers. Notably, the proportion of TUNEL-positive cells in the mesenchymal growth zone of regenerating antlers reaches up to 64%, a level higher than that reported in any

other adult tissue. This high rate of programmed cell death likely corresponds to the intense morphogenetic activity and tissue remodeling characteristic of antler regeneration.

2.7. Osteocyte survival

The osteocyte lifespan is determined by bone remodeling (osteoclasts resorb the bone and release osteocytes) (NIJWEIDE et al., 2002). Bone resorption is followed by a new bone formation, where up to half of these released osteocytes may become re-embedded (SUZUKI et al., 2000), but most of them will die by apoptosis and become phagocytosed (NIJWEIDE et al., 2002).

The survival period of osteocytes following a cessation of their blood supply is controversial. Some of the authors state that survival time after ischemia is longer than 48 hours (KENZORA et al., 1978), five days (BROWN and CRUESS, 1982) or even more (ABBOTT et al., 1947). The loss of osteocyte nuclei was rarely completed until the fourteenth day or even later in avascular necrosis of the femoral head after transcervical fractures (CATTO, 1965). Most of the osteocyte lacunae were empty or contained only pyknotic nuclei more than one week after infarction (YOUNG, 1966). The contours of osteocyte nuclei became rounder, and the chromatin mesh structures seemed more compact 12 hours after ending the blood supply. Other authors state that the period of survival is less than six hours (the period of reversible damage to osteocytes) (RÖSINGH and JAMES, 1969) or less than 12 hours (KUWATA et al., 1984). According to KENZORA et al. (1978), most osteocytes lost their viability within 12-24 hours of blood supply interruption. However, some of the osteocyte lacunae contained cellular elements and appeared normal or nearly normal for periods as long as 16 weeks after the induction of ischemia.

JAMES and STEIJN-MYAGKAYA (1986) showed different morphological changes in osteocytes from rabbit bone after being exposed to ischemia for different durations (15 minutes, one hour, two hours, four hours, 24 hours). Using electron microscopy in the control specimens, it was demonstrated that the largest part of the cell is occupied by the oval nucleus that is surrounded with narrow rim of cytoplasm. The nucleus contains fine granular chromatin, which is in a cape-like shape on the inner side of the nuclear envelope. Visible cell organelles are (poly)ribosomes

(majority were of the free type), rough endoplasmic reticulum, Golgi complex, mitochondria, and lysosomes.

After 15 minutes of ischemia, no changes were visible. In addition, there was no difference in changes between the samples that were exposed to ischemia for one or two hours. In both of these samples differences from the control specimen are visible. Osteocytes had irregular cellular surface, free ribosomes showed tendency for aggregation, perinuclear cisternae were enlarged, and condensations of chromatin against the nuclear envelope in the nucleus was enlarged (JAMES and STEIJN-MYAGKAYA, 1986).

Four hours after the onset of ischemia, the osteocytes occupied a smaller area of the lacuna. In the osteocyte's plasma membrane, local interruptions were present, and in places the plasma membrane was completely missing. Release of cytoplasmic contents and vesiculation of cytoplasmic matrix was present locally. Chromatin condensation into large aggregates and focal dilatations of the perinuclear cisternae were present in the nucleus. Mitochondria showed disorganization of the cristae, lack of matrix homogeneity, and sometimes membranous whorls in the inner compartment. Rough endoplasmic reticulum cisternae were swollen (inconspicuous in physiological osteocytes, or after one or two hours of ischemia). Irregularities of lacunar wall and protrusions into the lumen were present (JAMES and STEIJN-MYAGKAYA, 1986).

All lacunae were empty or contained only unidentifiable necrotic remnants of osteocytes 24 hours after onset of ischemia (mostly attached to the lacunar wall) (JAMES and STEIJN-MYAGKAYA, 1986).

Under the light microscope, two hours after the onset of ischemia osteocytes showed a denser nucleus with pyknotic appearance than in control specimens. After 24 hours after onset of ischemia, as seen with the electron microscope, all lacunae were empty with no trace of blood vessels in the Haversian canals (JAMES and STEIJN-MYAGKAYA, 1986).

USUI et al. (1989) analyzed changes observed in osteocytes under ischemic conditions in rabbit's femoral condyle (after 12 hours, two days, five days, eight days, 14 days).

By transmission electron microscopy, a physiological osteocyte with a large nucleus and a small amount of cytoplasm is visible in the lacuna. The cytoplasm of the control osteocytes contains several mitochondria and small amounts of endoplasmic reticulum. Around the osteocyte

is a narrow pericellular sheath which contains some flocculent material. Nuclear and cytoplasmic membranes are without interruptions. The inner rim of the nuclear membrane contains densely arranged chromatin granules, whereas the central region of the nucleus shows a sparse distribution (USUI et al., 1989).

After 12 hours of ischemia the osteocyte lacunar wall is preserved with a distinct lamina limitans, while the cytoplasm has become sparse with enlarged vacuoles. The cytoplasmic membrane is not clearly defined, and osteocyte processes are not visible in the canaliculi. The nuclear membrane is partially interrupted. Chromatin granules are more condensed and darker (indicative of the beginning of pyknosis). Sheath a flocculent material is visible in the pericellular. Thus, the osteocytes already show signs of pyknosis, but might still be diagnosed as normal under the light microscope (USUI et al., 1989).

On the second and fifth days of ischemia, the cytoplasmic and the nuclear membranes of the osteocyte have mostly disappeared. Vacuolar changes are visible in the cytoplasm, but also in the flocculent material. Throughout the osteocyte lacunae, numerous small vacuoles and degenerated intercellular organelles are present. After two days of ischemia, densely packed chromatin granules make the nuclear margin irregular. The nucleus becomes compact. These changes indicate osteocyte pyknosis. Five days after ischemia, the osteocyte nucleus is still round in shape but with a reduced density, and this osteocyte is in the transitional phase from pyknotic to pale (USUI et al., 1989).

Eight days after the onset of ischemia, indistinct osteocyte shape consists of degenerated cytoplasm and nucleus fragments. Membrane structures are not present, and the nucleus is not pyknotic. Described osteocyte is identical to a pale osteocyte (USUI et al., 1989).

After 14 days of ischemia, the osteocyte nucleus and cytoplasm have disappeared. Cell remnants remain in the osteocyte lacuna. Based on light microscopy, the lacuna is diagnosed as empty (USUI et al., 1989).

In the control specimens analyzed with a light microscope, more than half of the osteocyte lacunae contained physiological osteocytes (round or oval nucleus, smooth nuclear margins, inner rims of nucleus stained dark, while central parts were less stained). In comparison with ischemic specimens, the percentages of pale osteocytes and empty osteocyte lacunae were smaller. After 12

hours of ischemia, the percentage of physiological osteocytes decreased, while pyknotic osteocytes (rounded but compact-sized nuclei, nuclear margins relatively smooth, nuclei interior and periphery stained darker) increased. On the second day of ischemia, physiological osteocytes decreased significantly, while the percentages of pyknotic osteocytes, pale osteocytes (irregular and indistinct nuclei), and empty lacunae increased. On the fifth day of ischemia, the ratio of pale osteocytes reached a peak, and the number of empty lacunae increased. The frequency of empty lacunae reached more than 40% on the fourteenth day of ischemia (USUI et al., 1989).

Table 1. Classification of four types of osteocytes and lacunae under light microscopy (modified from USUI et al., 1989).

TYPE OF OSTEOCYTE	**NUCLEUS**		
	shape	**margin**	**stain**
NORMAL	round or oval	smooth	dark periphery, pale center
PYCNOTIC	round and compact	relatively smooth	dark
PALE	irregular and indistinct	irregular	pale
EMPTY LACUNA	only cell remnants left in lacuna or empty lacuna		

2.8. Live or dead hard antler bone

Most authors agree that, after velvet shedding, antlers are dead bones due to a disruption of their blood supply (WISLOCKI, 1942; BUBENIK, 1983; BUBENIK and BUBENIK, 1990; GOSS et al., 1992; GOSS, 1995). Nevertheless, there are authors who claim that antlers remain living bone even after the removal of velvet (BROCKSTEDT-RASMUSSEN et al., 1987; ROLF and ENDERLE, 1999; ROLF et al., 2001). BROCKSTEDT-RASMUSSEN et al. (1987) concluded that antlers do not die after velvet shedding and that continued bone formation within an antler goes on until they are cast. These authors said that it is more probable that antlers die immediately before they are cast, since the porosity approaches such minute values at the end of antler cycle that it seems unlikely that sufficient blood circulation can be sustained in antlers to maintain their requirements. According to them, the fact that they are living also explains how hard antlers can adhere to pedicle for several months without being cast.

ROLF and ENDERLE (1999) studied fallow deer (*Dama dama* L.) hard antlers. Samples obtained from different areas of hard antlers were taken at the time of velvet shedding, in December (after an artificially induced antler casting) and in March (3–4 weeks before the regular antler casting).

After velvet shedding, the pedicles were very porous macroscopically. Numerous vessels leading centrally through the pedicle into the spongy core of an antler were reported to occur by ROLF and ENDERLE (1999). Microscopically, in the antler sections, a capillary system within the cortical layers and in areas resembling bone marrow within the spongiosa was present. According to these authors, the capillary system also leads directly to the antler outer border. Early stages of trabecular microcallus formation were reported to occur in the inner spongiosa (ROLF and ENDERLE, 1999).

In December, some blood was observed macroscopically flowing from the core of antlers. In antler sections of the main branch blood remnants were concentrated at the transitional zone. Antler base was an almost completely mineralized area. At the periphery of antler base near to the detachment zone, according to ROLF and ENDERLE (1999), there were four to eight (sometimes even more) vessels filled with blood. Microscopically, within the transitional zone, these authors reported osteoblast lines that were forming osteoid seams (in some areas composed of different layers). The structures identified by ROLF and ENDERLE (1999) as active osteoblasts were

reported to show basophilic cytoplasm and peripherally located nuclei with a pale perinuclear area indicating an active Golgi apparatus. They even reported to have found some cells in mitotic divisions (progenitors of osteoblasts). Antler spongiosa was reported to contain blood cells. Presence of Howship's lacunae with osteoclast-like cells, according to the authors, indicated a low degree of osteoclastic resorption. The cortical layers and trabeculae of the spongy bone were reported to contain living osteocytes with intact nuclei (ROLF and ENDERLE, 1999).

In March, i.e., relatively shortly before casting, antlers were reported to contain larger amounts of blood. Microscopically within the bone, the presence of high amounts of living osteocytes was reported. Occasionally those cells contained pyknotic nuclei (indicating a dying bone). Authors claim that there was substantial number of living cells, and some of them were osteoblasts. They reported bridging osteoid seams (development of new trabeculae) in the transitional zone and spongiosa cells. Active osteoblasts were mainly observed in the transition zone, while the majority of detected cells within the spongiosa were diagnosed as less active forms of osteoblasts (ROLF and ENDERLE, 1999).

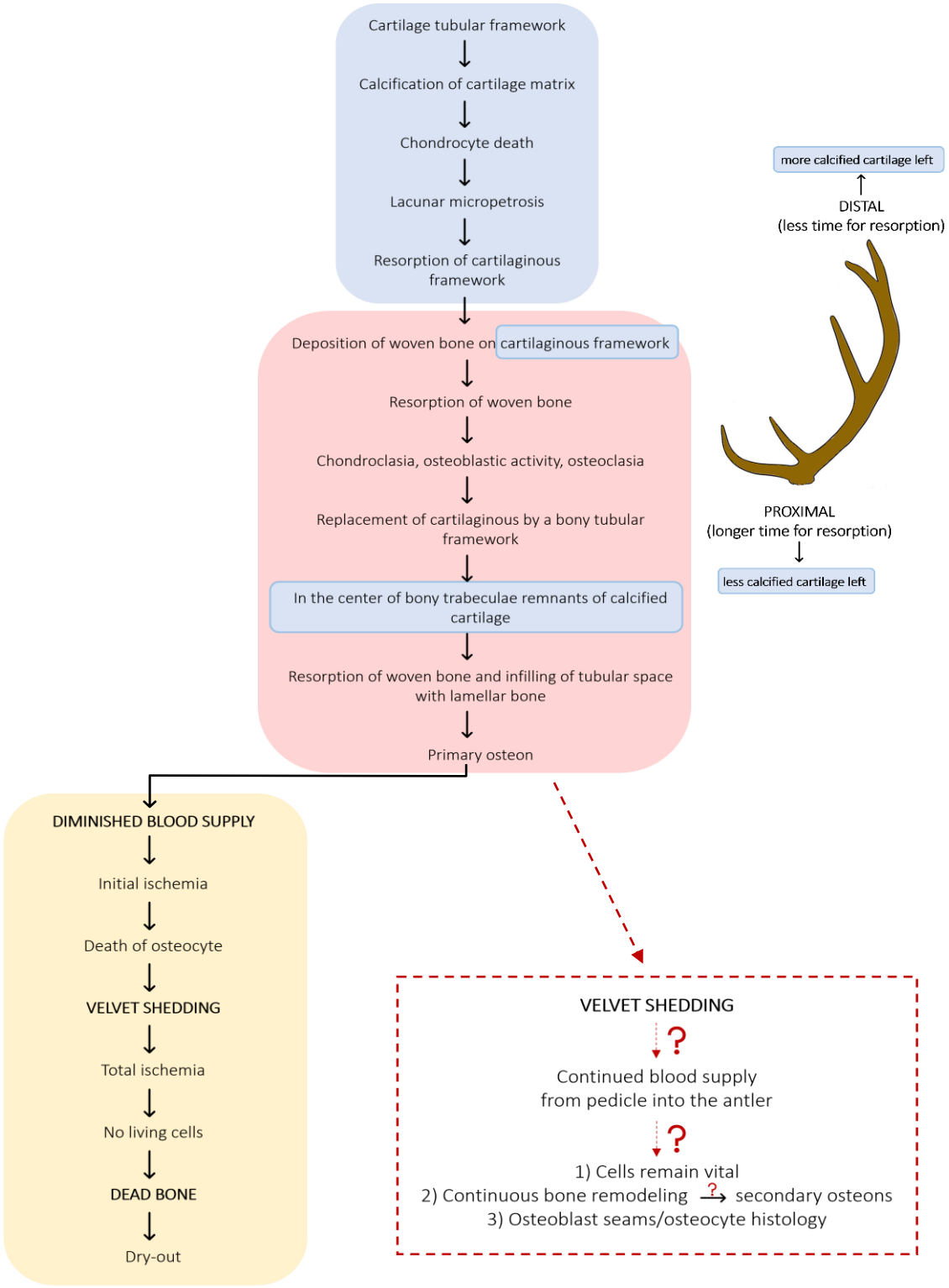

Figure 11. Schematic view of antler development; bottom left – after velvet shedding, the antler is dead bone; bottom right – the antler is living bone.

3. EXPLANATION OF RESEARCH TOPIC

Antlers are cranial bony appendages of cervids and the only mammalian organ capable of complete regeneration each year. They are growing from mesenchymal stem cells located in the antlerogenic periosteum and are initially formed out of cartilage that is subsequently replaced with bone. During the growth, antlers are covered with velvet. A debate about whether hard antlers are dead or living structures after velvet shedding and disruption of blood supply is still active. Understanding complex antler growth cycle and their composition is important for cervid biology and potentially also for different fields of human medicine, including regenerative medicine.

The hypothesis of this research is that hard antlers are a dead structure and that the remaining blood has no role in preserving osteocyte vitality.

To confirm or reject the hypothesis of this research, the following goals were set:

1) To determine the presence of blood in antlers monthly from before velvet shedding till casting.

2) To determine osteocyte vitality monthly from before velvet shedding till casting.

3) To determine intensity of lacunar micropetrosis monthly from before velvet shedding till casting.

4) To analyze the histological characteristics of antlers monthly from before velvet shedding till casting.

4. MATERIAL AND METHODS

4.1. Origin of samples

The materials and methods used in this dissertation were approved by the Faculty Council of the Faculty of Veterinary Medicine, University of Zagreb (Class: 640-01/21-02/07, Ref. No.: 251-61-01/139-21-40), on 16/06/2021 based on the approval of the Ethics Committee for Veterinary Medicine. The research design (non-probability sampling) of this study included sampling of mineralized antlers of two-year-old red deer (spikers). Animals originated from OG Letec farm in Bjelovar–Bilogora County, kept in outdoor enclosures, on pasture and with water available *ad libitum*. All animals on the farm are identified with ear tags, and precise data on the age of each individual is available (Fig. 12). Antlers were collected in two seasons of hard antlers (2021/2022, 2022/2023) monthly from final mineralization in velvet (end of August) to antler casting (end of April). Collected samples represent four different stages of the annual antler cycle: *antlers in velvet* (n = 2 antlers, i.e. 1 individual), *antlers at velvet shedding* (n = 2, i.e. 1 individual), *hard antlers* (n = 14, i.e. 7 individuals), *cast antlers* (n = 2, i.e. 1 individual) (Table 2, Fig. 13). A total of 10 male red deer (providing 20 antlers) participated in the study and remained in the herd after sampling of their antlers.

Figure 12. a) One of the enclosures of the red deer farm with a mixed red deer herd of stags and hinds; **b)** Red deer stag after cutting of hard antlers.

Table 2. List of collected antler samples.

Sampling number	Month of sampling	Sample ID	Stage of annual cycle of antler development
1.	August	Ba Bb	**Antlers in velvet**
2.	October	7a 7b	**Antlers at velvet shedding**
3.	October	2a 2b	**Hard antlers**
4.	November	3a 3b	**Hard antlers**
5.	December	8a 8b	**Hard antlers** (infested with larvae)
6.	December	4a 4b	**Hard antlers**
7.	January	9a 9b	**Hard antlers**
8.	February	10a 10b	**Hard antlers**
9.	March	11a 11b	**Hard antlers**
10.	April	12a 12b	**Cast antlers**

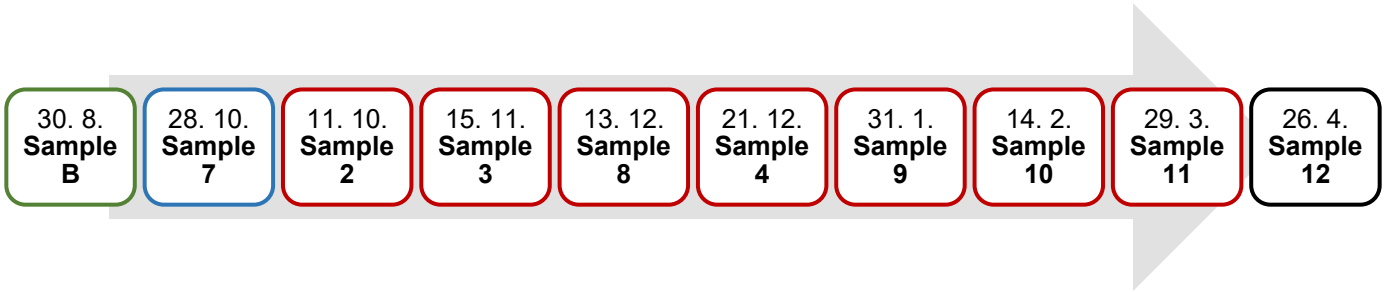

Figure 13. Timeline overview of the antler sampling. The samples were collected over two consecutive years. Sample 7 was collected in the second year of sampling, but at an earlier developmental stage than Sample 2.

4.2. Sampling

Antlers in velvet (Fig. 14a, 14d) were sampled in complete chemical immobilization caused by tiletamine-zolazepam and xylazine (1.2 mg/kg tiletamine + 1.2 mg/kg zolazepam and 2.3 mg/kg xylazine) in doses recommended for deer, according to body weight. Hard antlers (Fig. 14b, 14e) were removed with a fine-toothed saw in the crush system, approximately 5 cm above the pedicle-antler junction, a region that will represent coronet in the later sets of antlers. After delivery to the Faculty of Veterinary Medicine, the sampled pairs of antler beams (a and b) were measured in length, and divided into three equal segments (1 – proximal [part of an antler close to the head], 2 – middle, 3 – distal [top of an antler]) (Fig. 14c) by micromotor Ultimate 500 (NSK, Tokio, Japan) using a flex diamond separator, 45 mm (Flex Diamond Disc, Edenta, Switzerland). The incision site was cooled during cutting with tap water. Each segment was then cut longitudinally (N = 10) and transversely (N = 10). From 20 antlers and 3 segments each, a total of 1200 fragments were obtained. Out these, 600 were subjected to analysis in their mineralized form, while the remaining 600 were processed for demineralization. From each demineralized fragment, 20 histological slides were prepared, resulting in a total of 12,000 slides. Fragments (longitudinally and transversely sampled) for further demineralization were cut with micromotor Ultimate 500 (NSK, Tokio, Japan) using a flex diamond separator, 45 mm (Flex Diamond Disc, Edenta, Switzerland) with water cooling (Fig. 14d-14g) and put in 10% buffered formalin (pH 7.4). Fragments for further embedding in plastic (Biodur) and for staining of mineralized non-embedded antler samples were cut using a rotary saw with a water-cooled diamond-edged blade with a thickness of 0.7 mm (Mecatome T180 [Presi, Eybens, France]) and put in 10% buffered formalin (pH 7.4) or 70% ethanol. Non-fixed fragments for densitometry were cut in the same way (Fig. 14h).

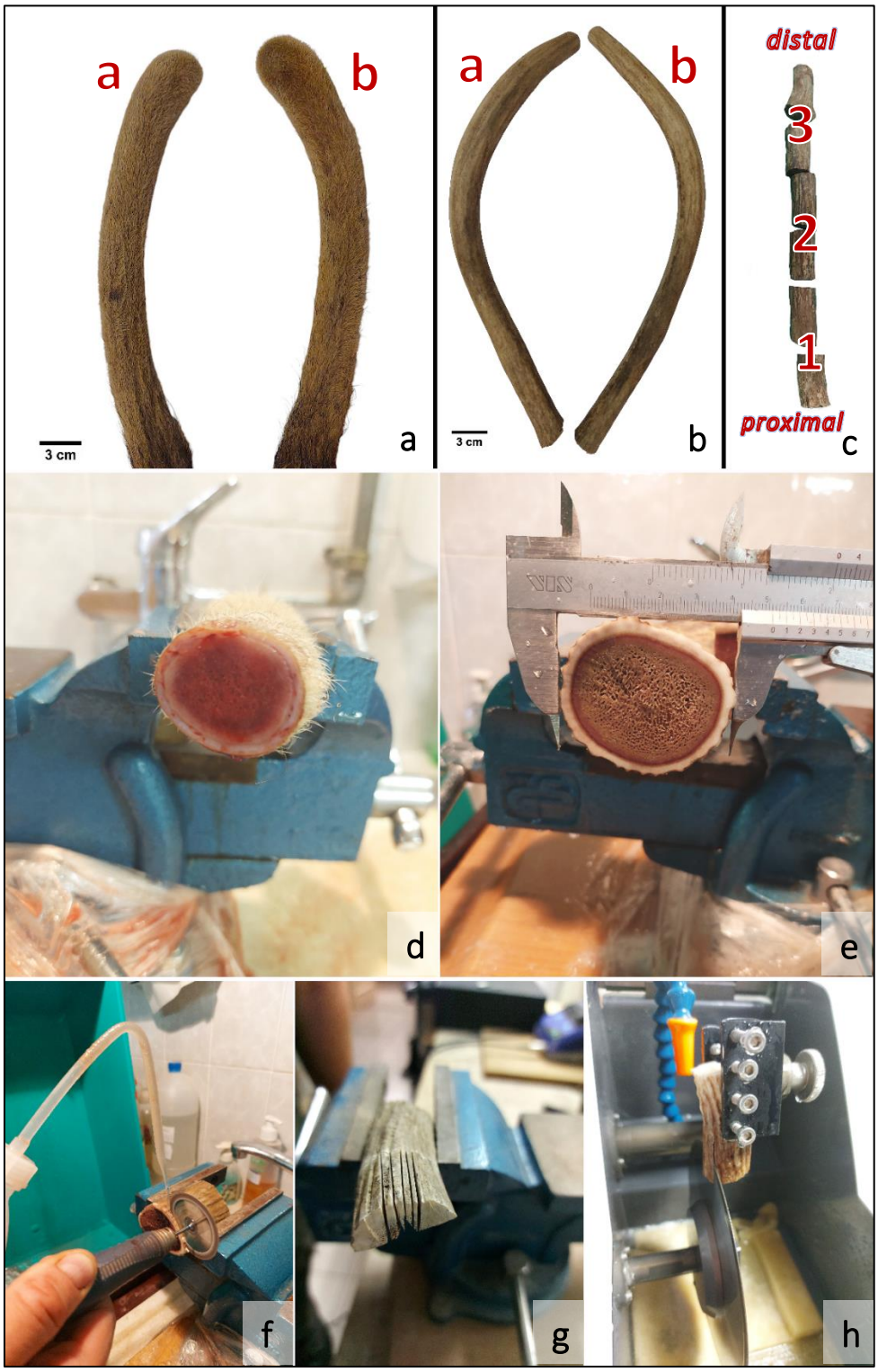

Figure 14. a) Sampled red deer (spiker) antler beams (a and b) in velvet; **b)** Sampled red deer (spiker) hard antler beams (a and b); **c)** Sampled antler beams divided into three equal segments (1 – proximal [part of the antler close to the head], 2 – middle, 3 – distal [top of the antler]); **d)** Transverse section of a segment of antler in the velvet; **e)** Transverse section of a segment of hard antler; **f)** Transversely sampled antler fragment cut with micromotor using a flex diamond

separator with water cooling; **g)** Longitudinally sampled antler fragments cut with micromotor using a flex diamond separator with water cooling; **h)** Fragment cut with rotary saw with a water-cooled diamond-edged blade.

4.3. Processing of mineralized antler samples

4.3.1. Non-embedded antler samples

4.3.1.1. Densitometry (DEXA – dual-energy x-ray absorptiometry)

Transverse antler fragments from each segment with a thickness of 1 cm (Fig. 15a) were analyzed using densitometry. This method was performed using the device HOLOGIC QDR 4500 W (Hologic, Inc., Bedford, USA) to test bone mineral density (BMD), which is a measurement of the amount of mineral matter (mostly calcium and phosphorus) per square centimeter of bones. The method used to obtain antler BMD involves comparing the DEXA values of antler specimens with those of phantoms (phantom values are used in the calibration of the device). A standardized imaging protocol for the lumbar spine segment was applied to three segments (proximal, middle, distal) of each antler, each representing a transversal section. A laser that did not cause damage to the samples was used to properly position the antler samples, and the radiation source was located below the samples (Fig. 15b). Densitometry was performed at the Dubrava University Hospital, Zagreb.

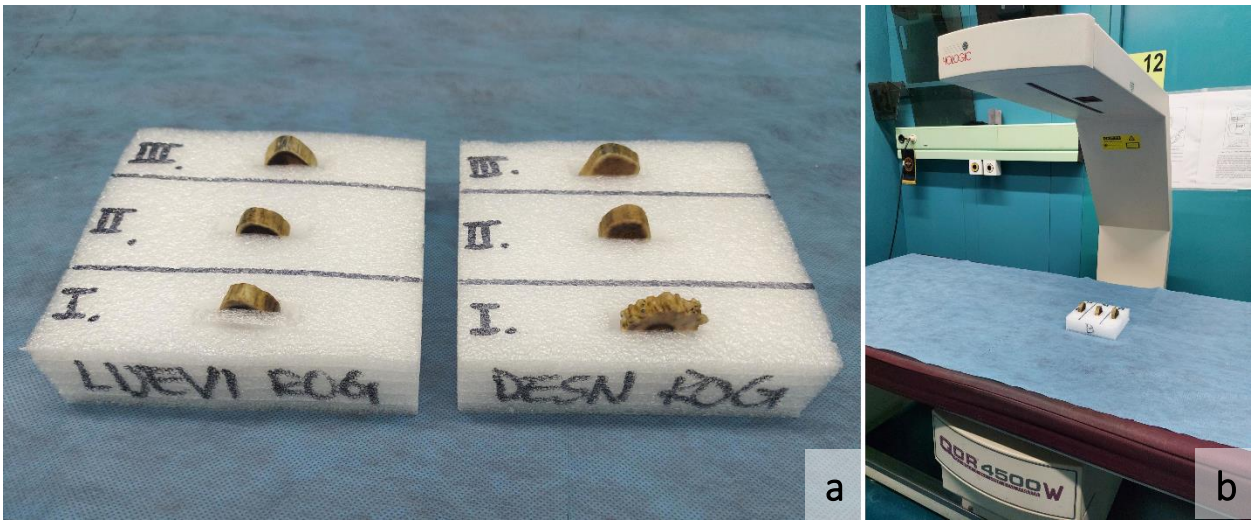

Figure 15. a) Transverse antler fragments from each segment; **b)** Device for testing bone mineral density.

4.3.1.2. Staining

4.3.1.2.1. Alcian Blue – Alizarin Red S

The Alcian Blue – Alizarin Red S method was used for distinguishing bone and cartilage tissue. Fragments of 100-120 µm in thickness were cut with a rotary saw with a water-cooled diamond-edged blade with a thickness of 0.7 mm (Mecatome T180 [Presi, Eybens, France]), then smoothed and polished by hand using whetstone (Naniwa, Osaka, Japan, grit 220 and 3000) to a thickness of 75-100 µm, and placed in 10% buffered formalin (pH 7.4). Non-embedded fragments were stained first with a mixture of solutions (10 mg Alcian Blue 8GX, 80 ml 95% ethanol, 20 ml glacial acetic acid) for 48 hours. After that, fragments were transferred in 2 changes of 95% ethanol for 2 to 3 hours each, then in 75%, 40%, 15% ethanol and distilled water for 2 to 3 hours each. Fragments were placed in 0.5% aqueous KOH solution with Alizarin Red S for 24 hours and then bleached with KOH-glycerin series (3:1, 1:1, 1:3) to pure glycerin by adding 3-4 drops of 3% hydrogen peroxide in 100 ml solution. This procedure removed the dark pigments from the tissue. At the end, fragments were stored in pure glycerin with the addition of thymol crystals (DINGERKUS and UHLER, 1977., modified). Samples were analyzed under the BRESSER Researcher ICD LED 20x-80x Stereo Microscope (Bresser, Rhede, Germany).

4.3.1.2.2. Villanueva´s tetrachrome bone staining

Villanueva´s tetrachrome bone staining was used for the visualization of different components of bone tissue. Fragments of 100-120 µm in thickness were cut with a rotary saw with a water-cooled diamond-edged blade of 0.7 mm thickness (Mecatome T180 [Presi, Eybens, France]), then smoothed and polished by hand using a whetstone (Naniwa, Osaka, Japan, grit 220 and 3000) to 75-100 µm thickness, and put in 70% ethanol. Non-embedded fragments were rehydrated by soaking in distilled water for an hour. Fragments were washed in 0.1% benzalkonium chloride in tap water for 1 minute and then rinsed in distilled water for 1 minute. Staining lasted for 15 hours with solution A (0.1 g Fast Green FCF, 2 g Orange G, 100 ml distilled water) that was adjusted to pH 6.5 with 3N acetic acid. Surface stains were removed by regrinding under tap water and sections were rinsed in distilled water. Followed by a counterstain with a mixture of 1 ml of solution B (solution B was prepared with 0.25 g Azure II, 100 ml 50% ethanol)

and 9 ml of solution C (solution C was prepared with 1 g basic fuchsin, 100 ml 50% ethanol) for 2 hours. Surface stains were removed by regrinding under tap water and sections were rinsed in distilled water. Fragments were washed in 0.1% benzalkonium chloride in tap water for 1 minute and then rinsed in distilled water for 1 minute. Differentiation was made with a solution of 0.01% acetic acid and 95% methanol for 5 minutes. Fragments were dehydrated in ascending concentrations of ethanol (96% for 9 min, 100% for 8 min) and purified in a solution of 100% ethanol and xylene (1:1 for 7 min, 1:3 for 6 min, 1:9 for 5 min) to pure xylene (4 min, 3 min). The fragments were placed on microscope slides (standard grade, VitroGnost), covered with Eukitt mounting medium and cover-slipped (SHEEHAN and HRAPCHAK, 1980). Antler sections were examined in a Digicyte DX50 (Digicyte digitalne tehnologije, Zagreb, Croatia) and scanned with NanoZoomer 2.0RS (Hammatsu, Japan).

4.3.2. Antler samples in plastic (Biodur®)

4.3.2.1. Embedding

Transverse antler fragments from each segment with a thickness of 2 cm were put in 70% ethanol. After fixation, fragments were transferred to dichloromethane for two days to replace the ethanol in the sample. The mixture for plastic embedding was prepared according to the manufacturer's instructions (BIODUR® E12 – standard epoxy resin in combination with standard amine hardener BIODUR® E1) (Biodur Products, Heidelberg, Germany). Standard epoxy resin (Biodur E12) had to be warmed to 70 °C and then stored at 30 °C before preparing the mixture. Fragments were put in plastic or paper cups coated with Vaseline and covered with the resin mixture. Cups were placed into a desiccator connected to the vacuum pump (Fig. 16a). Dichloromethane was evaporated from the fragments under low pressure and empty spaces in the fragments were filled with plastic. With the pressure regulator, the pressure inside the desiccator was moderately lowered up to 15 Pa (until bubbles were no longer visible) (Fig. 16b). After squeezing out all the bubbles from the fragments, the pressure regulator was slowly released and the desiccator vented. The samples were put in a thermostat (BTES, TMA Bodalec & Havoić, Dugo Selo, Croatia) to harden for 24 hours, and after that plastic or paper cups were removed from the Biodur (Fig. 16c). The excess plastic was cut with a rotary saw with a water-cooled diamond-

edged blade with a thickness of 0.4 mm (Dr. Steeg & Reuter, Bad Homburg, Germany), so at the end plastic got a cube-shape (Fig. 16d-16f).

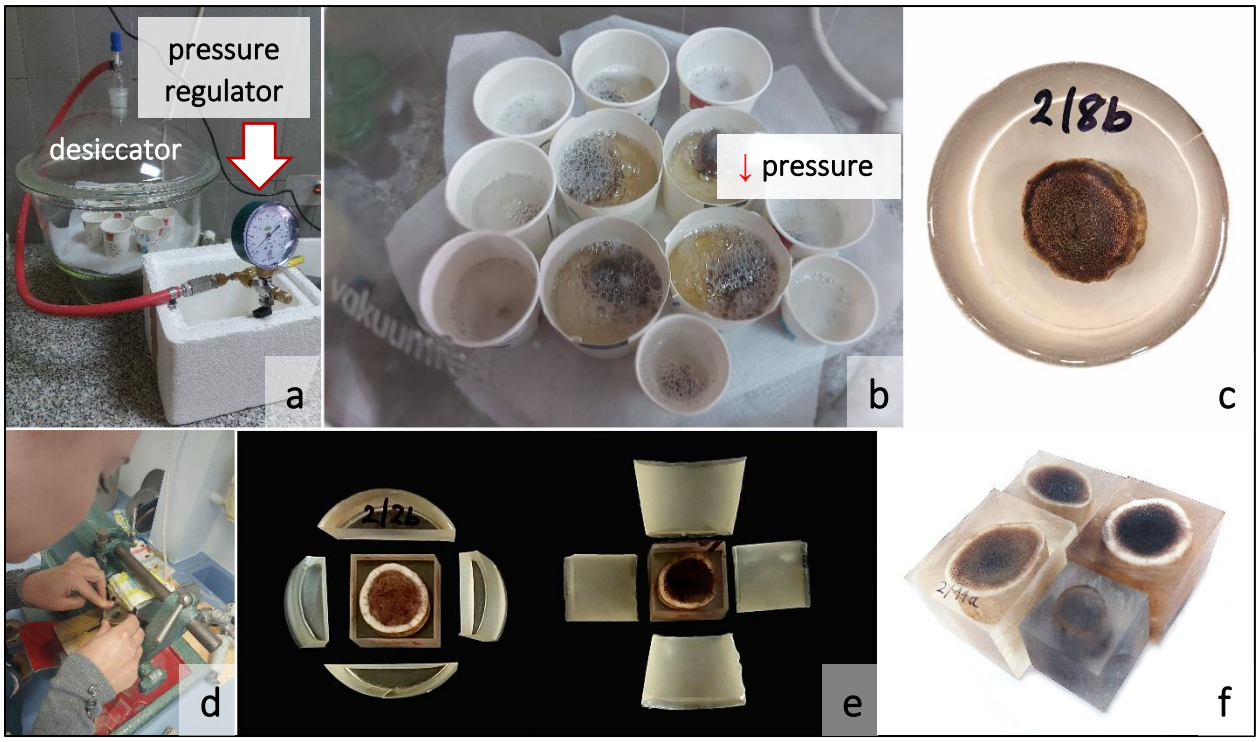

Figure 16. a) Closed vacuum system with desiccator and pressure regulator; **b)** Bubbles in the plastic visible due to pressure drop; **c)** Fragment of antler segment in the hardened plastic; **d)** Cutting the excess plastic; **(e, f)** Cube-shape finished antler samples in the plastic ready for further analysis.

4.3.2.2. Preparation for backscattered electron imaging in the electron microscope (SEM BSE)

A small section of the fragment (thickness ~ 0.5 cm) embedded in the plastic was cut with a rotary saw with a water-cooled diamond-edged blade with a thickness of 0.4 mm (Woko 50; Conrad Apparatebau, Clausthal-Zellerfeld, Germany). For backscattered electron (BSE) imaging of block surfaces of antlers, the cut surfaces of the plastic-embedded antler fragments were smoothed and polished by hand using a series of silicon carbide papers (grit 600, 1200, 2000, 3000) (Starcke GmbH & Co. KG, Melle, Germany) (Fig. 17a), followed by a final polishing step on a motorized polisher (Labopol 5, Struers, Ballerup, Denmark) using first a diamond suspension

of 3 μm particle size (DiaPro Dac 3, Struers, Ballerup, Denmark) and subsequently an alumina slurry of 0.3 μm particle size (AP-D Powder, Ballerup, Denmark). The direction of polishing was changed by 90 degrees after each transition to the next gradation of sandpaper or polishing solutions. The polishing of each step was carried out until the scratches from the previous step were no longer visible. During polishing, specimens were checked for scratches by microscope Zeiss 475052 – 9901 (Zeiss, Oberkochen, Germany) connected to fiber optic light source EK – 1 (Euromex, Duiven, The Netherlands) (Fig. 17b). For cleaning, after polishing with alumina slurry, plastic-embedded fragments were put in an ultrasonic cleaner (B200, Branson, Danbury, Connecticut, U.S.) filled with distilled water (Fig. 17c) on the automatic program for two to four minutes. After that, the plastic-embedded fragments were further cleaned in steps by alternately immersing in isopropanol and distilled water and again put in the ultrasonic cleaner. At the end, the polished surface of the plastic-embedded antler fragments was ready for further analysis (Fig. 17d). A self-adhesive copper foil was then attached around the edges of the specimen (Fig. 17e). The uncoated samples were studied (at 20 keV accelerating voltage) in low-vacuum mode in a scanning electron microscope (SEM, Evo Ma 15, Zeiss, Oberkochen, Germany), equipped with a high-definition thin five segment backscatter electron detector, with the polished surface oriented perpendicular to the primary electron beam.

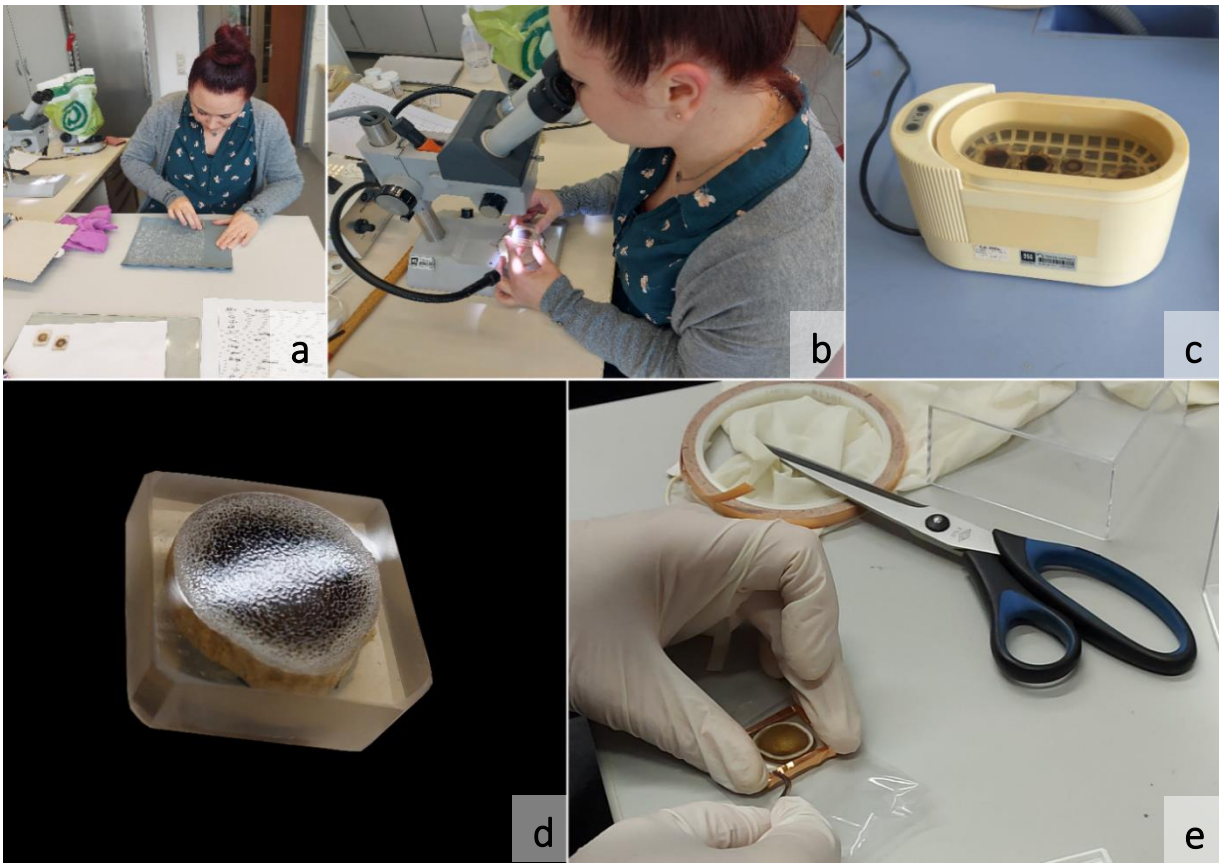

Figure 17. a) Cut surfaces of plastic-embedded antler fragment smoothed and polished by hand using a series of silicon carbide papers; **b)** Specimens were checked for scratches during polishing; **c)** Samples in the ultrasonic cleaner for removing adherent particles from the polishing process; **d)** Polished surface of plastic-embedded antler fragment; **e)** Copper foil attached to the edge of the plastic.

4.3.2.3. Preparation of the ground sections for light microscopy

The plastic-embedded antler bone fragments were smoothed, polished, and cleaned as previously described (method for SEM BSE). Samples were mounted with their polished sides down on glass slides, using the epoxy resin (Biodur) as glue, and dried in a thermostat (Memmert UN 30, Germany) for 48 hours. The mounted samples were then attached to the holder by vacuum and sectioned to a thickness of about 500 µm using a rotary saw with a water-cooled diamond-edged blade with a thickness of 0.4 mm (Woko 50; Conrad Apparatebau, Clausthal-Zellerfeld, Germany) (Fig. 18a), and subsequently ground and made plane-parallel (with a cup wheel) to approximately 200 µm (Fig. 18b) and finally polished to a thickness from 30 to 70 µm by hand using a series of silicon carbide papers (from grit 600 up to grit 3000) (Starcke GmbH & Co. KG, Melle, Germany) followed by a final polishing step using a deer leather cloth and a polishing compound (Menzerna, Ötigheim, Germany) (Fig. 18c). The direction of polishing was changed by 90 degrees after each transition to the next gradation of sandpaper or the deer leather cloth. The polishing of each step was carried out until the scratches from the previous step were no longer visible. The thickness of the glass and glass/plastic/antler fragment was checked with a micrometer screw (Fig. 18d). Ground sections (Fig. 18e) were examined in a Zeiss Axio–Imager M2 (Zeiss, Oberkochen, Germany) in normal transmitted light (bright field microscopy), in normal transmitted light with phase contrast (PHACO), in circularly polarized light (CPL), in circularly polarized light and 1λ-plate (CPL+1 λ), and with a Keyence digital microscope VHX 7000 (Keyence, Osaka, Japan).

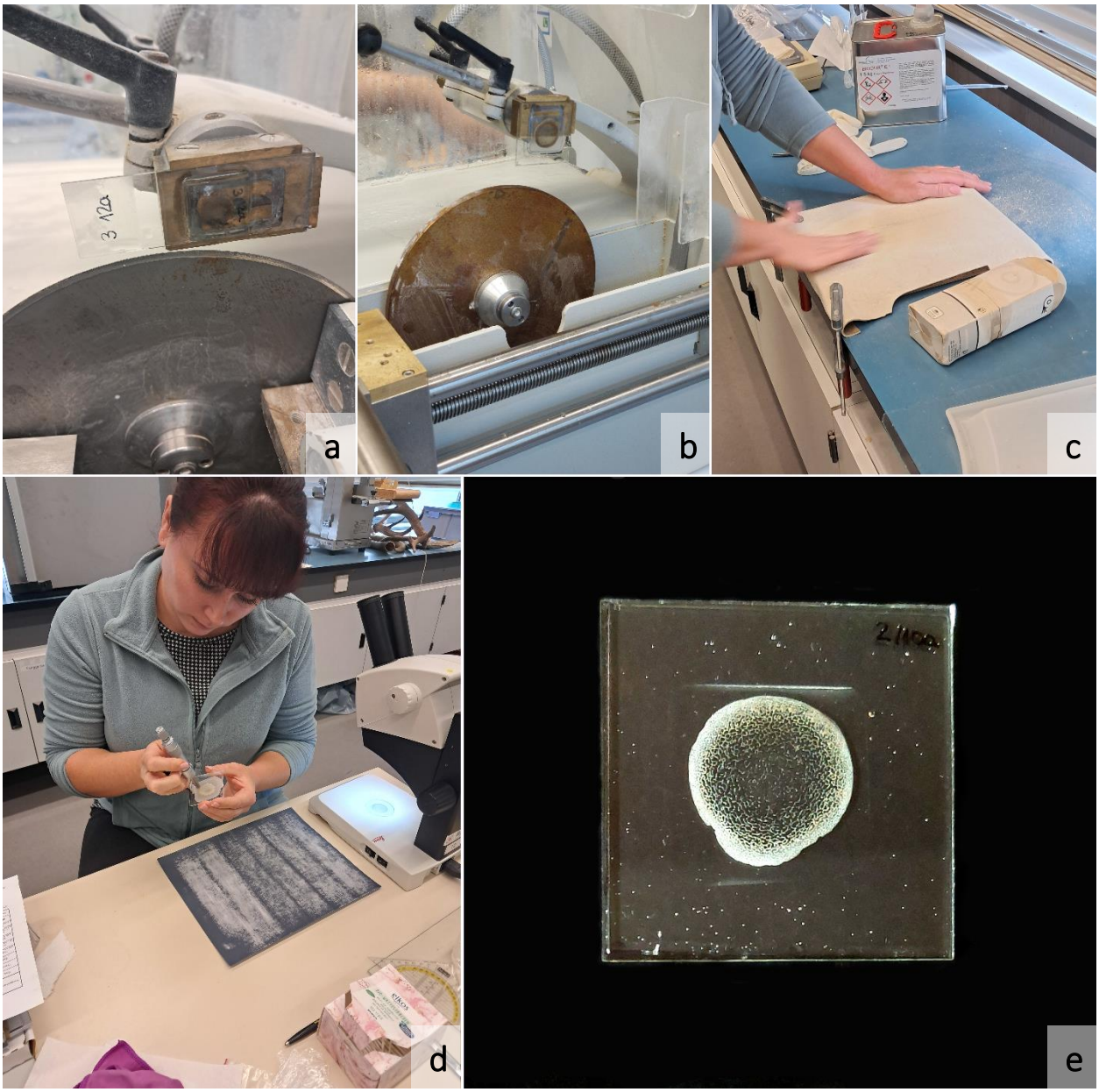

Figure 18. a) Mounted sample on a glass attached to a holder using vacuum and sectioned using a rotary saw with a water-cooled diamond-edged blade; **b)** Sample grinding (with cup wheel); **c)** Final polishing step with deer leather cloth and a polishing compound; **d)** The thickness of the glass and glass/plastic/antler fragment checked with a micrometer screw; **e)** Ground section of hard antler fragment.

4.3.2.4. Staining with von Kossa method

The von Kossa staining method was used for detection of calcium in tissue samples. The polished block surface was etched for 10 minutes with 2% acetic acid and after that washed with distilled water. The sample was then placed in 5% silver nitrate solution, exposed to bright sunlight for 10 minutes, and then washed with distilled water. At the end, the sample was placed in 5% sodium–thiosulphate for 5 minutes, washed with distilled water and dried (SHEEHAN and HRAPCHAK, 1980, modified). Stained surface of the sample was examined with a Keyence digital microscope VHX 7000 (Keyence, Osaka, Japan) and Zeiss Axioskop 2 Plus microscope (Carl Zeiss, Jena, Germany) in normal transmitted light.

4.4. Processing of demineralized antler samples

4.4.1. Fixation

For fixation, 10% buffered formalin (pH 7.4) was used, which was prepared by mixing 250 ml 10x phosphate buffered saline (PBS) (pH 7.2), 250 ml formalin, and 2000 ml distilled water. Adjustment of pH to 7.4 was done with 10 N NaOH or 1 N HCl.

Furthermore, 10xPBS (pH 7.2) was prepared by mixing 10.9 g anhydrous disodium phosphate (Na_2HPO_4), 3.2 g anhydrous monosodium phosphate (NaH_2PO_4), 90 g sodium chloride (NaCl), and up to 1000 ml distilled water. Adjustment of pH to 7.2 was done with 10 N NaOH.

4.4.2. Demineralization

After fixation in 10% buffered formalin (pH 7.4), demineralization of the antler bone samples was performed using Osteosens® solution (demineralization solution based on ethylenediaminetetraacetic acid, EDTA) (Biognost, Zagreb, Croatia) with the addition of 10% buffered formalin (pH 7.4). Antler fragments were put in a gauze, immersed in the solution, and put on a digital orbital shaker (RS-OS 20, Phoenix Instrument, Germany) (Fig. 19a, 19b). Demineralization lasted 4-8 weeks (depending on samples – antlers in velvet/hard antlers, sample segments – proximal/distal, and type of fragments – longitudinal/transversal) with regular changes of the solution every third day. The degree of demineralization was determined by sample bending

and needle sticking. After finishing the process of demineralization, the samples were washed in 1xPBS (3 days, with 3 changes of phosphate buffer per day).

4.4.3. Embedding in paraffin

Fixed and demineralized fragments were dehydrated with increasing ethanol concentrations (75%, 80%, 96%, 100%) and cleared with xylene. Paraffin embedding (Biowax plus 56/58, Biognost, Zagreb, Croatia) was performed in the thermostat (BTES-E, TMA Bodalec, Dugo Selo, Croatia).

4.4.4. Slide preparation

The paraffin blocks thus obtained were cut with a rotary microtome (CUT5062, Slee Mainz, Nieder-Olm, Germany) with a standard knife (surgery steel, 16 cm, D-edge, Gigatome, Germany) to a thickness of 6 μm (Fig. 19c). The tissue sections were flattened in a water bath (Hisbath4, Kaltek, Italy) in which gelatine was added (2 g of gelatine per 300 ml of tap water). Tissue sections were placed on adhesive microscope slides (VitroGnost Plus Ultra, Biognost, Zagreb, Croatia).

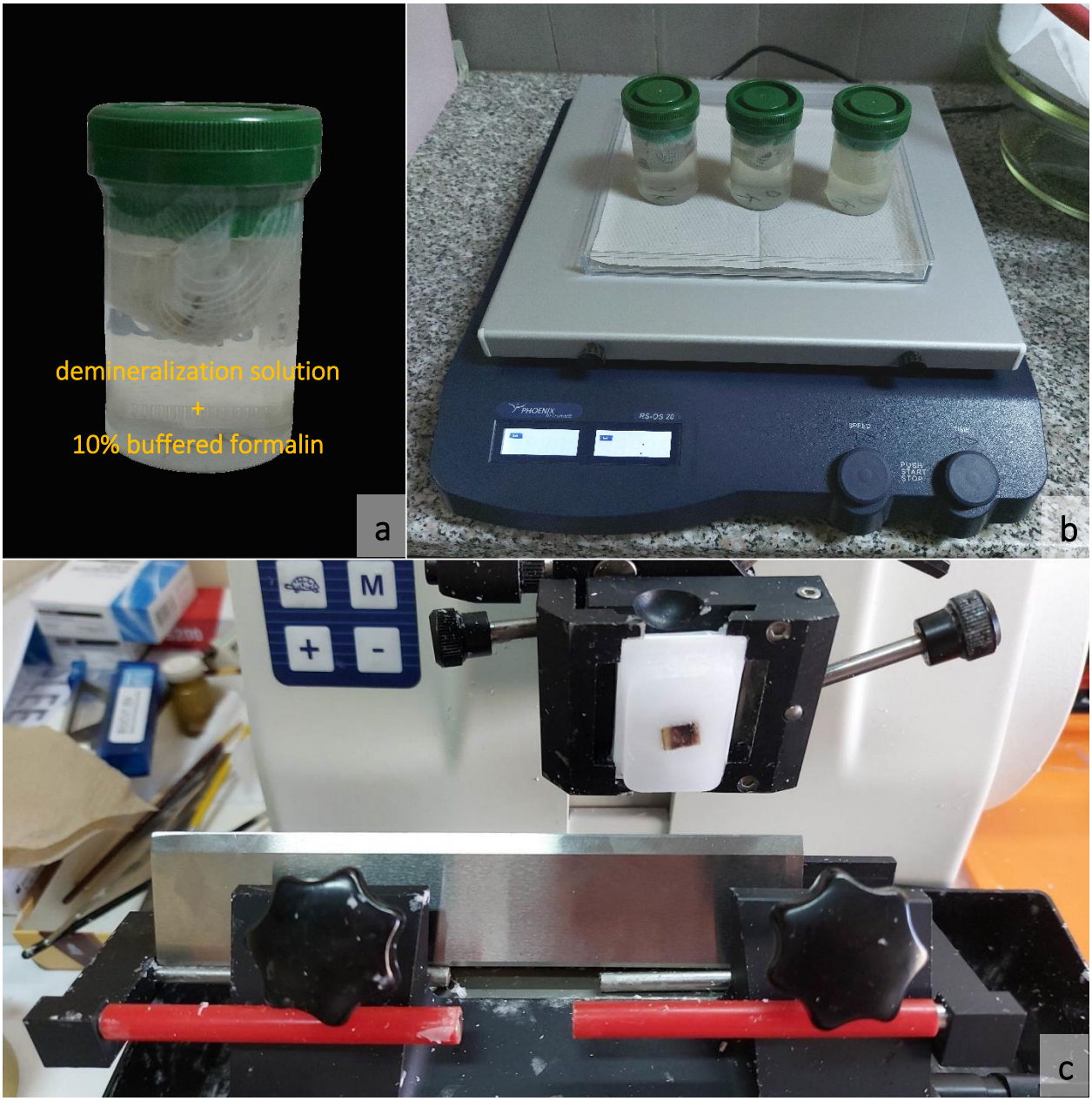

Figure 19. a) Process of demineralization. Antler fragments wrapped in gauze and immersed in the solution; **b)** Cups with antler fragments on a digital orbital shaker; **c)** Paraffin blocks cut with rotary microtome with a standard knife.

4.4.5. Deparaffinization and rehydration

Deparaffinization was done with xylene (2 x 10 minutes), and rehydration with descending concentrations of ethanol (from 100% to 75%, 5 minutes in each) to distilled water (2 x 5 minutes). Gelatine was removed in distilled water heated at 37℃ in the thermostat (BTES, TMA Bodalec & Havoić, Dugo Selo, Croatia) for 10 minutes.

4.4.6. Staining

4.4.6.1. Hematoxylin – eosin (HE)

To prepare *Mayer's hemalum,* 1 g of hematoxylin was dissolved in 1000 ml of distilled water. After that, 0.2 g of sodium iodate (NaJO3) and 50 g of chemically pure K-alum (KAl(SO4)2×12 H2O) were added. All components were dissolved while stirring on a magnetic stirrer (MSH-300, BioSan, Riga, Latvia). The solution became blue purple. Then 50 g of chloral hydrate and 1 g of crystalline citric acid were added. To prepare *Eosin Y*, 10 g Eosin Yellow was dissolved in 1000 ml of distilled water and 2 ml of glacial acetic acid was added.

Slides were put in Mayer's hemalum for 10 minutes, then in two changes of tap water for 5 minutes, in Eosin Y for 5 minutes, and in distilled water for 5 minutes. Dehydration was made with ascending concentrations of ethanol (75% 3 minutes, 96% 3 minutes, 2 x 100% 5 minutes) to xylene (2 x 5 minutes). Slides were covered with mounting medium Vitro-Clud (Deltalab, Barcelona, Spain) and closed with a cover glass (AESCHT et al., 2010).

4.4.6.2. Alcian Blue – Alizarin Red S

Solutions were prepared as follows:

- *3% acetic acid* (3 ml glacial acetic acid, 97 ml distilled water)

- *Alcian Blue (pH 2.5)* (1 g Alcian Blue 8GX, 100 ml 3% acetic acid, pH was adjusted with acetic acid)

- *Alizarin Red* (2 g Alizarin Red S C.I. 58005, 100 ml distilled water, pH was adjusted to 4.1 with 10% ammonium hydroxide)

Deparaffinization was made with xylene (2 x 10 minutes), and rehydration with descending concentrations of ethanol (100% for 5 minutes, 96% for 5 minutes), then 1 minute in tap water, and rinsed in distilled water. Gelatine was removed as previously described (in 4.4.5.). Slides were stained with Alcian Blue (pH 2.5) for 30 minutes, washed with 3 changes of tap water, washed with running tap water for 2 minutes and rinsed with distilled water. The slides were then stained with Alizarin Red S for 2 minutes. Excess dye was removed by shaking, and sections were blotted, then 20 times dipped in acetone, 20 times in acetone-xylene (1:1), and cleaned in a solution of xylene (2 x 2 minutes). The slides were finished as previously described (in 4.4.6.1.) (ANONYMOUS, 2024, modified).

4.4.6.3. Modified staining to show the ossification process

Solutions were prepared as follows:

- *Alcian Blue (pH 2.5)* (as previously described in 4.4.6.2.)
- *Mayer's hemalum* (as previously described in 4.4.6.1.)
- *Orange G – Eosin Y – Phloxin*
    - solution A (0.12% stock Eosin Y): 56 ml of 100% ethanol, 6.25 ml of distilled water, 0.075 g Eosin Y; Eosin Y was dissolved, and pH was adjusted to 4.6-5 (usually 4.8) with glacial acetic acid before adding solution B
    - solution B: 2 ml of 2% Orange G (40 mg/2 ml), 4.62 ml 1% Phloxin B (23.1 mg/4.62 ml); solution B was added to the solution A

Deparaffinization and gelatine removal was performed as previously described (in 4.4.5.). Slides were stained with Alcian Blue (pH 2.5) for 30 minutes, rinsed in two changes of distilled water for 5 minutes. The slides were stained with Meyer's hemalum for 2 minutes and washed with two changes of tap water for 5 minutes. Slides were placed in 96% ethanol for 1 minute, in Orange G - Eosin – Phloxin for 3 minutes, and subsequently in 96% ethanol for 10 seconds. Dehydration was finished by placing the slides in two changes of 100% ethanol for 5 minutes and two changes of xylene for 5 minutes.

Slides were finished as previously described (in 4.4.6.1.) (NOWALK and FLICK, 2008, modified).

4.4.7. TUNEL fluorescence assay

TUNEL was used as the method of choice for the detection of apoptotic cells (osteocytes). TUNEL was performed using a commercial kit QIA39-1EA FragEL™ DNA Fragmentation Detection Kit, Fluorescent – TdT Enzyme (Sigma-Aldrich, Merck, Germany) according to the manufacturer's instructions.

4.4.7.1. Kit components

The kit contains proteinase K (2 mg/ml proteinase K in 10mM Tris, pH 8), TdT equilibration buffer, fluorescein-FragEL^{TM} labelling reaction mix (3 vials containing a mixture of labelled and unlabeled deoxynucleotides at a ratio optimized for DNA fragment end labelling with TdT), TdT enzyme (Terminal Deoxynucleotidyl Transferase), fluorescent mounting media (an aqueous mounting media, containing DAPI, designed to preserve and enhance fluorescein fluorescence and to allow for the visualization of the total cell population), control slides (two similar slides, a mixture of HL-60 cells incubated with 0.5 µg/ml actinomycin D for 19 hours to induce apoptosis and HL-60 uninduced cells).

4.4.7.2. Deparaffinization and rehydration

Slides were immersed in xylene for 2 x 5 minutes, 100% ethanol for 2 x 5 minutes, 90% ethanol for 3 minutes, 80% ethanol for 3 minutes, and 70% ethanol for 3 minutes.

4.4.7.3. Permeabilization of specimen

Two mg/ml proteinase K 1:100 in 10 mM Tris (pH 8.0) was diluted (1 µl of 2 mg/ml proteinase K plus 99 µl 10 mM Tris per specimen). The entire specimen was covered with 100 µl of 20 µl/ml proteinase K and incubated at room temperature for 20 minutes. Slides were rinsed with 1xPBS (working solution), excess liquid was gently tapped off, and the glass slide was carefully dried around the specimen.

4.4.7.4. Equilibration and labelling reaction

5xTdT equilibration buffer was diluted 1:5 with distilled water (20 µl 5x buffer plus 80 µl distilled water per specimen). 5xTdT equilibration buffer is a concentrated solution that is 5 times (5x) stronger than the working concentration (1x). The entire specimen was covered with 100 µl of 1xTdT equilibration buffer and incubated at room temperature for 30 minutes while labelling reaction mixture was preparing. The working TdT labelling reaction mixture was prepared (contents of the fluorescein-FragEL^{TM} TdT labelling reaction mix tube were lightly vortexed for each sample to be labelled, transferred to a clean microfuge tube on ice, and mixed gently with 57 µl fluorescein-FragEL^{TM} TdT labeling reaction mix, and 3 µl TdT enzyme). 1x equilibration buffer was carefully blotted from the specimen, taking care not to touch the specimen. 60 µl of TdT labelling reaction mixture (prepared above) was immediately applied to each specimen. The specimen was covered with a piece of parafilm slightly larger than the specimen. Slides were placed in a humified chamber and incubated at 37℃ for 1-1.5 hours.

4.4.7.5. Termination of the method

The parafilm coverslip was removed and the slides were incubated in 1xPBS for 1 minute at room temperature. Excess liquid was briefly blotted, and slides were incubated in fresh 1xPBS for 1 minute at room temperature (2x). Excess PBS was wiped from the back of the slide and around the specimen. Glass coverslip was mounted using fluorescein-FragEL^{TM} mounting media.

After processing, the slides were analyzed using a Zeiss Axio – Imager M2 (Zeiss, Oberkochen, Germany). The total cell population was visualized using a filter for DAPI (330-380 nm). Labelled nuclei were analyzed using a standard fluorescein filter (465-495 nm).

4.5. Classification of osteocytes in antlers

For each sampled antler (n = 20), which was divided into three segments, longitudinal and transversal fragments were examined in slides stained with hematoxylin-eosin (HE) (hard antlers) or a modified staining to show the ossification process (antlers in velvet). Osteocytes were divided into five different groups (types A to E) based on the location and shape of the nucleus, the level

of filling of the lacunar area by the nucleus, and the level of chromatin condensation (Table 3). In each zone (*cortex*, *transition* and *trabecular*), one hundred osteocytes were examined and classified. The average value of the osteocyte types in each segment of the antler was calculated from the transverse and longitudinal sections of both antler beams (four counts per individual zone of each segment). Osteocyte counting was performed by Keyence digital microscope VHX 7000 (Keyence, Osaka, Japan) at 700x magnification.

Table 3. Classification of osteocytes (modified of MCKENZIE et al., 2019).

Type A	Type B	Type C	Type D	Type E
Nucleus fills most (> 80%) of lacunar area	Nucleus fills 50-80% of lacunar area	Nucleus is located centrally within lacuna, but covers less than 50% of lacunar area	Nucleus is mostly located in a peripheral position within the lacuna	Empty or almost empty lacuna
Nucleus with central weakly – stained portion, darker rim and some dark interior areas	Nucleus not completely dark, but with some weakly – stained areas	Nucleus is completely dark (chromatin completely condensed)	Nucleus is completely dark (chromatin completely condensed)	
Nucleus with round to oval shape	Nucleus with round to oval shape	Nucleus with oval, often elongated shape	Nucleus is considerably shrunken, often rim-like and sometimes fragmented	Only some remnants of condensed chromatin can be present in periphery of lacuna
Osteocyte alive	**Early stage of osteocyte devitalization**	**Dead osteocyte (shortly after death)**	**Dead osteocyte (moderately long after death)**	**Dead osteocyte (long after death)**
ALIVE	**DYING**	**DEAD**		

4.6. Additional analysis

During the sampling of antlers 8 (a, b), larvae were found in the antlers, and these larvae were later identified. Further bacteriological analysis and analysis of smears from the liquid material within the antlers were made for samples 8, 9 and B. Slides from all samples were stained to detect bacteria in the tissue.

4.6.1. Larvae sampling

The larvae present within the antlers were removed from the segments and fixed in 70% ethanol for further morphological and molecular identification.

4.6.2. Larvae identification

4.6.2.1. Morphological identification

For morphological identification, three larvae were collected from antlers and examined under a Motic SMZ-171 LED Stereo Zoom Microscopes (at 7.5x to 50x magnification). Two were third-instar larvae (L3), while one was a first instar larva (L1). Only the third-instar larvae (L3) were morphologically identified using previously described keys (MARTÍN-VEGA et al., 2012; MARTÍN-VEGA, 2014). Diagnosis was based mainly on the shape of the developed cephaloskeleton. Cephaloskleton dorsal edge appeared more rounded, the anterior part was broader, and the dorsal bridge was pointed in lateral view in our specimens compared to *Piophila casei*, in accordance with the figures provided by MARTÍN-VEGA et al. (2012). The mouth hook of *Prochyliza nigrimanus* is thicker in general appearance. Contrary to that, the mouth hook of *P. casei* is thinner, the dorsal edge is slightly concave in its basal part, and the distance between the base and the tips of the mouth hook is distinctly longer than the width of the mouth hook base (MARTÍN-VEGA et al., 2012). Given the small number of larvae selected for morphological inspection and their different developmental stages, the DNA barcoding method (HEBERT et al., 2003), using the mitochondrial gene cytochrome c oxidase I (COI), was employed to substantiate the morphological identification.

4.6.2.2. Sequencing and DNA Barcode Data Analysis

After the larvae were homogenized using Omni Tissue Homogenizer (Omni International), DNA extraction was performed according to the manufacturer's instructions using a DNeasy Blood & Tissue Kit (Qiagen Inc.). PCR reaction mixtures were prepared by combining 1 µL of DNA template (10 ng/µL), 13 µL of Qiagen Multiplex PCR Master Mix (Qiagen Inc.), 0.5 µM of each primer, and PCR grade water to complete 20 µL of PCR reaction volume. PCR amplification was performed under the following cycling conditions: initial denaturation at 94 °C for 15 min; 30 cycles at 94 °C (30 s), 48 °C (60 s), and 72 °C (60 s); and final extension at 72 °C for 10 min. The DNA amplicons obtained for two specimens, were sequenced by Macrogen Inc. (Amsterdam, The Netherlands) using the LCO1490 (5' – GGTCAACAAATCATAAAGATATTGG – 3') and HCO-2198 (5' – TAAACTTCAGGGTGACCAAAAAATCA – 3') amplification primers (FOLMER et al., 1994). After checking the chromatograms, sequences were edited using the BIOEDIT v.7.2 program (HALL, 1999). For species identification based on the DNA sequences, we used the BOLD Identification System (IDS) engine (RATNASINGHAM and HEBERT, 2007) and the Basic Local Alignment Search Tool (BLAST) (ALTSCHUL et al., 1990), to find similar sequences in BOLD (http://boldsystems.org, accessed on May 8, 2024) and NCBI (The National Center for Biotechnology Information, accessed on May 6, 2024) databases. For one sample, specimen and collection data, as well as obtained sequences, were uploaded to BOLD under Process ID ICRYO053-24.

4.6.3. Swabs for bacteriological examination for aerobic and anaerobic bacteria

Before cutting by micromotor Ultimate 500 (NSK, Tokio, Japan) using a flex diamond separator, 45 mm (Flex Diamond Disc, Edenta, Switzerland) with water cooling, the surface of the antler and diamond separator were treated with 70% ethanol. The incision site was cooled with saline solution. Swabs were taken from the cut surface and sent to the Department of Microbiology and Infectious Diseases with Clinic for bacteriological examination for aerobic and anaerobic bacteria. The species were identified by the MALDI TOF method.

4.6.4. Smears from the antler liquid material

After drying in the air, within 12 hours, the smears from the antler liquid material were stained with May-Grünwald Giemsa (Kemika, Zagreb, Croatia) and analyzed with Digicyte DX50 (Digicyte digitalne tehnologije, Zagreb, Croatia).

4.6.5. Identification of bacteria by Gram staining

Fixed (10% buffered formalin, pH 7.4), demineralized, embedded samples with a thickness of 6 μm were treated with BioGram Histo kit (Biognost, Zagreb, Croatia) for differentiation between Gram-positive and Gram-negative bacteria in histology sections according to the manufacturer's instructions. The kit contains Gram Crystal Violet 1% solution, stabilized Gram Lugol solution, Gram Decolorizer 2 solution, Gram Safranin solution and solution of picric acid in acetone.

Deparaffinization, rehydration and gelatine removal were performed as described previously (in 4.4.6.2.). Specimens were stained with Gram Crystal Violet 1% solution for 1 minute. Excessive dye was poured off the specimens and the specimens were carefully rinsed with stabilized Lugol solution. The dye was fixed by treating the specimens with stabilized Gram Lugol solution for 1 minute. The specimens were then rinsed carefully with distilled water for 5 seconds and treated using Gram Decolorizer 2 solution for 10-15 seconds (the process was finished when the specimen turned grey blue). The specimens were rinsed carefully with distilled water for 5 seconds and then were treated using Gram Safranin solution for 1 minute. The specimens were rinsed carefully with distilled water for 5 seconds and treated with picric acid in acetone for 10-30 seconds until the background pink color was washed away. Specimens were dehydrated in 100% ethanol in two exchanges (10 short dips in each) and cleared in 2 exchanges of xylene, 2 minutes in each. Slides were finished as previously described (in 4.4.6.2.).

4.7. Statistical analysis

Data distribution was tested using the Shapiro-Wilk test. The calculation of the correlation between variables was performed using the Kendall-Tau correlation coefficient (WILCOX, 2010).

Differences in average bone mineral density between beam segments were tested using analysis of variance (ANOVA), with Levene's test used to compare variances. In cases where no significant difference was detected, a factorial ANOVA was conducted, followed by Scheffé's post hoc test.

The distribution of osteocyte proportion data did not meet the assumptions of normality. Since the data were proportions (percentages), an ArcSin transformation was applied; however, this also failed to satisfy the normality assumption. Therefore, in cases where a significant correlation was found between antler sampling timeline and osteocyte proportion, group comparisons – by zones (cortex, transition, and trabecular) and beam segments (proximal, middle, and distal) – were conducted using regression analysis with a logarithmic function, employing the Levenberg-Marquardt algorithm (MORÉ, 1977).

All analysis were performed using Statistica software version 14.0.0.15 (TIBCO Software Inc., 2020).

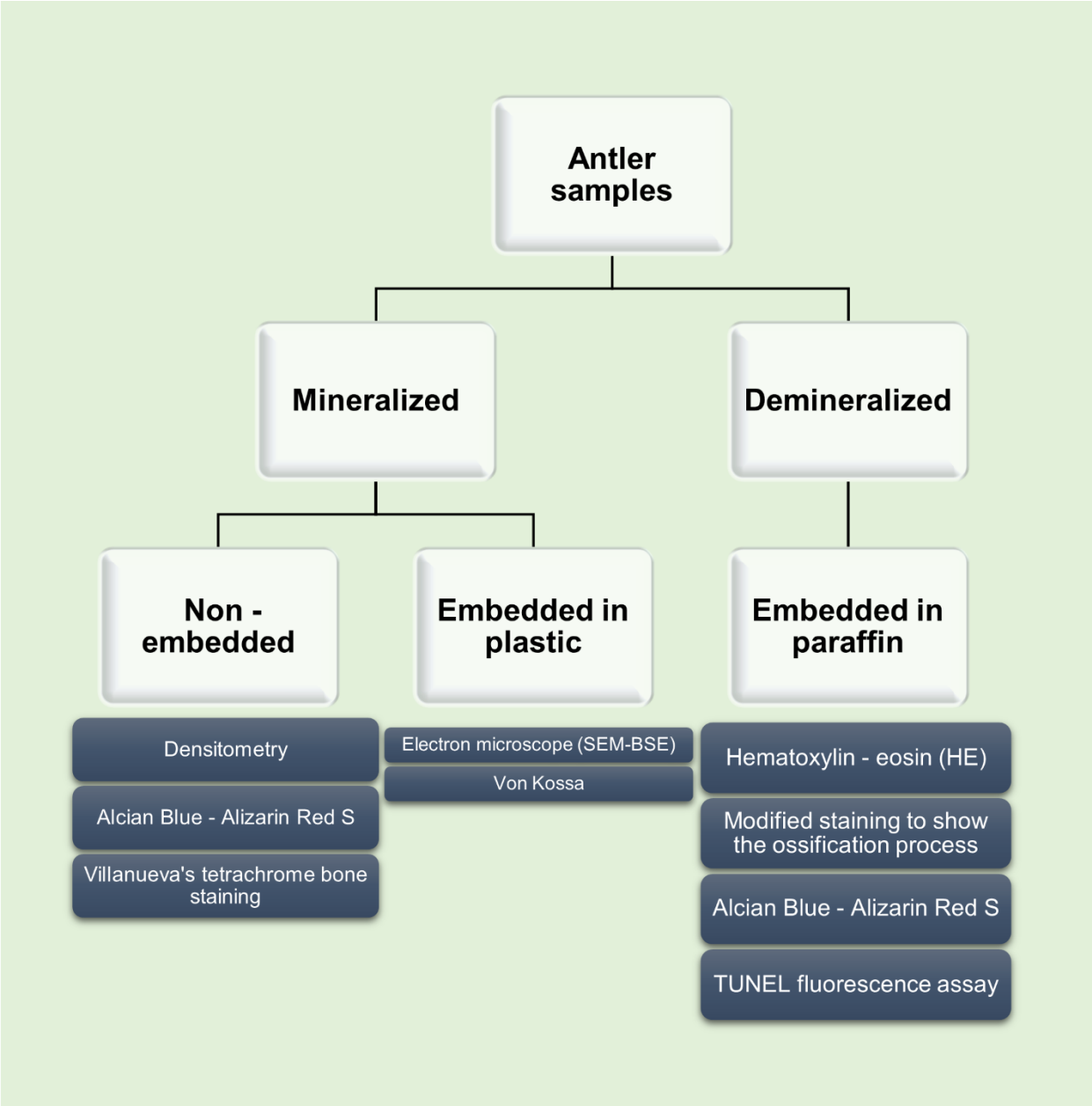

Figure 20. Overview of the methods used in the research.

Table 4. Abbreviations for different methods.

ABBREVIATION	MEANING
AB-ARS	Alcian Blue-Alizarin Red S
AV	antlers in velvet
AVS	antlers at velvet shedding
CA	cast antlers
CPL	circularly polarized light
CPL+1 λ	circularly polarized light and 1λ-plate
HA	hard antlers
HE	hematoxylin-eosin
MSOP	modified staining to show the ossification process
PHACO	normal transmitted light with phase contrast
TL	normal transmitted light (bright field microscopy)
SEM-BSE	scanning electron microscopy using a backscattered electron detector
TUNEL	TUNEL fluorescence assay
VTBS	Villanueva´s tetrachrome bone staining
VK	von Kossa

5. RESULTS

5.1. Densitometry

Table 5. Mean value of average bone mineral density (BMD) from the left and right antlers of each individual.

BMD (g/cm²)			
SEGMENT / SAMPLE	1	2	3
B	0.457	0.349	0.362
7	1.000	0.570	0.339
2	1.034	0.731	0.634
3	0.918	0.694	0.664
8	0.708	0.453	0.316
4	0.669	0.518	0.446
9	0.903	0.541	0.445
10	0.605	0.384	0.335
11	0.788	0.521	0.397
12	0.909	0.525	0.373

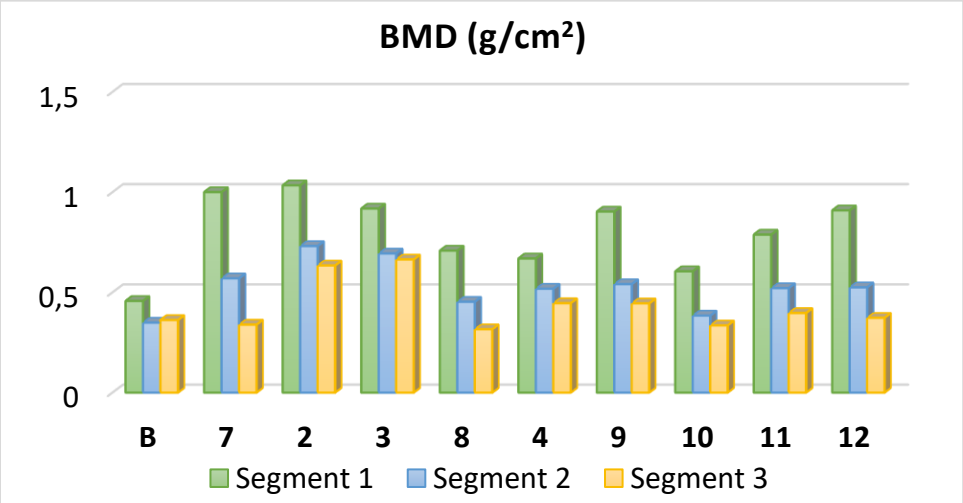

Figure 21. Summary of the average value of antler BMD by segments during the antler development cycle.

Over a period of months, a total of twenty red deer antlers representing different stages of the antler cycle were collected, and three segments representing proximal ("1"), middle ("2") and distal ("3") portions were sampled and processed using the previously described methods. Table 5 and Figure 21 show the mean value of average bone mineral density (BMD) from the left and right antlers of each individual.

Correlation analyzes revealed no statistically significant association between the stage of antler beam development (based on monthly sampling intervals) and the average bone mineral density in the proximal – segment 1 ($r = 0.035$), middle – segment 2 ($r = –0.136$), or distal – segment 3 ($r = –0.023$) portions of the beam.

The trait values showed no significant difference in variability ($F = 2.096$; $p = 0.143$), while a statistically significant difference in mineral density was observed between the analyzed segments on the beam ($F = 16.981$; $p < 0.00001$).

Table 6. Comparison of the mean mineral density in the antler between different segments of the beam. Different letters next to the trait values indicate a statistically significant difference.

FEATURE	Segment 1	Segment 2	Segment 3
Mean mineral density in the antler	0.799^{a}	0.529^{b}	0.431^{c}

According to Scheffé's post hoc test results (Table 6), there were statistically significant differences in BMD between the proximal portion (segment 1) of the antler (0.799), middle portion (segment 2) (0.529), and the distal portion (segment 3) (0.431).

Table 7. Markings and symbols used in description of the figures (from Fig. 22 to Fig. 66).

Symbol	Meaning
bv	blood vessel
↑	calcified cartilage
CL	chondrocyte lacuna
cf	collagen fibers
C	cortex
d	dermis
dCA	distal segment of cast antler
dHA	distal segment of hard antler
dVA	distal segment of velvet antler
dVS	distal segment of antler at velvet shedding
⇳	distoproximal antler axis
ed	epidermis
hf	hair follicles
◗	Howship's lacunae
⇪	hypermineralized seams
lb	lamellar bone
▲	lamellar infilling
mCA	middle segment of cast antler
mHA	middle segment of hard antler
mVA	middle segment of velvet antler
mVS	middle segment of antler at velvet shedding
○	multicanaled osteon
ob	osteoblast
ocl	osteoclast
★	osteocyte
OL	osteocyte lacuna
↑	osteoid seam
o	osteon
P	periosteum
pfl	periosteal fibrous layer

pol	periosteal osteogenic layer
pCA	proximal segment of cast antler
pHA	proximal segment of hard antler
pVA	proximal segment of velvet antler
pVS	proximal segment of antler at velvet shedding
RBC	red blood corpuscles
rb	residual blood
R	resorption cavity
⏵	resorption line
sg	sebaceous gland
⁂	soft tissue
S	trabecular zone
TZ	transitional zone
✖	tubular structures
✱	vascular canal
V	velvet
wb	woven bone

5.2. Histological analysis of antler samples

The results of histological analysis of red deer antlers according to the different methods are presented. Samples were divided into four groups (*antlers in velvet, antlers at velvet shedding, hard antlers, cast antlers*). According to the histological analysis, all sampled hard antlers (N = 14) had a similar structure within each segment, but also showed similar differences when comparing different segments.

5.2.1. Antlers in velvet (AV)

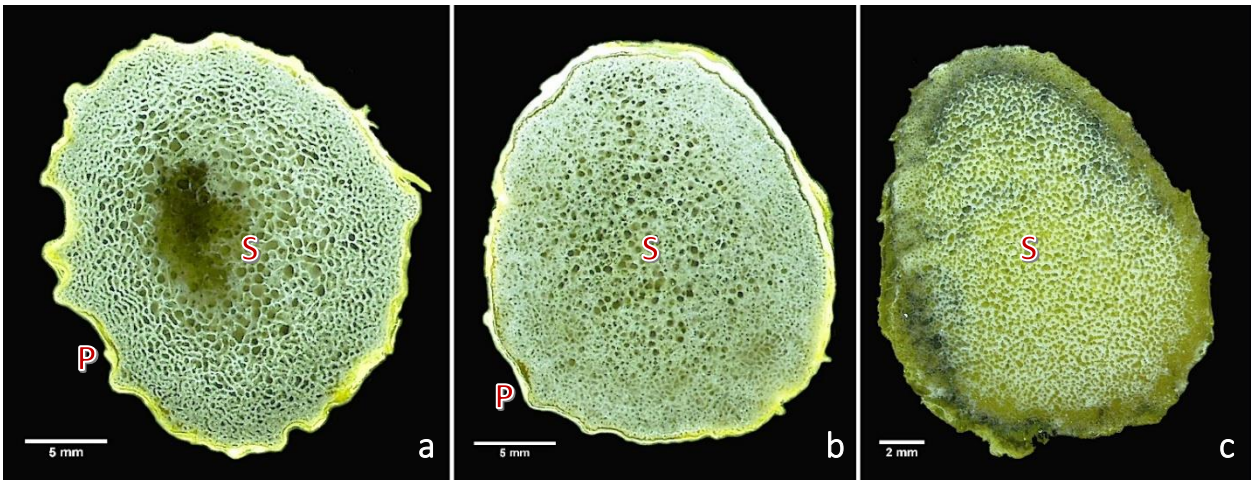

Figure 22. Transverse section of red deer antler segments in velvet: **a)** Segment 1, **b)** Segment 2, **c)** Segment 3. Mineralized, epoxy-resin embedded, unstained samples, Keyence VHX 500 (reflected light images of polished block surfaces).

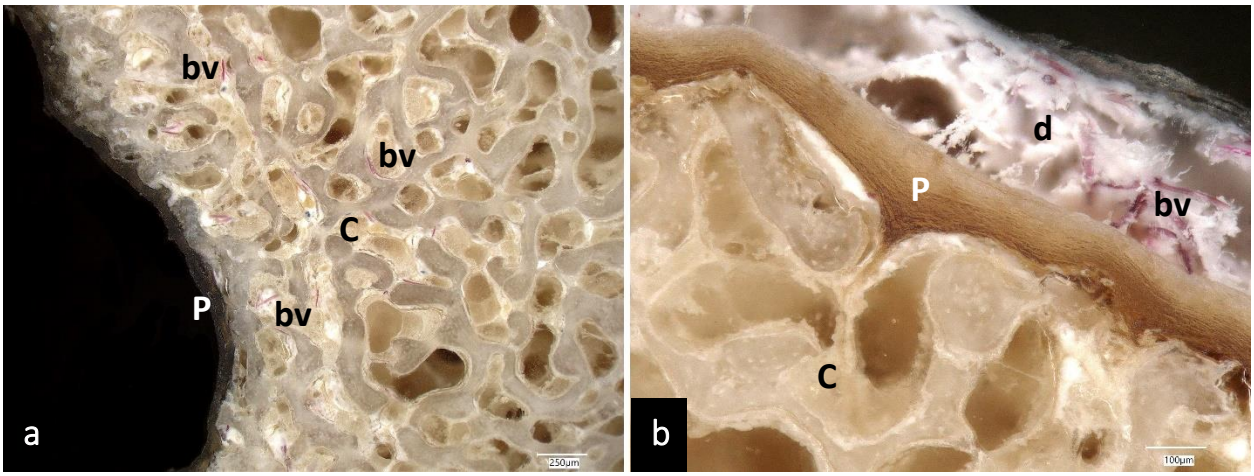

Figure 23. Transverse section of red deer antler samples in velvet: **a)** Segment 1, **b)** Segment 2. Mineralized, epoxy-resin embedded, unstained samples, Keyence VHX 7000 (reflected light images of polished block surfaces).

Figure 22 shows a microscopic view of three different antler segments in velvet (proximal, middle, distal). The cortex has not yet achieved a dense structure, while the periosteum covering the external surface of the antler bone and the middle trabecular zone is visible. Figure 23 shows antler outer periosteal part and inner cortical part. In both antler samples, areas containing blood vessels are visible (red areas).

5.2.1.1. Segment 3 (AV)

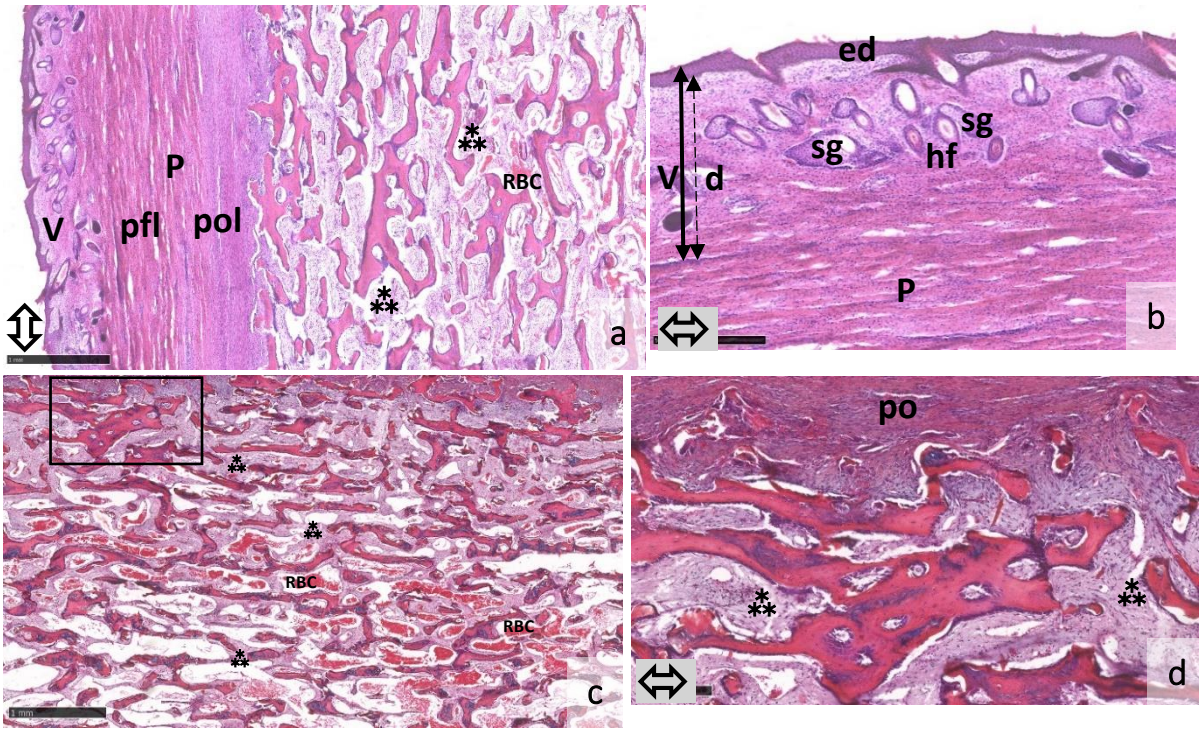

Figure 24. Section of red deer antlers in velvet, segment 3, longitudinal section, demineralized, paraffin embedded sample, (**a**, **b** – HE; **c**, **d** – MSOP), NanoZoomer 2.0RS.

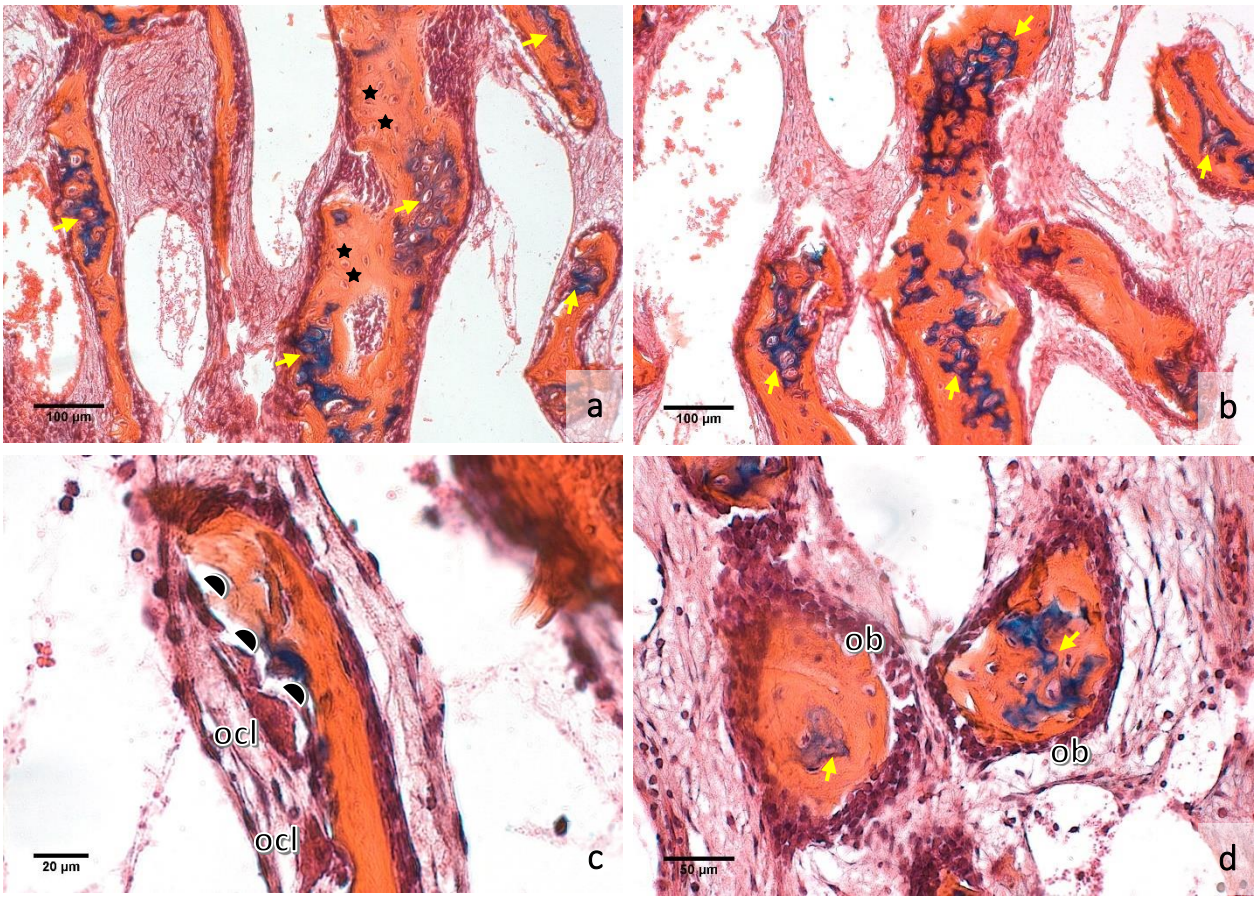

Figure 25. Longitudinal section of red deer antlers in velvet, segment 3, demineralized, paraffin embedded sample, MSOP, Axio Imager M2.

In Figure 24 it is visible that the antler is covered by an integumental layer – skin (velvet) consisting of two layers, epidermis (stratified squamous keratinized epithelium) and dermis (dense irregular connective tissue). Hair follicles and sebaceous glands are present in the dermis. Beneath the dermis lies the periosteum consisting of an outer fibrous and an inner osteogenic layer. A compact cortex is missing, and different antler zones are difficult to distinguish. Relatively high amounts of calcified cartilage (blue areas) are visible. In the intertrabecular spaces, red blood corpuscles and soft tissue are present. In Figure 25 resorption of calcified cartilage can be observed. Calcified cartilage and bone matrix is eroded by osteoclasts. Osteoclastic resorption has caused the presence of Howship's lacunae. Attached to the bone surface is a layer of osteoblasts, which is only missing in areas undergoing resorption. Osteocytes in lacunae are present in the bone matrix.

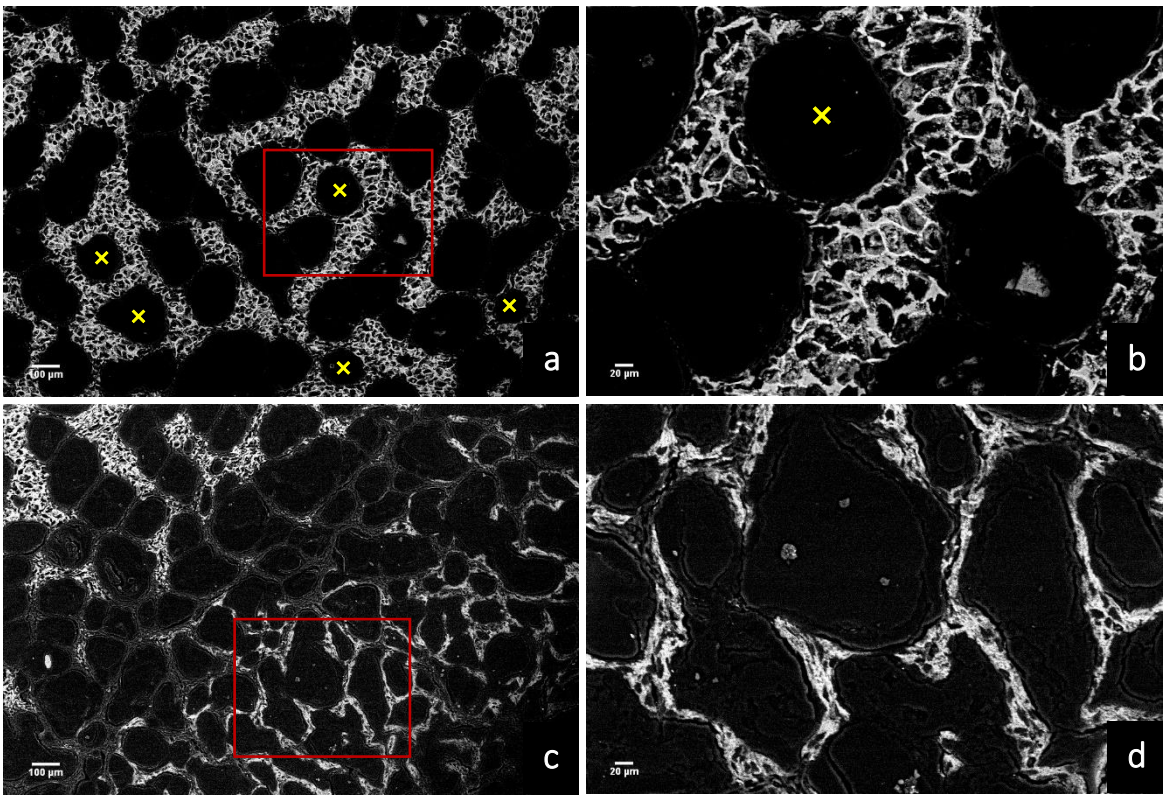

Figure 26. Polished block surfaces of the red deer antlers in velvet, segment 3, transverse sections, mineralized, epoxy-resin embedded, unstained sample, SEM-BSE.

In Figure 26 (26a, 26b), a mineralized cartilage framework (white) and cavities (black) are seen. White mineral precipitations are visible around each hypertrophic chondrocyte cell. The cavities between the calcified cartilage stacks are devoid of mineral. The framework of calcified cartilage forms longitudinally oriented tubular structures that surround cylindrical pores (x) containing vessels and soft tissue (that are not visible in the SEM-BSE images). Figures 26b and 26d show areas in red rectangles of Figure 26a and 26c at a higher magnification.

5.2.1.2. Segment 2 (AV)

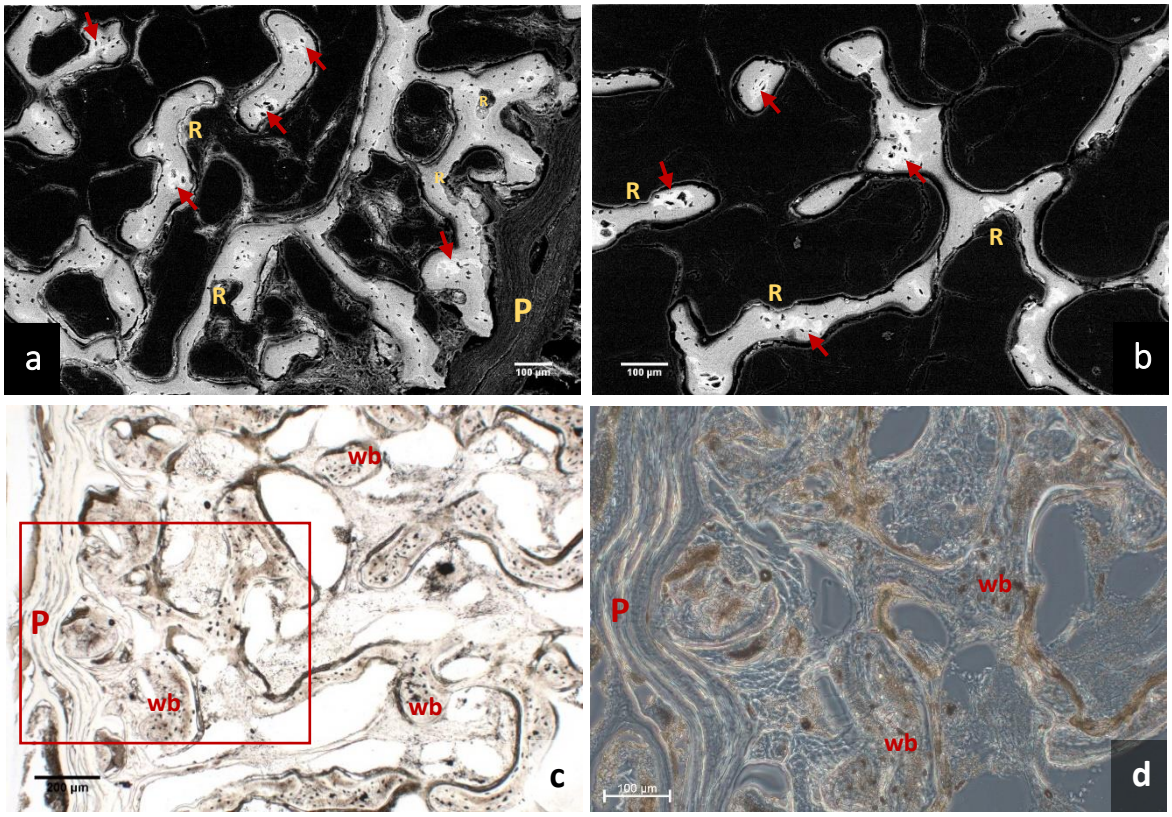

Figure 27. Red deer antlers in velvet, segment 2, transverse sections, mineralized, epoxy-resin embedded, unstained sample: **a), b)** Polished surface, SEM-BSE; **c), d)** Ground section, Axio Imager M2 (**c** – TL, **d** – PHACO).

Figure 27 shows the peripheral (cortical) part (Fig. 27a, 27c, 27d) and the trabecular zone of the antlers (Fig. 27b). Bony antler surface is overlain by a periosteum, which shows collagen fibers oriented in parallel (Fig. 27d). A dense cortex is missing. As demonstrated by SEM-BSE imaging, mineralization of the calcified cartilage matrix is more intense (brighter grey levels) than that of the mineralized bone matrix. There are several areas showing an irregular surface, indicating bone resorption by osteoclasts. In the ground sections, the cortical part contains areas of woven bone with larger and more numerous osteocyte lacunae compared to the osteons (dark areas in Fig. 27c). Figure 27d shows area in red rectangle of Figure 27c at a higher magnification.

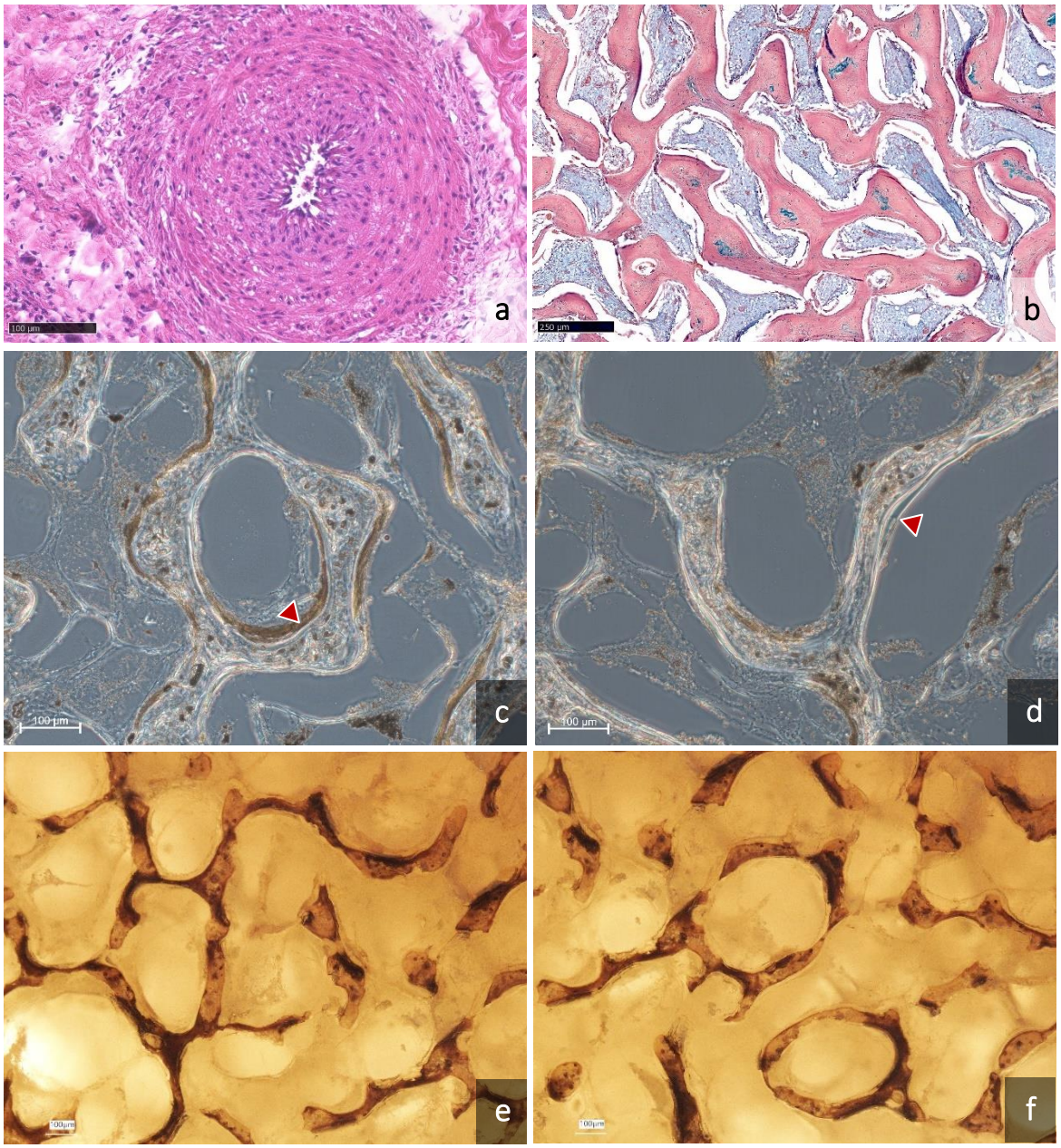

Figure 28. Red deer antlers in velvet, segment 2, transverse sections: **a)**, **b)** Demineralized, paraffin embedded samples, HE, ABARS, NanoZoomer 2.0RS; **c)**, **d)** Mineralized, ground sections, epoxy-resin embedded, unstained samples, Axio Imager M2 (PHACO); **e)**, **f)** Mineralized, polished surfaces, epoxy-resin embedded, VK, Keyence VHX 7000.

In Figure 28, blood vessels can be seen in the antler velvet. Figure 28a shows an artery with thick *tunica media* (smooth muscle cells). The number of calcified cartilage remnants (blue areas) is lower than in segment 3 (Fig. 28b). In Figures 28c and 28d, mostly woven bone is present,

but initial formation of lamellar bone can be seen. Using the von Kossa method, differences in bone tissue age can be observed: a newly-formed bone stains darker compared to an older bone, which appears lighter.

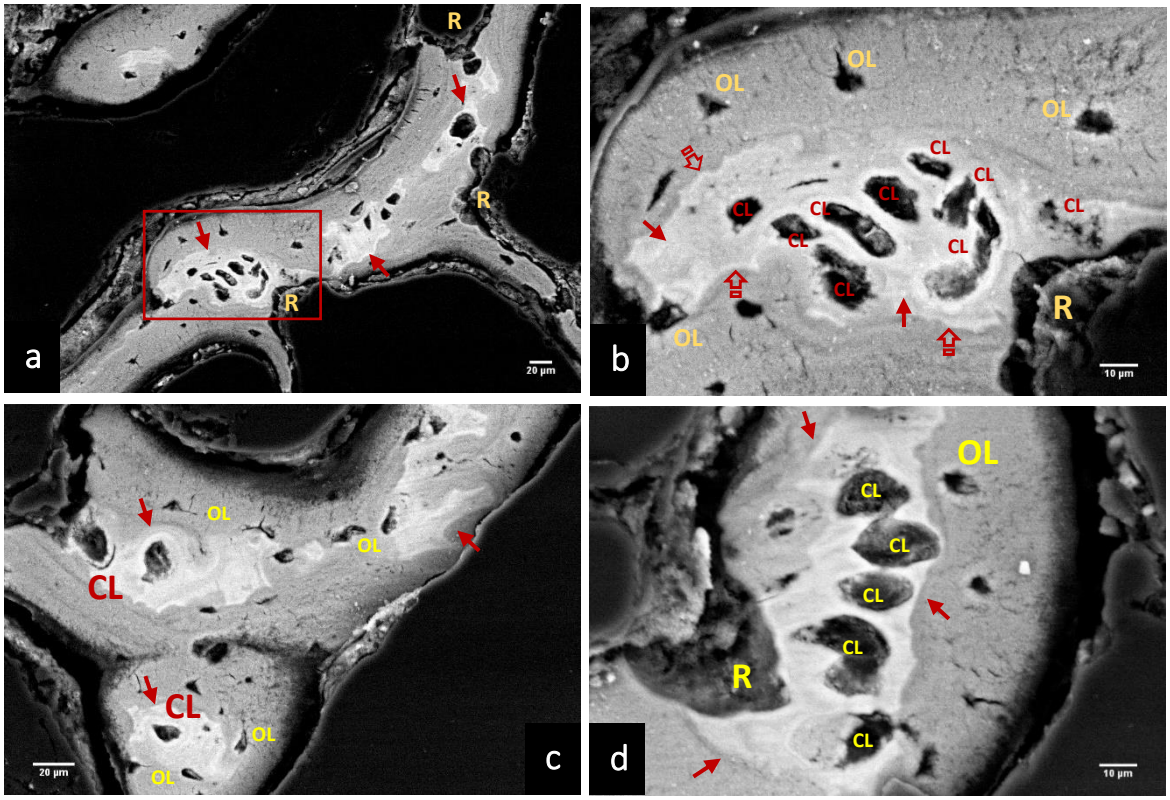

Figure 29. Polished surfaces of red deer antlers in velvet, segment 2, transverse sections, mineralized, epoxy-resin embedded, unstained sample, SEM-BSE.

Figure 29 shows remnants of calcified cartilage that have a scalloped surface due to the Howship's lacunae, indicating intense previous resorption activity. Hypermineralized (bright) seams, interpreted as reversal lines, are located along the margin of the calcified cartilage. In some places, signs of bone resorption are present. In chondrocyte and osteocyte lacunae mineral deposits can be seen (micropetrosis). Some of the mineral deposits in chondrocyte lacunae show a ring-like shape (Fig. 29c). Chondrocyte lacunae are larger, and rounder compared to the smaller and more lentiform osteocyte lacunae. Figure 30b shows area in red rectangle of Figure 30a at a higher magnification.

5.2.1.3. Segment 1 (AV)

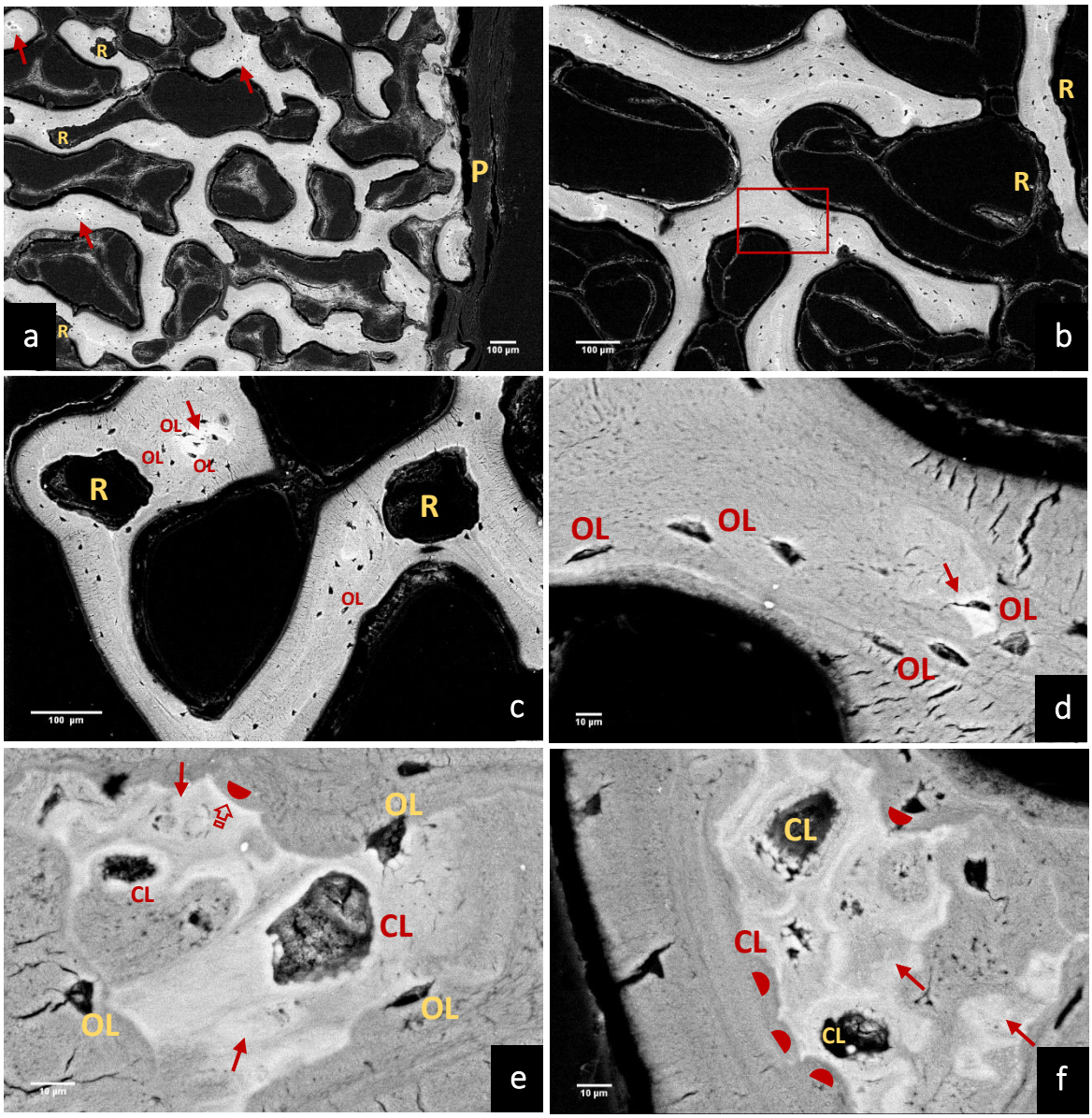

Figure 30. Polished surfaces of red deer antlers in velvet, segment 1, transverse sections, mineralized, epoxy-resin embedded, unstained samples, SEM-BSE.

Figure 30 shows the peripheral antler part with periosteum (Fig. 30a) and the inner part with bony trabeculae (Fig. 30b). A dense cortex is missing (Fig. 30a), and there are almost no remnants of calcified cartilage (Fig. 30a, 30b, 30c, 30d). Red rectangle of Figure 30b at a higher magnification is shown in Figure 30d. Smaller and larger areas of bone resorption are present (Fig. 30a, 30b, 30c). Figures 30e and 30f show areas of calcified cartilage with mineral deposits in

chondrocyte and osteocyte lacunae. Some of chondrocyte lacunae are only partially filled with minerals, while others are almost completely occluded.

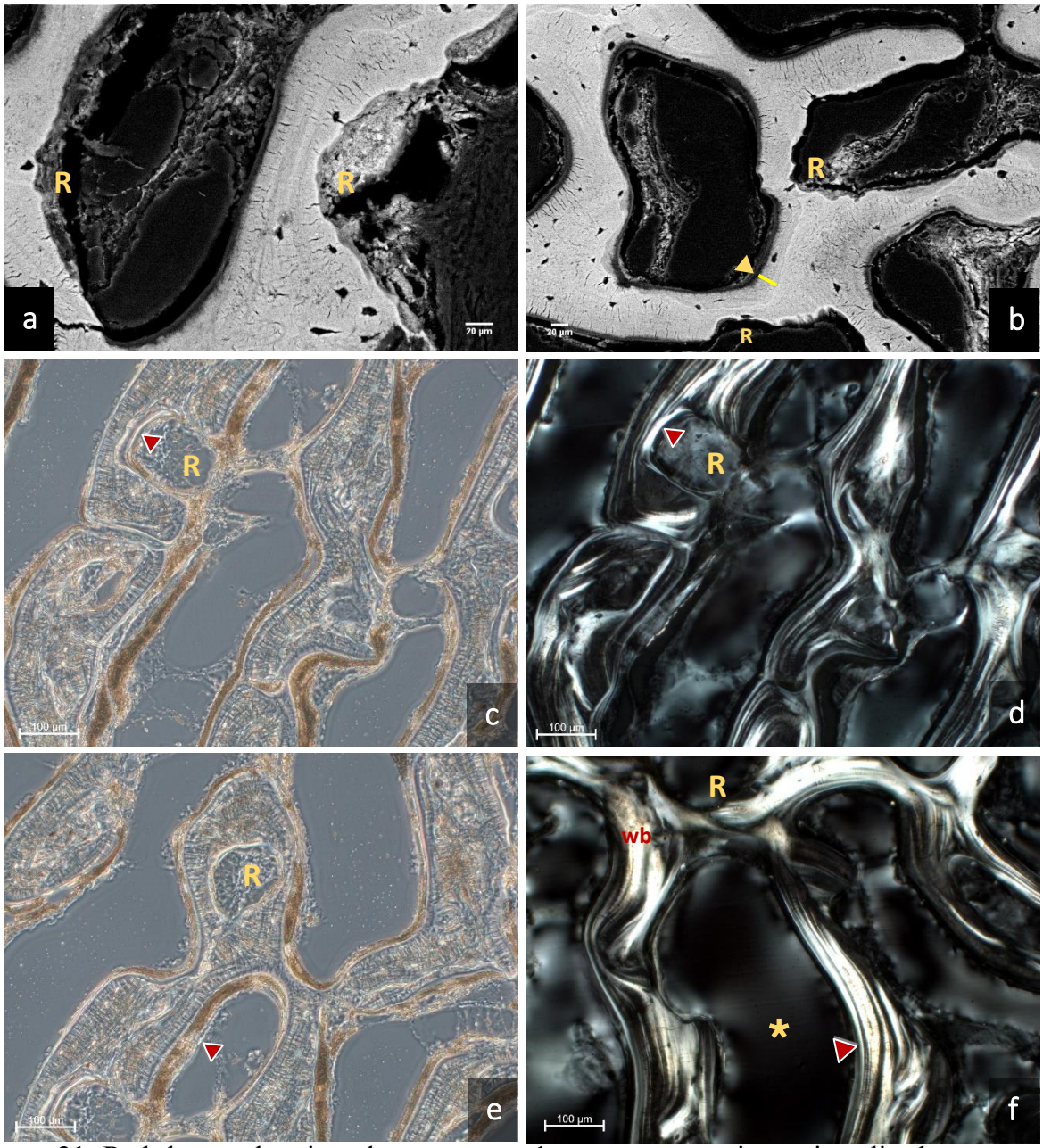

Figure 31. Red deer antlers in velvet, segment 1, transverse section, mineralized, epoxy-resin embedded, unstained samples: **a)**, **b)** Polished surface, SEM-BSE; **c)**, **d)**, **e)**, **f)** Ground section, Axio Imager M2 (**c, e** – PHACO; **d, f** – CPL).

Figure 31 shows areas of bone resorption and areas where infilling with lamellar bone occurs simultaneously. In Figure 31f, huge vascular canal and islands of woven bone are present. Brighter parts in Figures 31d and 31f demonstrate lamellar bony structures.

5.2.2. Antlers at velvet shedding (AVS)

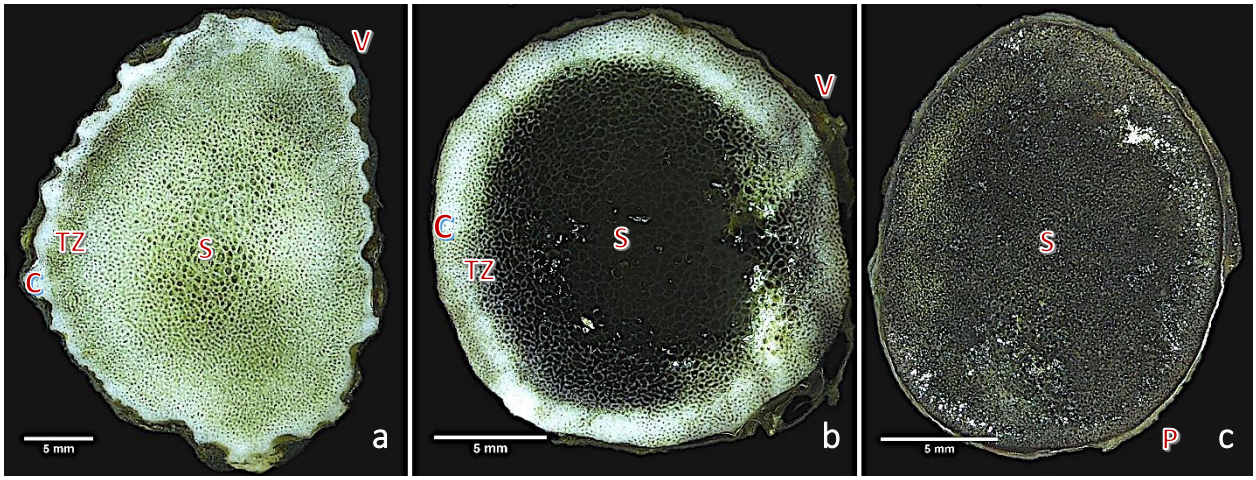

Figure 32. Transverse section of red deer antlers at velvet shedding: **a)** Segment 1, **b)** Segment 2, **c)** Segment 3. Mineralized, epoxy-resin embedded, unstained samples, Keyence VHX 500 (reflected light images of polished block surfaces).

In Figure 32, antlers at velvet shedding in some areas are surrounded with velvet remnants. Beneath the velvet is the periosteum (visible in segment 3). Different antler zones are visible: cortex, transitional zone, and trabecular zone. In segments 1 and 2, all mentioned zones are visible, while in segment 3 cortex and transitional zone are difficult to distinguish (the cortex is missing).

5.2.2.1. Segment 3 (AVS)

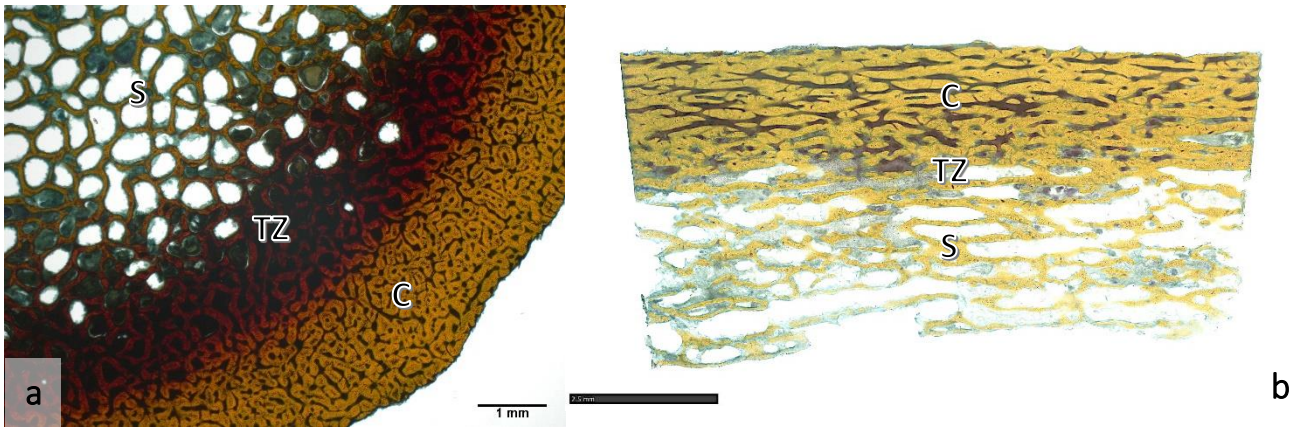

Figure 33. Red deer antlers at velvet shedding, segment 3, transverse and longitudinal sections, mineralized, unembedded samples, VTBS, Digicyte DX50, NanoZoomer 2.0RS.

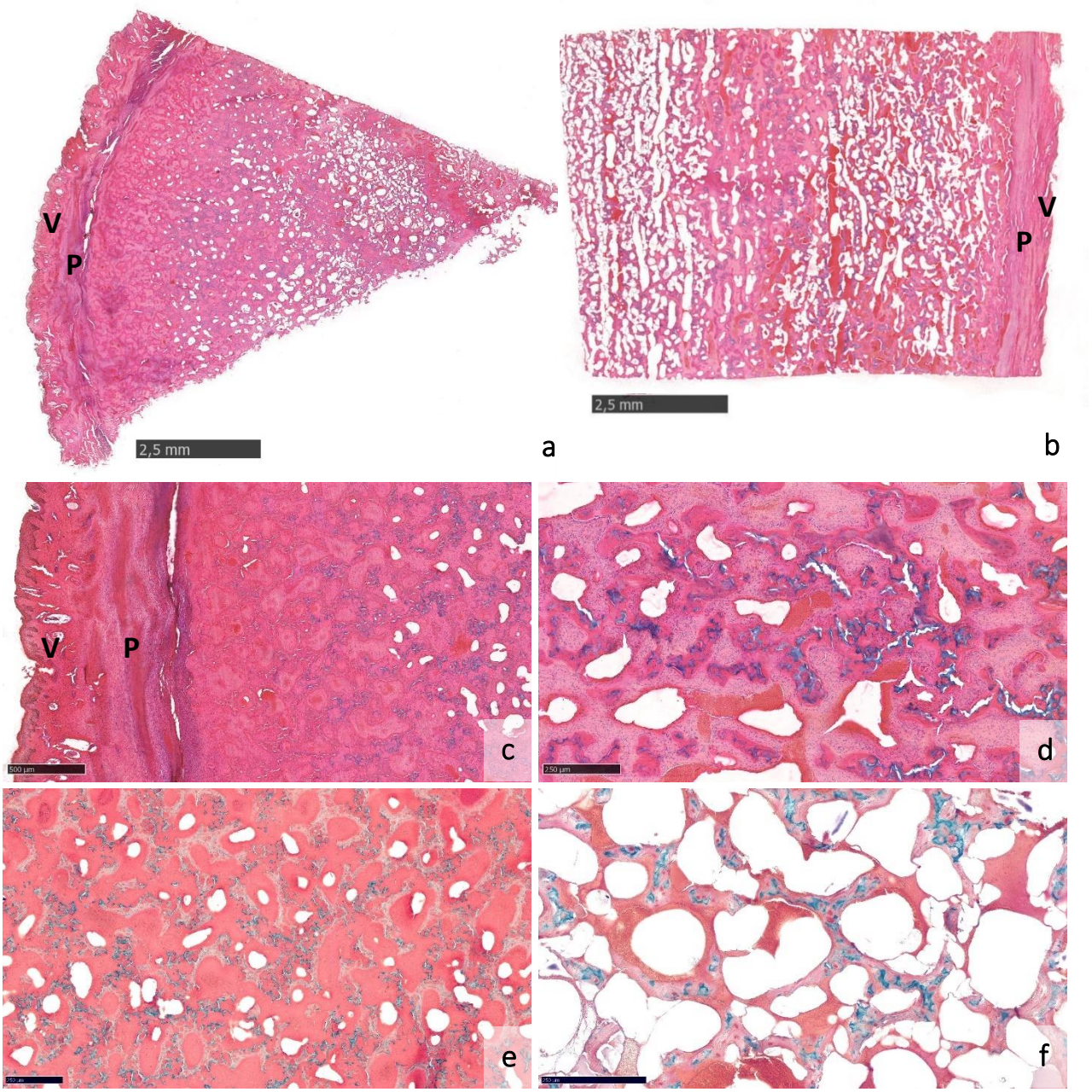

Figure 34. Red deer antlers at velvet shedding, segment 3, transverse (**a**, **c**, **e**, **f**) and longitudinal (**b**, **d**) sections, demineralized, paraffin embedded samples, NanoZoomer 2.0RS, (**a**, **b**, **c**, **d** – MSOP; **e**, **f** – ABARS).

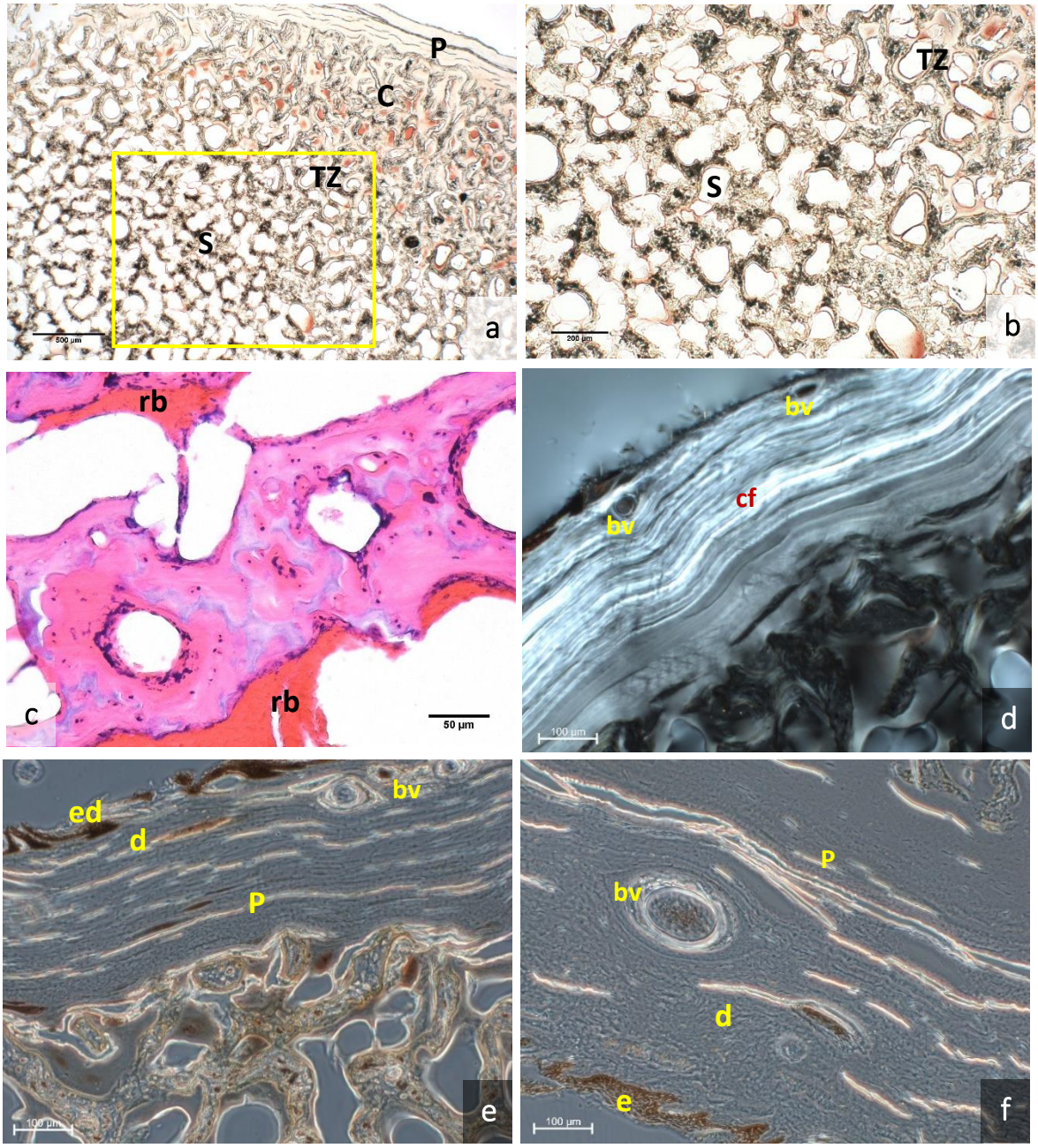

Figure 35. Red deer antlers at velvet shedding, segment 3, transverse section: **a)**, **b)**, **d)**, **e)**, **f)** Ground section, mineralized, epoxy-resin embedded, unstained samples, Axio Imager M2 (**a**, **b** – TL; **d** – CPL; **e**, **f** – PHACO); **c)** Demineralized, paraffin embedded, HE, Keyence, VHX 7000.

In Figure 33, different antler zones are visible: cortex, transitional zone, and trabecular zone. In Figures 34 and 35, the periosteum and velvet overlying the antler bone are seen. Proper cortex is not present (it is difficult to distinguish the cortex from the transitional zone). In Figure 34, larger amounts of calcified cartilage (blue) are observed. In the intertrabecular spaces, red material and other soft tissue are visible. The red material is most likely residual blood trapped in

the antler, also visible in Figure 35c. Figure 35b shows area in yellow rectangle of Figure 35a at a higher magnification. The darker portions of the trabecular framework are calcified cartilage, the lighter ones woven bone (Fig. 35a, 35b). In the antler dermis and periosteum, collagen fibers (bright lines) and blood vessels are visible (Fig. 35d, 35e, 35f). In Figure 35d, beneath the periosteum, areas without regular collagen structure are present.

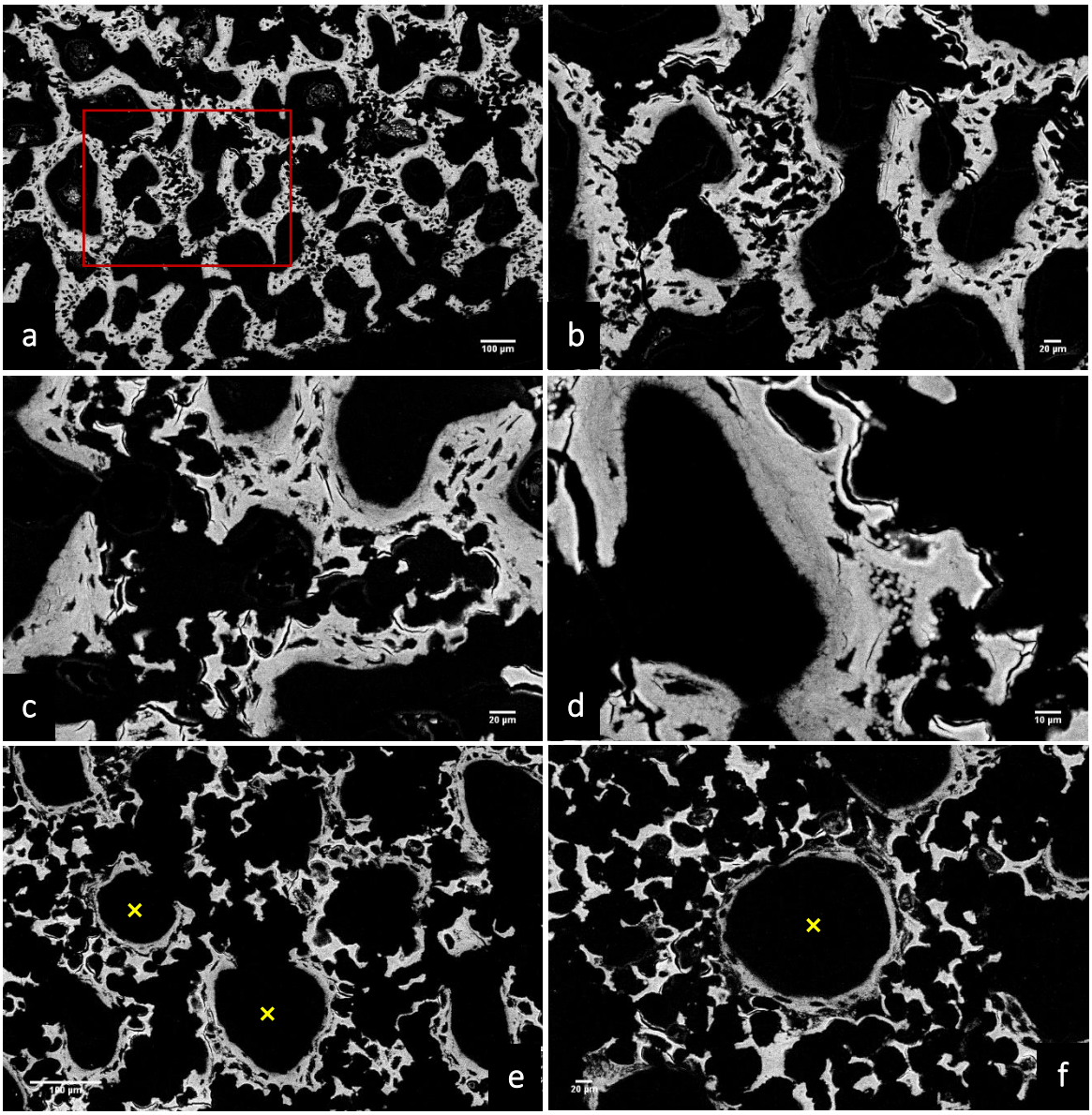

Figure 36. Polished surfaces of red deer antlers at velvet shedding, segment 3, transverse section, mineralized, epoxy-resin embedded, unstained sample, SEM-BSE.

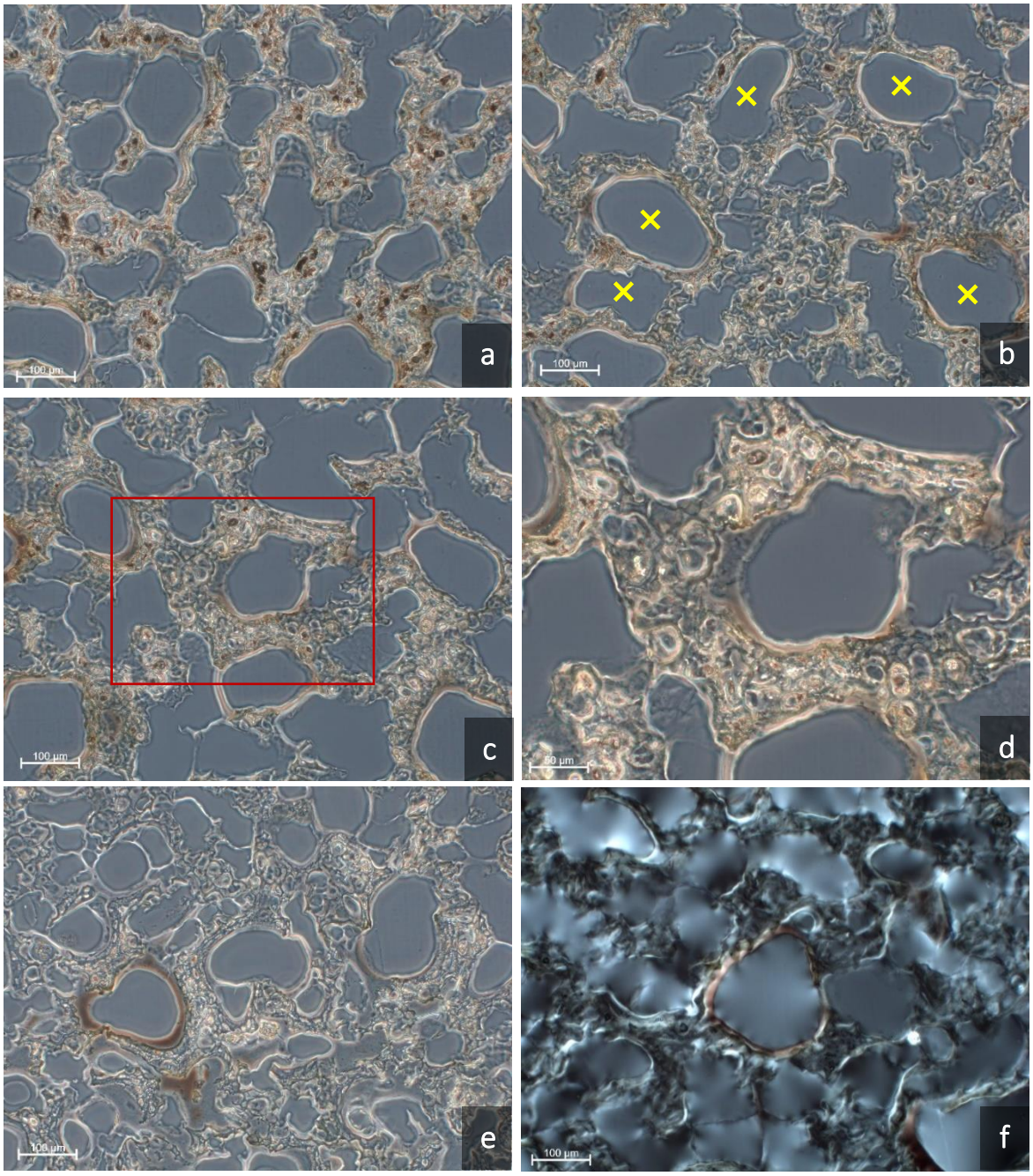

Figure 37. Ground section of red deer antler at velvet shedding, segment 3, transverse section, mineralized, epoxy-resin embedded, unstained sample, Axio Imager M2 (**a**, **b**, **c**, **d**, **e** – PHACO; **f** – CPL).

In Figures 36 and 37, the tubular framework is mostly cartilaginous, lamellar structures are not visible, and mineralization is not finished completely. Figures 36b and 37d show areas in red rectangles of Figures 36a and 37c at a higher magnification. In some areas, minor bone deposition

is present (Fig. 37c, 37d, 37e). In Figure 37f, there is no regular (lamellar) collagen structure in the framework, indicating that it is formed by woven bone.

5.2.2.2. Segment 2 (AVS)

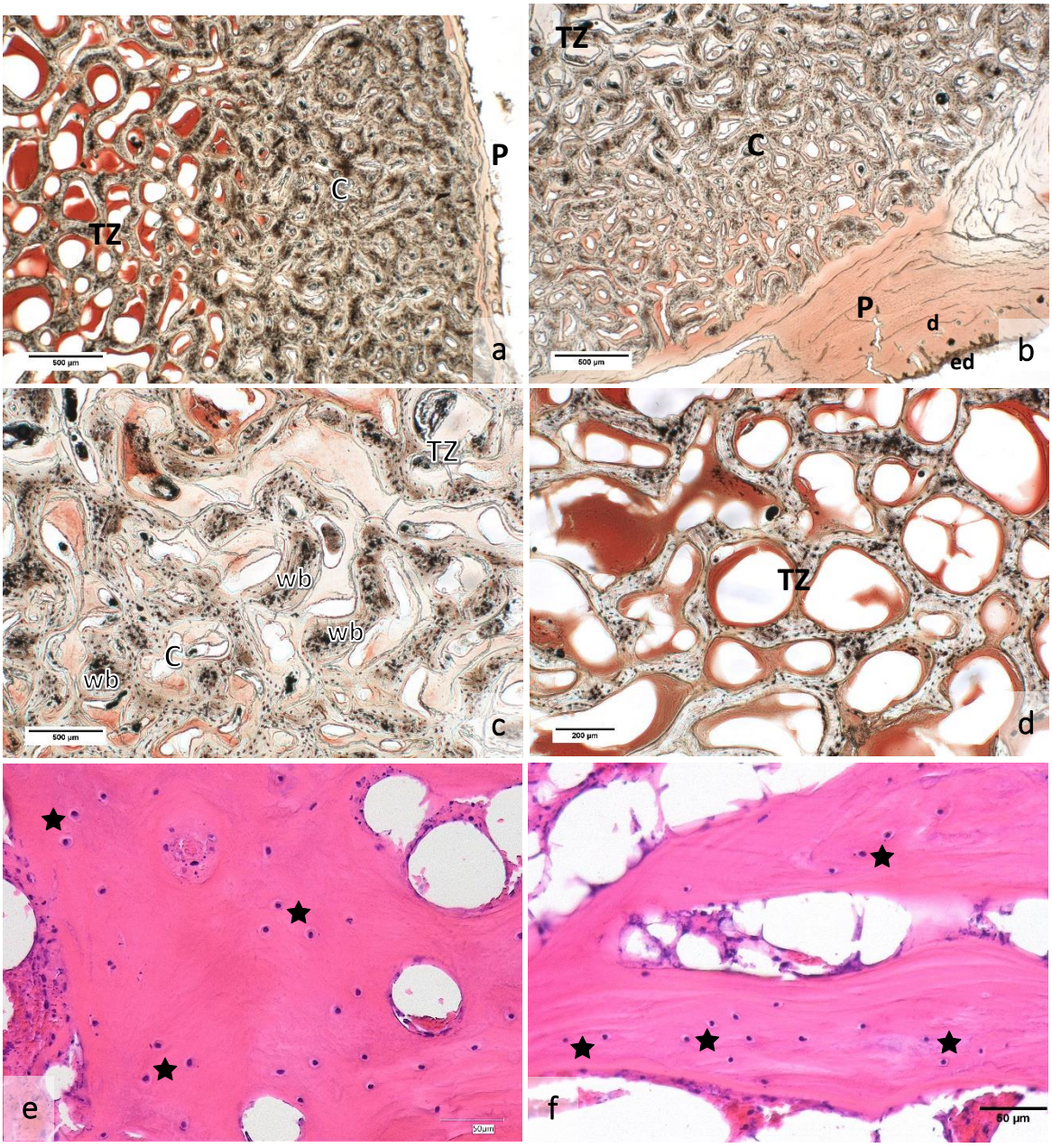

Figure 38. Red deer antlers at velvet shedding, segment 2: **a), b), c), d)** Ground section, transverse section, mineralized, epoxy-resin embedded, unstained sample, Axio Imager M2 (TL); **e), f)** Longitudinal section, demineralized, paraffin embedded, HE, Keyence VHX 7000.

In Figure 38, the antler is covered with velvet which consists of epidermis and dermis (Fig. 38b). Beneath the velvet is the periosteum, cortex and transitional zone. Figure 38e represents antler cortex, while Figure 38f represents a trabecular part. Osteocytes in lacunae are inside the bone matrix. In the cortex and the transitional zone, areas of woven bone are seen (Fig. 38a, 38b, 38c, 38d). Intertrabecular spaces (transitional and trabecular zone) contain residual blood.

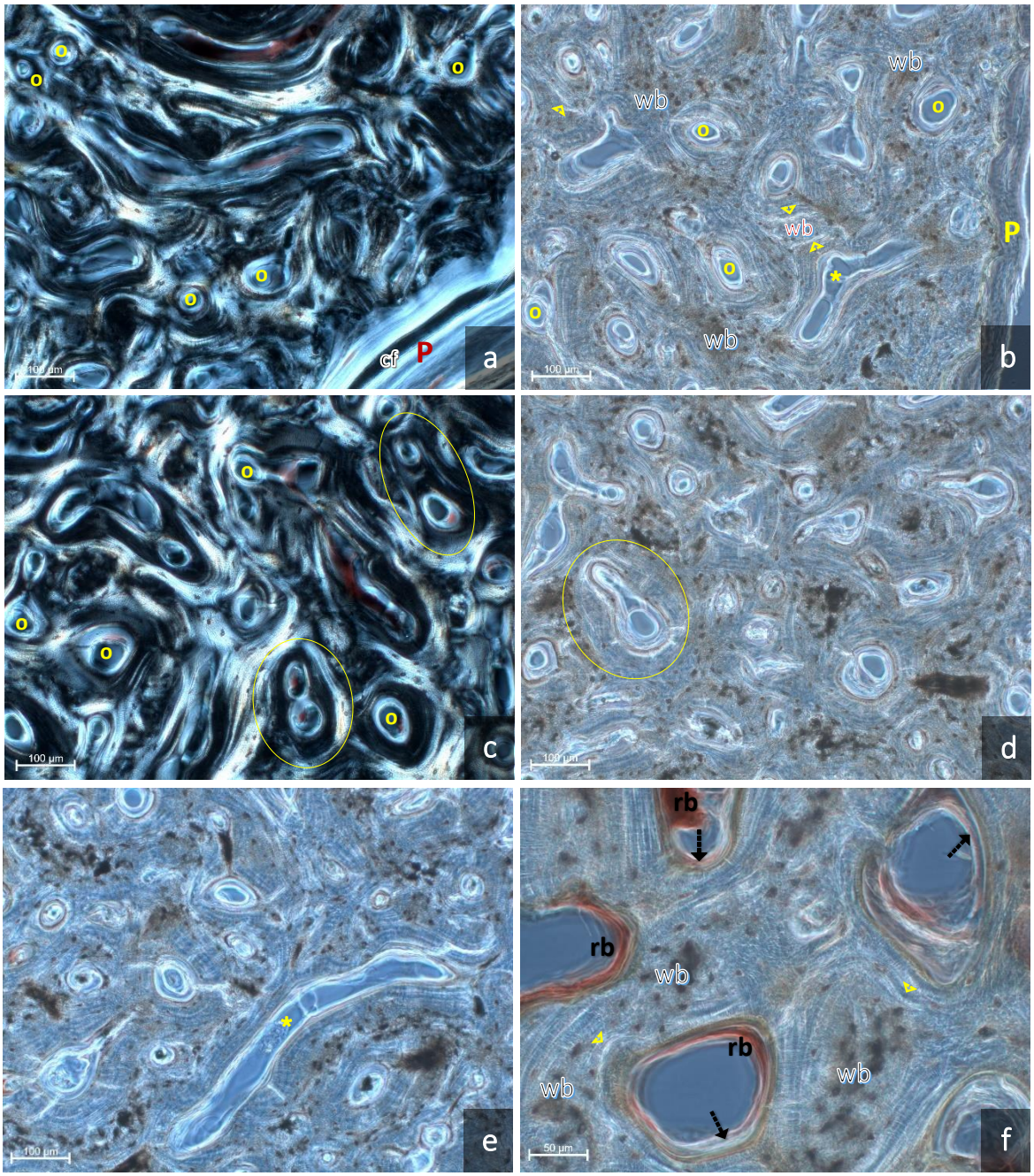

Figure 39. Ground section of red deer antler at velvet shedding, segment 2, transverse section, mineralized, epoxy-resin embedded, unstained sample, Axio Imager M2 (**a**, **c** – CPL; **b**, **d**, **e**, **f** – PHACO).

In Figure 39, collagen fibers (bright) are visible in the periosteum. Osteoid seam (bright unmineralized parts) lines osteons inside. Identified osteons are all primary osteons. Multiple canals and areas of woven bone are present. Using CPL method, it is demonstrated that there is no regular arrangement of collagen fibers in areas of woven bone. These areas have a higher amount of large and round osteocyte lacunae. In some areas large vascular canals are present (Fig. 39a, 39b, 39e). Inside some vascular canals residual blood is visible. Reversal lines are present along the boundary between lamellar and woven bone.

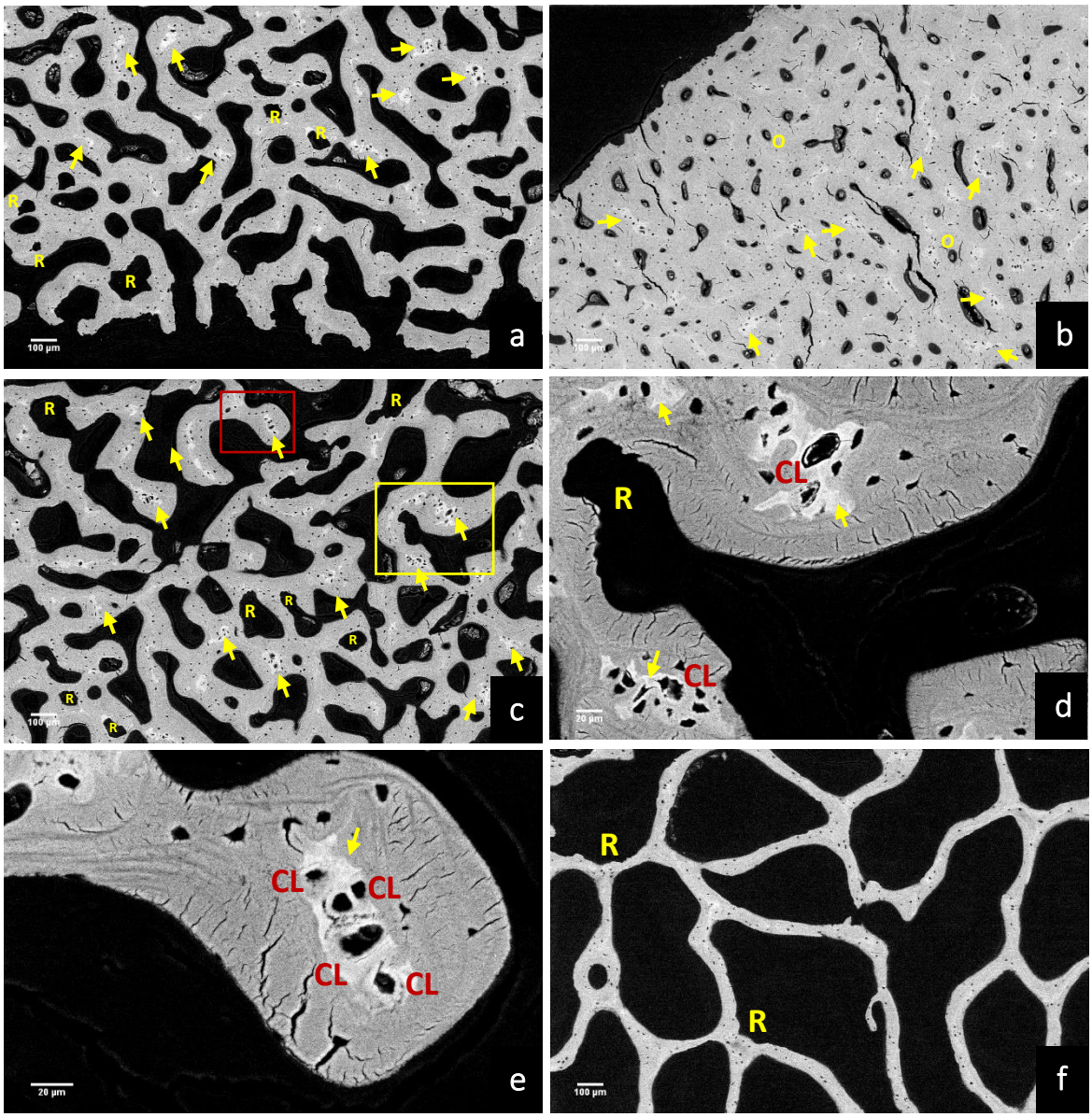

Figure 40. Polished surfaces of red deer antlers at velvet shedding, segment 2, transverse section, mineralized, epoxy-resin embedded, unstained sample, SEM-BSE.

In Figure 40a and 40b, there is antler surface and cortical part of the two opposite sides on the same cutting surface. Areas of calcified cartilage are present. In Figure 40a, there is no proper cortex, while in Figure 40b, osteons are visible in antler cortex. Areas marked by the rectangles in Figure 40c are shown at a higher magnification in Figure 40d (yellow rectangle) and Figure 40e (red rectangle). Cartilage and bone resorptions are visible in some areas. Chondrocyte lacunae contain mineral deposits. There are almost no areas of calcified cartilage in the antler trabecular part (Fig. 40f).

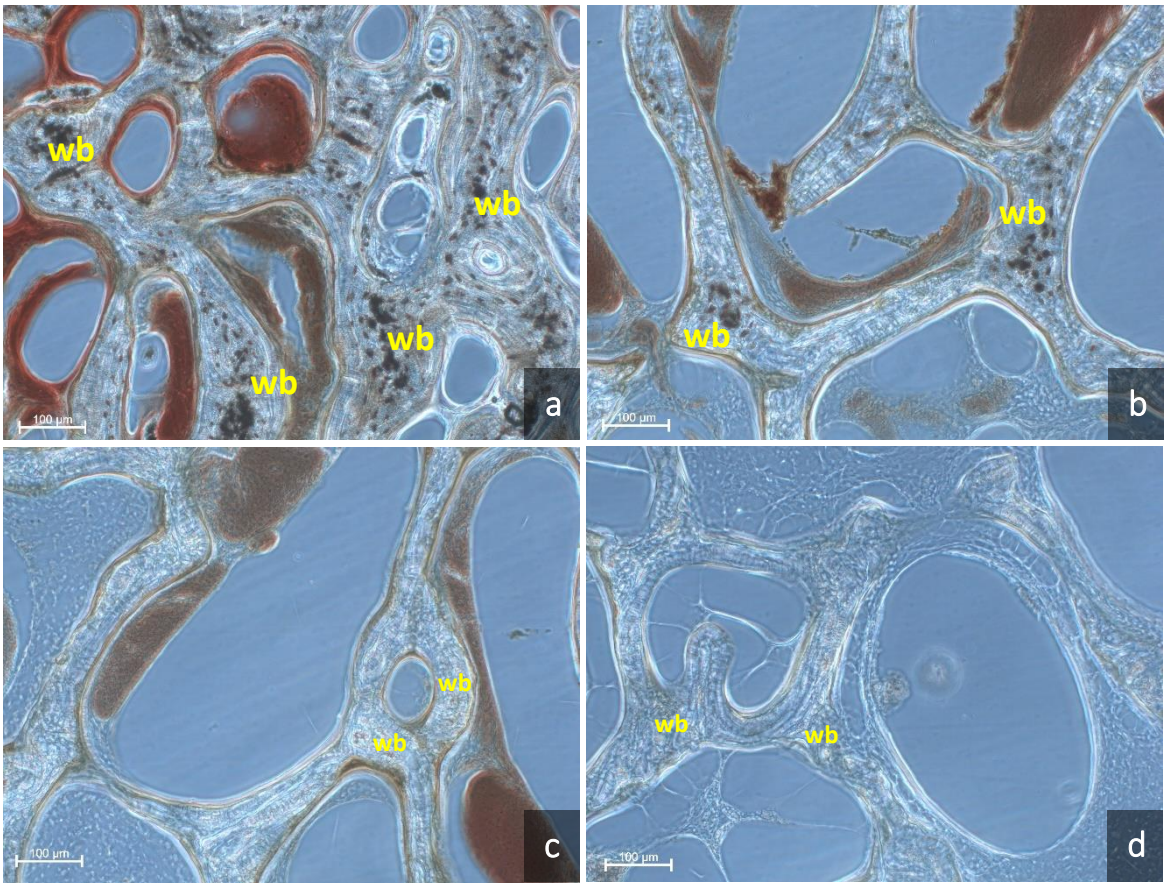

Figure 41. Ground section of red deer antler at velvet shedding, segment 2, transverse section, mineralized, epoxy-resin embedded, unstained sample, Axio Imager M2 (PHACO).

Figure 41 shows sections from cortical to trabecular part. All these figures show primarily woven bone. Residual blood is present in vascular canals.

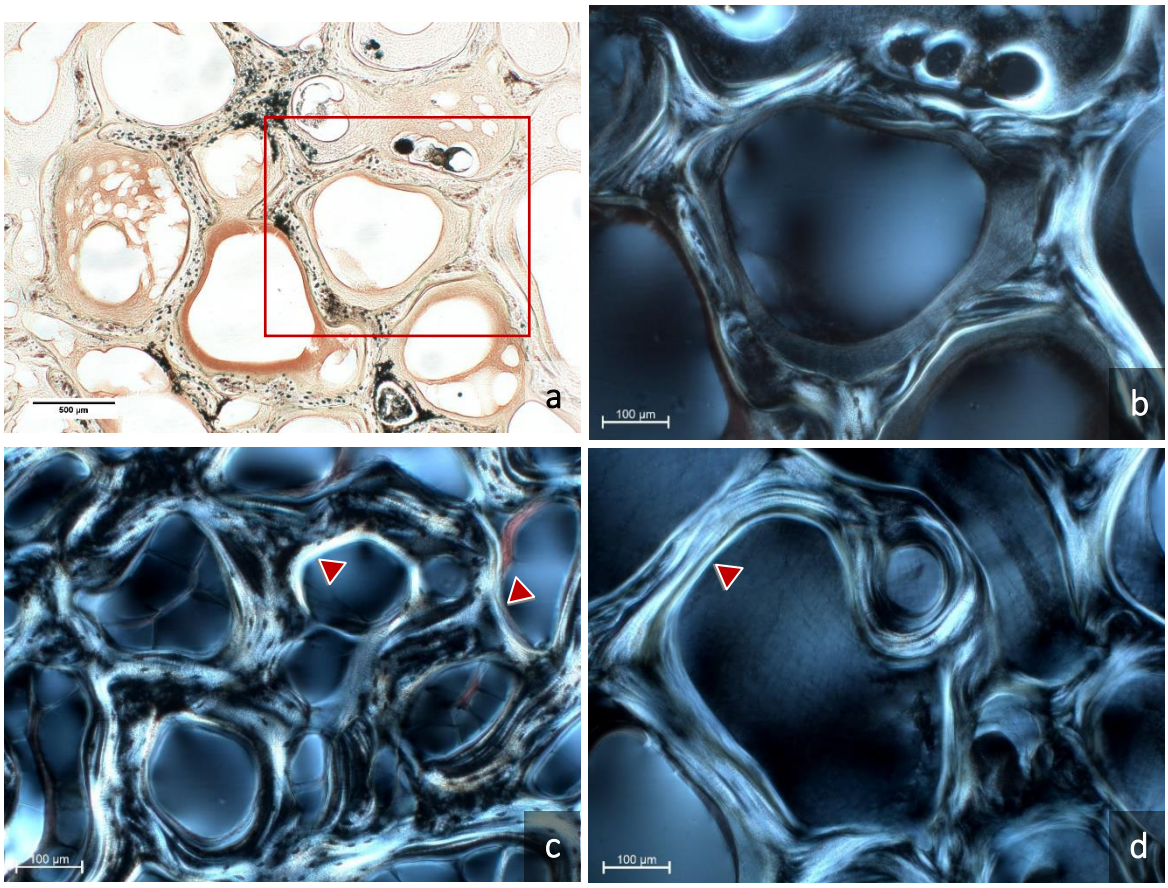

Figure 42. Ground section of red deer antlers at velvet shedding, segment 2, transverse section, mineralized, epoxy-resin embedded, unstained sample, Axio Imager M2 (**a** – TL; **b**, **c**, **d** – CPL).

Figure 42 shows a portion of the trabecular zone. There is a tubular framework consisting of woven bone and calcified cartilage (darker portions). Very early infilling of the intertrabecular pores with unmineralized lamellae (collagen showing birefringence in polarized light) of future primary osteons is observed. The pores are filled with soft tissue, which seems to include some vessels (Fig. 42a, 42b). In Figure 42a, residual blood is seen in the vascular spaces. Figure 42b shows area in red rectangle of Figure 42a at a higher magnification. In Figure 42c and Figure 42d the lighter parts represent lamellar bone, while darker parts represent woven bone. Higher amounts of woven bone are visible. The intertrabecular spaces are in a process of infilling with lamellar (primary osteonal) bone.

5.2.2.3. Segment 1(AVS)

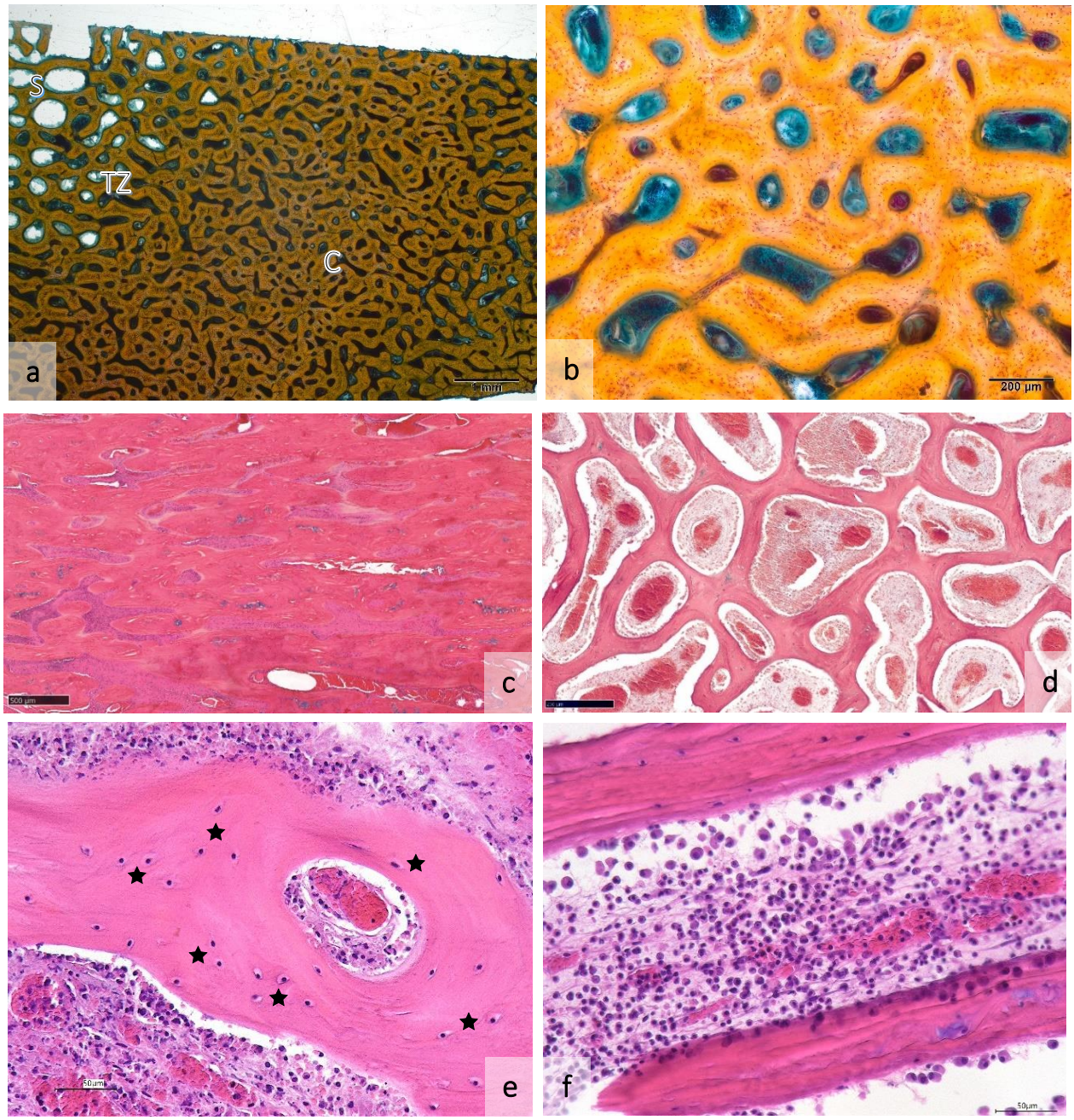

Figure 43. Red deer antlers at velvet shedding, segment 1: **a)**, **b)** Transverse section, mineralized, unembedded samples, VTBS, Digicyte DX50; **c)**, **d)**, **e)**, **f)** Transverse and longitudinal sections, demineralized, paraffin embedded samples (**c** – MSOP, NanoZoomer 2.0RS; **d** – ABARS, NanoZoomer 2.0RS; **e**, **f** – HE, Keyence VHX 7000).

In Figure 43, different antler zones are visible. Osteons and osteocytes in lacunae are present in the cortex. There is a small amount of calcified cartilage (blue areas) in the cortex (Fig. 43c) and in trabecular part (Fig. 43d). Vascular spaces and cavities are filled with soft tissue and residual blood (Fig. 43e and 43f).

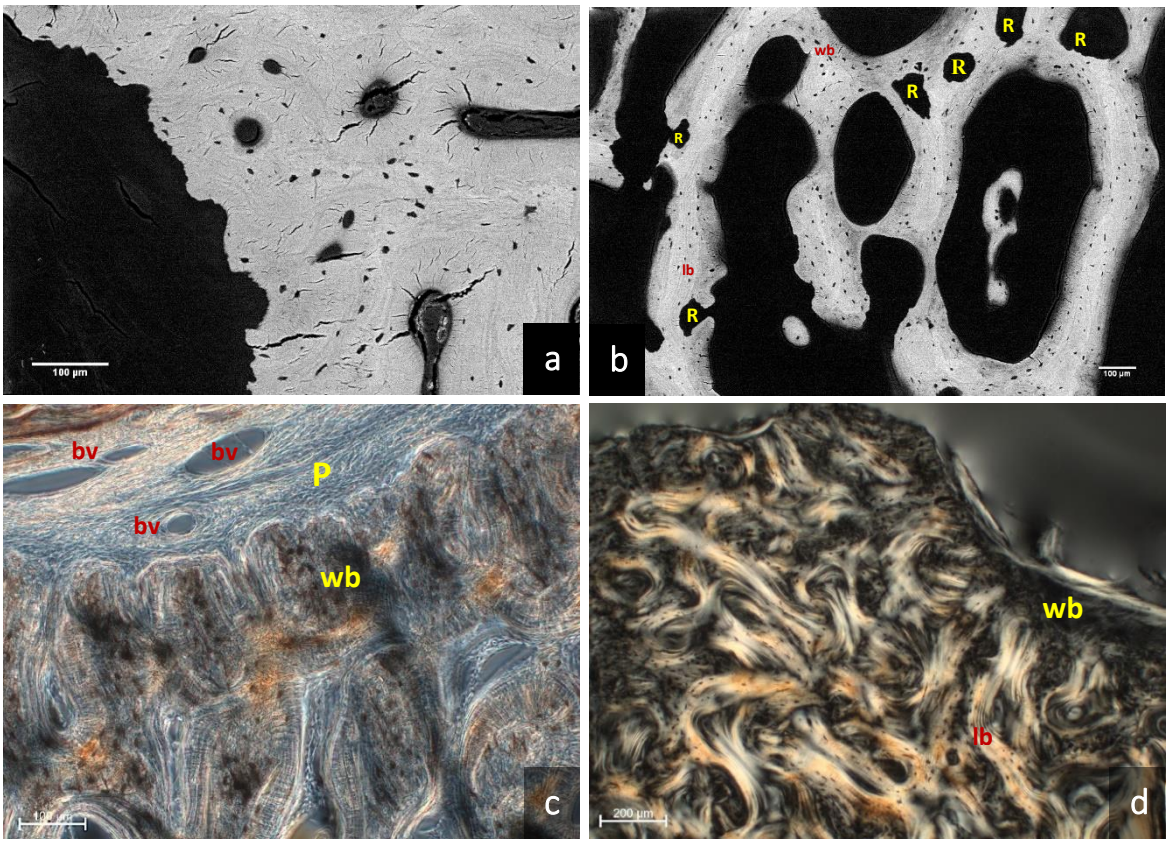

Figure 44. Polished surfaces of red deer antlers at velvet shedding, segment 1, transverse section, mineralized, epoxy-resin embedded, unstained sample (**a**, **b** – SEM-BSE; **c** – PHACO, **d** – CPL – Axio Imager M2).

In Figure 44, an irregular antler surface is visible. In cortex (Fig. 44a) and trabecular zone (Fig.44b), remnants of calcified cartilage are not present. In Figures 44b and 44d, difference between bone types (woven, lamellar) is observed. Lamellar bone has less osteocyte lacunae, which are smaller and lentiform. Bone resorption cavities are present in some areas. In Figure 44c, the antler is covered with periosteum that contains blood vessels. Areas of woven bone can be seen just beneath the periosteum (in the outermost portion of the bony antler).

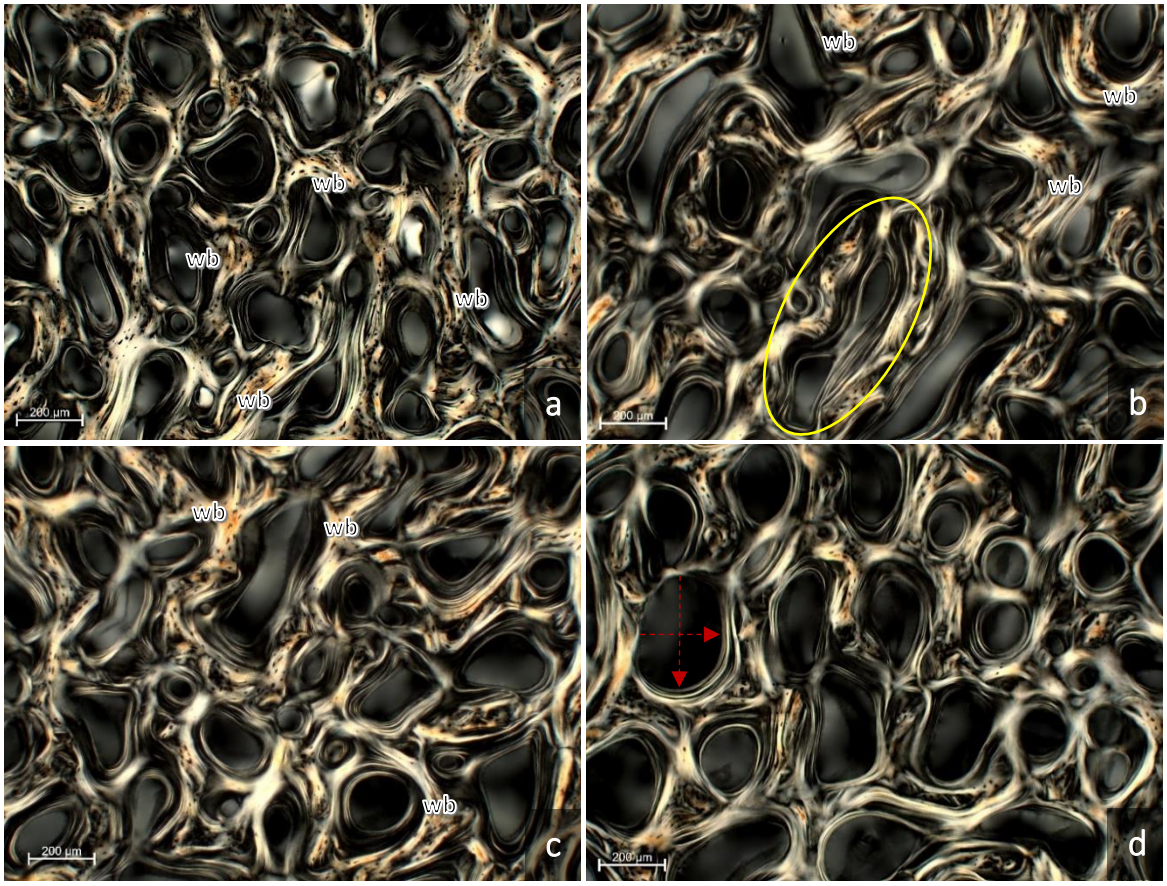

Figure 45. Ground section of red deer antler at velvet shedding, segment 1, transverse section, mineralized, epoxy-resin embedded, unstained sample, Axio Imager M2 (CPL).

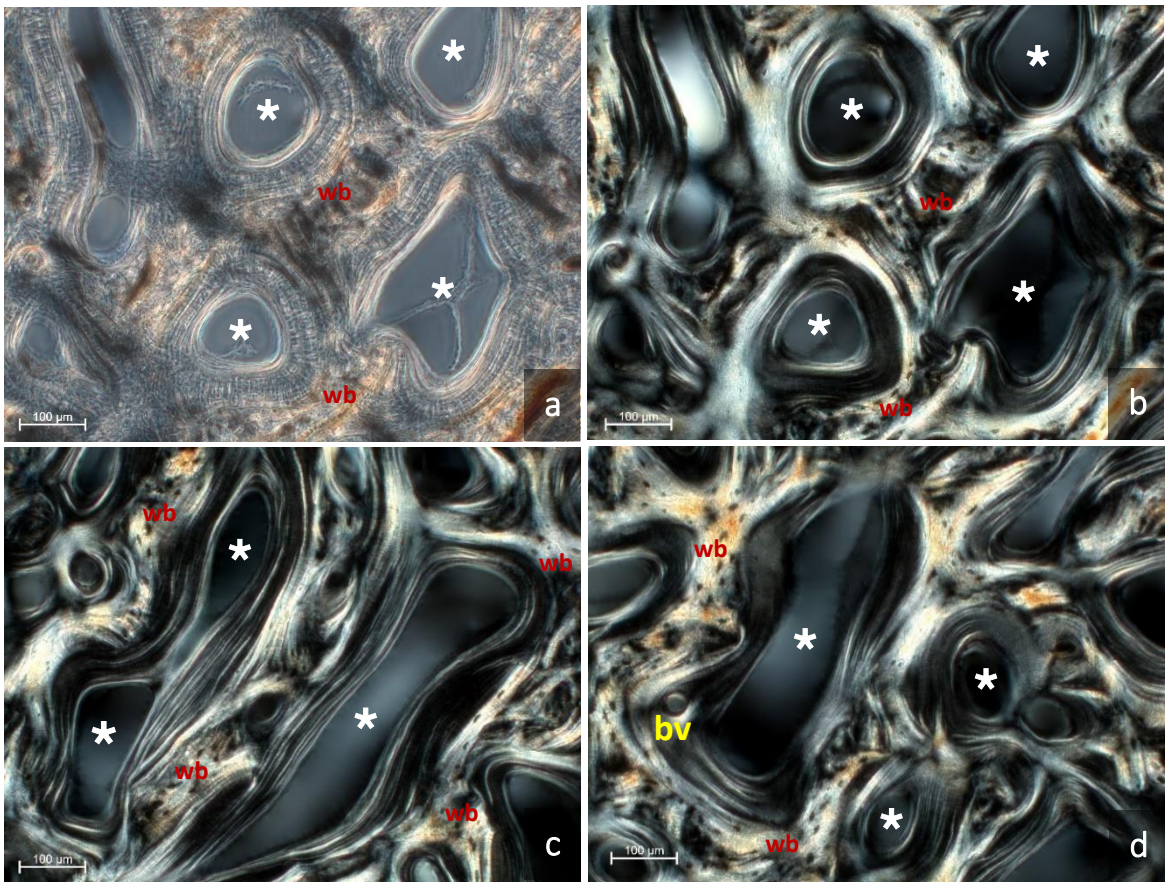

Figure 46. Ground section of red deer antlers at velvet shedding, segment 1, transverse section, mineralized, epoxy-resin embedded, unstained sample, Axio Imager M2 (**a** – PHACO; **b**, **c**, **d** – CPL).

In Figure 45, the bone framework is composed mostly of lamellar bone with varying fiber orientation. In places, remnants of woven bone are visible. Lamellar infilling is present. In Figure 45b, multicanaled primary osteon, and infilling in two different directions are visible. Toward the antler center, vascular spaces become wider (Fig. 45d). In Figure 46, vascular spaces are surrounded by lamellar bone, however, woven bone is present in central trabecular areas.

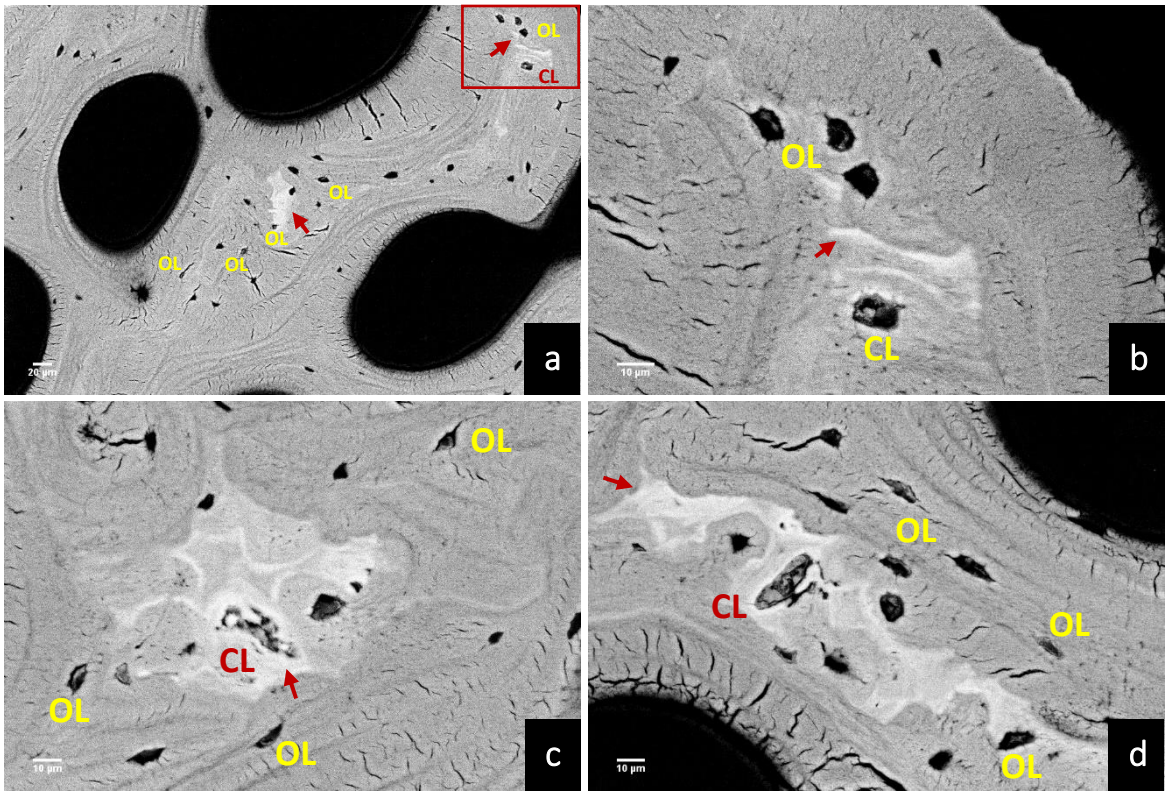

Figure 47. Polished surfaces of red deer antlers at velvet shedding, segment 1, transverse section, mineralized, epoxy-resin embedded, unstained sample, SEM-BSE.

In Figure 47, small amounts of calcified cartilage remnants are present. The border of the calcified cartilage is eroded (cartilage resorption). Mineralized deposits in chondrocyte and osteocyte lacunae are observed. Figure 47b shows area in red rectangle of Figure 47a at a higher magnification.

5.2.3. Hard antlers (HA)

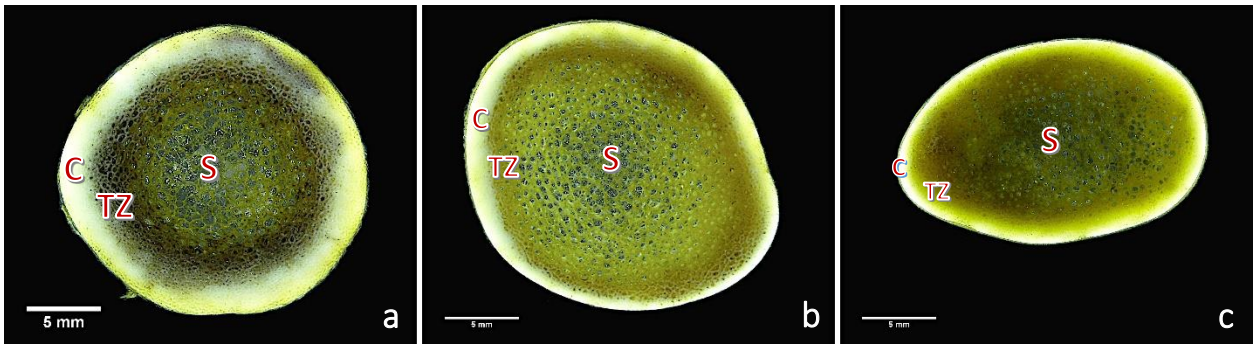

Figure 48. Transverse section of red deer hard antlers: **a)** Segment 1, **b)** Segment 2, **c)** Segment 3. Mineralized, epoxy-resin embedded samples, Keyence VHX 500 (reflected light images of polished block surfaces).

Figure 48 shows a microscopical view of different antler segments. Cortex, transitional zone and trabecular zone are visible.

5.2.3.1. Segment 3 (HA)

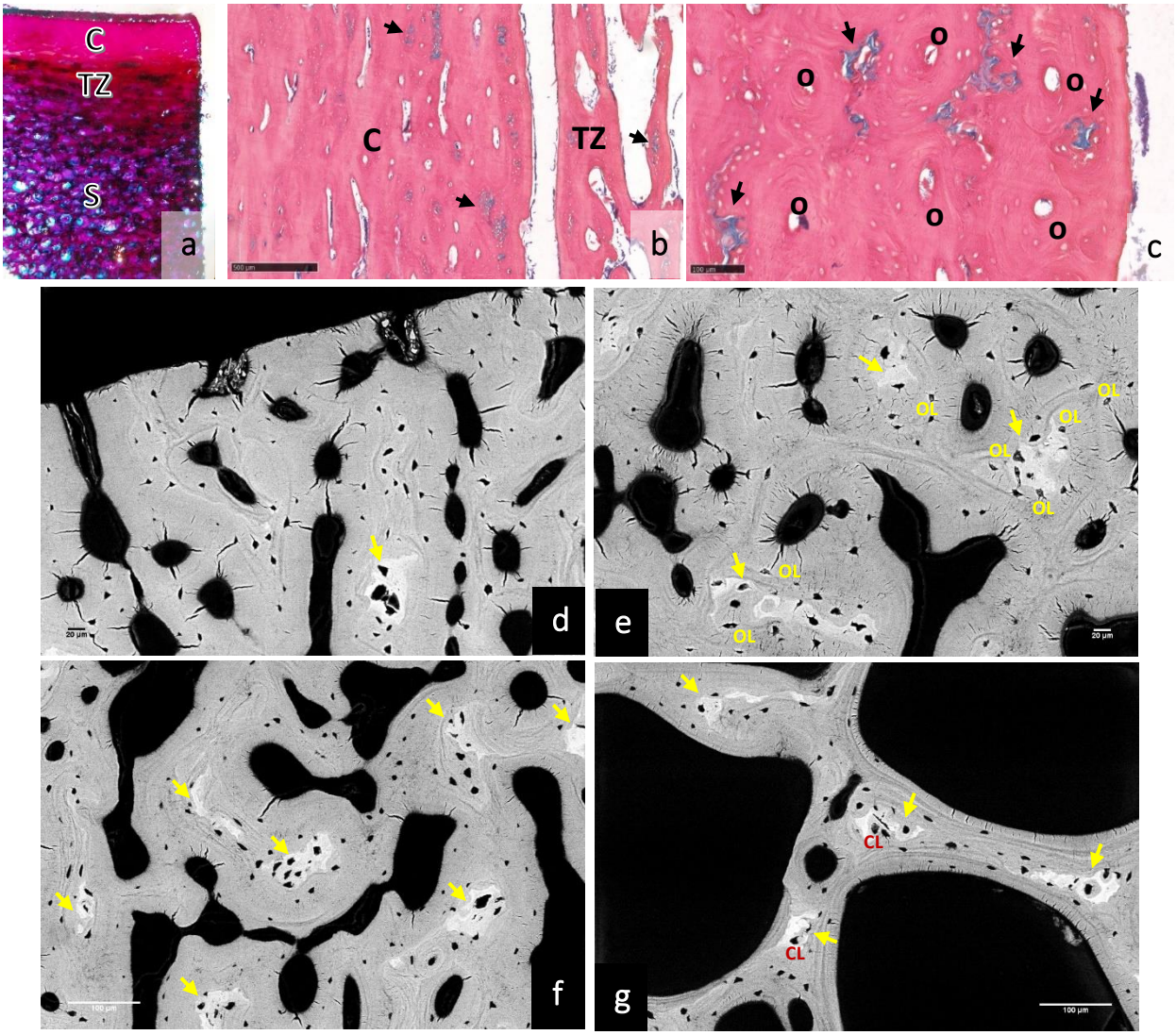

Figure 49. Red deer hard antlers, segment 3: **a)** Longitudinal section, mineralized, unembedded sample, ABARS; **b)**, **c)** Longitudinal section, demineralized, paraffin embedded samples, MSOP, NanoZoomer 2.0RS; **d)**, **e)**, **f)**, **g)** Polished surfaces, transverse section, mineralized, epoxy-resin embedded, unstained sample, SEM-BSE.

In Figure 49, different antler zones are visible: cortex (Fig. 49a, 49b, 49c, 49d, 49e), transitional zone (Fig. 49a, 49b, 49f), and trabecular zone (Fig. 49a, 49g). At the antler surface,

open vascular canals (cut osteons) can be observed (Fig. 49d), which indicates removal of an outer layer of bone during velvet shedding or later when the antlers were used for sparring, fighting or other purposes by the stags. Osteons can be seen in antler cortex. In each antler zone, areas with remnants of calcified cartilage are present. Osteocyte and chondrocyte lacunae are mostly empty.

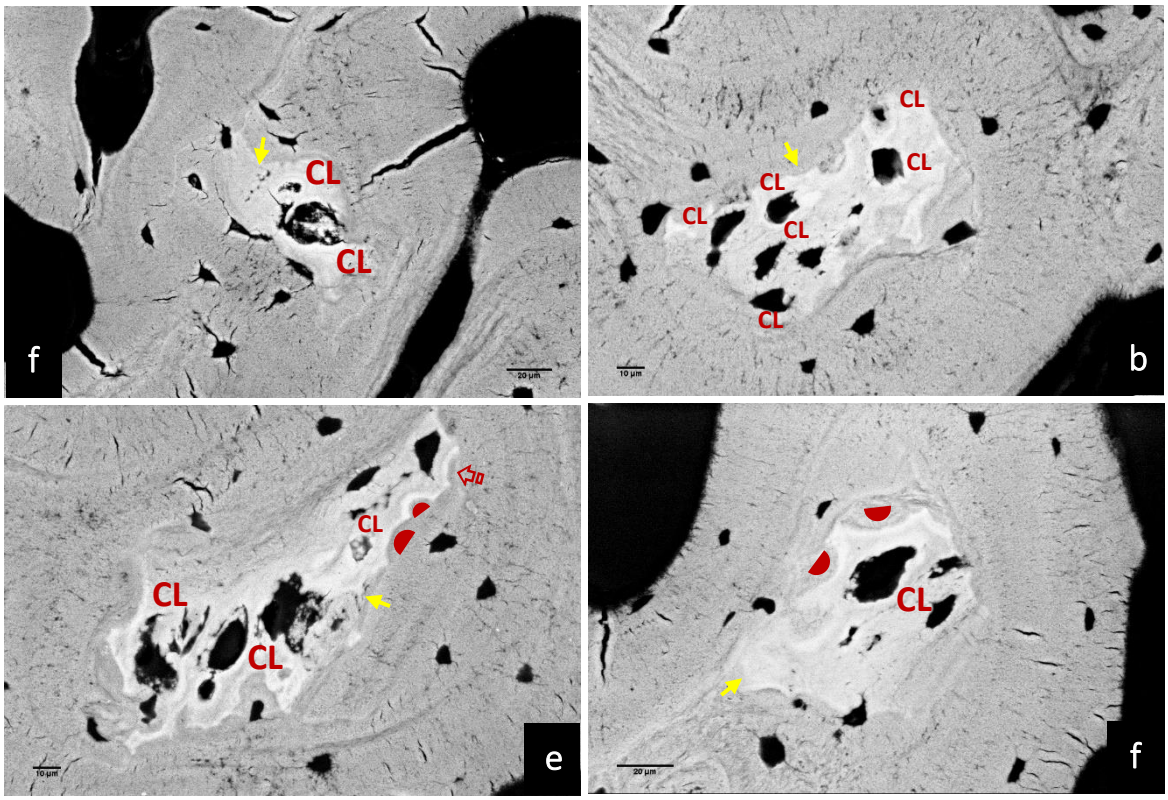

Figure 50. Polished surfaces of red deer hard antlers, segment 3, transverse section, mineralized, epoxy-resin embedded, unstained sample, SEM-BSE.

In areas of calcified cartilage remnants, chondrocyte lacunae are filled with mineral deposits to different extents (Fig. 50).

5.2.3.2. Segment 2 (HA)

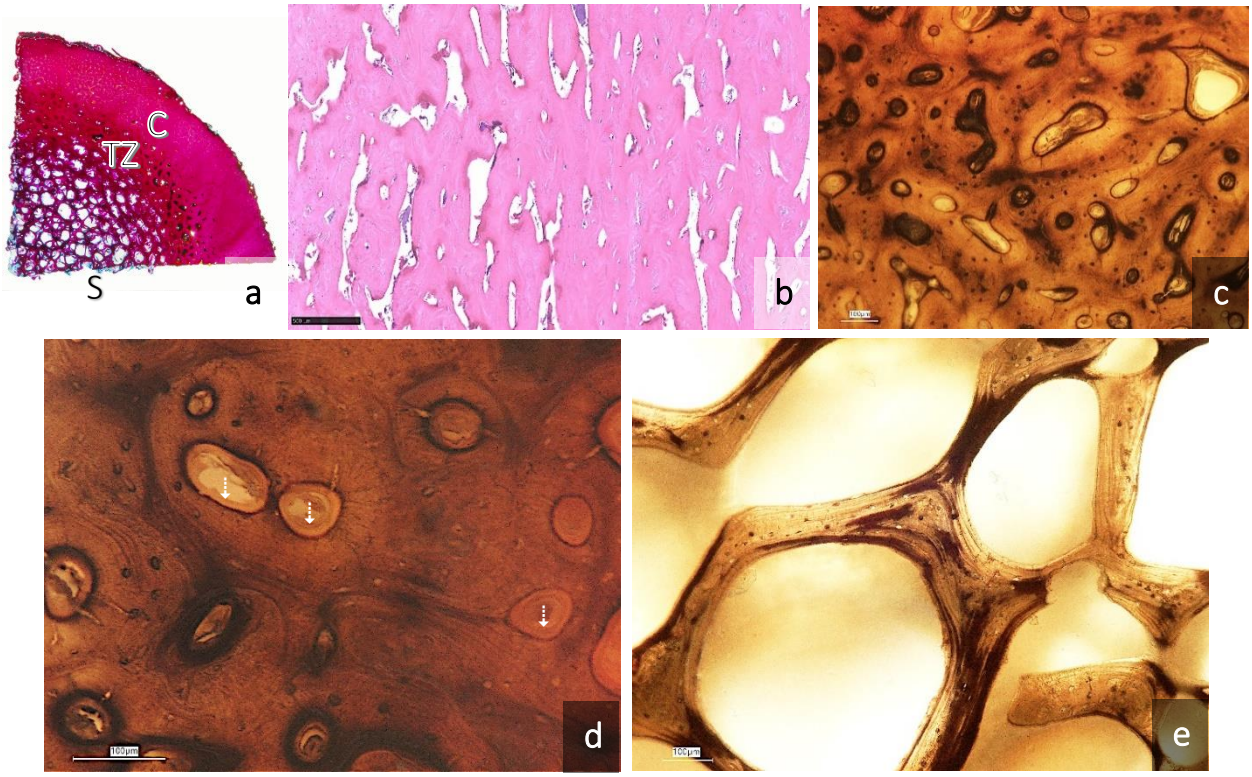

Figure 51. Red deer hard antlers, segment 2: **a)** Transverse section, mineralized, unembedded sample, ABARS; **b)** Longitudinal section, demineralized, paraffin embedded samples, MSOP, NanoZoomer 2.0RS; **c)**, **d)**, **e)** Transverse sections, mineralized, epoxy-resin embedded, VK, (Keyence VHX 7000).

In Figure 51a, different antler zones are visible. There are almost no areas with remnants of calcified cartilage (Fig. 51b). In Figures 51c, 51d and 51e, darker and lighter bony areas are present. An osteoid seam is observed inside the vascular canals (Fig. 51d).

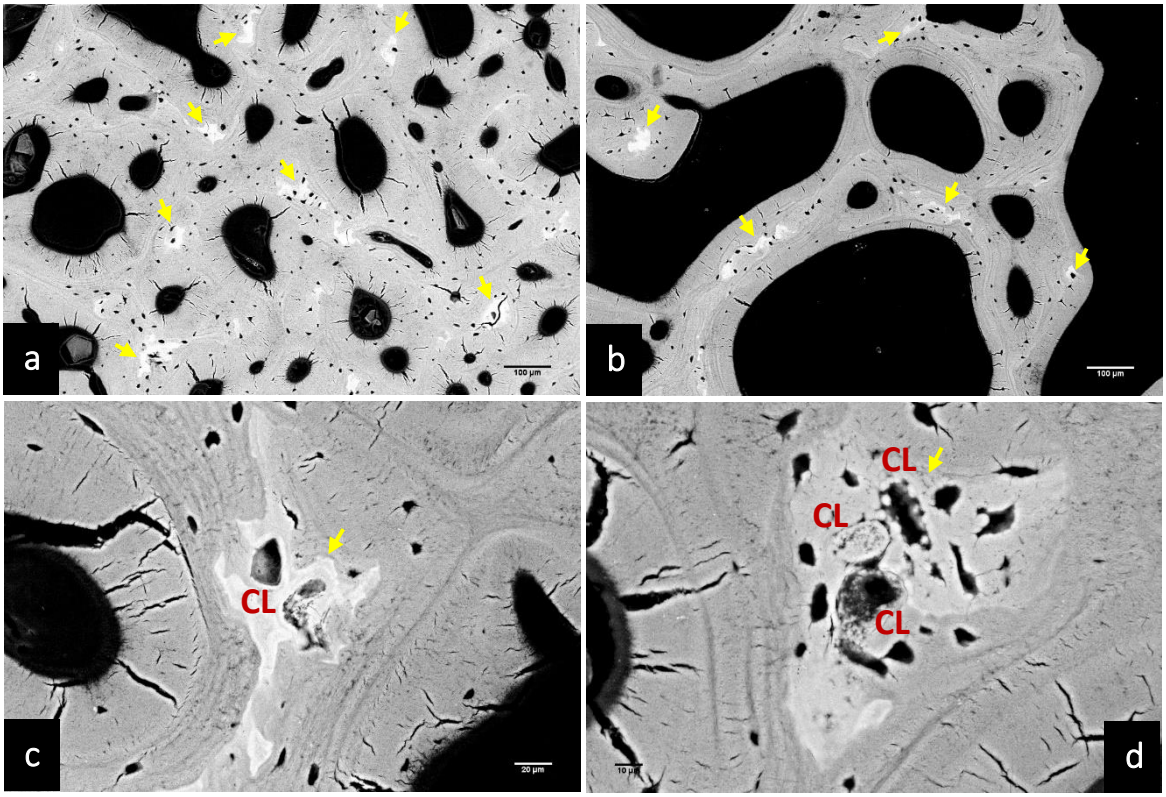

Figure 52. Polished surfaces of red deer hard antlers, segment 2, transverse section, mineralized, epoxy-resin embedded, unstained sample, SEM-BSE.

Figures 52a and 52b shows antler cortical and trabecular zones. Areas with remnants of calcified cartilage are present. In Figures 52c and 52d, mineral deposits in chondrocyte lacunae are visible. Bone canals (*canaliculi ossei*), through which osteocyte cytoplasmic processes extend, emanating from osteocyte lacunae are presented in Fig. 52d.

5.2.3.3. Segment 1 (HA)

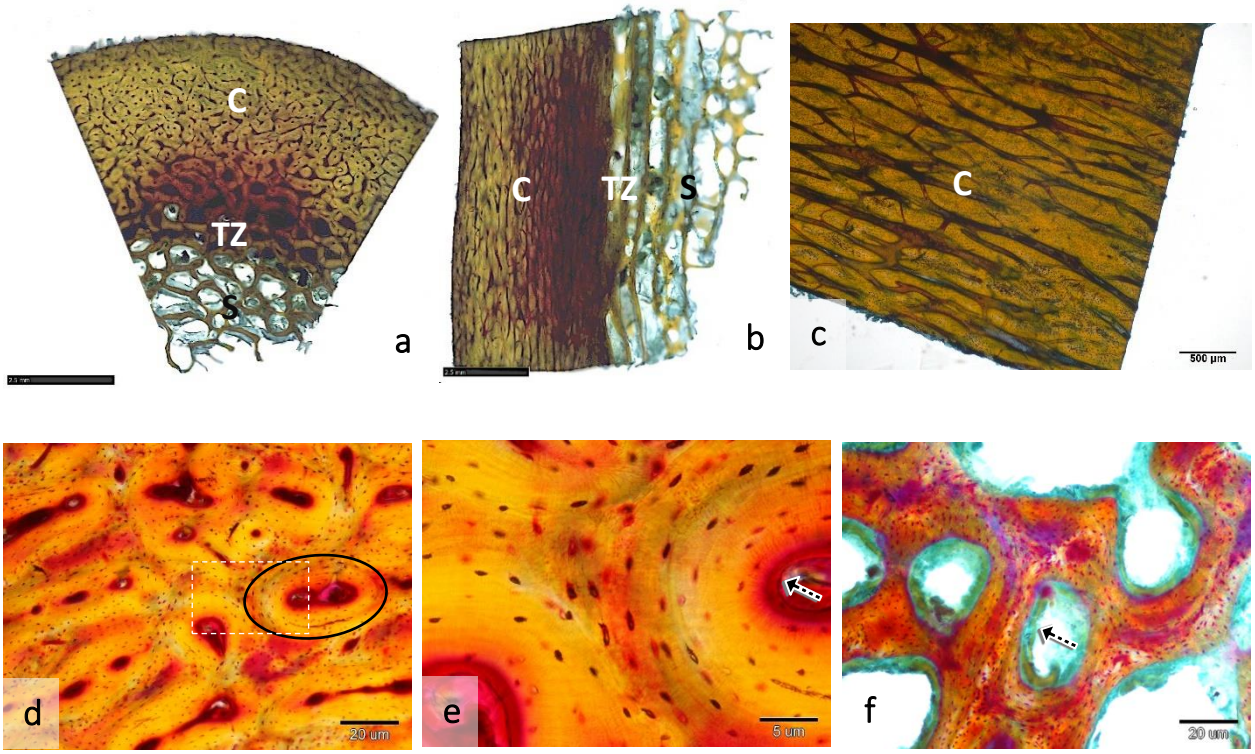

Figure 53. Red deer hard antlers, segment 1: Transverse (**a**, **d**, **e**, **f**) and longitudinal (**b**, **c**) sections, mineralized, unembedded samples, VTBS, (**a**, **b** – NanoZoomer 2.0RS; **c** - Digicyte DX50; **d**, **e**, **f** – Olympus BX41).

Figure 53 shows two different sections, each containing different antler zones. In Figures 53a and 53b, cortex, transitional zone and trabecular zone are visible. Figures 53c, 53d and 53e shows antler cortex, while trabecular zone is present in Figure 53f. The Haversian canals are straight, long and parallel to the longitudinal axis of the antler. The Volkmann's canals run perpendicular to the Haversian canals (Fig. 53c). Cortex contains osteons, some of which are multicanaled (Fig. 53d). Figure 53e shows area in white rectangle of Figure 53d at a higher magnification. In Figure 53e, bone canals (*canaliculi ossei*) can be observed. Along their internal border, the osteons are lined with osteoid seams (unmineralized bone matrix) (red areas), which is also observed around bone trabeculae (green areas) (Fig. 53f).

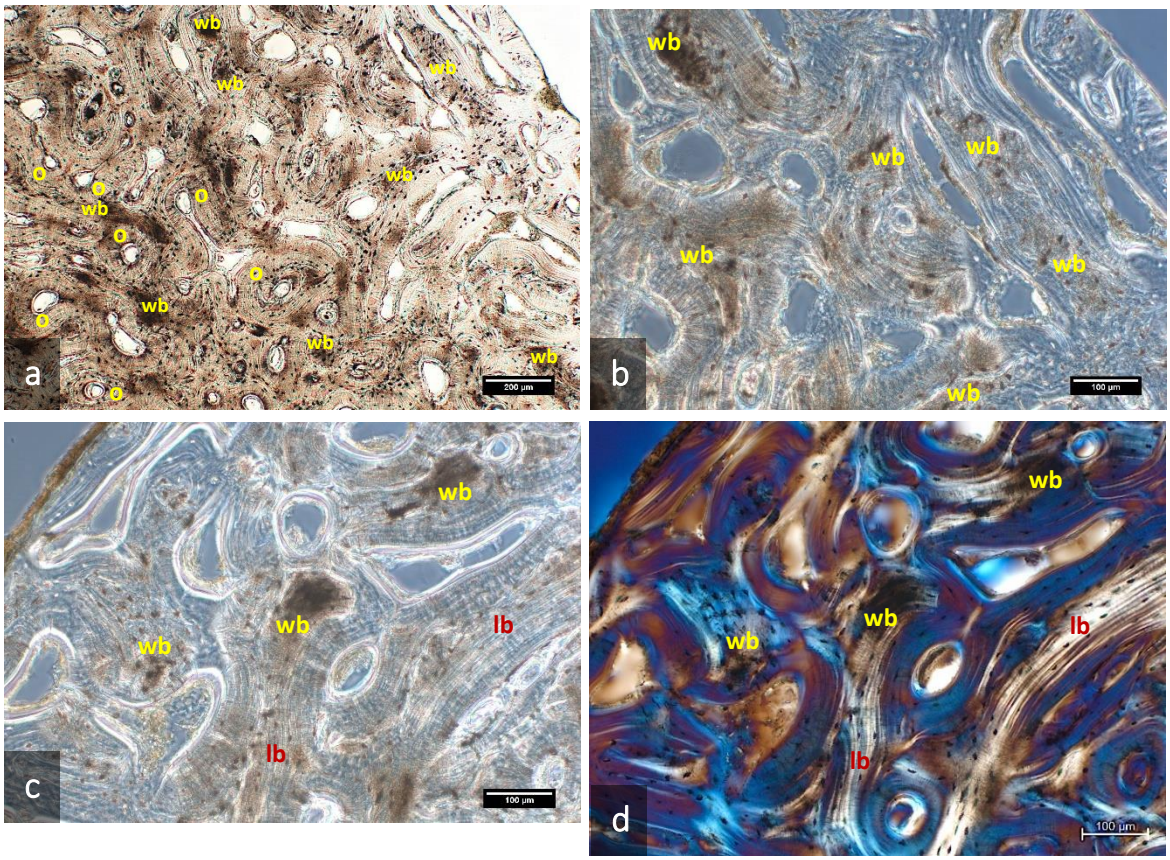

Figure 54. Ground section of red deer hard antlers, segment 1, transverse section, mineralized, epoxy-resin embedded, unstained sample, Axio Imager M2 (**a** – TL; **b**, **c** – PHACO; **d** – CPL + 1λ).

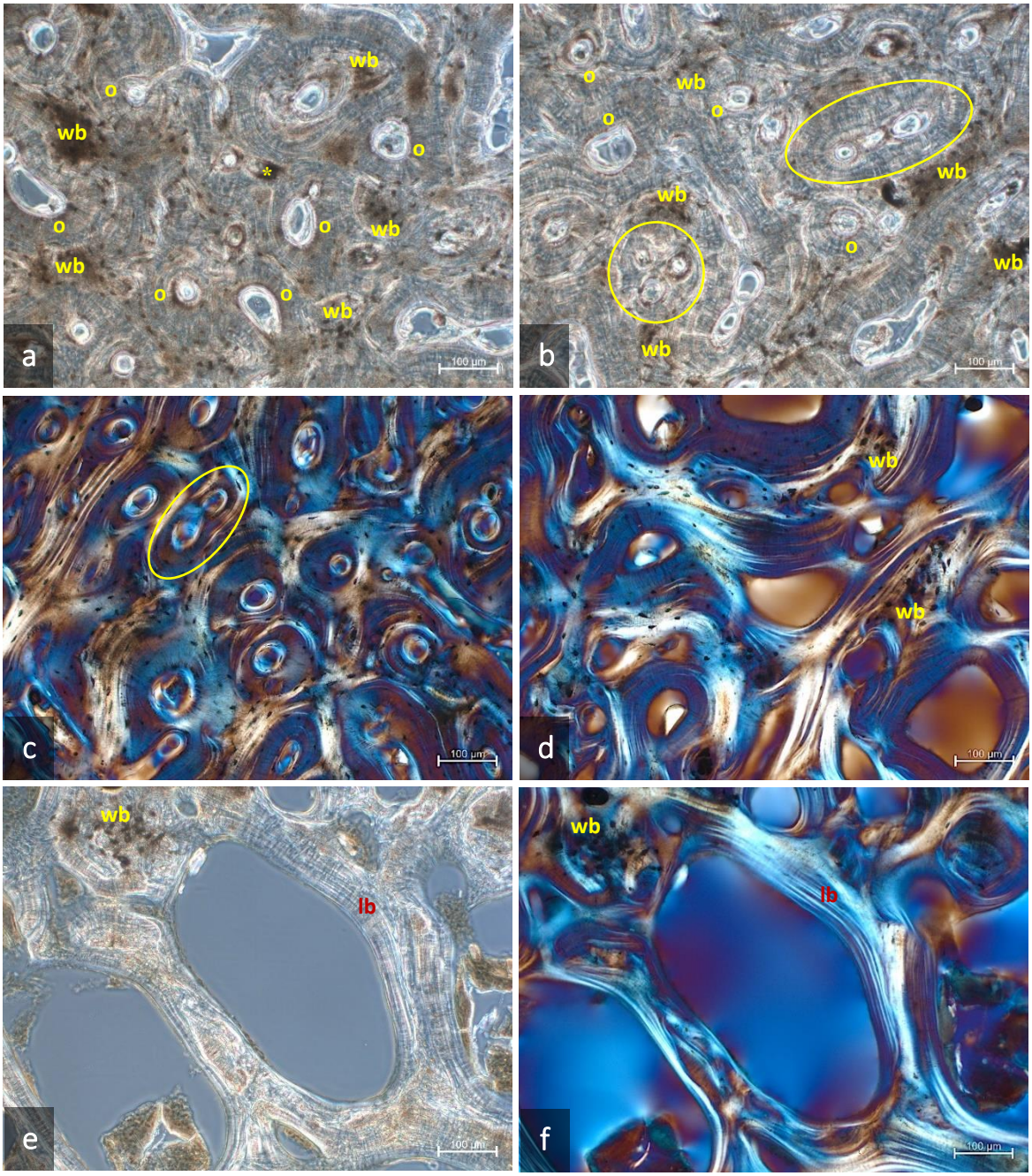

Figure 55. Ground section of red deer hard antlers, segment 1, transverse section, mineralized, epoxy-resin embedded, unstained sample, Axio Imager M2 (**a**, **b**, **e** – PHACO; **c**, **d**, **f** – CPL + 1λ).

In Figure 54, the antler surface and cortex are shown. In Figures 55a, 55b and 55c, the antler cortex, the transitional zone in Figure 55d and the trabecular zone in Figures 55e and 55f are shown. Antler cortex contains osteons (Fig. 54a, 55a, 55b, 55c), which are lined inside with osteoid (Fig. 54c, 55a, 55b). Osteon clusters are visible (Fig. 55b, 55c). The difference between lamellar and woven bone is observed (Fig. 54c, 54d, 55e, 55f). Osteons are internally lined with unmineralized bone matrix (osteoid) (Fig. 54b, 54c, 55a, 55b).

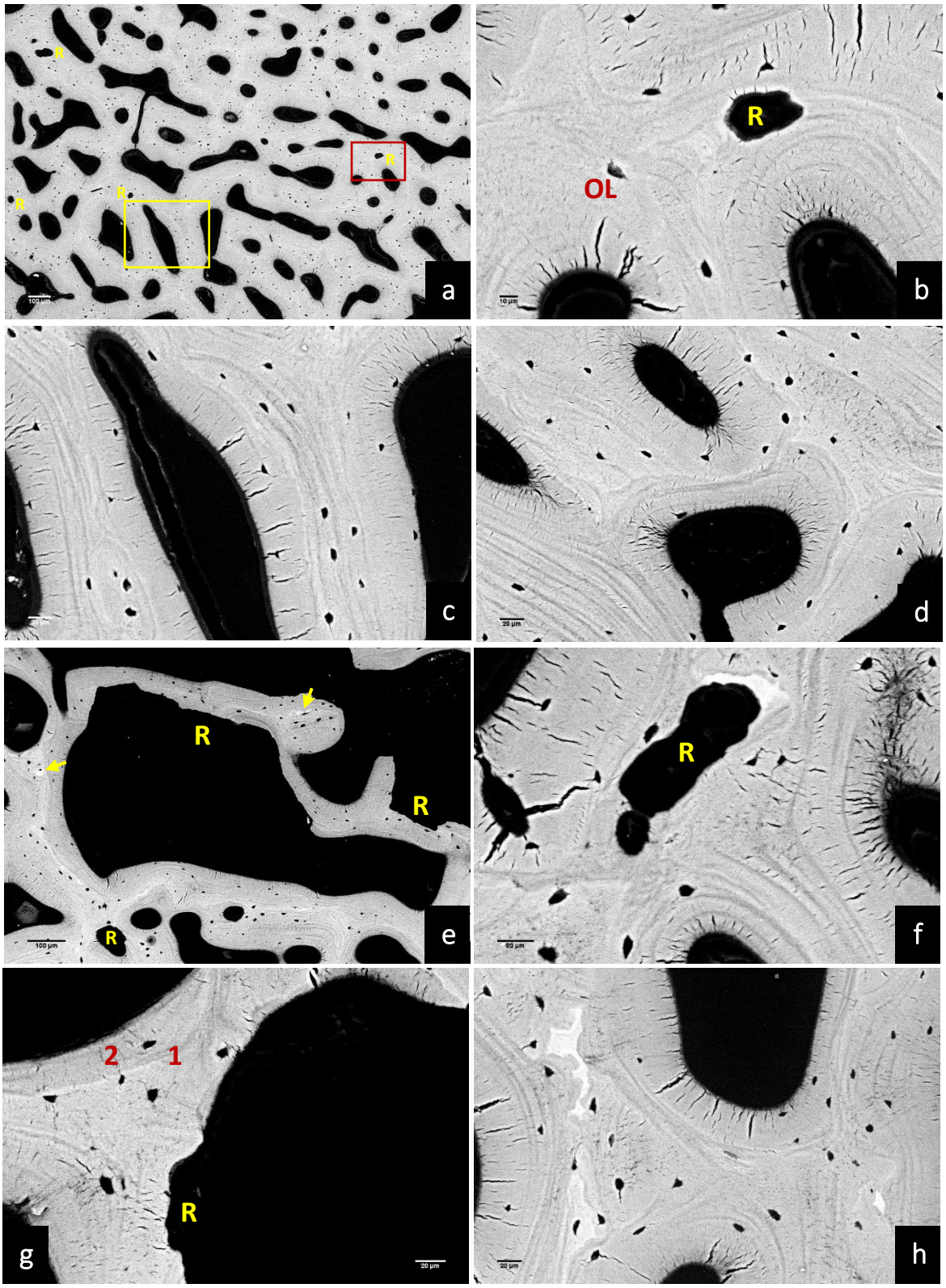

Figure 56. Polished surfaces of red deer hard antlers, segment 1, transverse section, mineralized, epoxy-resin embedded, unstained sample, SEM-BSE.

In Figure 56, there are almost no areas of calcified cartilage. Areas marked with the rectangles in Figure 56a are shown at a higher magnification in Figure 56b (red rectangle) and Figure 56c (yellow rectangle). Even at lower magnification, reversal lines, which are faintly hypermineralized, are visible (Fig. 56a, 56b, 56d). In some areas, bone resorption cavities are observed (Fig. 56b, 56e, 56g). Resorption of the last part of the cartilage matrix is less pronounced in the lamellar part, while it is larger in the scaffold (Fig. 56f). Figure 56h shows part of an old scaffold onto which lamellar (primary osteonal) bone has been deposited. In Figure 56b, one osteocyte lacuna is visible that appears to contain some mineral. In Figure 56g, the image indicates that an initial phase of resorption (demonstrated by a reversal line [1]) was followed by bone deposition [2]. The newly-formed bone [2] is somewhat less mineralized (darker) than the older (brighter) bone.

5.2.4. Cast antlers (CA)

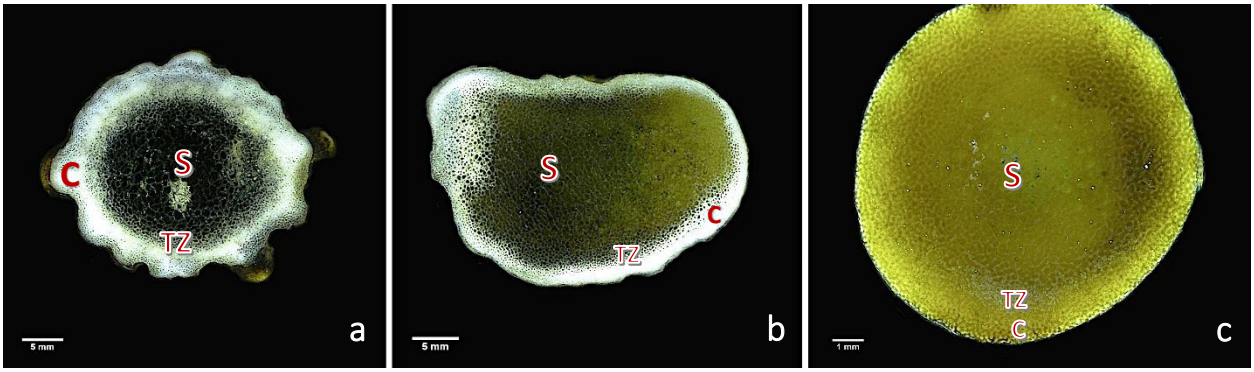

Figure 57. Transverse section of red deer cast antlers: **a)** Segment 1, **b)** Segment 2, **c)** Segment 3. Mineralized, epoxy-resin embedded, unstained samples, Keyence VHX 500 (reflected light images of polished block surfaces).

In Figure 57, different antler zones are visible: cortex, transitional zone, and trabecular zone. In segment 3, it is hard to distinguish cortex and transitional zone.

5.2.4.1. Segment 3 (CA)

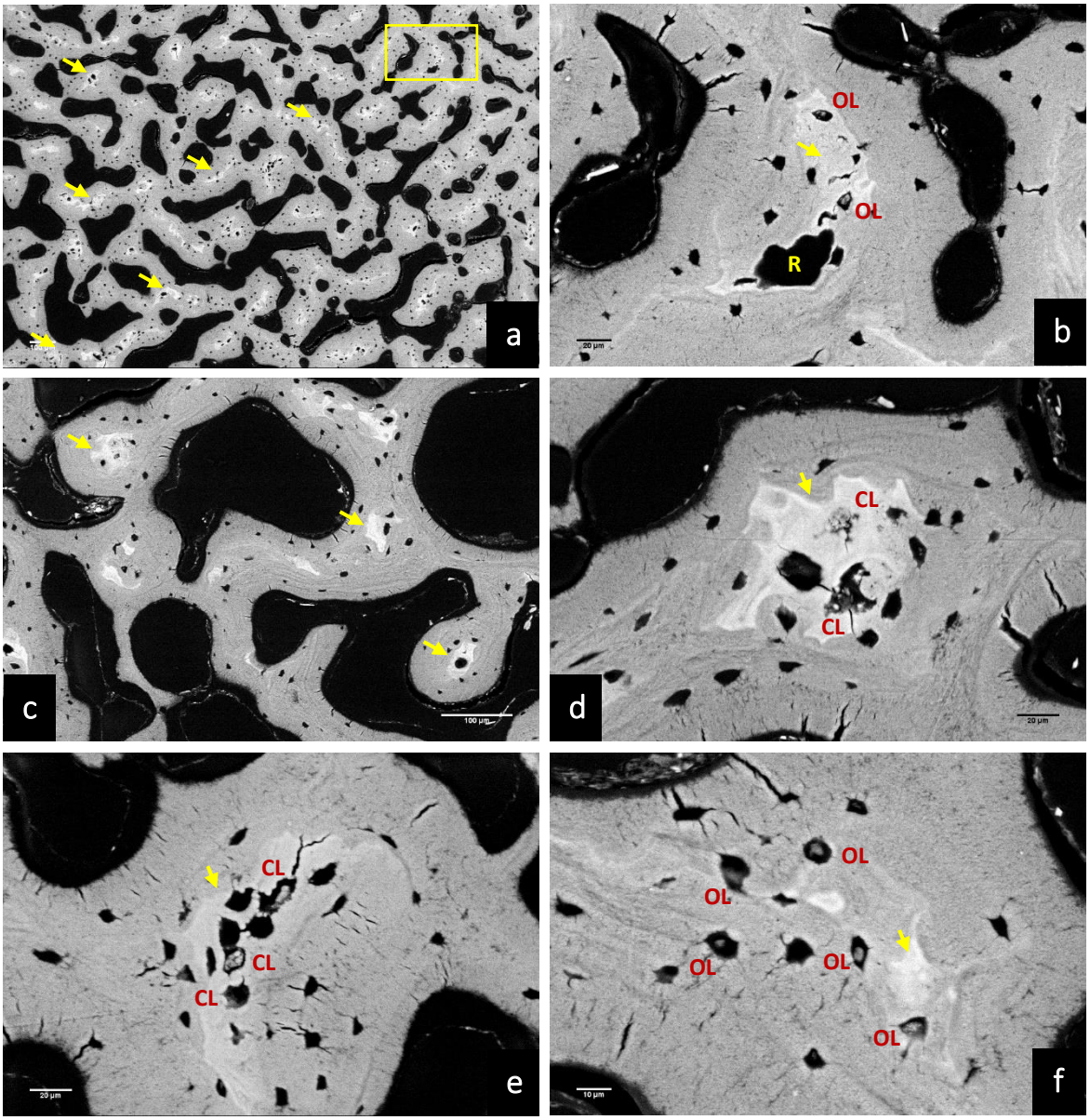

Figure 58. Polished surfaces of red deer cast antlers, segment 3, transverse section, mineralized, epoxy-resin embedded, unstained sample, SEM-BSE.

Larger amounts of calcified cartilage remnants are present in Figure 58a. Figure 58b shows area in yellow rectangle of Figure 58a at a higher magnification. A resorption cavity from former chondroclastic activity is visible in Figure 58b. There are chondrocyte and osteocyte lacunae filled with mineral deposits (Fig. 58b, 58d, 58e, 58f). Some chondrocyte lacunae are partially filled with minerals, while others are almost completely occluded (Fig. 58d).

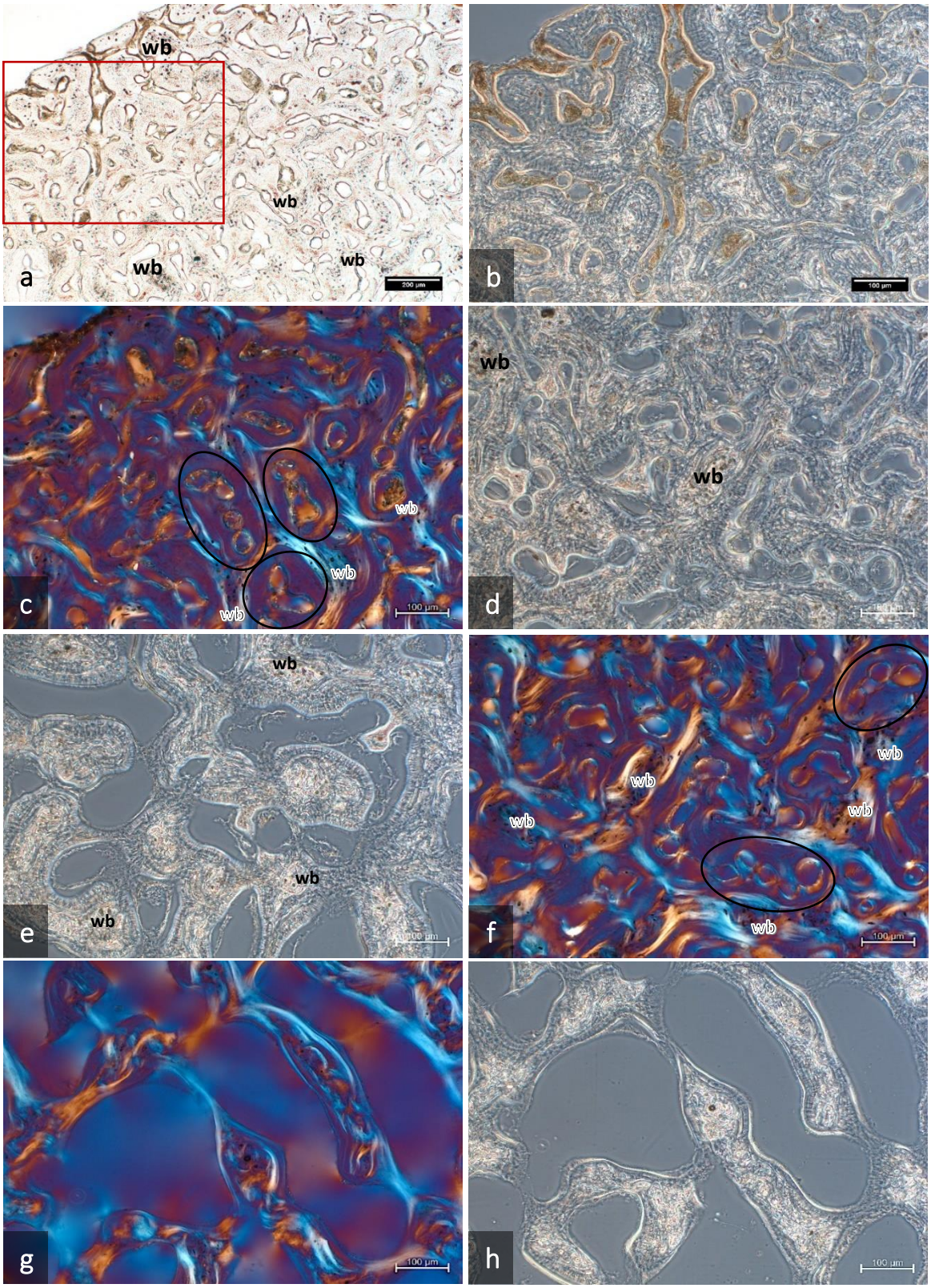

Figure 59. Ground section of red deer cast antlers, segment 3, transverse section, mineralized, epoxy-resin embedded, unstained sample, Axio Imager M2 (**a** – bright field; **b**, **d**, **e**, **h** – PHACO; **c**, **f**, **g** – CPL + 1λ).

In Figure 59, antler surface and cortex (Fig. 59a, 59b, 59c, 59d, 59f), transitional zone (Fig. 59e) and trabecular zone (Fig. 59g, 59h) are shown. Figure 59b shows area in red rectangle of Figure 59a at a higher magnification. It is visible that vascular canals are opened on the antler surface (Fig. 59a, 59b). Multicanaled osteons are present in the cortex (Fig. 59c, 59f). The antler consists predominantly of lamellar bone, with woven bone present only in smaller regions.

5.2.4.2. Segment 2 (CA)

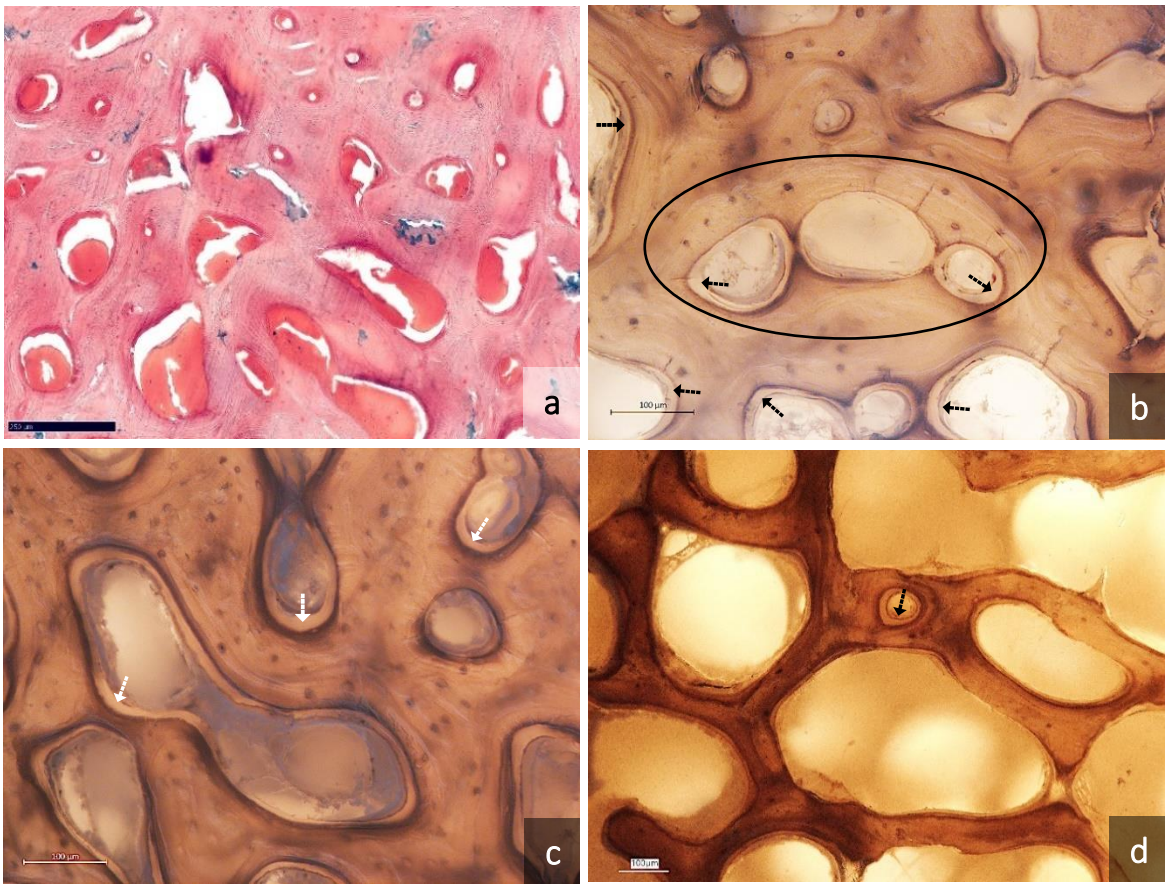

Figure 60. Red deer cast antlers, segment 2: **a)** Transverse section, demineralized, paraffin embedded samples, HE, NanoZoomer 2.0RS; **b)**, **c)**, **d)**, Transverse sections, mineralized, epoxy-resin embedded, VK, (**b**, **c** – Axioskop, 2Plus; **d** – Keyence VHX 7000).

In Figure 60, the antler cortex (Fig. 60a) and trabecular zone (Fig. 60d) are shown. Cortical vascular spaces are filled with residual blood. Areas of mineralized cartilage (blue) are visible (Fig. 60a). Multicanaled osteon is visible (Fig. 60b). Darker areas represent newly-formed bone,

while lighter areas are older bone. Osteons inside are lined with unmineralized bone matrix (osteoid) (Fig. 60b, 60c, 60d).

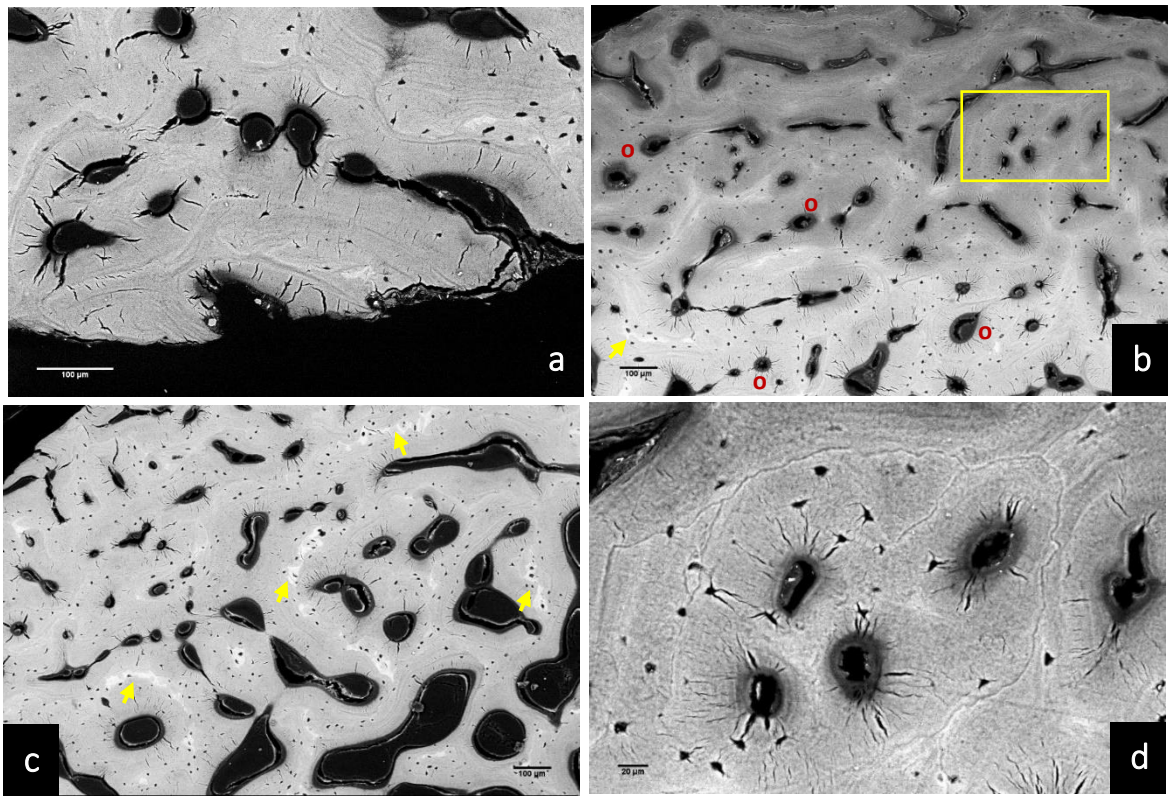

Figure 61. Polished surfaces of red deer cast antlers, segment 2, transverse section, mineralized, epoxy-resin embedded, unstained sample, SEM-BSE.

Figure 61 shows the antler surface and cortex. The surface is eroded and vascular canals are opened (Fig. 61a). Osteon clusters are present (Fig. 61b, 61d). The cortex contains osteons and small amounts of calcified cartilage remnants. Inside the osteons is an unmineralized bone matrix (osteoid). Figure 61d shows area in yellow rectangle of Figure 61b at a higher magnification.

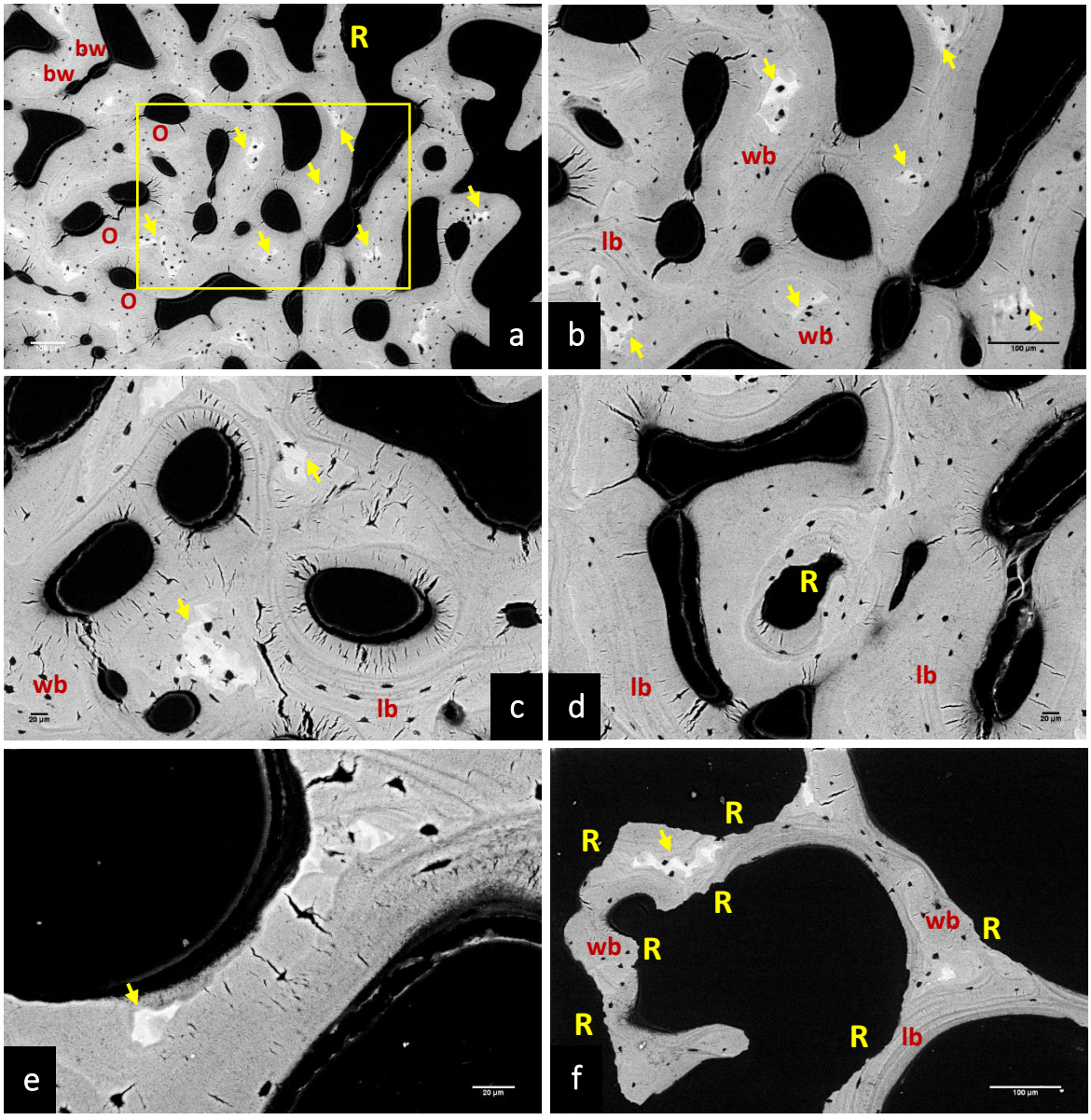

Figure 62. Polished surfaces of red deer cast antlers, segment 2, transverse section, mineralized, epoxy-resin embedded, unstained sample, SEM-BSE.

In Figure 62, areas of calcified cartilage remnants can be seen. There are not many areas showing bone resorption. Mostly there are primary osteons. Two vessels on the left side are visible (Fig. 62a). Figure 62b shows area in yellow rectangle of Figure 62a at a higher magnification. In Figure 62b, the bone surface is smooth, resorption cavities are not present. The difference between lamellar and woven bone is visible. Few osteocyte lacunae are located in lamellar bone, while more osteocyte lacunae are present in the scaffold of woven bone (Fig. 62b, 62c, 62d). While the resorption area is on one side of the vascular space, on the opposite side is a reversal line, as well as new bone formation (Fig. 62d). Trabecular zone is present in Figures 62e and 62f. Figure 62f

shows resorption areas, reversal lines, new lamellar bone and woven bone scaffold. Resorption cavities are present on both sides of trabecula, but there is no infilling.

5.2.4.3. Segment 1 (CA)

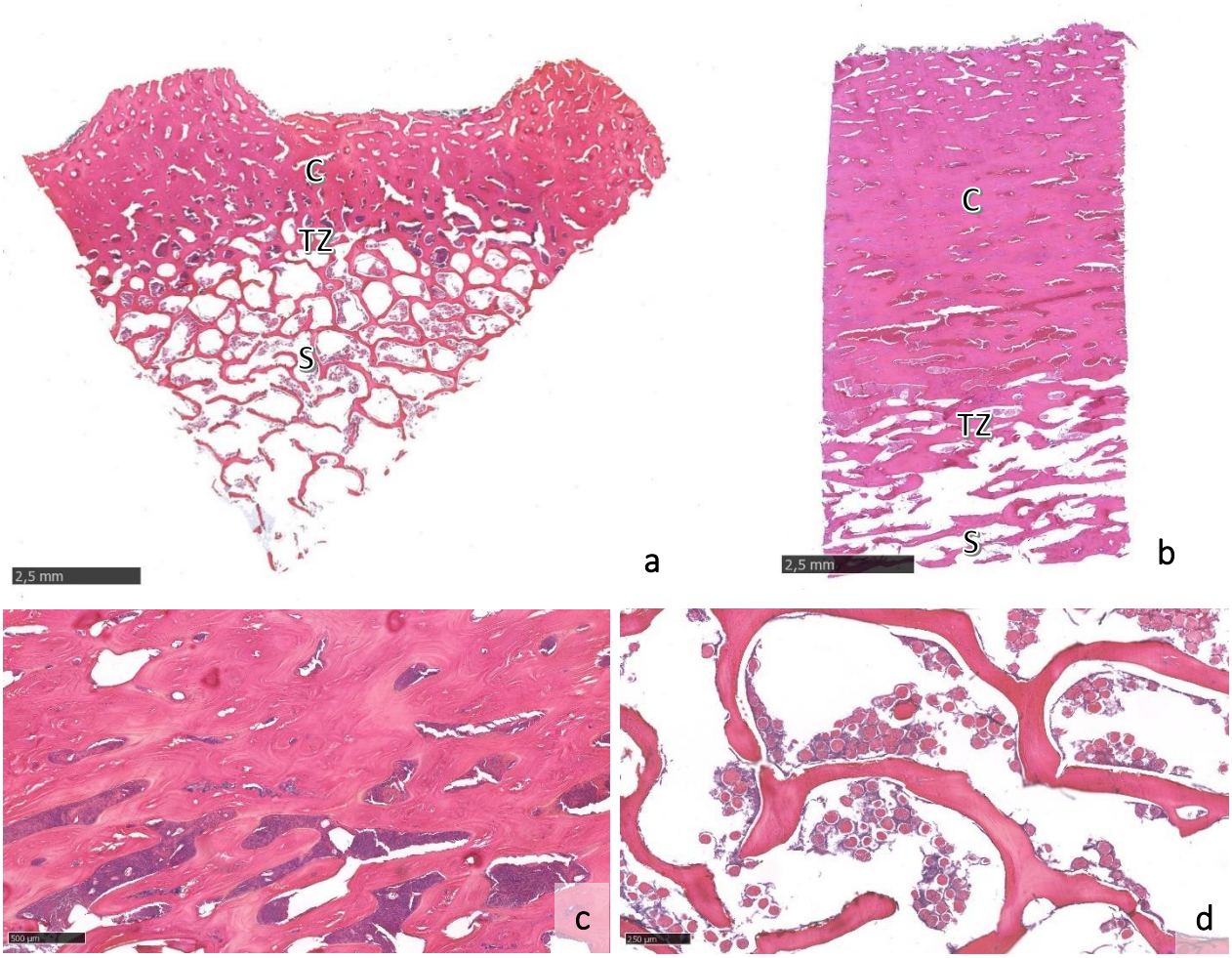

Figure 63. Red deer cast antlers, segment 1: **a), d)** Transverse sections; **b), c)** Longitudinal sections. Demineralized, paraffin embedded samples, HE, NanoZoomer 2.0RS.

In Figures 63a and 63b, different antler zones are visible in transverse and longitudinal sections. A few calcified cartilage remnants (blue areas) can be seen in the cortex, (Fig. 63c). Vascular spaces are filled with red or basophilic material (Fig. 63a, 63b, 63c). Round acidophilic structures surrounded with basophilic content are present in cavities of the trabecular part (Fig. 63d).

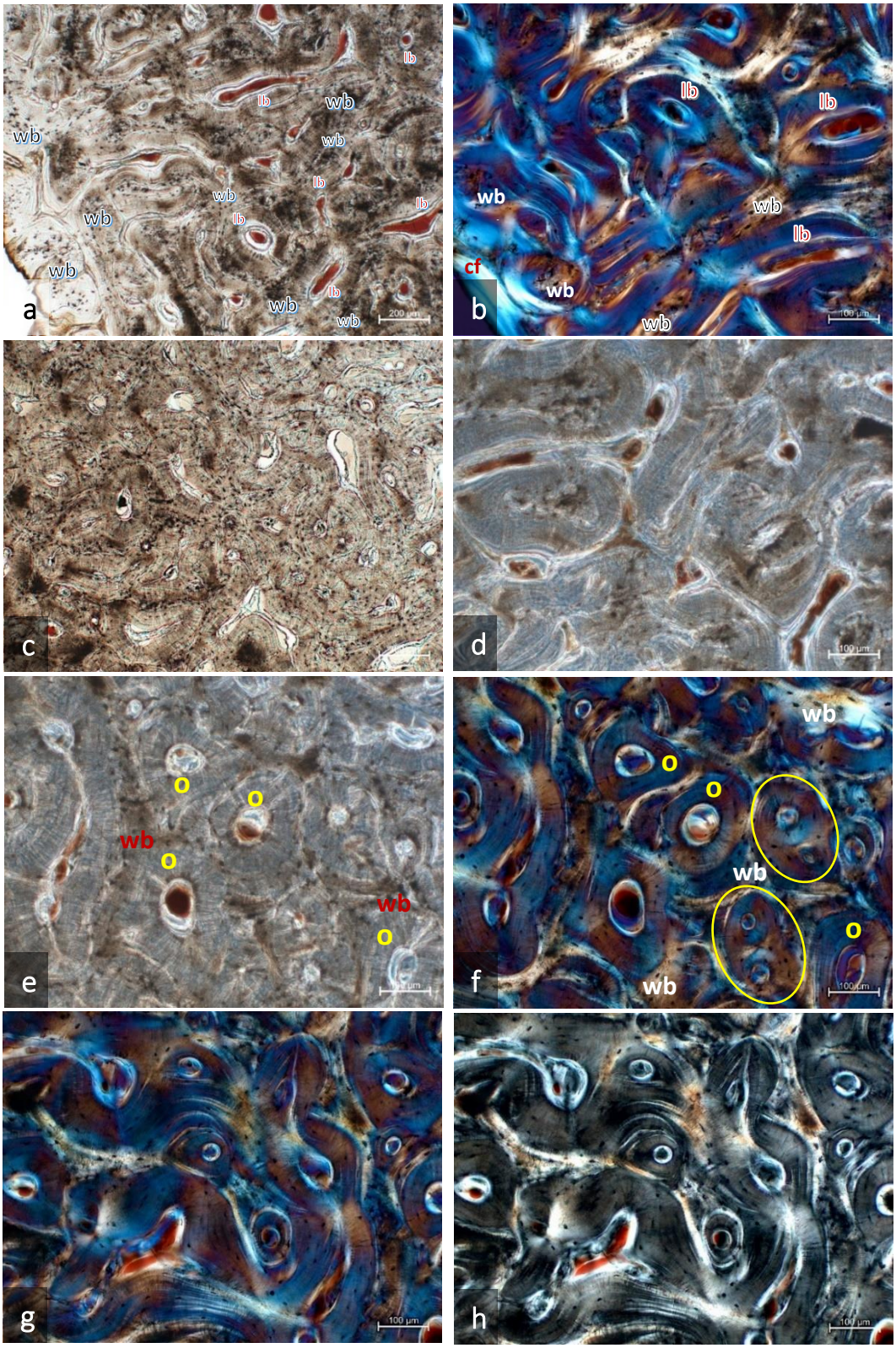

Figure 64. Ground section of red deer cast antlers, segment 1, transverse section, mineralized, epoxy-resin embedded, unstained sample, Axio Imager M2 (**a**, **c** – TL; **d**, **e** – PHACO; **b**, **f**, **g** – CPL + 1λ; **h** – CPL).

The antler periphery presented in Figures 64a and 64b is composed largely of woven bone, with single primary osteons more towards the interior. Vascular canals running in transverse directions (Volkmann's canals) are also present. Vascular spaces are filled with residual blood. Figure 64c is from a portion located more towards the interior (inner cortex), showing primary osteons within a framework of woven bone (visible in Fig. 64d and 64e as darker patches). The same applies to the other panels. In the CPL images, using the λ-plate, the yellowish-red and blue colors indicate different directions of the collagen fibers within the lamellae.

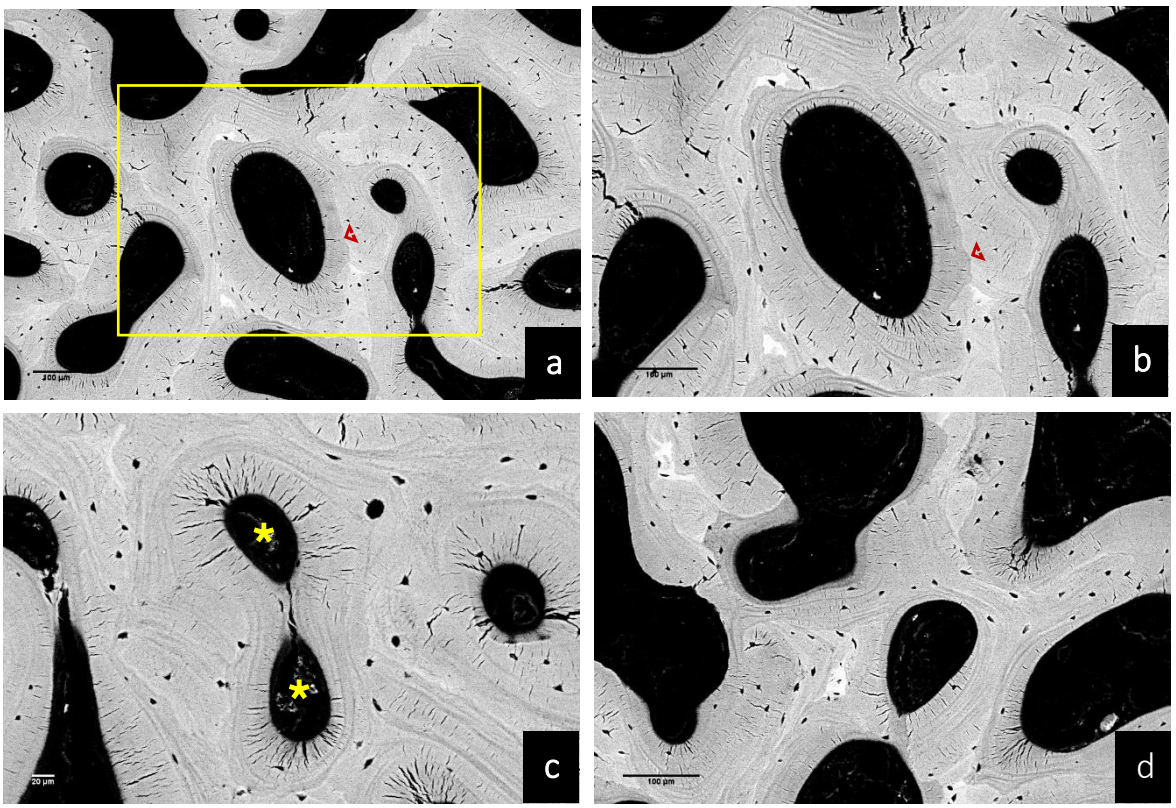

Figure 65. Polished surfaces of red deer cast antlers, segment 1, transverse section, mineralized, epoxy-resin embedded, unstained sample, SEM-BSE.

In Figures 65a and 65b, resorption lines are visible, and very small amount of calcified cartilage remnants. Figure 65b shows area in yellow rectangle of Figure 65a at a higher magnification. Bony lamellae separate two Haversian canals of one primary osteon (Fig. 65c). A mixture of older, more highly mineralized (brighter) and younger, less mineralized (darker) bone

areas with reversal lines appearing as particularly bright (relatively hypermineralized) thin lines, are visible in Figure 65d.

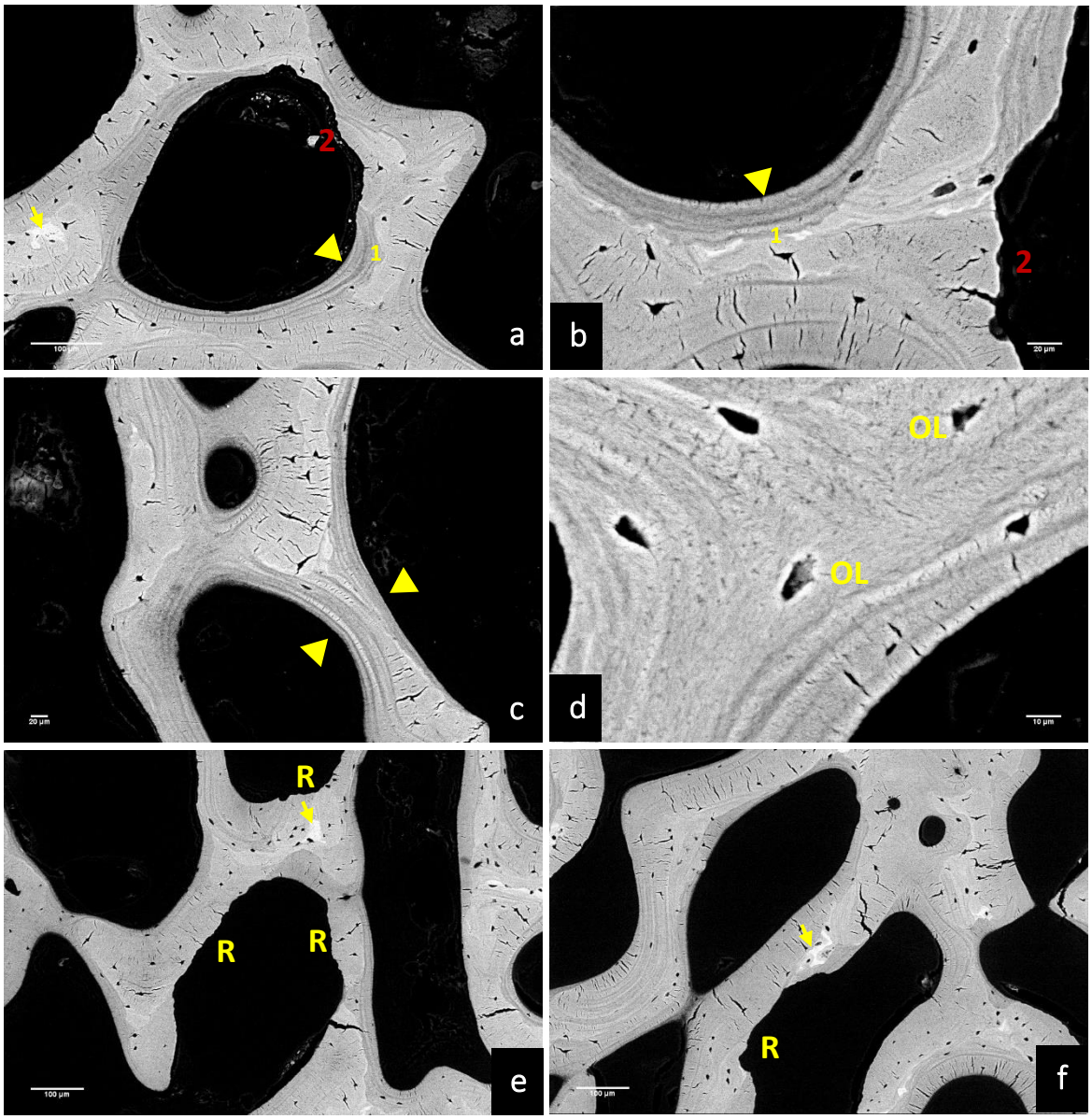

Figure 66. Polished surfaces of red deer cast antlers, segment 1, transverse section, mineralized, epoxy-resin embedded, unstained sample, SEM-BSE.

The first bone resorption cavity (1) has been filled before velvet shedding, while the second resorption cavity (2) is unfilled (Fig. 66a, 66b). In Figure 66c, resorption of the bony trabeculae occurred on both sides, which was later infilled with lamellar bone. There are some mineral deposits in osteocyte lacunae (Fig. 66d). Small areas of calcified cartilage are present (Fig. 66a, 66e, 66f).

5.2.5. Comparative view of antler segments using false-color SEM-BSE images

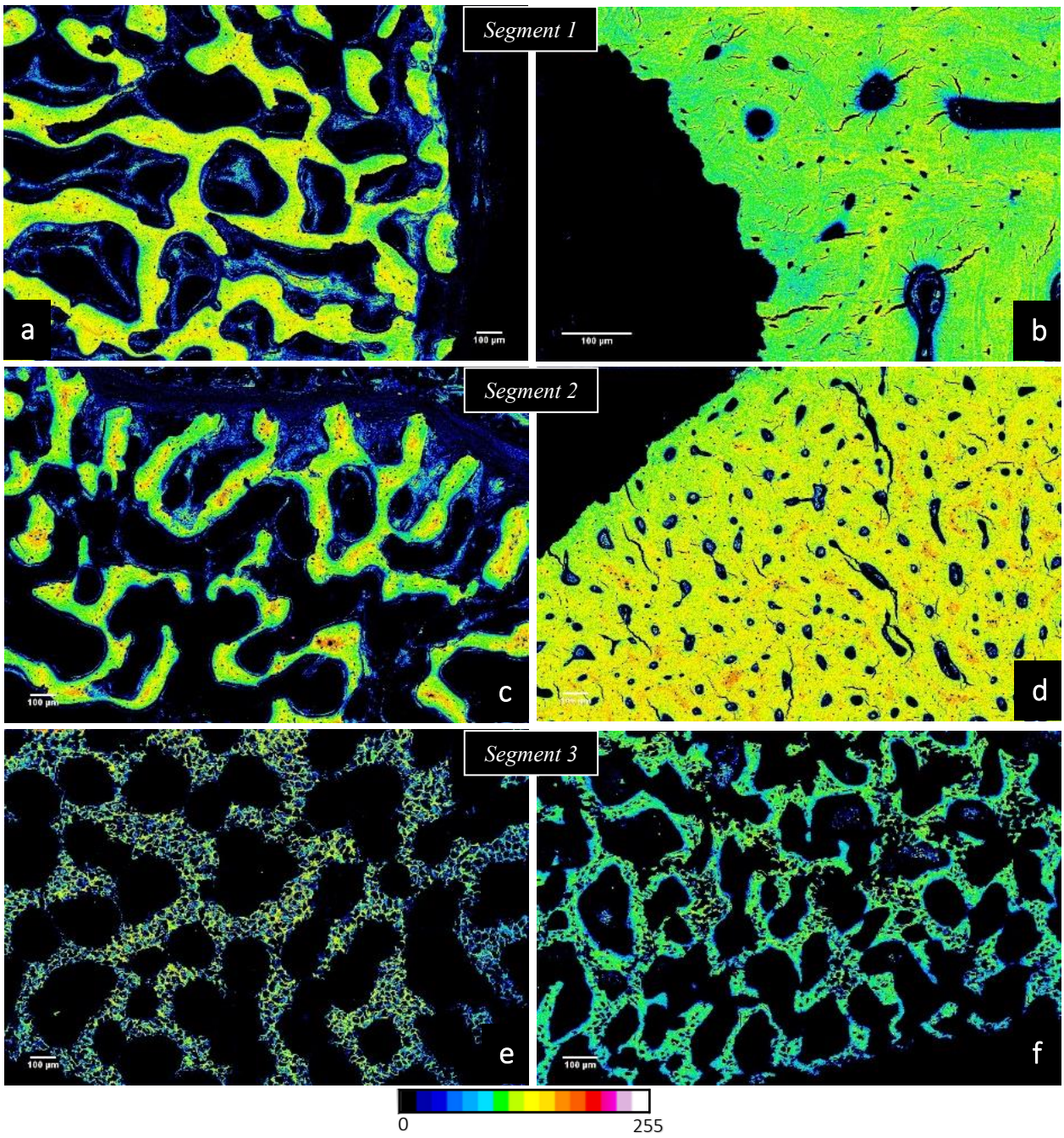

Figure 67. Pseudo-color SEM-BSE image of polished section surface of antler segments: **a)**, **c)**, **e)** Antlers in velvet; **b)**, **d)**, **f)** Antlers at velvet shedding. The 16 grey-level bands spanning the grey value range from 0 (black) to 255 (peak white) as indicated by the color bar below the figure.

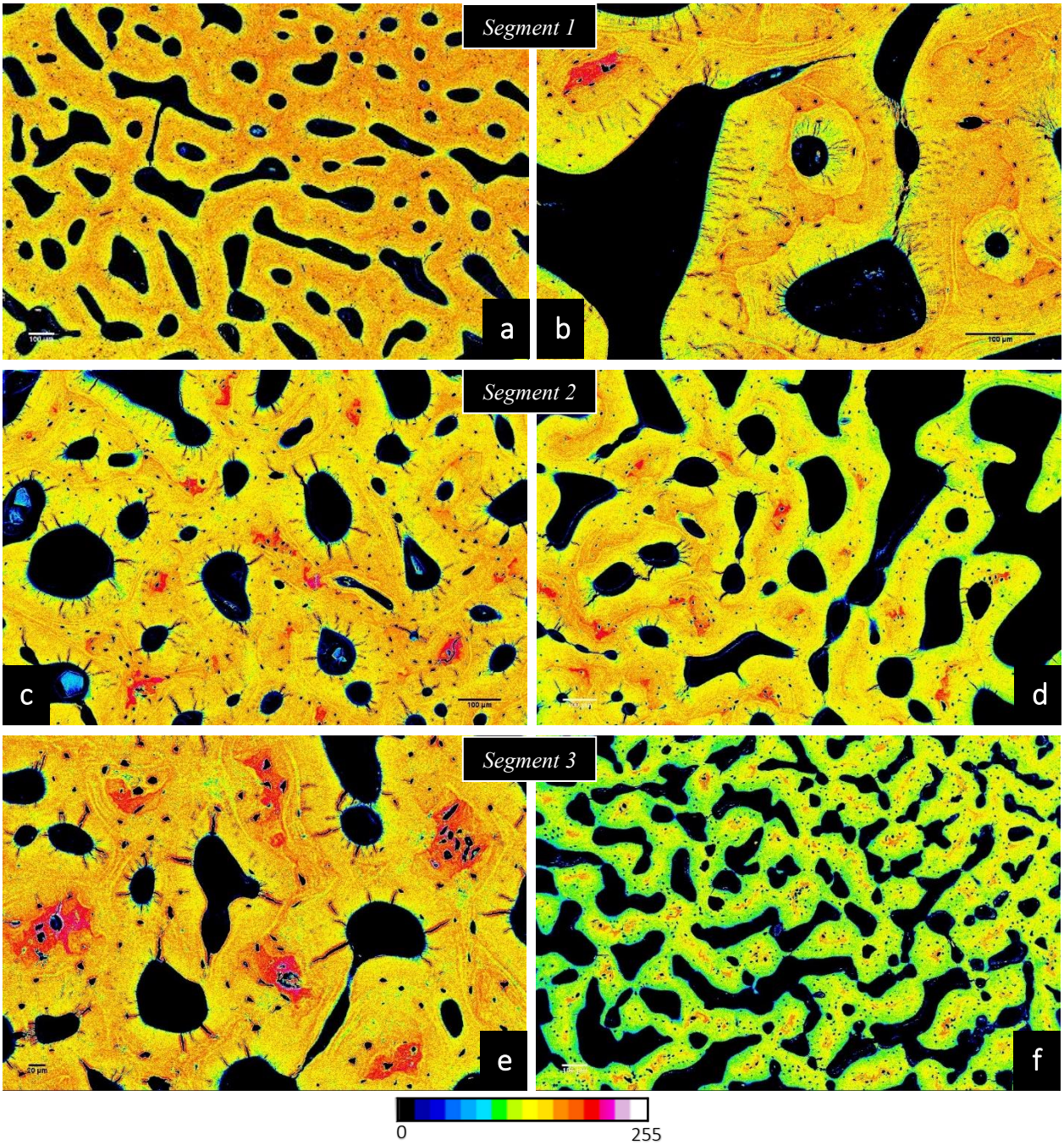

Figure 68. Pseudo-color SEM-BSE image of polished section surface of antler segments: **a)**, **c)**, **e)** Hard antlers; **b)**, **d)**, **f)** Cast antlers. The 16 grey-level bands spanning the grey value range from 0 (black) to 255 (peak white) as indicated by the color bar below the figure.

In Figures 67 and 68 with pseudo-color SEM-BSE, images show the degree of antlers mineralization. The color bars indicate increasing levels of mineralization from left to right. Figures 67a and 67c show the antler surface (cortex not yet formed in these growing antlers),

Figures 67b and 67d show dense antler cortex at velvet shedding. Figure 67e shows framework of calcified cartilage (only) in distal velvet antler, Figure 67f still shows framework with large areas of calcified cartilage covered by woven bone (green) in the distal antler portion at velvet shedding.

All panels in Figure 68 are either from the cortical or the transitional zone. An increase from proximal to distal in the fraction of calcified cartilage (which is more highly mineralized [red color] than bone [yellow to green colors]) can be observed. There is no significant difference in antler structure between cast and hard antlers. Minor variations may result from individual animal differences or the specific sampling location within the segment.

Table 8. Cross-sectional summary of the histological features of antlers in different developmental stages.

ANTLERS IN VELVET	- Covered with skin (epidermis, dermis) - Dermis contains blood vessels, hair follicles and sebaceous glands - Disto-proximal zonation of the antlers: mesenchymal zone at the tip, followed by a cartilaginous zone, followed by bone zone - The proper cortex is not visible - Chondroblast, chondroclasts and chondrocytes are present - Osteoblasts, osteoclast and osteocytes are present - In the vascular spaces blood elements are observed - In all antler portions remnants of calcified cartilage can be seen (most prevalent in distal portion) - Micropetrosis in some chondrocyte and osteocyte lacunae
ANTLERS AT VELVET SHEDDING	- In some areas, the antlers are covered by velvet remnants - Cortex is made mostly from primary osteons - In the vascular spaces red material (residual blood) and soft tissue are visible - Chondrocyte and osteocyte lacunae contain mostly cells - In all antler portions, remnants of calcified cartilage can be seen (most prevalent in distal portion) - Micropetrosis in some chondrocyte and osteocyte lacunae
HARD ANTLERS	- Cortex, transitional zone and trabecular zone are visible - Antler surface is eroded, and vascular canals are opened (cut osteons) - Cortex is made mainly from primary osteons - Osteocyte and chondrocyte lacunae are mostly empty - Vascular spaces are filled with residual blood - In all antler portions remnants of calcified cartilage can be seen (most prevalent in distal portion) - Mineral filled chondrocyte and osteocyte lacunae due to the former micropetrosis
CAST ANTLERS	- Cortex, transitional zone and trabecular zone are visible - Antler surface is eroded, and vascular canals are opened (cut osteons) - Cortex is made mainly from primary osteons - Osteocyte and chondrocyte lacunae are mostly empty - Vascular spaces are filled with residual blood - In all antler portions remnants of calcified cartilage can be seen (most prevalent in distal portion) - Mineral filled chondrocyte and osteocyte lacunae due to the former micropetrosis

5.2.6. Osteocyte classification

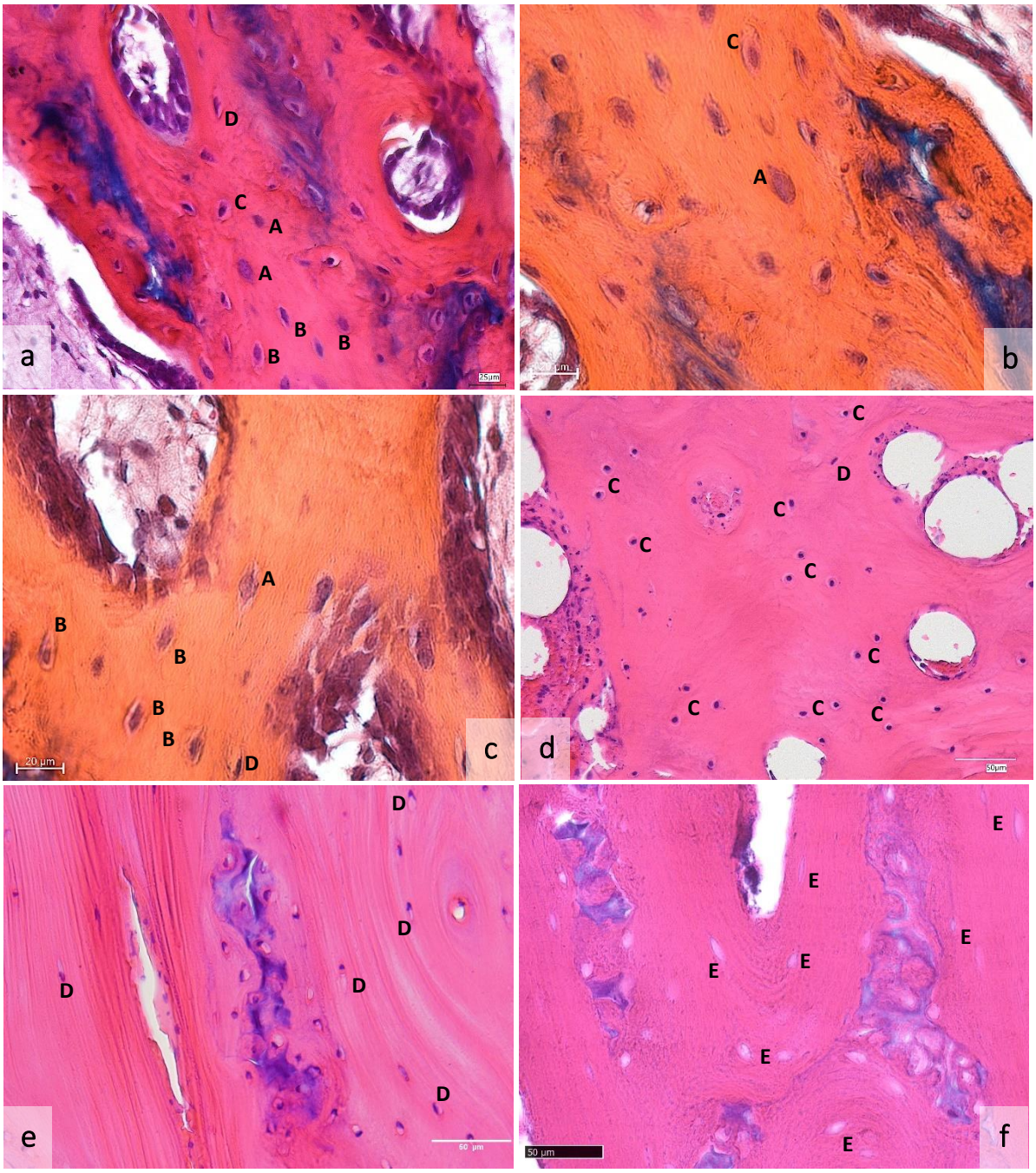

Figure 69. Osteocyte classification in five different types (alive [A], dying [B], dead [C, D, E]); (**a**, **b**, **c** – antlers in velvet, MSOP, Keyence VHX 7000/Axio Imager M2); (**d** – antlers at velvet shedding, HE, Keyence VHX 7000; **e** – hard antlers, HE, Olympus; **f** – cast antlers, HE, NanoZoomer 2.0RS).

In Figure 69, different osteocyte types are demonstrated. Detailed description is given in Table 3 (*Materials and methods*).

Table 9. Results of counting different osteocyte types (according to Table 3. Classification of osteocytes).

Specimen ID	Position	Type (%)				
		A	B	C	D	E
1/B	Cortex	-	24	45	30	1
	Transitional	4	23	30	40	3
	Trabecular	1	11	37	47	4
2/B	Cortex	-	16	41	42	1
	Transitional	-	32	39	25	4
	Trabecular	-	17	55	24	4
3/B	Cortex	8	31	43	17	1
	Transitional	10	29	48	9	4
	Trabecular	6	27	48	14	5
1/7	Cortex	-	-	21	73	6
	Transitional	-	-	15	73	12
	Trabecular	-	-	7	83	10
2/7	Cortex	-	-	1	87	12
	Transitional	-	-	37	63	-
	Trabecular	-	-	18	73	9
3/7	Cortex	-	-	14	84	2
	Transitional	-	-	3	89	8
	Trabecular	-	-	1	99	-
1/2	Cortex	-	-	-	97	3
	Transitional	-	-	2	86	12
	Trabecular	-	-	39	56	5
2/2	Cortex	-	-	-	85	15
	Transitional	-	-	1	80	19
	Trabecular	-	-	47	47	6
3/2	Cortex	-	-		84	16
	Transitional	-	-	34	64	2
	Trabecular	-	-	66	34	-
1/3	Cortex	-	-	1	75	24
	Transitional	-	-	1	88	11
	Trabecular	-	-	31	27	42
2/3	Cortex	-	-	-	88	12
	Transitional	-	-	11	86	3
	Trabecular	-	-	9	50	41
3/3	Cortex	-	-	1	94	5
	Transitional	-	-	1	95	4
	Trabecular	-	-	1	79	20

Specimen ID	Position	Type (%)				
		A	B	C	D	E
1/8	Cortex	-	-	1	83	16
	Transitional	-	-	6	59	35
	Trabecular	-	-	-	5	95
2/8	Cortex	-	-	1	73	26
	Transitional	-	-	-	44	56
	Trabecular	-	-	-	13	87
3/8	Cortex	-	-	-	74	26
	Transitional	-	-	-	12	88
	Trabecular	-	-	-	-	100
1/4	Cortex	-	-	3	97	-
	Transitional	-	-	11	89	-
	Trabecular	-	-	5	43	52
2/4	Cortex	-	-	2	91	7
	Transitional	-	-	4	89	7
	Trabecular	-	-	-	-	100
3/4	Cortex	-	-	-	88	12
	Transitional	-	-	7	86	7
	Trabecular	-	-	-	1	99
1/9	Cortex	-	-	-	43	57
	Transitional	-	-	-	76	24
	Trabecular	-	-	2	79	19
2/9	Cortex	-	-	-	78	22
	Transitional	-	-	1	92	7
	Trabecular	-	-	3	95	2
3/9	Cortex	-	-	-	12	88
	Transitional	-	-	1	95	4
	Trabecular	-	-	1	90	9
1/10	Cortex	-	-	-	90	10
	Transitional	-	-	-	-	100
	Trabecular	-	-	-	-	100
2/10	Cortex	-	-	1	87	12
	Transitional	-	-	-	-	100
	Trabecular	-	-	-	-	100
3/10	Cortex	-	-	2	84	14
	Transitional	-	-	-	1	99
	Trabecular	-	-	-	-	100

Specimen ID	Position	Type (%)				
		A	B	C	D	E
1/11	Cortex	-	-	1	92	7
	Transitional	-	-	-	-	100
	Trabecular	-	-	-	-	100
2/11	Cortex	-	-	-	90	10
	Transitional	-	-	-	3	97
	Trabecular	-	-	-	-	100
3/11	Cortex	-	-	1	50	49
	Transitional	-	-	-	35	65
	Trabecular	-	-	-	27	73
1/12	Cortex	-	-	-	2	98
	Transitional	-	-	-	7	93
	Trabecular	-	-	-	13	87
2/12	Cortex	-	-	-	18	82
	Transitional	-	-	1	22	77
	Trabecular	-	-	-	12	88
3/12	Cortex	-	-	-	6	94
	Transitional	-	-	-	4	96
	Trabecular	-	-	-	10	90

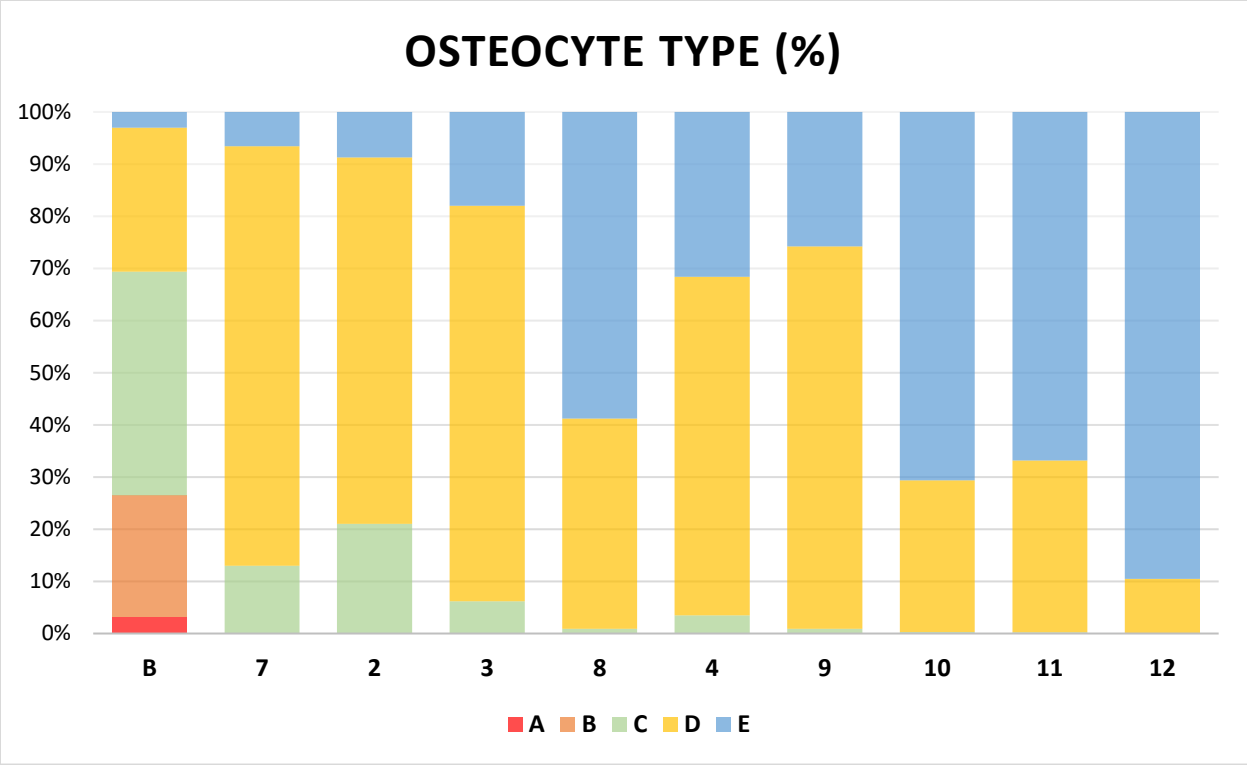

Figure 70. The proportion of certain types of osteocytes in different developmental stages of antlers (according to Table 3. Classification of osteocytes).

As is indicated by the results shown in Table 9 and Figure 70, living and dying osteocytes are present only in antlers in velvet. All observed osteocytes in antlers at velvet shedding, hard antlers and cast antlers were dead.

Since the distributions of most osteocyte type values deviate from normality, Kendall's Tau coefficient (τ) was used for assessing correlations.

Alive (viable) and dying osteocytes were observed almost exclusively in antlers during the velvet stage, whereas dead osteocytes of type C and particularly types D and E, were present across all other stages of antler development.

Table 10. Correlation (τ) between antler beam sampling timeline (Table 2, Fig. 13) with the proportion of dead osteocytes types C, D, and E. Coefficients highlighted in red indicate a significant ($p < 0.05$) association with the antler growth and development cycle.

Position	Segment								
	Segment 1	Segment 2	Segment 3	Segment 1	Segment 2	Segment 3	Segment 1	Segment 2	Segment 3
	Osteocyte type C			Osteocyte type D			Osteocyte type E		
Cortex	-0.497	-0.460	-0.358	-0.225	-0.067	-0.180	0.378	0.276	0.689
Transitional	-0.692	-0.597	-0.677	-0.449	-0.368	-0.225	0.523	0.539	0.460
Trabecular	-0.692	-0.680	-0.632	0.225	-0.276	-0.632	0.629	0.506	0.432

Osteocytes type C show the highest number of correlations in the proximal part (segment 1) of the beam. Their number decreases with different stages in antler sampling timeline across all three different antler zones (cortex, transitional, trabecular). In the middle (segment 2) and distal (segment 3) portions of the antler beam, within the cortex, their number remains relatively constant regardless of the sampling timeline. However, in the transitional and trabecular zones, their number significantly decreases as the antlers are collected at later stages following velvet shedding.

Osteocytes type D generally does not show correlations with the sampling timeline of the antler in any zone of the antler beam. The exception is the trabecular zone of the distal portion (segment 3) of the antler beam, where the abundance of osteocytes type D significantly decreases as the time from velvet shedding to sampling was longer.

Finally, osteocytes type E exhibit the greatest variability in abundance. Notably, the sign of the coefficient correlation changes, with all coefficient values being positive, which is opposite to the trends observed in other osteocyte types (types C and D). In the cortex, their number remains stable in the proximal (segment 1) and middle (segment 2) portions, but in the distal portion (segment 3), their number significantly increases on the sampling timeline ($\tau = 0.689$). The transitional and trabecular zones of the proximal (segment 1) and middle (segment 2) antler portion show a significant increase in osteocytes type E on the sampling timeline ($\tau = 0.506 – 0.629$).

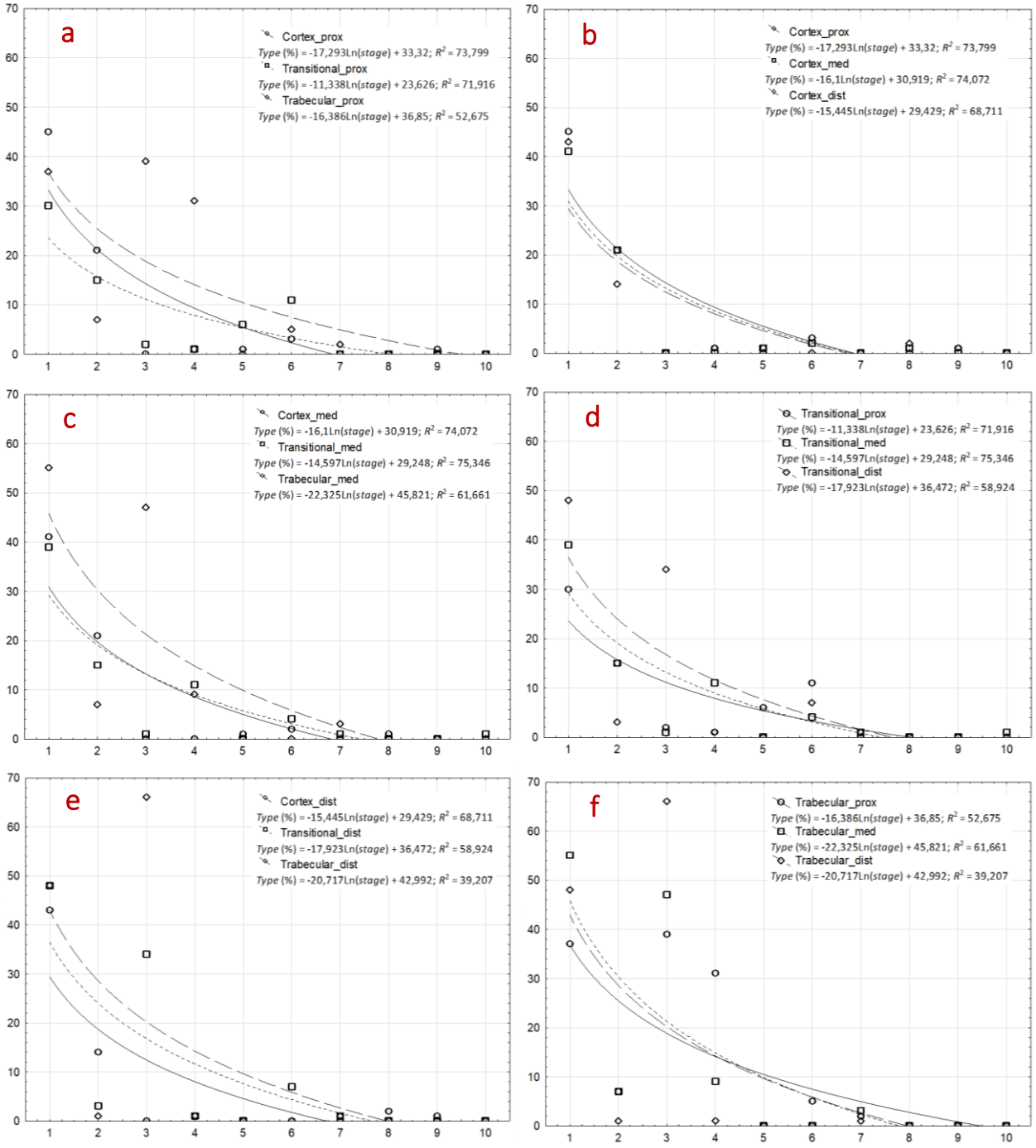

Figure 71. Dependence of the proportion of osteocytes type C (y-axis, [%]) over the sampling timeline (x-axis), across different antler zones and segments.

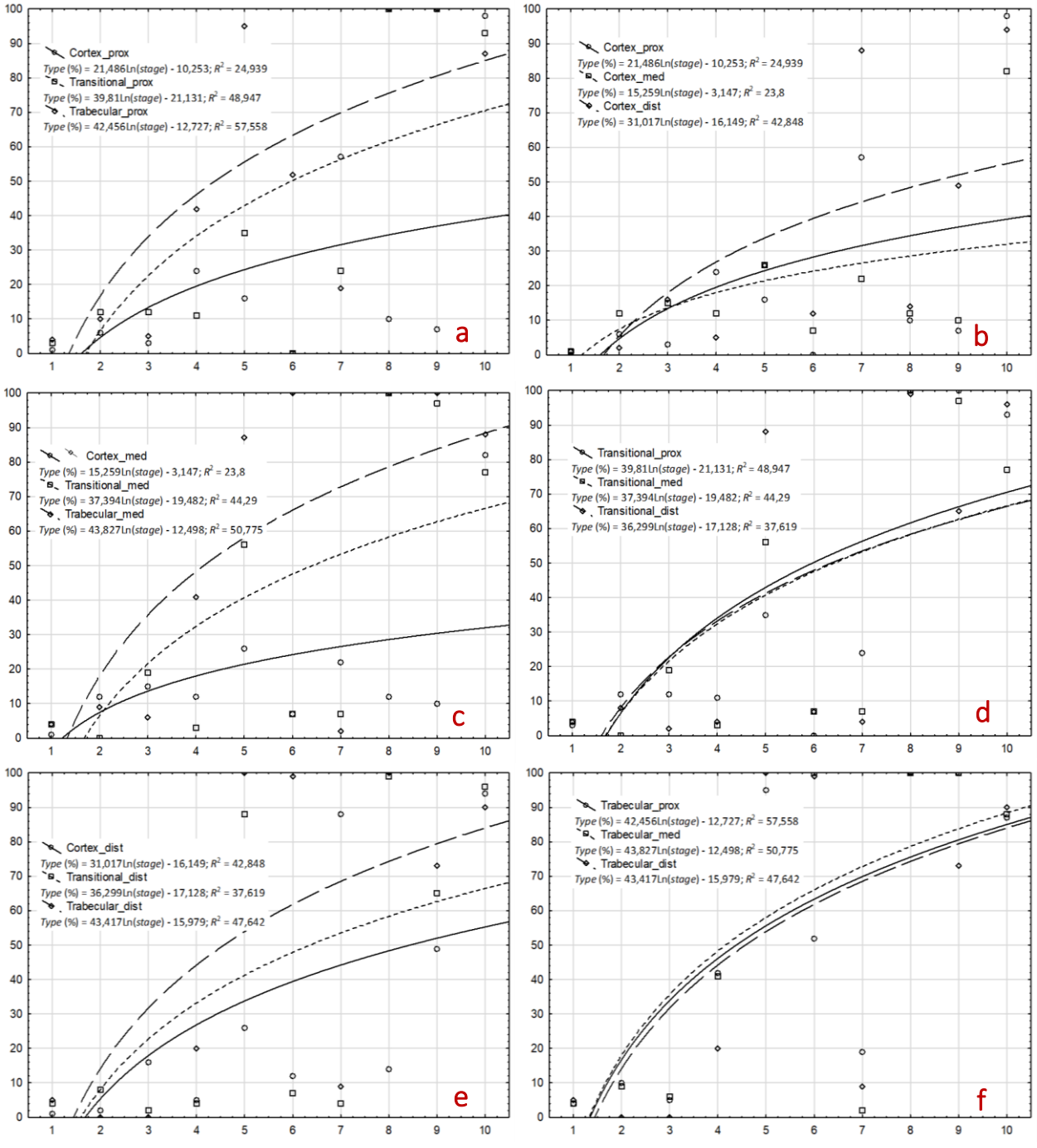

Figure 72. Dependence of the proportion of osteocytes type E (y-axis, [%]) over the sampling timeline (x-axis), across different antler zones and segments.

It has already been noted that the proportion of osteocytes type C decreases throughout the sampling timeline. This decline is specific to each proximal portion (segment 1) (Fig. 71a). The most pronounced decrease is observed in the cortex, while the least pronounced occurs in the transitional zone. The relationship between the proportion of osteocytes type C and the sampling timeline is relatively strong in both the cortex and transitional zones, with the sampling timeline explaining between 71.92% (R^2 = 71.916) and 73.99% (R^2 = 73.99) of the variability in osteocyte proportions. In the middle portion (segment 2) of the antler beam, this relationship is moderate, accounting for 52.68% (R^2 = 52.675) of the variability. Generally, at the beginning of the sampling timeline, there is a significant difference in the proportion of osteocytes type C between the cortex and transitional zones compared to the trabecular zone. Later in the timeline (in antlers sampled at different times after velvet shedding), no notable differences are observed between the cortex and trabecular zones. However, among all zones, the cortex is the first to lose osteocytes type C, followed by the trabecular zone, while the transitional zone retains a portion of type C osteocytes almost until the antler is cast.

In the middle portion (segment 2) of the antler beam, the cortex and transitional zones show almost no differences in the proportion of osteocytes type C (Fig. 71c), whereas the trabecular zone exhibits a noticeably higher proportion of these cells. The sampling timeline also explains a relatively large portion of the variability in the proportion of osteocytes type C, ranging from 74.07% (R^2 = 74.072) in the cortex to 75.35% (R^2 = 75.346) in the transitional zone. As in the proximal portion (segment 1) of the beam, the relationship between sampling timeline and the proportion of osteocytes type C is somewhat weaker in the trabecular zone, where the sampling timeline accounts for 61.66% of the variability (R^2 = 61.661). Around the beginning of the final third of sampling timeline, the cortex is the first to lose osteocytes type C, followed by the transitional zone, while the trabecular zone retains them the longest.

In the distal portion (segment 3) of the antler beam, the trend of osteocyte type C proportions in relation to the sampling timeline shows considerable variation between zones (Fig. 71e). However, compared to the proximal and middle portions of the beam, the percentage of variability explained here is somewhat lower, ranging from 39.21% (R^2 = 39.207) in the trabecular zone to 68.71% (R^2 = 68.711) in the cortex. It is important to note that in the cortex, the proportion of osteocytes type C is the lowest when compared to the proximal and middle portions of the beam.

Overall, when comparing the trends in osteocyte type C proportions across the proximal, middle, and distal portions of the beam and between different zones, the highest proportions are consistently observed in the antler trabecular zone. Nonetheless, the pattern of osteocyte type C loss follows the same sequence in all segments of the beam.

Figure 72 shows dependence of the proportion of osteocytes type E over the sampling timeline. As the sampling timeline goes on, the proportion of osteocytes type E also increases in all antler beam segments and different zones. The trabecular zone shows the strongest and steepest increase in all segments, suggesting it is most affected by the sampling timeline. The transitional zone follows a similar but less pronounced trend. The cortex shows the smallest increase and weakest correlation.

When analyzing all three segments across the respective antler zones, the correlation between osteocyte type E proportion and sampling timeline appears to be relatively consistent, R^2 range from 23.8 to 42.848 in cortex, 37.619 to 48.947 in transitional zone, and 47.642 to 57.558 in trabecular zone.

5.2.7. TUNEL assay

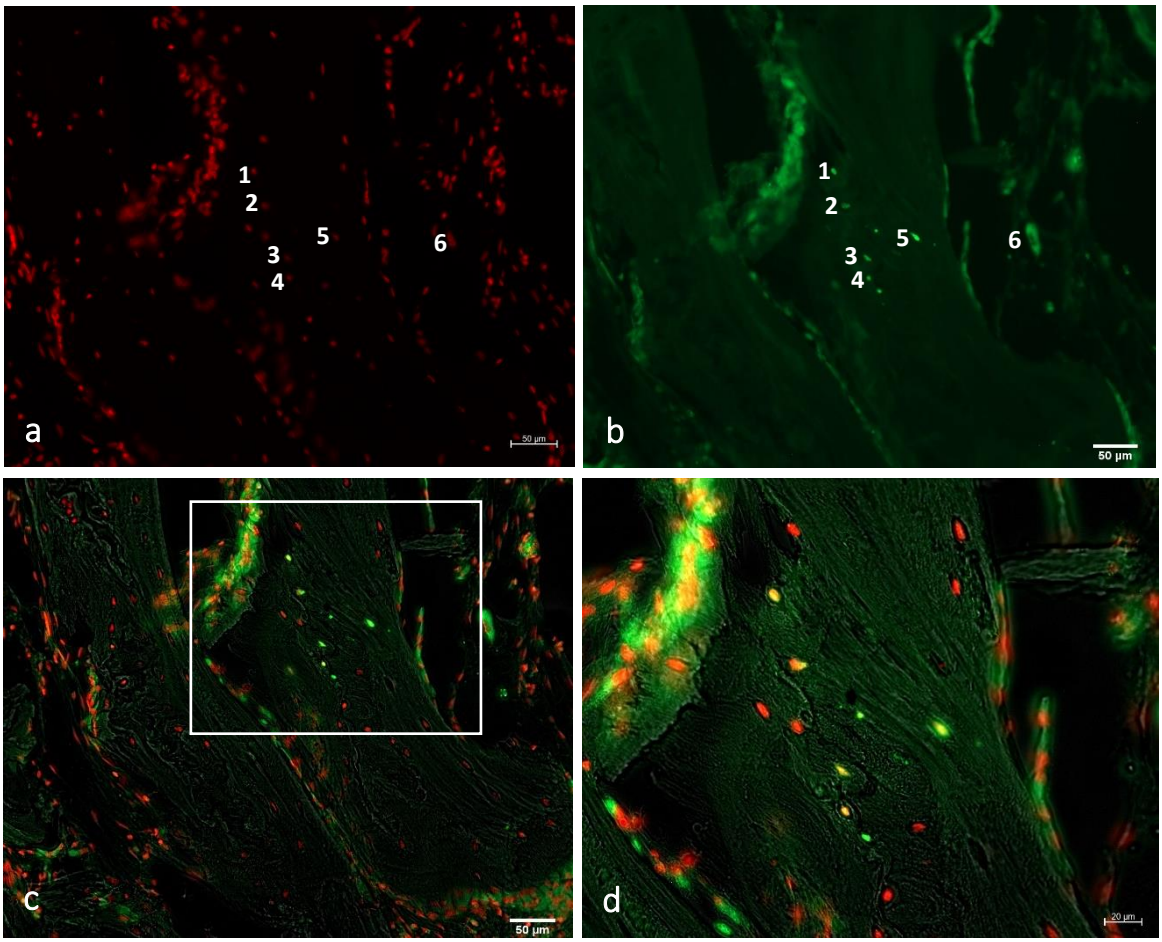

Figure 73. Red deer antlers in velvet, longitudinal section, demineralized, paraffin embedded samples, TUNEL, Axio Imager M2.

Figure 73a shows nuclei labelled with DAPI, while in Figure 73b the fluorescence signal indicates TUNEL positive DNA. Numbers 1-5 represent osteocytes, while number 6 identifies an osteoclast. Figure 73c shows overlapped Figures 73a and 73b, and Figure 73d is a higher magnification.

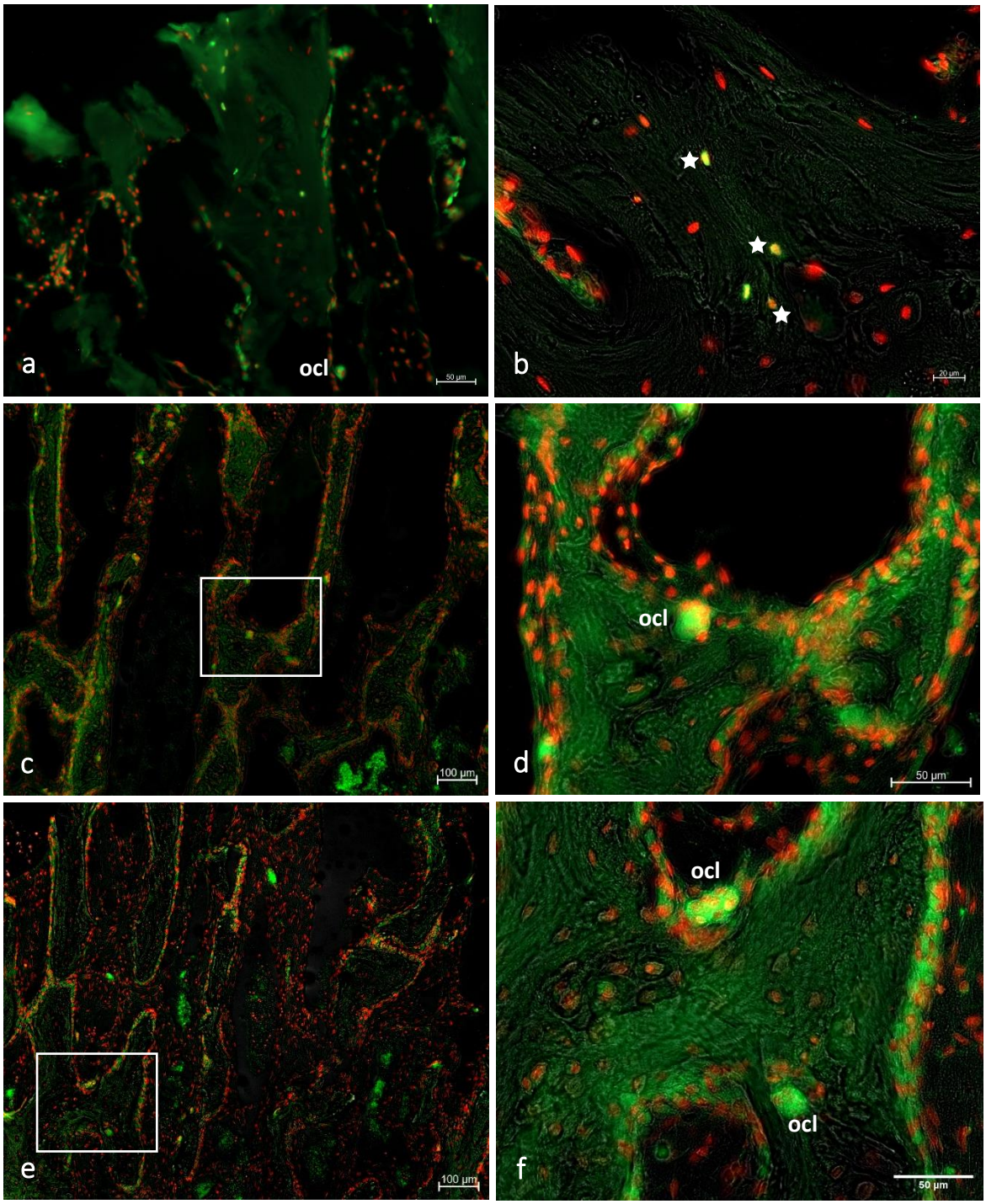

Figure 74. Red deer antlers in velvet, longitudinal section, demineralized, paraffin embedded samples, TUNEL, Axio Imager M2.

In Figure 74, examples of TUNEL positive osteocytes and osteoclasts in different magnifications are visible.

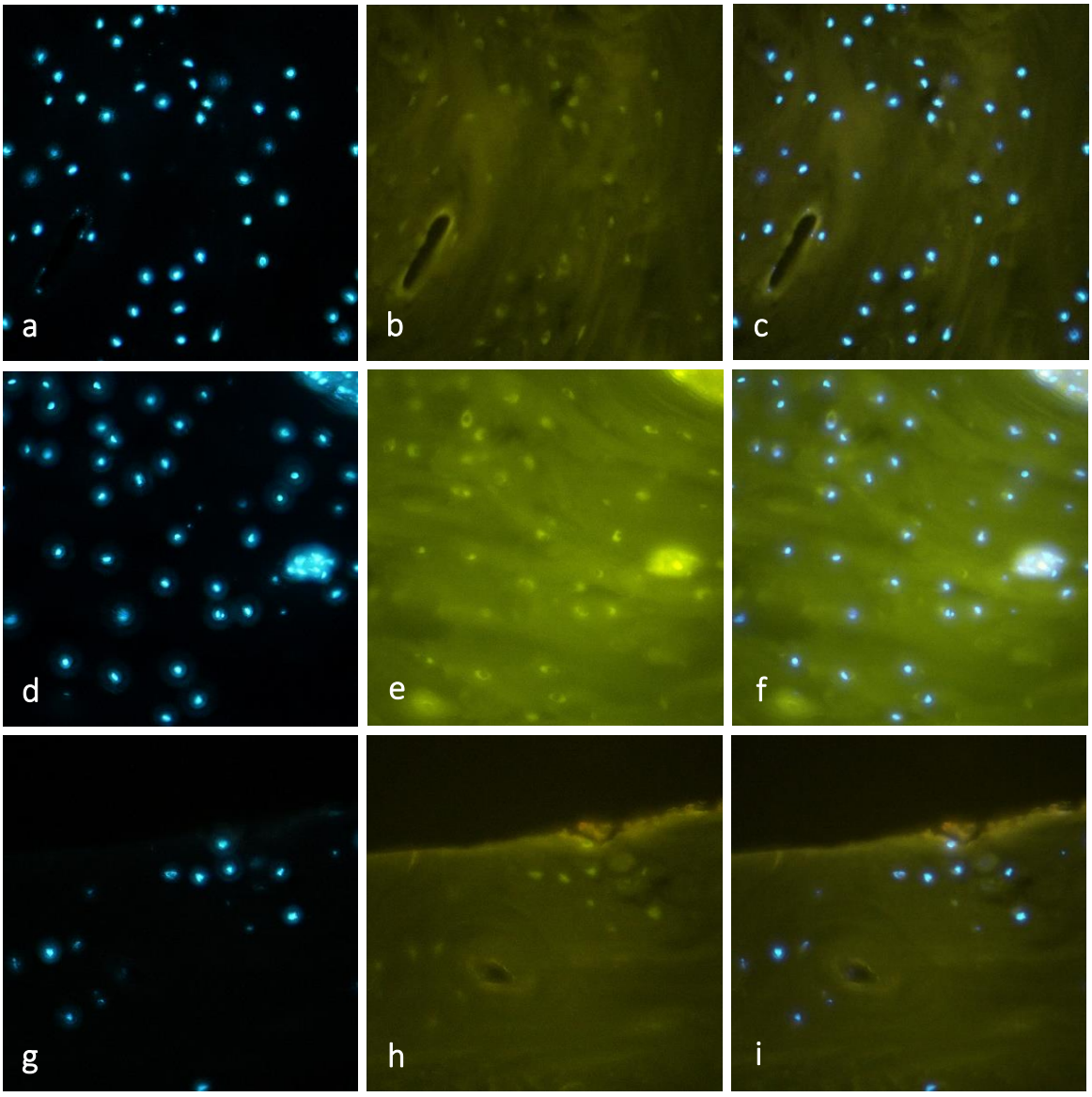

Figure 75. Red deer antlers: antlers at velvet shedding (**a-c**), hard antlers (**d-i)**, longitudinal section, demineralized, paraffin embedded samples, TUNEL, Olympus BX51.

In Figures 75a, 75d and 75g, nuclei labelled with DAPI are visible, while Figures 75b, 75e and 75h present histological slides exposed to TUNEL assay. Figures 75c, 75f and 75i shows overlapped figures labelled with DAPI and figures exposed to TUNEL assay.

5.3. Additional analysis

5.3.1. Smears from the antler liquid material

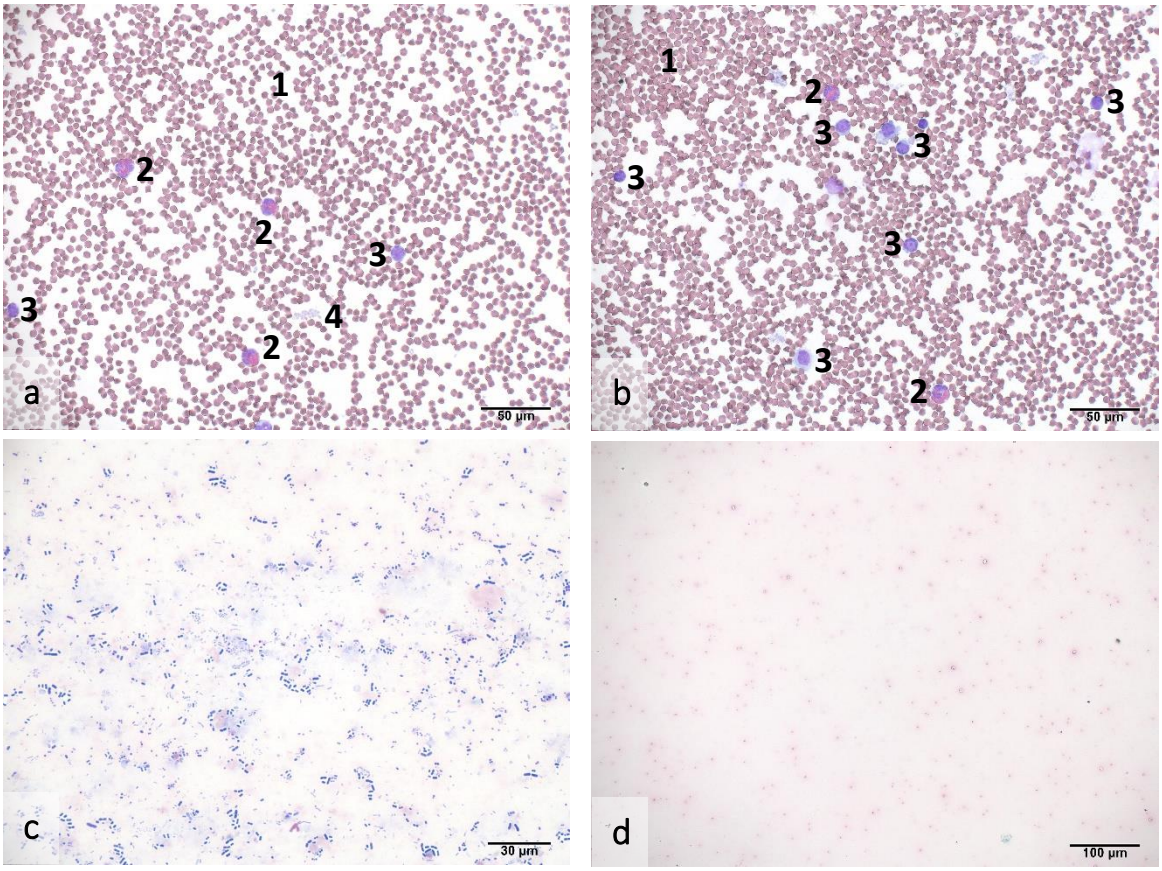

Figure 76. Smear from the antler liquid material (**a**, **b** – antlers in velvet; **c** – hard antlers (ID 8), larvae; **d** – hard antlers (ID 9)), MGG, Digicyte DX50.

In Figure 76, differences in the liquid material between antlers in different developmental phases (antlers in velvet and hard antlers) are presented. In smears from the antlers in velvet, red blood corpuscles (1), eosinophils (2), lymphocytes (3) and platelets (4) are visible. In smears from hard antlers with larvae, only bacteria are present. There are no red blood corpuscles or leukocytes. In smears from other hard antlers, red blood corpuscles, leukocytes and bacteria are also not visible. There is only a small amount of red protein content.

5.3.2. Identification of bacteria by Gram staining

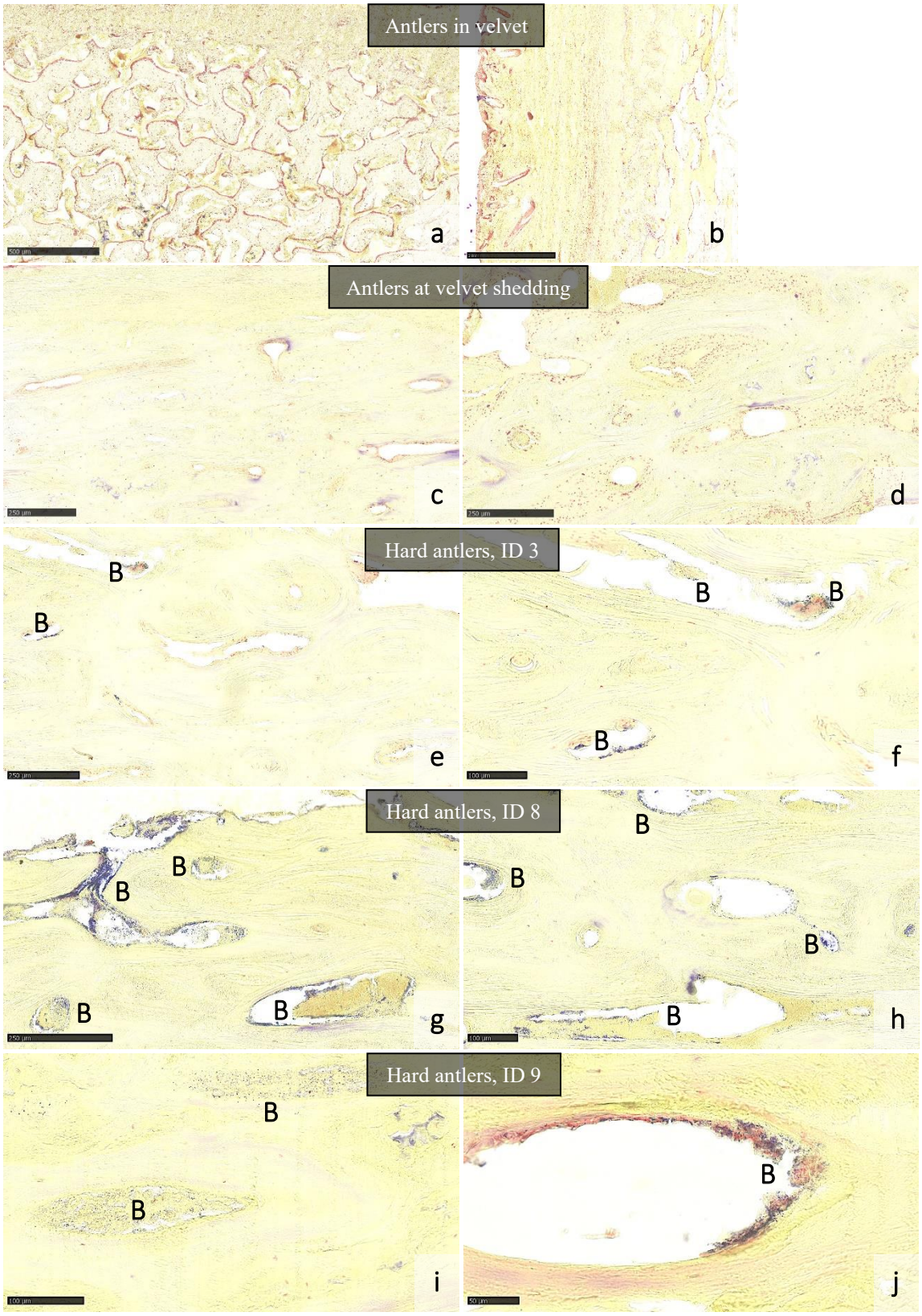

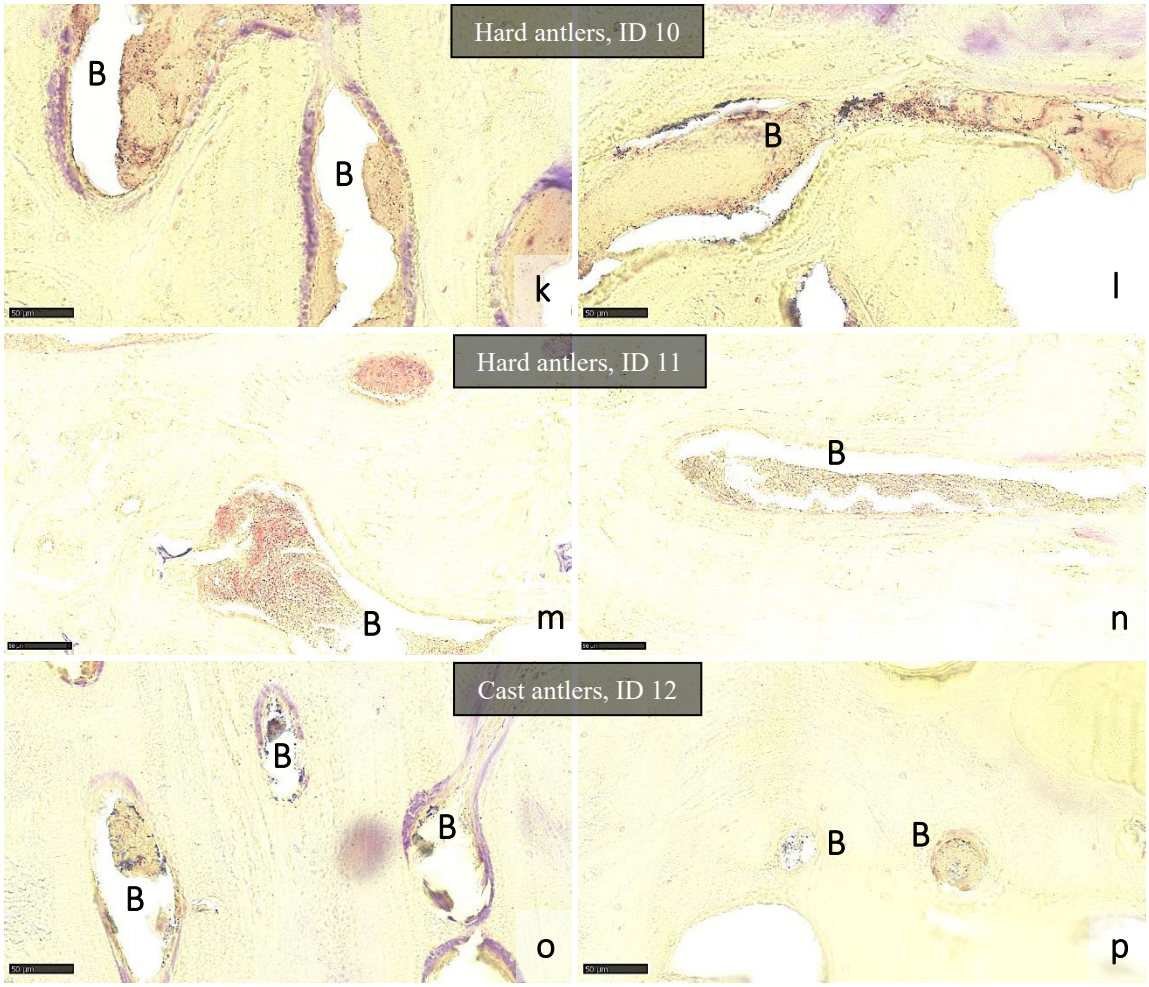

Figure 77. Section of antlers in different developmental phases, IBG, NanoZoomer 2.0RS.

In Figure 77, bacteria (B) (Gram +, Gram -) are present mostly in vascular spaces of hard and cast antlers, while bacteria are not visible in antlers in velvet and in antlers at velvet shedding.

5.3.3. Swabs for identification of aerobic and anaerobic bacteria

Swabs from antlers in velvet (ID B) were negative for aerobic and obligate anaerobic bacteria. Swabs from hard antlers with larvae (ID 8) were positive for *Erysipelothrix rhusiopathiae*, *Kurthia zopfii*, *Bacillus licheniformis*, *Macrococcus canis* and *Citrobacter freundii*. Swabs from hard antlers (ID 9) were positive for *Pseudomonas flavescens*. Obligate anaerobes were not isolated from ID 8 and ID 9 swabs.

5.3.4. Larvae in antlers

5.3.4.1. Histological analysis

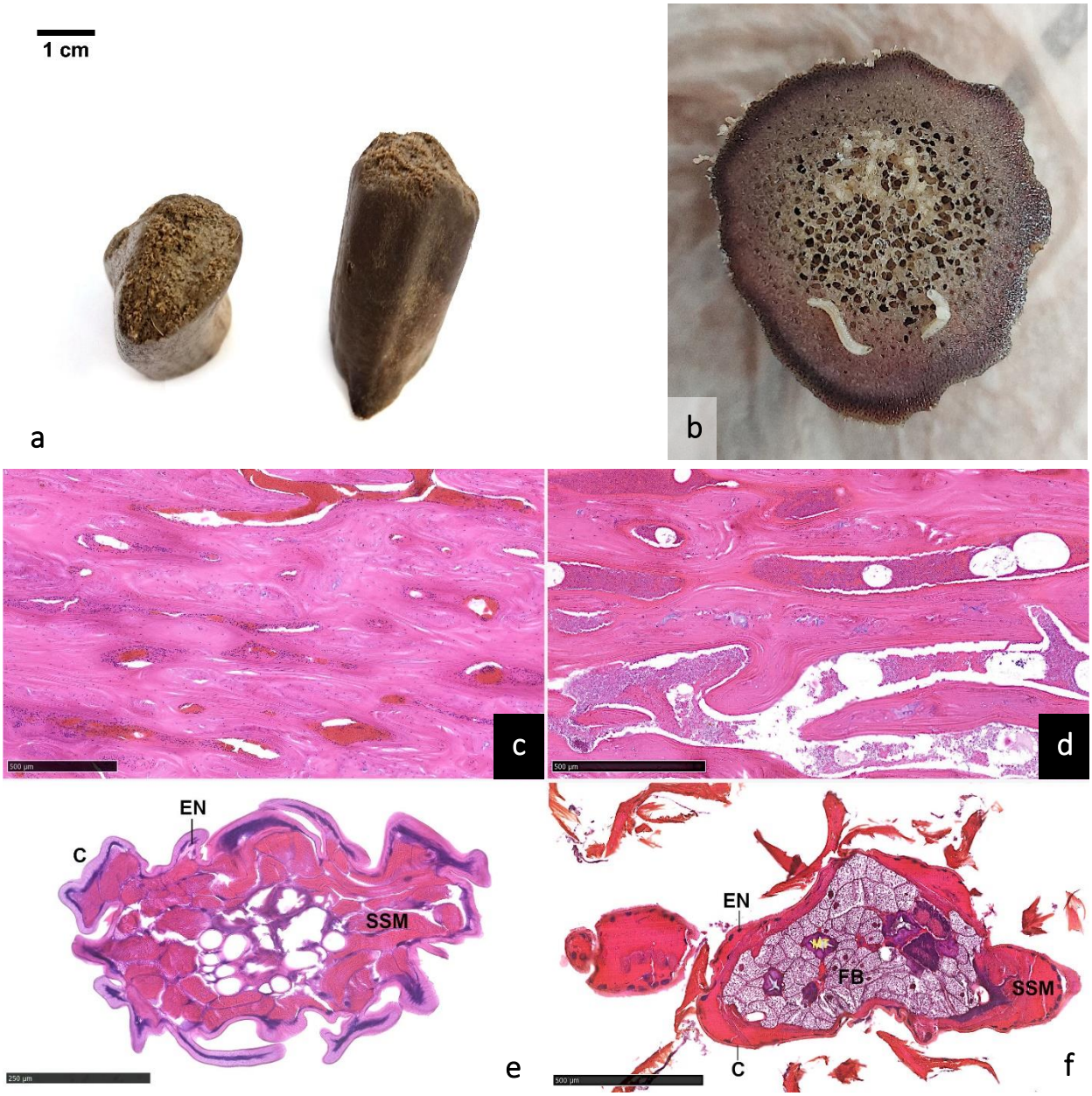

Figure 78. Red deer antlers (ID 8): **a**, **b** – macroscopic views; **c**, **e** – HE; **d**, **f** – MSOP, NanoZoomer 2.0RS.

In Figure 78, hard antlers tips are shown. Macroscopically, in some parts of the antler tips the compact part is missing. Figure 78b shows a transverse section of the hard antler containing larvae in the trabecular part. Inside the Haversian and Volkmann canals, a large number of bacteria,

scarce protein content and remnants of red blood corpuscles are visible. Figures 78c and 78d show longitudinal sections of antlers and a comparison of proximal (78c) and distal (78d) antler segments regarding the amount of red blood corpuscles. Proximal segments have more red blood corpuscles, while in the middle and distal segments, the amount of red blood corpuscles decreases, and the number of bacteria increases. In Figures 78e and 78f, transversely sectioned larvae are seen: C – cuticle, EN – epidermal nuclei, SSM – striated skeletal muscle. Additionally, in Figure 78f, the fat body (FB) and Malpighian tubules (MT) can be seen. The outer part of the larva's body wall consists of a cuticle with a single layer of round to flat epidermal nuclei. The larval body mainly consists of striated skeletal muscle. Most of the larva's body cavity is filled with a fat body made of large polygonal cells that contain numerous vacuoles within their cytoplasm. Malpighian tubules lined with a single-layer cubic epithelium are visible inside the fat body, some filled with minimal content. There were no indications of an inflammatory reaction observed around the larvae.

5.3.4.2. Morphological and molecular identification

Based on the shape of the cephaloskeleton, the third-instar larva (L3) was identified morphologically as *Prochyliza nigrimanus* (MEIGEN, 1826) (Diptera: Piophilidae). According to MARTÍN-VEGA et al. (2012), the distance between the base and the tips of the mouth hook was approximately equal to the width of the mouth hook base.

After alignments with data within COI databases, DNA sequences had the closest match with the BIN BOLD: ADL1379 (Barcode Index Number, RATNASINGHAM and HEBERT, 2013), within 3% of similarity to specimens identified as *Prochyliza nigrimanus* (basionym: *Piophila nigrimana* MEIGEN, 1826), and the highest similarity of 98.67%. The maximum distance within this BIN (BOLD: ADL1379) was 2.75% (p-distance). In GenBank, our sequences matched to OM791734.1 with 98.19% identity for amplicons sequenced using forward primer (LCO 1490) and the best matches were taxonomically denoted as *P. nigrimanus*.

6. DISCUSSION

Cranial appendages, sometimes also called headgear, come in various forms, shapes and sizes. As they differ morphologically and in origin, their fate and function are also different among different species. They appear in four main types, as ossicones in giraffids, pronghorns in *Antilocapra americana* and its fossil relatives, horns in bovids and antlers in cervids. Members of the family Giraffidae (*Giraffa camelopardalis* and *Okapia johnstoni*) possess the so-called ossicones. There are diverse scientific perspectives regarding the formation of ossicones. Certain authors consider that ossicones grow as cartilage and then mineralize from distal to the proximal part (GERAADS, 1991; NASOORI, 2020), while others support that the ossification process in ossicones is intramembranous (GANEY et al., 1990). These appendages develop separately from the cranial bones with which they fuse at the age of sexual maturity. Ossicones are present in both males and females, and in males are usually accompanied by a third one, which is positioned on the frontal bone. The paired ossicones are located on the frontal and parietal bone, their attachment site overlapping the frontoparietal suture (LANKESTER, 1907). Ossicones are used in a display of sexual behavior, and are highly vascularized and innervated, which, according to certain authors, is most probably a base that enables rapid healing and regeneration if damaged. They are permanently covered by the skin, except for their tips in older okapi males. Unlike ossicones, pronghorns combine characteristics of both horns and antlers. The North American pronghorn (*Antilocapra americana*) is the only extant member of the family Antilocapridae, which, despite being frequently related to antelopes, is actually more related to giraffids and cervids (PROTHERO and FOSS, 2007). Pronghorns are made of bony horn core and are covered by keratinous sheath, which is shed and formed annually under hormonal influence (O'GARA, 1990; MARRIOTT and PROTHERO, 2022). According to SOLOUNIAS (1988), there is no delayed fusion of the pronghorn core, i.e., the bony core is an apophysis of the frontal bone. Furthermore, unlike horns in bovids, pronghorns have two centers of keratin formation, a distal one for the main spike and the proximal one for prong (DAVIS et al., 2011). Both males and females possess pronghorns. Third type of cranial appendages are horns, permanent structures that grow throughout the life of an animal, and are found in the members of the Bovidae family. During horn development, the bony core grows from separated ossification centers, which are located in the dermis and hypodermis of the calves horn bud (CAPITAN et al., 2011). The predominant stance is that the base of the horn spike forms from ossifying hypodermal tissue and only later fuses with the skull.

However, other authors concluded that the horn core is a direct outgrowth (apophysis) of the frontal bone (SOLOUNIAS, 1988; DAVIS et al., 2014). The keratinous part is formed by the epidermis. When completely developed, horn is formed from bony core, keratinous sheath and connective tissue that is placed between them. Finally, the last type of headgear, the antlers, are found in cervids. Antlers are bony organs whose development exhibits distinct differences from typical mammalian osteogenesis in several aspects. Their growth involves both endochondral and perichondral (intramembranous) ossification (GRUBER, 1937; BANKS, 1974; BANKS and NEWBREY, 1983a, b; KIERDORF et al., 1995; PRICE et al., 1996). Undifferentiated mesenchymal stem cells are present at the tips of the main beam and tines. These cells differentiate into chondroblasts and chondrocytes, which form a longitudinally oriented cartilaginous tubular framework (scaffold) with large central cavities (vascular spaces) (WISLOCKI et al., 1947; BANKS, 1974; KIERDORF et al., 2003; LI et al., 2005, KRAUSS et al., 2011). Further proximally, the chondrocytes become hypertrophic and the cartilage matrix is mineralized, followed by the replacement of the cartilage by a woven-bone scaffold (BANKS and NEWBREY, 1983; KIERDORF et al., 1995; PRICE et al., 1996; FACHEUX et al., 2001; KRAUSS et al., 2011; GOMEZ et al., 2013). In addition to endochondral bone formation, a bony sleeve is formed at the antler periphery by osteoblasts derived from the osteogenic layer of the periosteum (KIERDORF et al., 2003). As this sleeve bone formation occurs without a cartilage precursor it constitutes a case of intramembranous (perichondral) ossification. During the growth phase, antlers are covered with a special type of skin known as velvet that differs from normal scalp skin (e.g. lack of arrector pili muscles) (BUBENIK, 1993; LI and SUTTIE, 2000). Along the antler vertical axis, there is a clear distal to proximal zonation. The antler tip (distal part) is the youngest, and the antler base (proximal part) is the oldest portion (GOMEZ et al., 2013; KIERDORF et al., 2022). Antlers are one of the fastest growing organs in mammals (peak growth rate range from 6-7 mm per day in wild red deer [TZALKIN, 1945] with up to 2.75 cm per day in wapiti (*Cervus canadensis*) [GOSS, 1970]), with their annual regenerative growth phase being completed in four to five months (CHAPMAN, 1975; GOSS, 1983; GOMEZ et al., 2013; WANG et al., 2019a).

The antler cycle is controlled by seasonal fluctuations in testosterone levels. During antler growth, circulating testosterone levels remain low. Rising testosterone levels prior to the rut cause cessation of growth, full mineralization of antler bone and velvet shedding, a process that exposes the bare antler bone. As long as testosterone levels remain high, the hard (polished) antlers are

carried by the males (WISLOCKI et al., 1947; GOSS, 1968; SUTTIE et al., 1995). A drop in testosterone after the rut triggers intense osteoclastic activity in the distal pedicle, eventually leading to antler casting (GRUBER, 1937; GOSS et al., 1992).

The activation of the antlerogenic periosteum (and thus the formation of the primary cranial appendages, i.e., pedicles and first antlers) depends on a testosterone impulse (BUBENIK, 1990), as it contains a high number of androgen binding sites (LI et al., 1998). The role of androgens (especially testosterone) in the antler cycle has been demonstrated experimentally by various authors using different methods (castration, application of sex steroids, application of antiandrogens) (KOLLE et al., 1993; KIERDORF et al., 1995b, 2004, 2021). The effects of castration on antler growth were already mentioned by Aristotle in his Historia Animalium: "*If deer are castrated when they have as yet no horns, they cease to grow horns; but if they already have them when castrated, the size of the horns remains the same and they do not cast them*" (ARISTOTLE, 1991). The second part of the sentence is correct only if it refers to antlers that are still in velvet. Castration when a stag is in hard antler leads to premature casting, followed by the growth of new antlers that remain in velvet permanently (peruke antlers).

In this study, results obtained on velvet antlers show that antler surface is covered with a thick layer of velvet, consisting of epidermis (stratified squamous keratinized epithelium) and dermis (blood vessels, hair follicles and sebaceous glands). This finding is in accordance with the previous studies. Thus, KIERDORF et al. (2004) have reported that the antler surface is covered by highly vascularized dermis, while the epidermis is poorly keratinized. Velvet is composed of epidermal and dermal layer, follicles and glands (KIERDORF et al., 2003). CEGIELSKI et al. (2009) divide the velvet into epidermis, dermis and subcutaneous tissue. Similarly to this study and previous ones, these authors also mention the rich blood supply of the velvet and its richness in sebaceous glands. Beneath the velvet is a periosteum that overlies the antler bone. The periosteum is essential for intramembranous bone formation (KIERDORF et al., 2004). Velvet antler samples also showed that the antler framework is initially cartilaginous, while bone is present in the proximal antler portions (segment 1). The amount of bone tissue in velvet antlers decreases towards the distal portion (segment 3). This study observed that velvet antler samples contain significant amount of blood (with functional blood elements) in the intertrabecular spaces. FAUCHEAUX et al. (2001) report similar findings and state that the extensive blood supply of

forming antlers not only provides oxygen and nutrients to meet the high metabolic needs of a rapidly growing tissue but is also a source of progenitors that subsequently differentiate into mature osteoclasts which are required for cartilage and bone resorption.

As stated before, antlers are peculiar organs that have intrigued researchers for a long period of time. Among many interesting topics related to antlers is also a long-term debate on whether hard antlers are a dead bone (WISLOCKI, 1942; GOSS, 1983; LANDETE-CASTILLEJOS et al., 2012; KIERDORF et al., 2021) or whether they can survive velvet shedding for longer periods of time (BROCKSTEDT-RASMUSSEN et al., 1987; ROLF and ENDERLE, 1999; ROLF et al., 2001). Each of the mentioned groups of scientists has presented arguments in support of their hypothesis. One of main prerequisites for antlers to remain alive is a permanent blood supply that should continue to function almost until the time when the hard antlers are cast. Specifically, observations indicating a disruption of the blood supply to the antlers at the time of velvet shedding has led many scientists to conclude that hard antlers are dead (WISLOCKI, 1942; BUBENIK, 1983; BUBENIK and BUBENIK, 1990; GOSS et al., 1992; GOSS, 1995). WISLOCKI (1942) observed the first signs of necrosis (in white-tailed deer antlers) even before velvet shedding and attributed this to the already diminished blood supply of the antlers during the late velvet stage. GRUBER (1937) states in his paper that the antlers die after velvet shedding. WISLOCKI (1942) indicated (1) that primary Haversian systems in antlers undergo only limited remodeling into secondary systems, (2) that interstitial lamellae are minimally present, and (3) that tertiary Haversian systems are not formed. In antler samples of white-tailed deer from August (antlers still in velvet), focal necrosis of marrow tissue suggests cessation of blood flow, signaling the imminent death of the antler and onset of velvet shedding. Furthermore, vascular injections of hard antlers demonstrated that while the pedicle remains vascularized, there were no blood vessels filled in the antler itself. In his extensive observations on horns and antlers, MODELL (1969) states that antlers have no blood supply or nerves and are insensitive to pain following velvet shedding. A study on red deer conducted by CURREY et al. (2009b) found that antlers dry out completely after velvet shedding and establish a hygric equilibrium with the environment. The above observations strongly suggest that after the cessation of antler growth, the blood supply of the antlers is diminished, which leads to initial ischemia, death of osteocytes, and consequently to velvet shedding. The actual fraying behavior is a response to rising testosterone levels, not to death of the velvet antlers, and occurs even if the antlers are immature (still living) (KIERDORF et al.,

1993). Finally, total ischemia is present, there are no living cells, the bone is dead and it dries out. If there was a continuous blood supply after velvet shedding, blood elements should be visible in the antler cavities, and this is completely opposite to the findings of this thesis. Rather, the results of this thesis show that blood elements (red blood corpuscles, eosinophils, lymphocytes) are present only in antlers in velvet. From velvet shedding (also including a sample of antler at the time of velvet shedding) onwards, antler cavities contain only residual red liquid. This red liquid, that one may call "residual blood", may resemble blood on initial inspection, however, histological analysis did not reveal any of blood elements, meaning that it is only a remnant of the blood once present in the growing antlers. Therefore, this red liquid should not be called blood, as obviously it has no functionality and cannot sustain life of the hard antlers. Even worse, according to this study, bacteria were present in all antler samples except for antlers in velvet and at velvet shedding. From this, it is obvious that not only is this liquid unable to promote life in hard antlers, but it also represents a toxic environment for potentially alive cells. Additionally, the residual red liquid decreases in quantity as the time span between velvet shedding and sampling increases. Therefore, the findings of this study fully support the view of previous authors that there is no blood supply in hard antlers. Contrary to these findings, a smaller group of authors holds that antlers are alive after velvet shedding and that they have a continuous blood supply from the pedicle into the antler (e.g. ROLF and ENDERLE, 1999 who studied antlers of fallow deer, *Dama dama*). They claim that cells within the antler remain vital after velvet shedding, and because of continuous bone remodeling, secondary osteons are present. The views of ROLF and ENDERLE (1999) have been cited as facts or at least well-supported hypothesis by quite a number of other authors (CEGIELSKI et al., 2009; CHEN et al., 2009; RÖSSNER et al., 2020; LI et al., 2024) who themselves did not study this issue. Thus, despite the poor evidence provided by ROLF and ENDERLE (1999), their views have been quite well received (instead of critically questioned) by parts of the "antler community". Results of this doctoral thesis contradict the claims made by ROLF and ENDERLE (1999) that hard antlers remain alive and vascularized structures with continuous blood supply that enables a normal metabolism within parts of the hard antler. A similar view on hard antlers as living structures was previously also brought up by BROCKSTEDT-RASMUSSEN et al. (1987) who concluded that the roe deer antlers survive the velvet shedding and that bone formation continues till their casting. They also claimed that the antlers most likely die just before casting.

Regarding the histological structure of the antlers, in this study, osteoclasts were found only in antlers in velvet, while in other samples of hard antlers they were not visible. Normally, active osteoblasts, located at the surfaces of bone matrix, typically form a single layer of cuboidal cells (MESCHER, 2018; LIEBICH, 2019). In this thesis, such active osteoblasts were present only in antlers in velvet, while in hard antlers they were visible only in the form of flat, inactive or resting osteoblasts that cover the bone matrix surface. In addition, histological analyzes in this thesis showed that the cortical part of hard antlers consists mostly of primary osteons. Contrary, in their study of fallow deer (*Dama dama* L.) antlers, ROLF and ENDERLE (1999) have concluded that hard antlers are a living tissue until approximately 3 weeks before casting. They report active osteoblasts and living osteocytes in cast antlers. According to them, antlers sampled 3 to 4 weeks prior to regular antler casting have fewer active osteoblasts, but contain some live and active cells that create "new bridges between osteoid seams". Furthermore, the same authors claim to have found visible osteocytes with pyknotic nuclei and even empty lacunae, from which they conclude that fallow deer antlers from this period are a slowly dying bone, and the process of dying will last 3 to 4 weeks until casting. According to ROLF and ENDERLE (1999), "these findings lead to the conclusion that from an osteological point of view the polished fallow deer antler without doubt represents living bone". Moreover, RÖSSNER et al. (2020) interpret antler osteons as secondary ones. This is contrary to the views of other authors (KRAUSS et al., 2011; GOMEZ et al., 2013; KIERDORF et al., 2013; SKEDROS et al., 2014) who state that antler osteons are predominantly primary ones, that there is no deposition of fluorochromes (oxytetracycline) in red deer antlers after velvet shedding, and that rather few secondary osteons are formed simultaneously with primary ones. Therefore, GOMEZ et al. (2013) refer to these secondary osteons that are formed during bone modelling (rather than remodeling) as modelling osteons.

The specific timeframe for the onset of DNA condensation in osteocytes after cell death is variable; however, it is generally considered that this process begins within a few hours after initiation of apoptosis/necrosis. There is variability in the data reported by different authors. KENZORA et al. (1978) report that most osteocytes lost their viability within 12-24 hours of blood supply interruption, however, they also state that osteocyte survival time can exceed 48 hours. According to BROWN and CRUESS (1982), the survival period is even longer and can be up to five days. This thesis shows that living osteocytes (type A) and dying osteocytes (type B) are present only in velvet antlers. In all antler samples obtained after velvet shedding, only dead

osteocytes (types C, D and E) were recorded. Due to technical limitations in sampling (inability to perform on-site sampling) and the distance between the sampling site and the laboratory, a brief time interval (2 to 3 hours) elapsed between the collection of the antler samples and their subsequent fixation in the present study, which is shorter than the time reported for osteocyte survival without blood supply (RÖSINGH and JAMES, 1969; KENZORA et al., 1978). Considering that the time interval was uniform across all sampling events, this factor can therefore be excluded as a potential human-related bias. The method for the detection of DNA damage, more specifically as a method for identifying apoptotic cells, is a TUNEL assay (LOO, 2002). The TUNEL assay is the method of choice for detecting apoptosis in situ, but this method is not limited to the detection of apoptotic cells. TUNEL can also be used to detect DNA damage associated with non-apoptotic events such as necrotic cell death induced by various insults (ANSARI et al., 1993). Programmed cell death (apoptosis) occurs in several skeletal cell types including chondrocytes, osteoclasts, osteoblasts and osteocytes (STEVENS et al., 2000; BODINE and KOMM, 2002; LI et al., 2002). In this thesis, osteocyte death was studied in antlers that had finished growth (late velvet stage) or even had already shed the velvet. Results of the TUNEL assay show that a few TUNEL-positive cells are found only in velvet antlers. Some of the TUNEL-positive cells were osteocytes, while others were multinuclear cells (osteoclasts). In all other samples (from antlers at velvet shedding till cast antlers), a positive signal was interpreted as a false signal (autofluorescence). Autofluorescence is visible in all sampled antlers, and was more frequent in the peripheral regions of antler tissue and within the vascular canals. KIERDORF et al. (2013) show that autofluorescence is present in roe deer antlers that have not been labelled with fluorochromes. In their research, the outer cortex showed a higher autofluorescence and a more immature structure than the main cortex, suggesting that it was secondarily formed by periosteal activity (younger part) and that it contains a higher proteoglycan content than the central cortex. In the regions of protuberances (pearls) of the antler surface, which is characteristic of the more proximal portions of roe deer antlers, marked autofluorescence was also visible. Furthermore, higher autofluorescence was present in more recently formed lamellar bone and osteoid. TAYLOR et al. (2012) also reported that there is a higher degree of autofluorescence of the bone matrix of newly-formed trabecular structures compared with the older matrix. Results of this thesis differ from the results obtained by COLITTI et al. (2005) who studied apoptosis in rapidly growing (regenerating) red deer antlers. This difference was expected since, contrary to their study, the

antlers studied in this thesis had finished their growth. COLITTI et al. (2005) found no TUNEL-positive cells in the velvet epidermis and dermis. Some TUNEL-positive cells were associated with hair follicles, while significant proportions of cells in the fibrous perichondrium and in the outer and inner mesenchyme of the antler growth region were TUNEL-positive. The apoptotic index was higher in non-mineralized than in mineralized cartilage of the growing antlers. Apoptotic chondrocytes were often observed adjacent to cells that appeared morphologically normal as well as adjacent to empty lacunae. The authors state that apoptotic bodies were also observed in some large lacunae. In the fibrous and cellular layers of the periosteum, a significant proportion of cells was TUNEL-positive, significantly more than in the overlying skin. At sites of intramembranous bone formation, a proportion of osteocytes and osteoblasts was TUNEL-positive, but no apoptotic osteoclasts were observed. The apoptosis observed by COLITTI et al. (2005) can (most likely) be linked to growth regulation and the control of morphogenesis, while the apoptosis found in the present thesis in the late velvet stage was probably related to changes in the course of an ischemic process. The findings of the present thesis demonstrated the presence of TUNEL-positive cells exclusively in velvet antlers, whereas no such cells were detected in hard antlers. Given that the applied kit is a non-isotopic system for the labelling of DNA breaks in (apoptotic) nuclei in paraffin-embedded tissue sections, tissue cryosections, cell preparations fixed on slides or cell suspensions (in accordance with the manufacturer's instructions), these observations are consistent with and confirm our previous results. It is, however, difficult to decide whether the observed cell death is a consequence of apoptosis or necrosis. Since it was observed only in velvet antlers, one can say that probably both types of death were present, i.e., some instances of apoptosis were linked to normal processes in growing antlers, while others represented necrosis attributed to ischemia due to the onset of a disruption in blood supply.

In the context of live vs. dead structure, it is necessary discuss a potential bone remodeling in hard antlers. ROLF and ENDERLE (1999) state that a progressive bone remodeling occurred in hard antler sections, including the presence of preosteoblasts undergoing mitotic cell division and active osteoblasts forming an osteoid seams. The process of bone remodeling would, however, also require the presence and action of osteoclasts in addition to osteoblasts. ROLF and ENDERLE (1999) did not describe osteoclasts or clear signs of bone resorption (Howship's lacunae) that should be present in the case of "remodeling". Furthermore, in a remodeled bone, several generations of secondary osteons should be present, and mineralized cartilage would not be

expected. In a study on fallow deer, KIERDORF et al. (2021) have shown that bone remodeling in antlers occurs only when their lifespan is experimentally prolonged by an antiandrogen treatment. The results of this thesis clearly support the view that short antler lifespan precludes significant remodeling of antler bone, explaining the small number of secondary osteons (GOMEZ et al., 2013). According to LANDETE-CASTILLEJOS et al. (2012) and KIERDORF et al. (2013, 2021, 2022), the growth phase of antlers is finished while they are still covered with velvet. The short lifespan of antlers results in an incomplete ossification, which is evidenced by the remnants of calcified cartilage. If remodeling of the bone in hard antlers really existed it should be visible by completion of ossification, existence of live cells and signs of osteoblastic and osteoclastic activity. Since ossification starts in the proximal parts of the antlers, remnants of calcified cartilage in proximal portions of antlers are either missing or present in only small amounts, while calcified cartilage is regularly present in their distal portions (LANDETE-CASTILLEJOS et al., 2012; KIERDORF et al., 2013, 2021, 2022). These findings are in accordance with the results of this thesis where the amount of calcified cartilage remnants was found to be highest in the distal antler portion (the youngest – "segment 3") and decreased toward the proximal portion (the oldest – "segment 1"). This difference between distal and proximal antler portions was found in all antler samples, from those still in velvet to the cast ones.

Another interesting finding is micropetrosis. It is a condition in which lacunae and canaliculi become filled with minerals (FROST, 1960a; BOYDE, 2003; BELL et al., 2008; MILOVANOVIC and BUSSE, 2020). It is associated with osteocyte apoptosis (BUSSE et al., 2010; MILOVANOVIC and BUSSE, 2020) and diagnostic of osteocyte death, leading to cessation of osteocyte activities in maintaining the lacunar space (BOYDE, 2003). The osteocyte lacunae can become occluded by mineral deposition after osteocyte death, a process referred to as passive lacunar mineralization (BUSSE et al., 2010; MILOVANOVIC and BUSSE, 2020). However, the release of matrix vesicles by dying osteocytes can also cause intralacunar mineral deposition while the cells are still alive, a process known as active lacunar mineralization (MILOVANOVIC et al., 2017; MILOVANOVIC and BUSSE, 2020). In addition to osteocyte lacunae, mineral deposits were also observed in chondrocyte lacunae of calcified cartilage remnants present in hard antlers (KIERDORF et al., 2022). In the present study, osteocyte and chondrocyte lacunae with mineral deposits were observed in antlers in velvet, antlers at velvet shedding, hard antlers and cast antlers. Given that apoptotic cells were identified only in velvet antlers, our results align with previous

findings that associate micropetrosis with osteocyte death. No cells were present in hard antlers. Following velvet shedding, due to the lack of all physiological/metabolic activity needed for both active and passive lacunar mineralization, the number of mineral-filled lacunae would not be expected to increase, which is consistent with the findings of this thesis. This further indicate complete disruption of blood supply, which does not allow for the formation of new mineral deposits.

One of the interesting hypotheses is that during the hard antler phase minerals used during the mineralization phase are gradually remobilized from antlers and returned to large bones of the deer organism. According to LI et al. (2024), deer can withdraw certain amount of calcium from antlers through preserved blood supply (referring partially to the observations reported by ROLF and ENDERLE, 1999), which should result in an increase in porosity due to bone resorption within the hard antlers. On the contrary, BROCKSTEDT-RASMUSSEN et al. (1987) analyzed the porosity of roe deer antlers and metacarpal bones collected during different months of the year and found a decrease of antler porosity over the hard antler period. Since velvet shedding in adult roe bucks occurs in March/April, it is important to note that the earliest antlers analyzed in this study were still in velvet. Although the results appear to be statistically significant, the methodology itself is questionable. First, an indirect indicator – porosity – was used without being confirmed by histological analysis, which complicates the interpretation of cellular and tissue-level changes. Second, the samples were collected over a period of 11 years, and in total, paired samples of antlers and metacarpal bones were obtained from 20 shot roe bucks. Furthermore, the authors did not report the exact age of the animals, which may be directly linked to porosity. Some samples were taken from roe bucks shot during the rut (July/August), and it is possible that these were territorial males in peak physical condition, while others may have been younger individuals harvested outside the rutting season. Such differences in age and physiological status could have influenced the porosity of both bone and antler tissue. Complete disruption of blood supply observed in this thesis inhibits potential withdrawal of minerals from hard antlers to the skeletal bones. Additionally, the densitometric results of the present study clearly show that there is no loss of mineral density of hard antlers. Therefore, it is obvious that once incorporated in hard antlers, minerals will stay there. At the same time, minerals taken from skeletal bones are replaced with calcium obtained via nutrition. Antler eating behavior (osteophagia) was observed in deer, showing that when antler minerals are re-used, it occurs in that way (BARRETTE, 1985).

Growing evidence supports the hypothesis that hard antlers are dead structures. LANDETE-CASTILLEJOS et al. (2019) have concluded that probably the main reason for the annual regeneration of antlers is the fact that hard antlers are dead bony structures. RÖSSNER et al. (2020) found no lines of arrested growth or other features indicating that antlers are longer-lived organs in recently shed muntjac antlers. All results presented in this thesis also suggest that osteocyte death occurs during the end of the velvet antler phase, indicating that by the time when velvet shedding takes place, viable osteocytes are no longer present. Histological analysis conducted in this thesis clearly demonstrates that deer antlers, after velvet shedding, are entirely avascular and acellular, confirming that they are a "dead", i.e., metabolically inactive organ. The results of this thesis thus support previous claims describing antlers as a "dead" organ, while also refuting scientific studies that characterize antlers as a "living" structure. This insight has direct applications in deer farming, particularly during various handling procedures. During the velvet phase, any intervention involving antlers is permitted only under anesthesia and analgesia administered by a licensed veterinarian. On the other hand, manipulation with hard antlers is more common, especially the removal of hard antlers in farmed deer. This practice helps to prevent potential injuries among males and to females due to possible fights, or to farm workers and infrastructure. This study confirms that such procedures do not cause pain or bleeding (with the exception of exudation of residual red fluid). In this study, the main factor that may have potentially influenced the results was the time interval between field sample collection and tissue fixation. Additionally, due to the fact that procedures were performed on live animals and in accordance with the 3R principle, the number of sampled animals was kept to a minimum. In future research, sampling and fixation should be carried out directly in the field immediately after antler removal, and, if possible, the results should be validated using a larger sample size.

7. CONCLUSIONS

- Blood is present only in velvet antlers. In all other samples, there was only residual red fluid, without corpuscular blood elements and the antler cavities were filled with bacteria.
- There is no blood supply in hard antlers that could promote antler life or withdrawal of minerals to the skeletal bones.
- Active/live osteoblasts and osteoclasts are present in antlers in velvet, while in the other samples no vital cells were present.
- The proportion of osteocytes type C (dead) decreases significantly, while the proportion of osteocytes type E (empty lacuna) increases significantly as the sampling time progresses after velvet shedding.
- Lacunar micropetrosis is observed in all sampled antlers from before velvet shedding till casting without changes in intensity, confirming disruption of blood supply.
- Bone mineral density is the lowest in velvet antlers, while in later samples it is higher, but without statistically significant difference between sampling dates. A statistically significant difference in bone mineral density was confirmed between proximal, middle, and distal segments.
- In all antlers sampled monthly from before velvet shedding till casting, remnants of calcified cartilage are present (with higher amount in distal portions).
- All obtained results indicate that hard antlers are a dead structure.

8. LITERATURE

ABBOTT, L. C., E. R. SCHOTTSTAEDT, J. B. SAUNDERS, C. M. DE, F. C. BOST (1947): The evaluation of cortical and cancellous bone grafting material: a clinical and experimental study. J. Bone Joint Surg. Am. 29, 381-414.

AESCHT, E., S. BÜCHL-ZIMMERMANN, A. BURMESTER, S. DÄNHARDT-PFEIFFER, C. DESEL, C. HAMERS, G. JACH, M. KÄSSENS, J. MAKOVITZKY, M. MULISCH, B. NIXDORF-BERGWEILER, D. PÜTZ, B. RIEDELSHEIMER, F. VAN DEN BOOM, R. WEGERHOFF, U. WELSCH (2010): Färbungen. In: Romeis - Mikroskopische Technik. Mulisch M., U. Welsch (eds), Spektrum Akademischer Verlag Heidelberg, pp. 183–297.

AIGNER, T., M. HEMMEL, D. NEUREITER, P. M. GEBHARD, G. ZEILER, T. KIRCHNER, L. MCKENNA (2001): Apoptotic cell death is not a widespread phenomenon in normal aging and osteoarthritis human articular knee cartilage: a study of proliferation, programmed cell death (apoptosis), and viability of chondrocytes in normal and osteoarthritic human knee cartilage. Arthritis Rheum. 44, 1304–1312. doi: 10.1002/1529-0131(200106)44:6<1304::AID-ART222>3.0.CO;2-T

AITCHISON, J. (1946): Hinged Teeth in Mammals: A Study of the Tusks of Muntjacs (Muntiacus) and Chinese Water Deer (*Hydropotes inermis*). Proc. Zool. Soc. Lond., 116, 329–338. doi: 10.1111/j.1096-3642.1946.tb00125.x

ALLEN, M. R., D. B. BURR (2014): Bone modeling and remodeling. In: Basic and Applied Bone Biology. (Burr, D. B., M. R. Allen, Eds.), Elsevier, Amsterdam, pp. 75–90. doi: 10.1016/B978-0-12-416015-6.00004-6

ALTSCHUL, S. F., W. GISH, W. MILLER, E. W. MYERS, D. J. LIPMAN (1990): Basic local alignment search tool. J. Mol. Biol. 215:403–410. doi: 10.1016/S0022-2836(05)80360-2

ANONYMOUS (2024): https://healthsciences.usask.ca/facility-services/Histology/alcian-blue-and-alizarin-red-s_ffpe-tissues-version-0.1-july-2022.pdf (accessed on: 07/15/2024).

ANSARI, B., P. J. COATES, B. D. GREENSTEIN, P. A. HALL (1993): In situ end-labelling detects DNA strand breaks in apoptosis and other physiological and pathological states. J. Pathol. 170, 1–8. doi: 10.1002/path.1711700102

ARCHANA, M, BASTIAN, T. L. YOGESH, K. L. KUMARASWAMY (2013): Various methods available for detection of apoptotic cells-a review. Indian J. Cancer, 50, 274-283. doi: 10. 4103/ 0019- 509X. 118720

ARENDS, M. J., R. G. MORRIS, A. H. WYLLIE (1990): Apoptosis: The role of the endonuclease. Am. J. Pathol. 136, 593–608.

ARISTOTLE (1991): History of Animals, Books VII-X, p. 401. Edited and translated by D.M. Balme. Loeb Classical Library, Harvard University Press, Cambridge, MA, USA.

ARNDT-JOVIN, D. J., T. M. JOVIN (1977): Analysis and sorting of living cells according to deoxyribonucleic acid content. J. Histochem. Cytochem. 25, 585–589. doi: 10.1177/25.7.70450

ASHKENAZI, A. (2002): Targeting death and decoy receptors of the tumour-necrosis factor superfamily. Nat. Rev. Cancer 2, 420–430. doi: 10.1038/nrc821

ASSAD, M., N. LEMIEUX, C. H. RIVARD (1997): Immunogold electron microscopy in situ end-labeling (EM-ISEL): Assay for biomaterial DNA damage detection. Bio-Med. Mater. Eng. 7, 391–400. doi: 10.1177/09592989199700700600 8

BACH-GANSMO, F. L., S. C. IRVINE, A. BRÜEL, J. S. THOMSEN, H. BIRKEDAL (2013): Calcified cartilage in rat cortical bone. Calcif. Tissue Int. 92, 330–338. doi: 10.1007/s00223-012-9682-6

BANKS, W. J. (1974): The Ossification Process of the Developing Antler in the White-tailed Deer (*Odocoileus virginianus*). Calcif. Tissue Res. 14, 257—274. doi: 10.1007/BF02060300

BANKS, W. J., J. W. NEWBREY (1983a): Light microscopic studies of the ossification process in developing antlers. In: Antler Development in Cervidae. (Brown, R. D., Ed.). Caesar Kleberg Wildlife Research Institute, Kingsville, USA, pp. 231–260.

BANKS, W. J., J. W. NEWBREY (1983b): Antler development as a unique modification of mammalian endochondral ossification. In: Antler development in Cervidae. (Brown R. D., Ed.). Caesar Kleberg Wildlife Research Institute, Kingsville, USA. p 279 –306.

BANKS, W., J. EPLING, R. KAINER, R. DAVIS (1968): Antler growth and osteoporosis. I. morphological and morphometric changes in the costal compacta during the antler growth cycle, Anat. Rec. 162, 387–398, doi: 10.1002/ar.1091620401

BARRETTE, C. (1977): Fighting Behavior of Muntjac and the Evolution of Antlers. Evolution 31, 169-176. doi: 10.2307/2407555

BARRETTE, C. (1985): Antler eating and antler growth in wild Axis deer. Mammalia 49, 491–500. doi: 10.1515/mamm.1985.49.4.491

BARTOŠ, L. (1990): Social Status and Antler Development in Red Reer. In: Horns, pronghorns, and antlers. (Bubenik, G. A., A. B. Bubenik, Eds.). Springer, New York, New York. pp. 424–459. doi: 10.1007/978-1-4613-8966-8_17

BAXTER, B. J., R. N. ANDREWS, G. K. BARRELL (1999): Bone turnover associated with antler growth in red deer (*Cervus elaphus*). Anat. Rec. 256: 14–19, doi: 10.1002/(SICI)1097-0185(19990901)256:1<14::AID-AR3>3.0.CO;2-A

BELL, L. S., M. KAYSER, C. JONES (2008): The mineralized osteocyte: a living fossil. Am. J. Phys. Anthropol. 137, 449–456. doi: 10.1002/ajpa.20886

BELLIDO, T., M. HUENING, M. RAVAL-PANDYA, S. C. MANOLAGAS, S. CHRISTAKOS (2000): Calbindin-D28k is expressed in osteoblastic cells and suppresses their apoptosis by inhibiting caspase-3 activity. J. Biol. Chem. 275, 26328–26332. doi: 10.1074/jbc.M003600200

BENINDE, J. (1937): Zur Naturgeschichte des Rothirschs. Verlag Paul Schöps. Leipzig, Germany.

BERGHE, T., A. LINKERMANN, S. JOUAN-LANHOUET, H. WALCZAK, P. VANDENABEELE (2014): Regulated necrosis: the expanding network of non-apoptotic cell death pathways. Nat. Rev. Mol. Cell Biol. 15, 135–147. doi: 10.1038/nrm3737

BODINE, P. V. N., B. S. KOMM (2002): Tissue Culture Models for Studies of Hormone and Vitamin Action in Bone Cells. In: Vitamins and Hormones, Vol. 64. (Litwack, G., Ed.), Academic Press, New York, pp. 101–151. doi: 10.1016/S0083-6729(02)64004-X

BONFIGLIO, M. (1954): Aseptic necrosis of the femoral head in dogs. Effects of drilling and bone grafting. Surg. Gynecol. Obstet. 98, 591-599.

BOWYER, R. T. (1983): Osteophagia and antler breakage among Roosevelt elk. Calif. Fish and Game 69, 84–88.

BOYCE, B. F., L. XING, R. L. JILKA, T. BELLIDO, R. S. WEINSTEIN, A. MICHAEL PARFITT, S. C. MANOLAGAS (2002): Apoptosis in Bone Cells. In: Principles of Bone Biology. (Bilezikian, J. P., L. G. Raisz, G. A. Rodan, Eds.). Academic Press, pp. 151 – 168.

BOYDE, A. (2003): The real response of bone to exercise. J. Anat. 203, 173–189. doi: 10.1046/j.1469-7580.2003.00213.x

BOYDE, A. (2021): The bone cartilage interface and osteoarthritis. Calcif. Tissue Int. 109, 303–328. doi: 10.1007/s00223-021-00866-9

BROCKSTEDT-RASMUSSEN, H., P. LETH SØRENSEN, H. EWALD, F. MELSEN (1987): The Rhythmic Relation between Antler and Bone Porosity in Danish Deer. Bone 8, 19-22. doi: 10.1016/8756-3282(87)90127-X

BROWN, K. L., R. L. CRUESS (1982): Bone and cartilage transplantation in orthopaedic surgery: a review. J. Bone Joint Surg. Am. 64, 270-279.

BROWN, R. D. (1990): Nutrition and Antler Development. In: Horns, pronghorns, and antlers. (Bubenik, G. A., A. B. Bubenik, Eds.). Springer, New York, New York, pp. 426–441. doi: 10.1007/978-1-4613-8966-8_16

BUBENIK, A. B. (1968): The significance of antlers in the social life of the Cervidae. Deer 1: 208-214.

BUBENIK, G. A. (1983): The endocrine regulation of the antler cycle. In: Antler development in Cervidae (Brown, R. D., Ed.). Caesar Kleberg Wildlife Res. Inst., Kingsville, Texas, pp. 73– 107.

BUBENIK, G. A. (1990): Neuroendocrine regulation of the antler cycle. In: Horns, pronghorns, and antlers. (Bubenik, G. A., A. B. Bubenik, Eds.). Springer, New York, New York, pp. 265-297.

BUBENIK, G. A. (1993): Morphological differences in the antler velvet of Cervidae. In: Deer of China. Biology and Management, (Ohtaishi, N., H. I. Sheng, Eds.), Elsevier, Amsterdam, pp. 56–64.

BUBENIK, G. A., A. B. BUBENIK (1990): Horns, Pronghorns, and Antlers: Evolution, Morphology, Physiology, and Social Significance. Springer Verlag, New York, USA.

BUBENIK, G. A., A. B. BUBENIK, G. M. BROWN, A. TRENKLE, D. I. WILSON (1975): Growth hormone and cortisol levels in the annual cycle of white-tailed deer (*Odocoileus virginianus*). Can. J. Physiol. Pharmacol 53, 787–792. doi: 10.1139/y75-108

BUSSE, B., D. DJONIC, P. MILOVANOVIC, M. HAHN, K. PÜSCHEL, R. O. RITCHIE, M. DJURIC, M. AMLING (2010): Decrease in the osteocyte lacunar density accompanied by hypermineralized lacunar occlusion reveals failure and delay of remodeling in aged human bone. Aging Cell. 9, 1065–1075. doi: 10.1111/j.1474-9726.2010.00633.x

CABRERA, D., T. STANKOWICH (2020): Stabbing Slinkers: Tusk Evolution Among Artiodactyls. Journal of Mammalian Evolution 27: 265–272. doi: 10.1007/s10914-018-9453-x

CALAMARI, Z. T., J. J. FLYNN (2024): Gene expression supports a single origin of horns and antlers in hoofed mammals. Commun. Biol. 7, 509. doi: 10.1038/s42003-024-06134-4

CAPITAN, A., C. GROHS, B. WEISS, M. N. ROSSIGNOL, P. REVERSE, A. A. EGGEN (2011): A newly described bovine type 2 scurs syndrome segregates with a frame-shift mutation in TWIST1. PLoS ONE 6: e22242. doi: 10.1371/journal.pone.0022242

CAPPELLI, J., A. S. ATZORI, F. CEACERO, T. LANDETE-CASTILLEJOS, A. CANNAS, L. GALLEGO, A. J. GARCÍA DÍAZ (2017): Morphology, chemical composition, mechanical properties and structure in antler of Sardinian red deer (*Cervus elaphus corsicanus*), Hystrix 28, 110–112. doi: 10.4404/hystrix–28.1-12270

CARO, T. M., C. M. GRAHAM, C. J. STONER, M. M. FLORES (2003): Correlates of horn and antler shape in bovids and cervids. Behavioral Ecology and Sociobiology, 55, 32–41. doi: 10.1007/s00265-003-0672-6

CATTO, M. (1965): A histological study of avascular necrosis of the femoral head after transcervical fracture. J. Bone Joint Surg. Br. 47, 749-776. doi: 10.1302/0301-620X.47B4.749

CATTO, M. (1976): Pathology of aseptic bone necrosis. In: Aseptic necrosis of bone. 1st ed. (Davidson, J. K., Ed.), Excerpta Medica, Amsterdam, Nederlands, pp. 3-100.

CEGIELSKI, M., I. IZYKOWSKA, M. PODHORSKA-OKOLOW, B. GWORYS, M. ZABEL, P. DZIEGIEL (2009): Histological studies of growing and mature antlers of red deer stags (*Cervus elaphus*). Anat. Histol. Embryol. 38, 184-188. doi: 10.1111/j.1439-0264.2008.00906.x

CHAPMAN, D. I. (1975): Antlers-bones of contention. Mamm. Rev. 5, 121-172. doi: 10.1111/j.1365-2907.1975.tb00194.x

CHAPMAN, D. I. (1981): Antler structure and function: a hypothesis. J. Biomech. 14, 195–197. doi: 10.1016/0021-9290(81)90026-9

CHEN, P. – Y., A. G. STOKES, J. MCKITTRICK (2009): Comparison of the structure and mechanical properties of bovine femur bone and antler of the North American elk (*Cervus elaphus canadensis*). Acta Biomater. 5, 693-706. doi: 10.1016/j.actbio.2008.09.011

CHEN, Q., J. KANG, C. FU (2018): The independence of and associations among apoptosis, autophagy, and necrosis. Signal Transduct. Target. Ther. 3, 18. doi: 10.1038/s41392-018-0018-5

CHURCHER, C. S. (1990): Cranial appendages of Giraffoidea, In: Horns, Pronghorns, and Antlers. (Bubenik, G. A., A. B. Bubenik, Eds.), Springer, New York, pp. 180–194. doi: 10.1007/978-1-4613-8966-8_5

CLUTTON-BROCK, T. H. (1982): The functions of antlers. Behaviour. 79, 108–124. doi: 10.1163/156853982X00201

CLUTTON-BROCK, T. H., S. D. ALBON, P. H. HARVEY (1980): Antlers, body size and breeding group size in the Cervidae. Nature, 285, 565–567. doi: 10.1038/285565a0

COLBERT, E. H. (1955): The evolution of vertebrates. Wiley, New York.

COLITTI, M., S. P. ALLEN, J. S. PRICE (2005): Programmed cell death in the regenerating deer antler. J. Anat., 207, 339–351. doi: 10.1111/j.1469-7580.2005.00464.x

COOPE, G. R. (1968): The evolutionary origin of antlers. Deer 1, 215-217.

COWAN, R. L., E. W. HARTSOOK, J. B. WHELAN (1968): Calcium-strontium metabolism in white-tailed deer as related to age and antler growth. Proc. Soc. Exp. Biol. Med. 129, 733-737. doi: 10.3181/00379727-129-33412

CROITOR, R. (2021): Taxonomy, systematics and evolution of giant deer *Megaloceros giganteus* (Blumenbach, 1799) (Cervidae, Mammalia) from the Pleistocene of Eurasia. Quaternary, 4, 36. doi: 10.3390/quat4040036

CRONIN, M. A., R. STUART, B. J. PIERSON, J. C. PATTON (1996): K-casein gene phylogeny of higher ruminants (Pecora, Artiodactyla). Mol. Phylogenet. Evol. 6: 295–311. doi: 10.1006/mpev.1996.0078

CUMMINGS, J., T. H. WARD, A. GREYSTOKE, M. RANSON, C. DIVE (2008): Biomarker method validation in anticancer drug development. Br. J. Pharmacol. 153, 646-656. doi: 10.1038/sj.bjp.0707441

CURREY J. D., T. LANDETE-CASTILLEJOS, J. A. ESTÉVEZ, A. OLGUÍN, A. J. GARCÍA, L. GALLEGO (2009a): The Young's modulus and impact energy absorption of wet and dry deer cortical bone, The Open Bone Journal 1, 38–45. doi: 10.2174/1876525400901010038

CURREY, J. D. (1979a): Mechanical properties of bone with greatly differing functions, J. Biomech. 12, 313–319. doi: 10.1016/0021-9290(79)90073-3

CURREY, J. D. (1979b): Changes in the impact energy absorption of bone with age, J. Biomech. 12, 459–469. doi: 10.1016/0021-9290(79)90031-9

CURREY, J. D. (1988): The effect of porosity and mineral content on the Young's modulus of elasticity of the compact bone, J. Biomech. 21, 131–139. doi: 10.1016/0021-9290(88)90006-1

CURREY, J. D. (1999): The design of mineralised hard tissues for their mechanical functions, J. Exp. Biol. 202, 3285–3294. doi: 10.1242/jeb.202.23.3285

CURREY, J. D. (2002): Bones: Structure and Mechanics, Princeton University Press, Princeton.

CURREY, J. D., T. LANDETE-CASTILLEJOS, J. ESTÉVEZ, F. CEACERO, A. OLGUÍN, A. GARCÍA, L. GALLEGO (2009b): The mechanical properties of deer antler bone when used in fighting, J. Exp. Biol. 212, 3985–3993. doi: 10.1242/jeb.032292

CZABOTAR, P. E., G. LESSENE, A. STRASSER, J. M. ADAMS (2014): Control of apoptosis by the BCL-2 protein family: implications for physiology and therapy. Nat. Rev. Mol. Cell Biol. 15, 49–63. doi: 10.1038/nrm3722

DARZYNKIEWICZ, Z., D. GALKOWSKI, H. ZHAO (2008): Analysis of apoptosis by cytometry using TUNEL assay. Methods. 44, 250-254. doi: 10.1016/j.ymeth.2007.11.008

DAVIS, E. B., K. A. BRAKORA, A. H. LEE (2011): Evolution of ruminant headgear: a review. Proc. Biol. Sci. 278, 2857–2865. doi: 10.1098/rspb.2011.0938

DAVIS, E. B., K. A. BRAKORA, K. STILSON (2014): Evolution, development and functional role of horns in cattle, In: Ecology, Evolution and Behaviour of Wild Cattle: Implications for Conservation. (Melletti, M., J. Burton, Eds.). Cambridge University Press, Cambridge, pp. 72−82. doi: org/10.1017/CBO9781139568098.010

DAVIS, R. W. (1962): Studies on antler growth in mule deer. In: Proceedings of the first national white-tailed deer disease symposium, Athens: Univ. Georgia p. 61-64.

DAVISON, K. S., K. SIMINOSKI, J. D. ADACHI, D. A. HANLEY, D. GOLTZMAN, A. B. HODSMAN, R. JOSSE, S. KAISER, W. P. OLSZYNSKI, A. PAPAIOANNOU, L. G. STE-MARIE, D. L. KENDLER, A. TENENHOUSE, J. P. BROWN (2006): Bone strength: the whole is greater than the sum of its parts, Semin. Arthritis Rheum. 36, 22–31. doi: 10.1016/j.semarthrit.2006.04.002

DE BUFFRÉNIL, V., A. DE RICQLÉS, C. E. RAY, P. P. DOMNING (1990): Bone histology of the ribs of the Archaeocetes (Mammalia: Cetacea). J. Vert. Paleontol. 10, 455–466. doi: 10.1080/02724634.1990.10011828

DE BUFFRÉNIL, V., H. ASTIBIA, X. PEREDA SUBERBIOLA, A. BERRETEAGA, N. BARDET (2008): Variation in bone histology of middle Eocene sirenians from western Europe. Geodiversitas 30, 425–432. doi: 10.5281/zenodo.5376687

DEMARAIS, S., B. K. STRICKLAND (2011): Antlers. In: Biology and management of white-tailed deer. (Hewitt, D. G., Ed.), CRC Press, Boca Raton, Florida, pp. 107–145.

DEMIGUEL, D., B. AZANZA, J. MORALES (2014): Key innovations in ruminant evolution: a paleontological perspective. Integr. Zool. 9, 412–433. doi: 10.1111/1749-4877.12080

DHURIYA, Y. K., D. SHARMA (2018): Necroptosis: a regulated inflammatory mode of cell death. Journal of Neuroinflammation 15, 199. doi: 10.1186/s12974-018-1235-0

DINGERKUS, G., L. D. UHLER (1977): Enzyme Clearing of Alcian Blue Stained Whole Small Vertebrates for Demonstration of Cartilage. Stain Technol., 52, 229-232. doi: 10.3109/10520297709116780

ECKLE, V. S., A. BUCHMANN, W. BURSCH, R. SCHULTE-HERMANN, M. SCHWARZ (2004): Immunohistochemical detection of activated caspases in apoptotic hepatocytes in rat liver. Toxicol. Pathol., 32, 9-15. doi: 10.1080/01926230490260673

ELLIOTT, J. L., J. M. OLDHAM, G. R. AMBLER, J. J. BASS, G. S. SPENCER, S. C. HODGKINSON, B. H. BREIER, P. D. GLUCKMAN, J. M. SUTTIE (1992): Presence of insulin-like growth factor-I receptors and absence of growth hormone receptors in the antler tip. Endocrinology, 130, 2513–2520. doi: 10.1210/endo.130.5.1315246

ELLIOTT, J. L., J. M. OLDHAM, G. R. AMBLER, P. C. MOLAN, G. S. G. SPENCER, S. C. HODGKINSON, B. H. BREIER, P. D. GLUCKMAN, J. M. SUTTIE, J. J. BASS (1993): Receptors for insulin-like growth factor-II in the growing tip of the deer antler. J. Endocrinol. 138, 233–242. doi: 10.1677/joe.0.1380233

ELMORE, S. (2007): Apoptosis: a review of programmed cell death. Toxicol. Pathol. 35, 495–516. doi: 10.1080/01926230701320337

EVANS, F. G., M. LEBOW (1951): Regional differences in some of the physical properties of the human femur. J. App. Physiol. 3, 563 -572. doi: 10.1152/jappl.1951.3.9.563

FAUCHEUX, C., S. A. NESBITT, M. A. HORTON, J. S. PRICE (2001): Cells in regenerating deer antler cartilage provide a microenvironment that supports osteoclast differentiation. J. Exp. Biol. 204, 443–455. doi: 10.1242/jeb.204.3.443

FAWCETT, D. W. (1942): The amedullary bones of the Florida manatee (*Trichechus latirostris*). Am. J. Anat. 71, 271–309. doi: 10.1002/aja.1000710206

FENNESSY, P. F. (1984): Deer Antlers: Regeneration, function and evolution, Journal of the Royal Society of New Zealand, 14, 290-291. doi:10.1080/03036758.1984.10426948

FERGUSON, V. L., A. J. BUSHBY, A. BOYDE (2003): Nanomechanical properties and mineral concentration in articular calcified cartilage and subchondral bone. J. Anat. 203, 191–202. doi: 10.1046/j.1469-7580.2003.00193.x

FOLMER, O., M. BLACK, W. HOEH, R. LUTZ, R. VRIJENHOEK (1994): DNA primers for amplification of mitochondrial cytochrome c oxidase subunit I from diverse metazoan invertebrates. Mol. Mar. Biol. Biotechnol. 3, 294–299.

FRASIER, M. B., W. J. BANKS (1973): Characterization of antler mucosubstances by selected histochemical techniques. Anat. Rec. 175, 323.

FROST, H. M. (1960a): Micropetrosis. J. Bone Joint Surg. Am. 42, 144–150.

FROST, H. M. (1960b): In vivo osteocyte death. J. Bone Joint Surg. Am. 42, 138–143.

GALEA, G. L., M. R. ZEIN, S. ALLEN, P. FRANCIS-WEST (2021): Making and shaping endochondral and intramembranous bones. Dev. Dyn. 250, 414–449. doi: 10.1002/dvdy.278

GANEY T., J. OGDEN, J. OLSEN (1990): Development of the giraffe horn and its blood supply. Anat. Rec. 227, 497–507. doi: 10.1002/ar.1092270413

GAVRIELI, Y., Y. SHERMAN, S. A. BEN-SASSON (1992): Identification of programmed cell death in situ via specific labeling of nuclear DNA fragmentation. J. Cell Biol. 119, 493–501. doi: 10.1083/jcb.119.3.493

GEIST, V. (1981): Behaviour: Adaptive strategies in mule deer. In: Mule and black-tailed deer of North America. (Wallmo. O. C., Ed.), University of Nebraska Press, Lincoln, Nebraska, pp. 157-223.

GEIST, V. (1998): Deer of the World, their Evolution, Behavior, and Ecology. Stackpole Books, Mechanisburg, Pennsylvania.

GENTRY, A. W. (2000): The ruminant radiation. In: Antelopes, Deer, and Relatives. (Vrba, E. S., G. B. Schaller, Eds.), Yale University Press, New Haven, Connecticut, pp. 11–25.

GERAADS, D. (1991): Derived features of giraffid ossicones. J. Mamm. 72, 213-214. doi: 10.2307/1382003

GHOBRIAL, I. M., T. E. WITZIG, A. A. ADJEI (2005): Targeting apoptosis pathways in cancer therapy. CA Cancer J. Clin. 55, 178–194. doi: 10.3322/canjclin.55.3.178

GILBERT, C., A. ROPIQUET, A. HASSANIN (2006): Mitochondrial and nuclear phylogenies of Cervidae (Mammalia, Ruminantia): Systematics, morphology, and biogeography. Mol. Phylogenet. Evol., 40, 101–117. doi: 10.1016/j.ympev.2006.02.017

GOLD, R., M. SCHMIED, G. GIEGERICH, H. BREITSCHOPF, H. P. HARTUNG, K. V. TOYKA, H. LASSMANN (1994): Differentiation between cellular apoptosis and necrosis by the combined use of in situ tailing and nick translation techniques. Lab. Invest. 71, 219–225.

GOLD, R., M. SCHMIED, G. ROTHE, H. ZISCHLER, H. BREITSCHOPF, H. WEKERLE, H. LASSMANN (1993): Detection of DNA fragmentation in apoptosis: Application of in situ nick translation to cell culture systems and tissue sections. J. Histochem. Cytochem., 41, 1023–1030. doi: 10.1177/41.7.8515045

GOLSTEIN, P., G. KROEMER (2007): Cell death by necrosis: towards a molecular definition. Trends Biochem. Sci. 32, 37–43. doi: 10.1016/j.tibs.2006.11.001

GOMEZ S., A. J. GARCÍA, S. LUNA, U. KIERDORF, H. KIERDORF, L. GALLEGO, T. LANDETE-CASTILLEJOS (2013): Labeling studies on cortical bone formation in the antlers of red deer (*Cervus elaphus*), Bone, 52, 506–515. doi: 10.1016/j.bone.2012.09.015

GÓMEZ, J. A., J. PÉREZ-BARBERÍA, A. J. GARCÍA, J. CAPPELLI, L. CHONCO, F. CEACERO, M. PÉREZ-SERRANO, T. LANDETE-CASTILLEJOS (2022): Factors affecting antler growth period and casting date in red deer. J. Mammal. 103, 169-177. doi: 10.1093/jmammal/gyab097

GOSS, R. J. (1961): Experimental investigations of morphogenesis in the growing antler. J. Embryol. Exp. Morphol., 9, 342–354.

GOSS, R. J. (1968): Inhibition of growth and shedding of antlers by sex hormones. Nature 220, 83–85. doi: 10.1038/220083a0

GOSS, R. J. (1970): Problems of antlerogenesis, Clin. Orthop. Relat. Res. 69, 227–238.

GOSS, R. J. (1983): Deer Antlers: Regeneration, Function, and Evolution, Academic Press, New York.

GOSS, R. J. (1984): Epimorphic regeneration in mammals. In: Soft and hard tissue repair. (Hunt, T. K., R. B. Heppenstall, E. Pines, D. Rovee, Eds.), Praeger, New York, pp. 554 –573.

GOSS, R. J. (1990): Of antlers and embryos. In: Horns, pronghorns and antlers. (Bubenik, G. A., A. B. Bubenik, Eds.), Springer, New York, pp 298-312. doi: 10.1007/978-1-4613-8966-8_9

GOSS, R. J. (1992): Regeneration versus repair. In: Wound healing— biochemical and clinical aspects. (Cohen, I. K., R. F. Diegelmann, W. J. Lindblad, Eds.), Saunders, Philadelphia, pp. 20 –39.

GOSS, R. J. (1995): Future directions in antler research. Anat. Rec. 241, 291– 302. doi:10.1002/ar.1092410302

GOSS, R. J., A. VAN PRAAGH, P. BREWER (1992): The mechanism of antler casting in fallow deer. J. Exp. Zool. 264, 429– 436. doi: 10.1002/jez.1402640408

GOSS, R. J., R. S. POWEL (1985): Induction of deer antlers by transplanted periosteum. I. Graft size and shape. J. Exp. Zool. 235, 359–373. doi: 10.1002/jez.1402350307

GOULD, S. J. (1973): Positive Allometry of Antlers in the "Irish Elk", *Megalocerus giganteus*. Nature 244, 375–376. doi: 10.1038/244375a0

GRASL-KRAUPP, B., B. RUTTKAY-NEDECKY, H. KOUDELKA, K. BUKOWSKA, W. BURSCH, R. SCHULTE-HERMANN (1995): In situ detection of fragmented DNA (TUNEL assay) fails to discriminate among apoptosis, necrosis, and autolytic cell death: A cautionary note. Hepatology 21, 1465–1468. doi: 10.1002/hep.1840210534

GROVES, C. P., P. GRUBB (1990): Muntiacidae. In: Horns, Pronghorns, and Antlers. (Bubenik, G. A., A. B. Bubenik, Eds.), Springer, New York, pp. 134–168.

GRUBER, G. B. (1937): Morphobiologische Untersuchungen am Cerviden-Geweih. Werden, Weehsel und Wesen des Rehgehorns. Wiss. Nachr. Biol. 3, 9-63.

GUO, M., B. A. HAY (1999): Cell proliferation and apoptosis. Curr. Opin. Cell Biol., 11, 745–752. doi: 10.1016/s0955-0674(99)00046-0

GUTIÉRREZ, E. E., K. M. HELGEN, M. M. MCDONOUGH, F. BAUER, M. T. HAWKINS, L. A. ESCOBEDO-MORALES, B. D. PATTERSON, J. E. MALDONADO (2017): A gene-tree test of the traditional taxonomy of American deer: the importance of voucher specimens, geographic data, and dense sampling. ZooKeys, 697, 87-131. doi: 10.3897/zookeys.697.15124

HABERMEHL, K. H. (1985): Altersbestimmung bei Wild- und Pelztieren, 2nd ed., Paul Parey, Hamburg. doi: 10.1111/j.1439-0442.1986.tb00521.x

HALL, B. K. (2015): Bones and Cartilage: Developmental and Evolutionary Skeletal Biology (Second edition), Elsevier, Amsterdam.

HALL, T. A. (1999): BioEdit: a user-friendly biological sequence alignment editor and analysis program for Windows 95/98/NT. Nucleic Acids Symp. Ser. 41, 95–98.

HARDY, M. H. (1992): The secret life of the hair follicle. Trends Genet. 8, 55–61. doi: 10.1016/0168-9525(92)90350-d

HARRINGTON, R. (1985): Evolution and distribution of the cervidae. In: Biology of deer production. (Fennessy, P. F., K. R. Drew, Eds.), The Royal Society of New Zealand, Wellington, pp. 3-11.

HARTWIG, H. (1967): Experimentelle Untersuehungen znr Entwicklungsphysiologie der Stangenbildung beim Reh (*Capreolus C. capreolus* L. 1758). Wilhelm Roux' Arch. Entwickl.- Mech. Org. 158, 358-384.

HARTWIG, H., J. SCHRUDDE (1974): Experimentelle Untersuchungen zur Bildung der primären Stirnauswüchse beim Reh (*Capreolus capreolus* L.). Z. Jagdwiss. 20, 1-13.

HASSANIN, A., E. J. P. DOUZERY (2003): Molecular and Morphological Phylogenies of Ruminantia and the Alternative Position of the Moschidae. Systematic Biology 52, 206–228. doi: 10.1080/10635150390192726

HASSANIN, A., F. DELSUC, A. ROPIQUET, C. HAMMER, B. JANSEN VAN VUUREN, C. MATTHEE, M. RUIZ-GARCIA, F. CATZEFLIS, V. ARESKOUG, T. T. NGUYEN, A. COULOUX (2012): Pattern and timing of diversification of Cetartiodactyla (Mammalia, Laurasiatheria), as revealed by a comprehensive analysis of mitochondrial genomes. C. R. Biol., 335, 32–50. doi: 10.1016/j.crvi.2011.11.002

HEBERT, P. D. N., A. CYWINSKA, S. L. BALL, J. R. DE WAARD (2003): Biological identifications through DNA barcodes. Proc. Biol. Sci., 270, 313–321. doi: 10.1098/rspb.2002.2218

HECKEBERG, N. S., D. ERPENBECK, G. WÖRHEIDE, G. E. RÖSSNER (2016): Systematic relationships of five newly sequenced cervid species. PeerJ. 4:e2307. doi: 10.7717/peerj.2307

HECKEBERG, N. S., F. E. ZACHOS, U. KIERDORF (2023): Antler tine homologies and cervid systematics: A review of past and present controversies with special emphasis on *Elaphurus davidianus*. Anat. Rec. (Hoboken)., 306, 5–28. doi: 10.1002/ar.24956

HILLMAN, J. R., R. W. DAVIS, Y. Z. ABDELBAKI (1973): Cyclic bone remodeling in deer, Calc.Tiss. Res. 12, 323–330. doi: 10.1007/BF02013745

HU, X. M., Z. X. LI, R. H. LIN, J. Q. SHAN, Q. W. YU, R. X. WANG, L. S. LIAO, W. T. YAN, Z. WANG, L. SHANG, Y. HUANG, Q. ZHANG, K. XIONG (2021): Guidelines for Regulated Cell Death Assays: A Systematic Summary, A Categorical Comparison, A Prospective. Front. Cell Dev. Biol., 4:9:634690. doi: 10.3389/fcell.2021.634690

HUGHES, S., T. J. HAYDEN, C. J. DOUADY, C. TOUGARD, M. GERMONPRÉ, A. STUART, L. LBOVA, R. F. CARDEN, C. HÄNNI, L. SAY (2006): Molecular phylogeny of the extinct giant deer, *Megaloceros giganteus*. Mol. Phylogenet. Evol., 40, 285–291. doi: 10.1016/j.ympev.2006.02.004

JAMES, J., G. L. STEIJN-MYAGKAYA (1986): Death of osteocytes. Electron microscopy after in vitro ischaemia. J. Bone Joint Surg. Br., 68, 620-624. doi: 10.1302/0301-620x.68b4.3733842

JANICKI, Z., A. SLAVICA, D. KONJEVIĆ, K. SEVERIN (2007): Zoologija divljači. Zavod za biologiju, patologiju i uzgoj divljači Veterinarskog fakulteta Sveučilišta u Zagrebu, Zagreb, pp. 17-22.

JIN, J. J. H., P. SHIPMAN (2010): Documenting natural wear on antlers: A first step in identifying use-wear on purported antler tools. Quaternary International 211, 91–102. doi: 10.1016/j.quaint.2009.06.023

JING, Y., J. JING, L. YE, X. LIU, S. E. HARRIS, R. J. HINTON, J. Q. FENG (2017): Chondrogenesis and osteogenesis are one continuous developmental and lineage defined biological process. Sci. Rep. 7, 10020. doi: 10.1038/s41598-017-10048-z

JUDKINS, R. L. (1958): Microscopic anatomy of the deer antler, M. S. Thesis. Fort Collins: Colorado State University. p. 81.

KANDUC, D., A. MITTELMAN, R. SERPICO, E. SINIGAGLIA, A. A. SINHA, C. NATALE, R. SANTACROCE, M. G. DI CORCIA, A. LUCCHESE, L. DINI, P. PANI, S. SANTACROCE, S. SIMONE, R. BUCCI, E. FARBER (2002): Cell death: apoptosis versus necrosis (review). Int. J. Oncol. 21, 165–170. doi: 10.3892/ijo.21.1.165

KARI S., K. SUBRAMANIAN, I. A. ALTOMONTE, A. MURUGESAN, O. YLI-HARJA, M. KANDHAVELU (2022): Programmed cell death detection methods: a systematic review and a categorical comparison. Apoptosis 27, 482–508. doi: 10.1007/s10495-022-01735-y

KAUFMANN, S. H., P. W. JR MESNER, K. SAMEJIMA, S. TONÉ, W. C. EARNSHAW (2000): Detection of DNA cleavage in apoptotic cells. Methods Enzymol., 322, 3–15. doi: 10.1016/s0076-6879(00)22003-x

KELLY, K. J., R. M. SANDOVAL, K. W. DUNN, B. A. MOLITORIS, P. C. DAGHER (2003): A novel method to determine specificity and sensitivity of the TUNEL reaction in the quantitation of apoptosis. Am. J. Physiol. Cell Physiol., 284,C1309–C1318. doi: 10.1152/ajpcell.00353.2002

KENZORA, J. E., R. E. STEELE, Z. H. YOSIPOVITCH, M. J. GLIMCHER (1978): Experimental osteonecrosis of the femoral head in adult rabbits. Clin. Orthop. Relat. Res., 130, 8-46.

KERR, J. F., A. H. WYLLIE, A. R. CURRIE (1972): Apoptosis: a basic biological phenomenon with wide-ranging implications in tissue kinetics. Br. J. Cancer, 26, 239–257. doi: 10.1038/bjc.1972.33

KERSCHNITZKI, M., W. WAGERMAIER, P. ROSCHGER, J. SETO, R. SHAHAR, G. N. DUDA, S. MUNDLOS, P. FRATZL (2011): The organization of the osteocyte network mirrors the extracellular matrix orientation in bone. J. Struct. Biol., 173, 303–311. doi: 10.1016/j.jsb.2010.11.014

KHALID, N., M. AZIMPOURAN (2020): Necrosis. Treasure Island (FL). StatPearls Publishing.

KIERDORF, H., U. KIERDORF (1992): State of determination of the antlerogenic tissues with special reference to double-head formation. In: The biology of deer. (Brown, R. D., Ed.), Springer, New York. pp. 525 -531.

KIERDORF, H., U. KIERDORF, T. SZUWART, G. CLEMEN (1995a): A light microscopic study of primary antler development in fallow deer (*Dama dama*). Ann. Anat., 177, 525–532. doi: 10.1016/S0940-9602(11)80085-3

KIERDORF, H., U. KIERDORF, T. SZUWART, U. GATH, G. CLEMEN (1994): Light microscopic observations on the ossification process in the early developing pedicle of fallow deer (*Dama dama*). Ann. Anat. 176, 243-249. doi: 10.1016/S0940-9602(11)80485-1

KIERDORF, U., C. LI, J. S. PRICE (2009): Improbable appendages: Deer antler renewal as a unique case of mammalian regeneration. Semin. Cell Dev. Biol. 20, 535–542. doi: 10.1016/j.semcdb.2008.11.011

KIERDORF, U., D. STOFFELS, H. KIERDORF (2014): Element concentrations and element ratios in antler and pedicle bone of yearling red deer (*Cervus elaphus*) stags – a quantitative X-ray fluorescence study, Biol. Trace Elem. Res. 162, 124–133. doi: 10.1007/s12011-014-0154-x

KIERDORF, U., E. STOFFELS, D. STOFFELS, H. KIERDORF, T. SZUWART, G. CLEMEN (2003): Histological studies of bone formation during pedicle restoration and early antler regeneration in roe deer and fallow deer. Anat. Rec. A. Discov. Mol. Cell Evol. Biol., 273, 741–751. doi: 10.1002/ar.a.10082

KIERDORF, U., H. KIERDORF (2000): Delayed ectopic antler growth and formation of a double-head antler in the metacarpal region of a fallow buck (*Dama dama* L.) following transplantation of antlerogenic periosteum. Ann. Anat. 182, 365-370. doi: 10.1016/s0940-9602(00)80013-8

KIERDORF, U., H. KIERDORF (2012): Antler regrowth as a form of epimorphic regeneration in vertebrates – a comparative view. Front. Biosci. (Elite Ed)., 4, 1606-1624. doi: 10.2741/483

KIERDORF, U., H. KIERDORF, M. SCHULTZ, H. J. ROLF (2004): Histological structure of antlers in castrated male fallow deer (*Dama dama*). Anat. Rec. A. Discov. Mol. Cell Evol. Biol. 281, 1352–1362. doi: 10.1002/ar.a.20127

KIERDORF, U., H. KIERDORF, S. KNUTH (1995b): Effects of castration on antler growth in fallow deer (*Dama dama* L.). J. Exp. Zool. 273, 33-43. doi: 10.1002/jez.1402730105

KIERDORF, U., H. KIERDORF, T. SZUWART (2007): Deer antler regeneration: cells, concepts, and controversies. J. Morphol. 268, 726–738. doi: 10.1002/jmor.10546

KIERDORF, U., M. SCHULTZ, H. KIERDORF (2021): The consequences of living longer—Effects of an experimentally extended velvet antler phase on the histomorphology of antler bone in fallow deer (*Dama dama*). J. Anat. 239, 1104–1113. doi: 10.1111/joa.13495

KIERDORF, U., M. SCHULTZ, K. FISCHER (1993): Effects of an antiandrogen treatment on the antler cycle of male fallow deer (*Dama dama* L.). J. Exp. Zool. 266, 195-205. doi: 10.1002/jez.1402660305

KIERDORF, U., S. FLOHR, S. GOMEZ, T. LANDETE-CASTILLEJOS, H. KIERDORF (2013): The structure of pedicle and hard antler bone in the European roe deer (*Capreolus capreolus*): a light microscope and backscattered electron imaging study, J. Anat. 223, 364–384. doi: 10.1111/joa.12091

KIERDORF, U., S. R. STOCK, S. GOMEZ, O. ANTIPOVA, H. KIERDORF (2022): Distribution, structure, and mineralization of calcified cartilage remnants in hard antlers. Bone Rep., 16, 101571. doi: 10.1016/j.bonr.2022.101571

KITCHENER, A. (1985): The effect of behaviour and body weight on the morphological design of horns. Journal of Zoology, 205, 191–203.

KLINKHAMER, A. J., N. WOODLEY, J. M. NEENAN, W. C. H. PARR, P. CLAUSEN, M. R. SANCHEZ-VILLAGRA, G. SANSALONE, A. M. LISTER, S. WROE (2019): Head to head: The case for fighting behavior in *Megaloceros giganteus* using finite-element analysis. Proc. Biol. Sci., 286, 20191873. doi: 10.1098/rspb.2019.1873

KLUCK, R. M., E. BOSSY-WETZEL, D. R. GREEN, D. D. NEWMEYER (1997): The release of cytochrome c from mitochondria: a primary site for Bcl-2 regulation of apoptosis. Science 275, 1132–1136. doi: 10.1126/science.275.5303.1132

KOCKX, M. M., J. MUHRING, M. W. M. KNAAPEN, G. R. Y. DE MEYER (1998): RNA synthesis and splicing interferes with DNA in situ end labeling techniques used to detect apoptosis. Am. J. Pathol. 152, 885–888.

KOLLE, R., U. KIERDORF, K. FISCHER (1993): Effects of an antiandrogen treatment on morphological characters and physiological functions of male fallow deer (*Dama dama* L.). J. Exp. Zool. 267, 288-298. doi: 10.1002/jez.1402670307

KOUSTENI, S., T. BELLIDO, L. I. PLOTKIN, C. A. O'BRIEN, D. L. BODENNER, L. HAN, K. HAN, G. B. DIGREGORIO, J. A. KATZENELLENBOGEN, B. S. KATZENELLENBOGEN, P. K. ROBERSON, R. S. WEINSTEIN, R. L. JILKA, S. C. MANOLAGAS (2001): Nongenotropic, sex-nonspecific signaling through the estrogen or androgen receptors: dissociation from transcriptional activity. Cell 104, 719–730.

KRAUSS, S., P. FRATZL, J. SETO, J. D. CURREY, J. A. ESTEVEZ, S. S. FUNARI, H. S. GUPTA (2009): Inhomogeneous fibril stretching in antler starts after macroscopic yielding: Indication for a nanoscale toughening mechanism. Bone 44, 1105–1110. doi: 10.1016/j.bone.2009.02.009

KRAUSS, S., W. WAGEMEIER, J. A. ESTEVEZ, J. D. CURREY, P. FRATZL (2011): Tubular frameworks guiding orderly bone formation in the antler of the red deer (*Cervus elaphus*), J. Struct. Biol., 175, 457–464. doi: 10.1016/j.jsb.2011.06.005

KUHLMAN, R. E., R. RAINEY, R. O'NEILL (1963): Biochemical investigations of deer antler. II. Quantitative microchemical changes associated with antler bone formation. J. Bone and Joint Surg. 45 A, 345-350.

KUWATA, N., S. KAWAI, K. DOI (1984): Clinical and experimental studies of bone union in reimplantation of digits: a preliminary report on ischemic interval. Microsurgery. 5, 31-35. doi: 10.1002/micr.1920050107

KUZNETSOVA, M. V., M. V. KHOLODOVA, A. A. DANILKIN (2005): Molecular phylogeny of deer (Cervidae: Artiodactyla). Russ. J. Genet., 41: 742–749. doi: 10.1007/s11177-005-0154-1

LANDETE-CASTILLEJOS, T., A. GARCÍA, L. GALLEGO (2007a): Body weight, early growth and antler size influence antler bone mineral composition of Iberian red deer (*Cervus elaphus hispanicus*). Bone. 40, 230–235. doi: 10.1016/j.bone.2006.07.009

LANDETE-CASTILLEJOS, T., H. KIERDORF, S. GOMEZ, S. LUNA, A. J. GARCIA, J. CAPPELLI, M. PÉREZ-SERRANO, J. PÉREZ-BARBERÍA, L. GALLEGO, U. KIERDORF (2019): Antlers - Evolution, development, structure, composition, and biomechanics of an outstanding type of bone. Bone. 128, 115046. doi: 10.1016/j.bone.2019.115046

LANDETE-CASTILLEJOS, T., J. A. ESTEVEZ, A. MARTÍNEZ, F. CEACERO, A. GARCIA, L. GALLEGO (2007b): Does chemical composition of antler bone reflect the physiological effort made to grow it? Bone. 40, 1095–1102. doi: 10.1016/j.bone.2006.11.022

LANDETE-CASTILLEJOS, T., J. A. ESTEVEZ, F. CEACERO, A. J. GARCIA, L. A. GALLEGO (2012a): Review of factors affecting antler composition and mechanics. Front. Biosci. (Elite Ed). 4, 2328-2339. doi: 10.2741/e545

LANDETE-CASTILLEJOS, T., J. D. CURREY, F. CEACERO, A. J. GARCIA, L. GALLEGO, S. GOMEZ (2012b): Does nutrition affect bone porosity and mineral tissue distribution in deer antlers? The relationship between histology, mechanical properties and mineral composition. Bone. 50, 245–254. doi: 10.1016/j.bone.2011.10.026

LANDETE-CASTILLEJOS, T., J. D. CURREY, J. A. ESTEVEZ, E. GASPAR-LÓPEZ, A. J. GARCIA, L. GALLEGO (2007c): Influence of physiological effort of growth and chemical composition on antler bone mechanical properties. Bone. 41, 794–803. doi: 10.1016/j.bone.2007.07.013

LANDETE-CASTILLEJOS, T., J. D. CURREY, J. A. ESTEVEZ, Y. FIERRO, A. CALATAYUD, F. CEACERO, A. GARCIA, L. GALLEGO (2010): Do drastic weather effects on diet influence changes in chemical composition, mechanical properties and structure in deer antlers? Bone. 47, 815–825. doi: 10.1016/j.bone.2010.07.021

LANKESTER, E. R. (1907): The Origin of the Lateral Horns of the Giraffe in Foetal Life on the Area of the Parietal Bones. Proc. Zool. Soc. Lond., 77, 100-115.

LAUNEY, M. E., P. Y. CHEN, J. MCKITTRICK, R. O. RITCHIE (2010): Mechanistic aspects of the fracture toughness of elk antler bone. Acta Biomater. 6, 1505–1514. doi: 10.1016/j.actbio.2009.11.026

LI, C. (2012): Deer antler regeneration: a stem cell-based epimorphic process. Birth Defects Res. C. Embryo. Today. 96, 51-62. doi: 10.1002/bdrc.21000

LI, C., A. J. HARRIS, J. M. SUTTIE (1998): Autoradiographic localization of androgen-binding in the antlerogenic periosteum of red deer (*Cervus elaphus*). Recent Developments in Deer Biology: Proceedings of the 3rd International Congress on the Biology of Deer. (Milne, J. A., Ed.), MLURI, Aberdeen, p. 220.

LI, C., J. M. SUTTIE (1994): Light microscopic studies of pedicle and early first antler development in red deer (*Cervus elaphus*), Anat. Rec. 239: 198–215. doi: 10.1002/ar.1092390211

LI, C., J. M. SUTTIE (1998): Electron microscopic studies of antlerogenic cells from five developmental stages during pedicle and early antler formation in red deer (*Cervus elaphus*), Anat. Rec. 252: 587–599. doi: 10.1002/(SICI)1097-0185(199812)252:4<587:AID-AR9>3.0.CO;2-I

LI, C., J. M. SUTTIE (2000): Histological studies of pedicle skin formation and its transformation to antler velvet in red deer (*Cervus elaphus*), Anat. Rec. 260; 62–71. doi: 10.1002/1097-0185(20000901)260:1<62::AID-AR70>3.0.CO;2-4

LI, C., J. M. SUTTIE, D. E. CLARK (2004): Morphological observation of antler regeneration in red deer (*Cervus elaphus*). J. Morphol. 262, 731–740. doi: 10.1002/jmor.10273

LI, C., J. M. SUTTIE, D. E. CLARK (2005): Histological examination of antler regeneration in red deer (*Cervus elaphus*). Anat. Rec. A. Discov. Mol. Cell Evol. Biol. 282, 163–174. doi: 10.1002/ar.a.20148

LI, C., W. WANG, G. ZHANG, H. BA, H. LIU, J. WANG, W. LI, G. MELINO, Y. SHI (2024): Bone metabolism associated with annual antler regeneration: a deer insight into osteoporosis reversal. Biol. Direct. doi: 10.1186/s13062-024-00561-3

LI, G., G. WHITE, C. CONNOLLY, D. MARSH (2002): Cell proliferation and apoptosis during fracture healing. J. Bone Miner. Res. 17, 791–799. doi: 10.1359/jbmr.2002.17.5.791

LIEBICH, H.-G. (2019): Veterinary Histology of Domestic Mammals and Birds. 5M Publishing Ltd, UK, pp. 80-90.

LINCOLN, G. A. (1972): The role of antlers in the behaviour of red deer. J. Exp. Zool. 182, 233-249. doi: 10.1002/jez.1401820208

LINCOLN, G. A. (1984): Antlers and their regeneration - a study using hummels, hinds and haviers. Proc. Royal Soc. Edinburgh 82, 243 -259. doi:10.1017/S026972700000372

LINCOLN, G. A. (1989): Seasonal aspects of testicular function. In: The testis, 2nd ed. (Burger, H., D. de Kretser, Eds.), Raven Press, New York, 329-386.

LINCOLN, G. A. (1992): Biology of antlers. J. Zool. 226, 517–528. doi: 10.1111/j.1469-7998.1992.tb07495.x

LISTER, A. M. (1987): Diversity and evolution of antler form in Quaternary deer. In: Biology and Management of the Cervidae. (Wemmer, C. M., Ed.), Smithsonian Institution Press., Washington, pp. 81–98. doi: 10.13140/2.1.2517.6961

LOCKSLEY, R. M., N. KILLEEN, M. J. LENARDO (2001): The TNF and TNF receptor super-families: integrating mammalian biology. Cell. 104, 487–501. doi: 10.1016/s0092-8674(01)00237-9

LOJDA, A. (1956): Histogenesa parohu našich Cervidu a její histochemický obraz. Čs. Morfol. 4, 43-62.

LOO, D. T. (2002): TUNEL Assay. In: In Situ Detection of DNA Damage: Methods and Protocols. Methods in Molecular Biology (Didenko, V. V., Ed.), Humana Press Inc., Totowa, pp. 21-30. doi: 10.1385/1-59259-179-5:21

MACEWEN, W. (1920): The growth and shedding of the antler of the deer. Jackson and Co., Glasgow, Maclehose, p. 105.

MANOLAGAS, S. C., A. M. PARFITT (2010): What old means to bone. Trends Endocrinol. Metab. 21, 369–374. doi: 10.1016/j.tem.2010.01.010

MARRIOTT, K. L., D. R. PROTHERO (2022): Variability of the horns and pronghorns (Mammalia: Artiodactyla: Antilocapridae): implications for pronghorn systematics. In: Fossil Record 8 (Lucas, S. G., R. B. Blodgett, A. J. Lichtig, A. P. Hunt, Eds.). Bulletin 90, New Mexico Museum of Natural History & Science, Albuquerque, pp. 289-294.

MARTINEZ, M. M., R. D. REIF, D. PAPPAS (2010): Detection of apoptosis: A review of conventional and novel techniques. Anal. Methods. 2, 996-1004. doi: 10.1039/C0AY00247J

MARTÍN-VEGA, D. (2014): On the identity of *Prochyliza nigrimana* (Meigen) and *Prochyliza nigricornis* (Meigen) (Diptera: Piophilidae), with a synopsis of *Prochyliza* Walker and description of a new species. Zootaxa. 3893, 277–292. doi: 10.11646/zootaxa.3893.2.7

MARTÍN-VEGA, D., A. BAZ, L. M. DÍAZ-ARANDA (2012): The immature stages of the necrophagous fly, *Prochyliza nigrimana*: comparison with *Piophila casei* and medicolegal considerations (Diptera: Piophilidae). Parasitol. Res. 111, 1127–1135. doi: 10.1007/s00436-012-2943-5

MCCARTHY, E. F. (1982): Aseptic necrosis of bone. An historic perspective. Clin. Orthop. Relat. Res. 168, 216-221.

MCKENZIE, J., C. SMITH, K. KARUPPAIAH, J. LANGBERG, M. J. SILVA, D. M. ORNITZ (2019): Osteocyte Death and Bone Overgrowth in Mice Lacking Fibroblast Growth Factor Receptors 1 and 2 in Mature Osteoblasts and Osteocytes. J. Bone Miner. Res. 34, 1660–1675. doi: 10.1002/jbmr.3742

MEDH, R. D., E. B. THOMPSON (2000): Hormonal regulation of physiological cell turnover and apoptosis. Cell Tissue Res. 301, 101–124. doi: 10.1007/s004419900159

MEIGEN, J. W. (1826): Systematische Beschreibung der bekannten europäischen zweiflügeligen Insekten, Volume 5. Hamm, Aachenbei Friedrich Wilhelm Forstmann: Gedruckt bei Beaufort Sohn. pp 412. doi: 10.5962/bhl.title.12464

MEISTER, W. W. (1956): Changes in histological structure of the long bones of white-tailed deer (*Odocoileus virginianus*) during the growth of the antlers, Anat. Rec. 124, 709–721. doi: 10.1002/ar.1091240407

MESCHER, A. L. (2018): Junqueira's Basic Histology. McGraw-Hill Education, New York pp. 138 - 151.

MILOVANOVIC, P., B. BUSSE (2020): Phenomenon of osteocyte lacunar mineralization: indicator of former osteocyte death and a novel marker of impaired bone quality? Endocr. Conn. 9, R70-R80. doi: 10.1530/ec-19-0531

MILOVANOVIC, P., E. A. ZIMMERMANN, A. VOM SCHEIDT, B. HOFFMANN, G. SARAU, T. YORGAN, M. SCHWEIZER, M. AMLING, S. CHRISTIANSEN, B. BUSSE (2017): The Formation of Calcified Nanospherites during Micropetrosis Represents a Unique Mineralization Mechanism in Aged Human Bone. Small. 13:1602215. doi: 10.1002/smll.201602215

MIYAMOTO, M. M., F. KRAUS, O. A. RYDER (1990): Phylogeny and evolution of antlered deer determined from mitochondrial DNA sequences. Proc. Natl. Acad. Sci. U. S. A. 87, 6127–6131. doi: 10.1073/pnas.87.16.6127

MODELL, W. (1969): Horns and antlers. Sci. Am. 220, 114–122.

MODELL, W., C. V. NOBACK (1931): Histogenesis of bone in the growing antler of the cervidae. Amer. J. Anat. 49, 65-95. doi: 10.1002/aja.1000490104

MORÉ, J., J. (1977): The Levenberg-Marquardt Algorithm: Implementation and Theory. In: Lecture Notes in Mathematics. (Watson, G. A., Ed.), Springer-Verlag, Berlin, pp. 105-116.

MUIR, P. D., A. R. SYKES, G. K. BARRELL (1987): Calcium metabolism in red deer (*Cervus elaphus*) offered herbages during antlerogenesis: kinetic and stable balance studies, J. Agric. Sci. 109, 357–364. doi: 10.1017/S0021859600080783

NAGATA, S. (2000): Apoptotic DNA fragmentation. Exp. Cell Res. 256, 12–18. doi: 10.1006/excr.2000.4834

NASOORI, A. (2020): Formation, structure, and function of extra-skeletal bones in mammals. Biol. Rev. Camb. Philos. Soc. 95, 986–1019. doi: 10.1111/brv.12597

NICOLETTI, I., G. MIGLIORATI, M. C. PAGLIACCI, F. GRIGNANI, C. RICCARDI (1991): A rapid and simple method for measuring thymocyte apoptosis by propidium iodide staining and flow cytometry. J. Immunol. Methods. doi: 10.1016/0022-1759(91)90198-o

NIJWEIDE, P. J., E. H. BURGER, J. KLEIN-NULEND (2002): The Osteocyte. In: Principles of Bone Biology (Bilezikian, J. P., L. G. Raisz, G. A. Rodan, Eds.). Academic Press, San Diego, pp. 93 – 108.

NOBACK, C. V. (1929): The internal structure and seasonal growth changes of deer antlers. Bull. N. Y. Zool. Soc. 49, 65-86.

NOWALK, J. R., L. M. FLICK (2008): Visualization of Different Tissues Involved in Endochondral Ossification With Alcian Blue Hematoxylin and Orange G/Eosin Counterstain. J. Histotechnol. 31, 19–21. doi: 10.1179/his.2008.31.1.19

O'GARA, B. W. (1990): The pronghorn (*Antilocapra americana*). In: Horns, pronghorns, and antlers: evolution, morphology, physiology, and social significance (Bubenik G. A., A. B. Bubenik, Eds.). Springer, New York, USA, pp. 231–264.

OUITHAVON, K., N. BHUMPAKPHAN, J. DENDUANGBORIPANT, B. SIRIAROONRAT, S. TRAKULNALEAMSAI (2009): An analysis of the phylogenetic relationship of thai cervids inferred from nucleotide sequences of protein kinase C iota (PRKCI) intron. Agriculture and Natural Resources. 43, 709–719.

OW, Y. - L. P., D. R. GREEN, Z. HAO, T. W. MAK (2008): Cytochrome c: functions beyond respiration. Nat. Rev. Mol. Cell Biol. 9, 532–542. doi: 10.1038/nrm2434

PARFITT, A. M. (1977): The cellular basis of bone turnover and bone loss: a rebuttal of the osteocytic resorption-bone flow theory. Clin. Orthop. Relat. R. 127, 236-247. doi: 10.1097/00003086-197709000-00036

PARHAMIFAR, L., H. ANDERSEN, S. M. MOGHIMI (2019): Lactate dehydrogenase assay for assessment of polycation cytotoxicity. Methods Mol. Biol. doi: 10.1007/978-1-62703-140-0_2

PARK W., S. WEI, B. S. KIM, B. KIM, S. J. BAE, Y. C. CHAE, D. RYU, K. T. HA (2023): Diversity and complexity of cell death: a historical review. Exp. Mol. Med. 55, 1573–1594. doi: 10.1038/s12276-023-01078-x

PAUS, R., T. ROSENBACH, N. HAAS, B. M. CZARNETZKI (1993): Patterns of cell death: the significance of apoptosis for dermatology. Exp. Dermatol. 2, 3–11. doi: 10.1111/j.1600-0625.1993.tb00192.x

PHEMISTER, D. B. (1915): Necrotic bone and subsequent changes which it undergoes. J. Am. Med. Assoc. 64, 211-216.

PHEMISTER, D. B. (1930): Repair of bone in the presence of aseptic necrosis resulting from fractures, transplantations and vascular obstruction. J. Bone Joint Surg. 12, 769-787.

PICAVET, P. P., M. BALLIGAND (2016): Organic and mechanical properties of Cervidae antlers: a review. Vet. Res. Commun. 40, 141–147. doi: 10.1007/s11259-016-9663-8

POMPEIANO, M., M. HVALA, J. CHUN (1998): Onset of apoptotic DNA fragmentation can precede cell elimination by days in the small intestinal villus. Cell Death Differ. 5, 702–709. doi: 10.1038/sj.cdd.4400403

PRICE, J. S., B. O. OYAJOBI, A. M. NALIN, A. FRAZER, G. G. R. RUSSELL, LJ. SANDELL (1996): Chondrogenesis in the regenerating antler tip in red deer: expression of collagen types I, IIA, IIB, and X demonstrated by in situ nucleic acid hybridization and immunocytochemistry. Dev. Dyn. 205, 332–347. doi: 10.1002/(sici)1097-0177(199603)205:3%3C332::aid-aja12%3E3.0.co;2-6

PRICE, J. S., B. O. OYAJOBI, R. O. OREFFO, R. G. RUSSELL (1994): Cells cultured from the growing tip of red deer antler express alkaline phosphatase and proliferate in response to insulin-like growth factor-I. J. Endocrinol. 143, R9–R16. doi: 10.1677/joe.0.143r009

PRICE, J. S., C. FAUCHEUX, S. ALLEN (2005): Deer antlers as a model of mammalian regeneration, Curr. Top. Dev. Biol. 67, 1–48. doi: 10.1016/S0070-2153(05)67001-9

PRITCHARD, J. J. (1972): General histology of bone. In: The Biochemistry and Physiology of Bone. (Bourne, G. H., Ed.), Structure, second edition, vol. I. Academic Press, New York, pp. 1–20.

PROTHERO, D. R., S. E. FOSS (2007): Summary. In: The evolution of Artiodactyls (Prothero, D. R., S. E. Foss, Eds.). John Hopkins University Press, Baltimore, MD, pp. 303-316.

RANDI, E., N. MUCCI, F. CLARO-HERGUETA, A. BONNET, E. J. P. DOUZERY (2001): A mitochondrial DNA control region phylogeny of the Cervinae: speciation in Cervus and implications for conservation. Anim. Conserv. 4, 1–11. doi: 10.1017/S1367943001001019

RANDI, E., N. MUCCI, M. PIERPAOLI, E. DOUZERY (1998): New phylogenetic perspectives on the Cervidae (Artiodactyla) are provided by the mitochondrial cytochrome b gene. Proc. Biol. Sci. 265, 793–801. doi: 10.1098/rspb.1998.0362

RATNASINGHAM, S., P. D. N. HEBERT (2007): BOLD: the Barcode of Life Data System. Mol. Ecol. Notes. 7, 355–364. doi: 10.1111/j.1471-8286.2007.01678.x

RATNASINGHAM, S., P. D. N. HEBERT (2013): A DNA-based registry for all animal species: the barcode index number (BIN) system. PLoS One. 8, e66213. doi: 10.1371/journal.pone.0066213

REDZA-DUTORDOIR, M., D. A. AVERILL-BATES (2016): Activation of apoptosis signaling pathways by reactive oxygen species. Biochim. Biophys. Acta. 1863, 2977–2992. doi: 10.1016/j.bbamcr.2016.09.012

RHUMBLER, L. (1929): Zur Entwicklungsmechanik von Korkziehergeweihbildungen und verwandter Erscheinungen. Arch. f. Entw.-Mech. Bd. 119, 441-515.

RIEDL, S. J., Y. SHI (2004): Molecular mechanisms of caspase regulation during apoptosis. Nat. Rev. Mol. Cell Biol. 5, 897–907. doi: 10.1038/nrm1496

ROBERTS, S. C. (1996): The Evolution of Hornedness in Female Ruminants. Behaviour. 133, 399–442.

ROLF, H. J., A. ENDERLE (1999): Hard fallow deer antler: a living bone till antler casting? Anat. Rec. 255, 69–77. doi: 10.1002/(SICI)1097-0185(19990501)255:1<69::AID-AR8>3.0.CO;2-R

ROLF, H. J., K. FISCHER (1996): Serum testosterone, 5-α-dihydrotestosterone and different sex characteristics in male fallow deer (*Cervus dama*): a long-term experiment with accelerated photoperiods. Comp. Biochem. Physiol. A. Physiol. 115, 207–221. doi: 10.1016/0300-9629(96)00051-5

ROLF, H. J., K. FISCHER, F. W. DÜWEL, F. KAUER, A. ENDERLE (2001): Histomorphology and physiology of “living” hard antlers: Evidence for a substance transport into polished antlers via the vascular system. In: Antler Science and Product Technology, Part I, Antler Biology (Jeong-Sim, S., H. H. Sunwoo, R. J. Hudson, B. T. Jeon, Eds.). ASPT Research Center, University of Alberta, Edmonton, Canada, pp. 97–108.

RÖSSNER, G. E., L. COSTEUR, T. M. SCHEYER (2020): Antiquity and fundamental processes of the antler cycle in Cervidae (Mammalia). Sci. Nat. 108, 3. doi: 10.1007/s00114-020-01713-x

RÖSINGH, G. E., J. JAMES (1969): Early phases of avascular necrosis of the femoral head in rabbits. J. Bone Joint Surg. Br. 51, 165-174.

SADIGHI, M., S. R. HAINES, A. SKOTTNER, A. J. HARRIS, J. M. SUTTIE (1994): Effects of insulin-like growth factor-I (IGF-I) and IGF-II on the growth of antler cells in vitro. J. Endocrinol. 143, 461–469. doi: 10.1677/joe.0.1430461

SARASTE, A., K. PULKKI (2000): Morphologic and biochemical hallmarks of apoptosis. Cardiovasc. Res. 45, 528-537. doi: 10.1016/s0008-6363(99)00384-3

SCHALLER, G. B. (1967): The deer and the tiger. University of Chicago Press. Chicago.

SCHERFT, J. P. (1972): The lamina limitans of the organic matrix of calcified cartilage and bone. J. Ultrastruct. Res. 38, 318-331. doi: 10.1016/s0022-5320(72)90008-1

SCOTT, K. M., C. M. JANIS (1987): Phylogenetic relationships of the Cervidae, and the case for a superfamily ‘Cervoidea’. In: Biology and management of the Cervidae. (Wemmer C., Ed.), Smithsonian Institution, Washington, London, pp. 3–20.

SEMPERE, A. J., J. BOISSIN, B. DUTOURNE, A. LACROIX, M. R. BLANC, J. P. RAVAULT (1983): Variations in the plasma concentration of prolactin, LH and FSH and in testicular activity during the first year of life in the roe deer (*Capreolus capreolus* L.). Gen. Comp. Endocrinol. 52, 247–254. doi: 10.1016/0016-6480(83)90119-3

SEMPERE, A. J., R. GRIMBERG, C. SILVE, C. TAU, M. GARABEDIAN (1989): Evidence for extrarenal production of 1,25-dihydroxyvitamin during physiological bone growth: in vivo and in vitro production by deer antler cells. Endocrinology. 125, 2312– 2319. doi: 10.1210/endo-125-5-2312

SHEEHAN, D. C., B. B. HRAPCHAK (1980): Theory and practice of Histotechnology. 2nd ed., Battelle Press, Columbus, Ohio, pp. 100-101.

SHI, Z. D., G. K. BARRELL (1994): Thyroid hormones are required for the expression of seasonal changes in red deer (*Cervus elaphus*) stags. Reprod. Fertil. Dev. 6, 187–192. doi: 10.1071/rd9940187

SIMPSON, G. G. (1949): The meaning of evolution. Yale University Press.

SKEDROS, J. G., J. L. HOLMES, E. G. VAJDA, R. D. BLOEBAUM (2005): Cement lines of secondary osteons in human bone are not mineral-deficient: new data in a historical perspective. Anat. Rec. A. Discov. Mol. Cell Evol. Biol. 286, 781–803. doi: 10.1002/ar.a.20214

SKEDROS, J. G., K. E. KEENAN, D. M. L. COOPER, R. D. BLOEBAUM (2014): Histocompositional organization and toughening mechanisms in antler. J. Struct. Biol. 187, 129–148. doi: 10.1016/j.jsb.2014.06.004

SKEDROS, J. G., M. R. DAYTON, C. L. SYBROWSKY, R. D. BLOEBAUM, K. N. BACHUS (2006): The influence of collagen fiber orientation and other histocompositional characteristics on the mechanical properties of equine cortical bone. J. Exp. Biol. 209, 3025–3042. doi: 10.1242/jeb.02304

SOLOUNIAS, N. (1988): Evidence from horn morphology on the phylogenetic relationships of the pronghorn (*Antilocapra americana*). J. Mammal. 69, 1–3.

SPINAGE, C. A. (1970): Giraffid horns. Nature. 227, 735-736. doi: 10.1038/227735a0

STADELMANN, C., H. LASSMANN (2000): Detection of apoptosis in tissue sections. Cell Tissue Res. 301, 19–31. doi: 10.1007/s004410000203

STENN, K. S., R. PAUS (2001): Controls of hair follicle cycling. Physiol. Rev. 81, 449–494. doi: 10.1152/physrev.2001.81.1.449

STEVENS H. Y., J. REEVE, B. S. NOBLE (2000): Bcl-2, tissue transglutaminase and p53 protein expression in the apoptotic cascade in ribs of premature infants. J. Anat. 196, 181–191. doi: 10.1046/j.1469-7580.2000.19620181.x

SUTTIE, J. M., G. A. LINCOLN, R. N. KAY (1984): Endocrine control of antler growth in red deer stags. J. Reprod. Fertil. 71, 7–15. doi: 10.1530/jrf.0.0710007

SUTTIE, J. M., P. D. GLUCKMAN, J. H. BUTLER, P. F. FENNESSY, I. D. CORSON, F. J. LAAS (1985): Insulin-like growth factor 1 (IGF-1) antler stimulating hormone? Endocrinology. 116, 846–848. doi: 10.1210/endo-116-2-846

SUTTIE, J. M., P. F. FENNESSY, K. R. LAPWOOD, I. D. CORSON (1995): Role of steroids in antler growth of red deer stags. J. Exp. Zool. 271, 120–130. doi: 10.1002/jez.1402710207

SUZUKI, R., T. DOMON, M. WAKITA (2000): Some osteocytes released from their lacunae are embedded again in the bone and not engulfed by osteoclasts during bone remodeling. Anat. Embryol. (Berl). 202, 119–128. doi: 10.1007/s004290000101

SZUWART, T., H. KIERDORF, U. KIERDORF, G. CLEMEN (1998): Ultrastructural aspects of cartilage formation, mineralization, and degeneration during primary antler growth in fallow deer (*Dama dama*). Ann. Anat. 180, 501–510. doi: 10.1016/S0940-9602(98)80055-1

SZUWART, T., H. KIERDORF, U. KIERDORF, G. CLEMEN (2002): Histochemical and ultrastructural studies of cartilage resorption and acid phosphatase activity during antler growth in fallow deer (*Dama dama*). Anat. Rec. 268, 66–72. doi: 10.1002/ar.10135

SZUWART, T., U. GATH, J. ALTHOFF, H. J. HÖHLING (1994): Biochemical and histological study of the ossification in the early developing pedicle of the fallow deer (*Dama dama*). Cell Tissue Res. 277, 123 -129. doi: 10.1007/bf00303088

TAFT, E. B., T. C. HALL, J. C. AUB (1956): The growth of the deer antler. NY State Conserv. 10, 4 - 5.

TAYLOR, A. M., A. BOYDE, J. S. DAVIDSON, J. C. JARVIS, L. R. RANGANATH, J. A. GALLAGHER (2012): Identification of trabecular excrescences, novel microanatomical structures, present in bone in osteoarthropathies. Eur. Cell Mater. 23, 300–309. doi: 10.22203/ecm.v023a23

TIBCO Software Inc. (2020): Data Science Workbench, version 14. http://tibco.com

TROHAR, J. (2004): Jelen. In: Lovstvo (Mustapić, Z., ed.). Hrvatski lovački savez, Zagreb, pp. 43-60.

TURNER, C. H. (2002): Biomechanics of bone: determinants of skeletal fragility and bone quality. Osteoporos. Int. 13, 97–104. doi: 10.1007/s001980200000

TZALKIN, V. J. (1945): Data for a study on the horns of the true deer (*Cervus elaphus* L.). Zool. Zh. 24, 224–236.

USUI, Y., K. KAWAI, K. HIROHATA (1989): An Electron Microscopic Study of the Changes Observed in Osteocytes Under Ischemic Conditions. J. Orthop. Res. 7, 12-21. doi: 10.1002/jor.1100070103

VAN DER EEMS, K. L., R. D. BROWN, C. M. GUNDBERG (1988): Circulating levels of 1,25 dihydroxyvitamin D, alkaline phosphatase, hydroxyproline, and osteocalcin associated with antler growth in white-tailed deer. Acta Endocrinol. (Copenh). 118, 407–414. doi: 10.1530/acta.0.1180407

VERMES I., C. HAANEN, C. REUTELINGSPERGER (2000): Flow cytometry of apoptotic cell death. J. Immunol. Methods. 243, 167-190. doi: 10.1016/S0022-1759(00)00233-7

VOGT, F. (1936): Neue Wege der Hege. Verlag J. Neumann-Neudamm, Vienna.

VON KORFF, K. (1914): Über den Geweihwechsel der Hirsche, besonders über den Knorpel- und Knochenbildungsprozess der Substantia spongiosa der Baststangen. Anatomische Hefte I. Abteilung 51, 691–731.

WAJANT, H. (2002): The Fas signaling pathway: more than a paradigm. Science 296, 1635–1636. doi: 10.1126/science.1071553

WALDO, C. M., G. B. WISLOCKI, D. W. FAWCETT (1949): Observations on the blood supply of growing antlers, Am. J. Anat. 84, 27–61. doi: 10.1002/aja.1000840103

WANG, D., D. BERG, H. BA, H. SUN, Z. WANG, C. LI (2019b): Deer antler stem cells are a novel type of cells that sustain full regeneration of a mammalian organ – deer antler. Cell Death Dis. 10, 443. doi: 10.1038/s41419-019-1686-y

WANG, Y., C. ZHANG, N. WANG, Z. LI, R. HELLER, R. LIU, Y. ZHAO, J. HAN, X. PAN, Z. ZHENG, X. DAI, C. CHEN, M. DOU, S. PENG, X. CHEN, J. LIU, M. LI, K. WANG, C. LIU, Z. LIN, L. CHEN, F. HAO, W. ZHU, C. SONG, C. ZHAO, C. ZHENG, J. WANG, S. HU, C. LI, H. YANG, L. JIANG, G. LI, M. LIU, T. S. SONSTEGARD, G. ZHANG, Y. JIANG, W. WANG, Q. QIU (2019a): Genetic basis of ruminant headgear and rapid antler regeneration. Science. 364, eaav6335. doi: 10.1126/science.aav6335

WATANABE, M., M. HITOMI, K. VAN DER WEE, F. ROTHENBERG, S. A. FISHER, R. ZUCKER, K. K. H. SVOBODA, E. C. GOLDSMITH, K. M. HEISKANEN, A. L. NIEMINEN (2002): The pros and cons of apoptosis assays for use in the study of cells, tissues, and organs. Microsc Microanal. 8, 375-391. doi: 10. 1017/ S1431 92760 20103 46

WEBB, S. D. (2000): Evolutionary history of New World Cervidae. In: Antelopes, Deer, and Relatives: Fossil Record, Behavioral Ecology, Systematics, and Conservation. (Vrba, E., G. Schaller, Eds.), Yale University Press, New Haven, pp. 38–64.

WIJSMAN, J. H., R. R. JONKER, R. KEIJZER, C. J. VAN DE VELDE, C. J. CORNELISSE, J. H. VAN DIERENDONCK (1993): A new method to detect apoptosis in paraffin sections: in situ end-labeling of fragmented DNA. J. Histochem. Cytochem. 41, 7–12. doi: 10.1177/41.1.7678025

WILCOX, R. R. (2010): Fundamentals of Modern Statistical Methods – Substantially Improving Power and Accuracy. Springer, New York, Dordrecht, Heidelberg, London. doi: 10.1007/978-1-4419-5525-8

WISLOCKI, G. (1943): Studies on growth of deer antlers. In: Essays in Biology. (Berkeley, C. A., Ed.), University of California Press., Los Angeles, pp. 631–653.

WISLOCKI, G. B. (1942): Studies on the growth of deer antlers. I. On the structure and histogenesis of the antlers of the Virginia deer (*Odocoileus virginianus borealis*), Am. J. Anat. 71, 371–415. doi: 10.1002/aja.1000710304

WISLOCKI, G. B., H. L. WEATHERFORD, M. SINGER (1947): Osteogenesis of antlers investigated by histological and histochemical methods. Anat. Rec. 99, 265-284.

WISLOCKI, G. B., J. C. AUB, C. M. WALDO (1947): The effects of gonadectomy and the administration of testosterone propionate on the growth of antlers in male and female deer. Endocrinology. 40, 202–224. doi: 10.1210/endo-40-3-202

WISLOCKI, G. B., M. SINGER (1946): The occurrence and function of nerves in the growing antlers of deer. J. Comp. Neurol. 85, 1-19. doi: 10.1002/cne.900850102

WYLLIE, A. H., J. F. KERR, A. R. CURRIE (1980): Cell death: The significance of apoptosis. Int. Rev. Cytol. 68, 251 - 306. doi: 10.1016/s0074-7696(08)62312-8

YELLOWLEY, C. E., Z. LI, Z. ZHOU, C. R. JACOBS, H. J. DONAHUE (2000): Functional gap junctions between osteocytic and osteoblastic cells. J. Bone Miner. Res. 15, 209-217. doi: 10.1359/jbmr.2000.15.2.209

YENI, Y. N., T. L. NORMAN (2000): Calculation of porosity and osteonal cement line effects on the effective fracture toughness of cortical bone in longitudinal crack growth, J. Biomed. Mater. Res. 51, 504–509. doi: 10.1002/1097-4636(20000905)51:3<504:AID-JBM27>3.0.CO;2-I

YOUNG, J. Z. (1962): The life of vertebrates. 2nd ed., Oxford University Press, Oxford, pp. 741-760.

YOUNG, M. H. (1966): Epiphysial infarction in a growing long bone. An experimental study in the rabbit. J. Bone Joint Surg. 48, 826-840.

9. BIOGRAPHY

Nikolina Škvorc was born on September 23, 1994 in Zagreb. After graduating from the XV. gimnazija (MIOC) in 2013, she enrolled at the Faculty of Veterinary Medicine, University of Zagreb. In her fifth year of study, she received the City of Zagreb Scholarship for the academic year 2017/2018. She received the Rector's Awards for team scientific work in the academic year 2016/2017 and for individual scientific work in the academic year 2018/2019. She graduated on September 17, 2019. She started working as an assistant at the Department of Anatomy, Histology and Embryology of the Faculty of Veterinary Medicine and enrolled in the doctoral study of Veterinary Sciences on February 10, 2020. She defended her dissertation topic in front of the Committee on July 1, 2022, entitled "Characterization of antler bone formation and osteocyte viability from velvet phase till antler casting in red deer (*Cervus elaphus* L.)". She participated in 24 international congresses and conferences, where she presented six oral and nine poster presentations, and is also a co-author of 18 presentations. In addition, she authored one scientific article, 3 professional articles and co-authored two professional articles. She was a member of the organizing committees of three international congresses and co-editor of a collection of abstracts. She trained at 15 workshops and seminars, and was one of the leaders of two workshops. She trained scientifically and professionally at three domestic and one foreign institution and at the Laboratory of Cytology and Histopathology of the Department of Veterinary Pathology. She was an associate on two projects (DEVet, HKO), and is currently an associate on the HRZZ project (IP-2024-05-8056). She is a member of the Croatian Veterinary Chamber, the European Association of Veterinary Anatomists, the International Society of Education in Animal Sciences, the Hunting Section of the Faculty of Veterinary Medicine, University of Zagreb "dr. OTO ROHR" and the AMAC-VEF Association.

List of published works by the author

1. **ŠKVORC, N.**, M. BUJANIĆ, Z. ŠTRITOF, S. KUŽIR, D. KONJEVIĆ (2025): Presence of bacteria in red deer antlers during different stages of development. 14th European Vertebrate Management Conference: Book of Abstracts, May 12-16, Ankaran, Slovenia, p. 177.
doi: 10.20315/evmc.2025.159

2. **ŠKVORC, N.**, M. BUJANIĆ, G. LYKOTHANASIS, K. KRAPINEC, K. PINTUR, B. REINDL, D. KONJEVIĆ (2025): Reliability of dental wear for age evaluation in roe deer. Book of Abstracts 60th Croatian & 20th International Symposium on Agriculture, June 1-6, Brač, Croatia, p. 108.

3. KONJEVIĆ, D., E. KLARIĆ, M. BUJANIĆ, **N. ŠKVORC**, Z. JANICKI, V. JUMIĆ, K. KRAPINEC (2025): The impact of *Fascioloides magna* infection on characteristics of red deer antlers. Book of Abstracts 60th Croatian & 20th International Symposium on Agriculture, June 1-6, Brač, Croatia, p. 96.

4. **ŠKVORC, N.**, M. BUJANIĆ, K. SEVERIN, L. ŠERIĆ JELASKA, M. PALIĆ, A. GUDAN KURILJ, S. KUŽIR, D. KONJEVIĆ (2024): Red deer (*Cervus elaphus*) antler myiasis caused by *Prochyliza nigrimanus* (Meigen 1826). Parasitol. Res., 123, 1-7.
doi: 10.1007/s00436-024-08421-9

5. **ŠKVORC, N.**, M. BUJANIĆ, S. KUŽIR, D. KONJEVIĆ (2024): Jelensko rogovlje – funkcionalno modificirana kost. Hrvat. vet. vjesn. 32, 34-42.

6. **ŠKVORC, N.**, L. DEVČIĆ, M. BUJANIĆ, D. KONJEVIĆ, S. KUŽIR (2024): Histology of selected glands in the Eurasian red squirrel (*Sciurus vulgaris*) – Case report. Anat. Histol. Embryol., 53, pp. 19-20.
doi: 10.1111/ahe.13066

7. BASTIANČIĆ, L., V. BENKO, **N. ŠKVORC**, I. FRANIN, S. FARAGUNA, M. LOVRIĆ, D. VALIĆ, S. KUŽIR (2024): Mast cells or macrophages – description of cells found in the digestive tract of piper gurnard (*Trigla lyra*). Anat. Histol. Embryol., 53, p. 15.
doi: 10.1111/ahe.13066

8. FRANKO, R., N. GUNJEVIĆ, **N. ŠKVORC**, J. MILJKOVIĆ, T. GOJAK, D. LISIČIĆ, L. BASTIANČIĆ (2024): Histological study of the osteoderms in the skin of the common wall gecko (*Tarentola mauritanica*). Proceedings of 3rd International Scientific and Professional Meeting on Reptiles and Exotic Animals "Reptilia", May 24-25, Zagreb, Croatia, p. 150.

9. KUŽIR, S., L. BASTIANČIĆ, **N. ŠKVORC**, M. POLETTO, K. BILIĆ MEŠTRIĆ (2024): Veterinary Medicine – Open Educational Resources. Book of Abstracts 10th International Scientific Meeting "Days of Veterinary Medicine" and 2nd European Conference on Veterinary and Medical Education 2024, September 22-25, Ohrid, R. N. Macedonia, p. 143.

10. KUŽIR, S., L. DEVČIĆ, **N. ŠKVORC**, M. POLETTO, A. SHEK VUGROVEČKI, D. HORVATEK TOMIĆ (2024): Vertikalni nastavni materijali: vrijednost za studente i praktičare. Zbornik radova međunarodnog znanstveno stručnog skupa 7. Hrvatski veterinarski kongres, October 24-27, Dubrovnik, Croatia, p. 125.

11. KUŽIR, S., L. DEVČIĆ, **N. ŠKVORC**, J. IVANIĆ, M. POLETTO (2024): Projekt e-Sveučilišta - Plimni val! THECUC 2024 – Sveučilišta nove generacije, November 6-8, Pula, Croatia.

12. **ŠKVORC, N.**, L. BASTIANČIĆ, M. POLETTO, S. KUŽIR (2023): Exploring modern learning preferences: the impact of computerization on younger generation students. ICEAS III Proceedings Book, June 15-16, Zagreb, Croatia, p. 64.

13. DEVČIĆ, L., D. HUBER, **N. ŠKVORC**, S. KUŽIR (2023): Variations in the histological methods of processing samples in histology and histopathology. ICEAS III Proceedings Book, June 15-16, Zagreb, Croatia, p. 53.

14. **ŠKVORC, N.**, S. KUŽIR, M. BUJANIĆ, L. BASTIANČIĆ, D. KONJEVIĆ (2023): Histological structure of *Fascioloides magna* pseudocysts in red deer livers. Book of Abstracts International Symposium on Animal Sciences, September 18-20, Novi Sad, Serbia, p. 32.

15. **ŠKVORC, N.**, D. KONJEVIĆ, M. BUJANIĆ, L. DEVČIĆ, S. KUŽIR (2023): Visualization of ossification during intrauterine development of wild boar. Book of Abstracts of 10th International Congress Veterinary Science and Profession. October 5-7, Zagreb, Croatia, p. 112.

16. KONJEVIĆ, D., M. BUJANIĆ, **N. ŠKVORC**, A. GUDAN KURILJ (2023): Red deer livers and fascioloidosis: from infection to regeneration. Zbornik radova znanstveno-stručnog skupa s međunarodnim sudjelovanjem Veterinarski dani 2023., October 26-29, Zagreb, Croatia, p. 142.

17. TURK, V., M. BUJANIĆ, K. KRAPINEC, **N. ŠKVORC**, C. GIBERT, D. KONJEVIĆ (2023): Metode za procjenu dobi u srne obične (*Capreolus capreolus* L.). Veterinar 61, 20-26.

18. **ŠKVORC, N.**, S. KUŽIR, M. BUJANIĆ, D. KONJEVIĆ (2022): Histological structure of mineralised red deer antler: application of three staining methods. Book of Abstracts of 57th Croatian & 17th International Symposium on Agriculture, June 19-24, Vodice, Croatia, p. 246.

19. **ŠKVORC, N.**, L. BASTIANČIĆ, S. KUŽIR, D. KONJEVIĆ, N. ŠPREM, M. BUJANIĆ (2022): Cytomorphological characteristics of European mouflon (*Ovis aries musimon*) blood cells. Anat. Histol. Embryol. 51, pp. 53-54.
doi:10.1111/ahe.12759

20. BUJANIĆ, M., P. VERZAK, **N. ŠKVORC**, Z. JANICKI, D. KONJEVIĆ (2022): Anatomical distribution of *Fascioloides magna* pseudocysts in the red deer (*Cervus elaphus*) livers. Anat. Histol. Embryol. 51, pp. 11-12.
doi:10.1111/ahe.12759

21. BASTIANČIĆ, L., **N. ŠKVORC**, V. KUBALE DVOJMOČ, M. LUKAČ, S. KUŽIR (2022): Histological study of the skin in yellow-headed water monitor (*Varanus cumingi*). Anat. Histol. Embryol. 51, 6-7.
doi:10.1111/ahe.12759

22. **ŠKVORC, N.**, M. BUJANIĆ, A. MUTVAR, L. TARLE, L. BASTIANČIĆ, S. KUŽIR, D. KONJEVIĆ (2022): Mineral density of red deer (*Cervus elaphus*) antlers up to two and half months after velvet shedding – preliminary results. Proceedings of the 10th International Deer Biology Congress, September 4-9, Osijek, Croatia, p. 144.

23. BUJANIĆ, M., **N. ŠKVORC**, C. GIBERT, E. AUBINEAU, C. DEREGNAUCOURT, K. KRAPINEC, D. KONJEVIĆ (2022): Comparison of different methods for age estimation in roe deer (*Capreolus capreolus*) – preliminary study. Book of Abstracts 10th International Deer Biology Congress, September 4-9, Osijek, Croatia, pp. 125-126.

24. **ŠKVORC, N.**, L. BASTIANČIĆ, M. BUJANIĆ, D. KONJEVIĆ, S. KUŽIR (2022): Macroscopic and microscopic structure of the adrenal glands in the Eurasian badger (*Meles meles*) – case study. Proceedings of the 11th Meeting of the Young Generation of Veterinary Anatomists, July 20-22, Zürich, Switzerland, p. 31.

25. BUJANIĆ, M., **N. ŠKVORC**, I.-C. ŠOŠTARIĆ-ZUCKERMANN, D. KONJEVIĆ (2022): Microscopic appearance of the liver lesions caused by *Fascioloides magna* in a roe deer. Proceedings of the 11th Meeting of the Young Generation of Veterinary Anatomists, July 20-22, Zürich, Switzerland, pp. 26-27.

26. BASTIANČIĆ, L., K. MATANOVIĆ, E. GJURČEVIĆ, **N. ŠKVORC**, M. LOVRIĆ, D. VALIĆ, S. KUŽIR (2022): Histological characteristics of the posterior part of digestive tract in small-spotted catshark (*Scyliorhinus canicula*). Proceedings of the 11th Meeting of the Young Generation of Veterinary Anatomists, July 20-22, Zürich, Switzerland, p. 17.

27. BUJANIĆ, M., **N. ŠKVORC**, I.-C. ŠOŠTARIĆ-ZUCKERMANN, L. MEDVEN ZAGRADIŠNIK, D. KONJEVIĆ (2022): First record of *Fascioloides magna* infection in Alpine ibex (*Capra ibex*) kept in fenced area shared with red and fallow deer. Book of Proceedings 5th International Conference on Avian, Herpetological and Exotic Mammal Medicine, March 27-30, Budapest, Hungary, p. 413.

28. ERMAN, V., M. BUJANIĆ, **N. ŠKVORC**, S. MANDEK, D. KONJEVIĆ (2022): Značajke invazije divljih svinja (*Sus scrofa* L.) metiljem *Fascioloides magna*. Zbornik radova Veterinarski dani 2022, October 20–23, Poreč, Croatia, pp. 81-84.

29. BASTIANČIĆ, L., K. MATANOVIĆ, E. GJURČEVIĆ, **N. ŠKVORC**, V. BENKO, M. LOVRIĆ, D. VALIĆ, S. KUŽIR (2022): Histology of the digestive tract in the European hake (*Merluccius merluccius*). Book of Abstracts of the 9th International Scientific Meeting Days of Veterinary Medicine 2022, September 22-25, Ohrid, R. N. Macedonia, p. 136.

30. **ŠKVORC, N.**, M. BUJANIĆ, I.-C. ŠOŠTARIĆ-ZUCKERMANN, S. KUŽIR, D. KONJEVIĆ (2021): Histološki prikaz hidatidoze u divlje svinje (*Sus scrofa* L.). Hrv. vet. vjesn. 29, 48-54.

31. **ŠKVORC, N.**, I.-C. ŠOŠTARIĆ-ZUCKERMANN, M. BUJANIĆ, D. KONJEVIĆ (2021): Inflammatory response in livers of red deer and wild boar infected with *Fascioloides magna*. Book of Abstracts of 56th Croatian & 16th International Symposium on Agriculture, September 5-10, Vodice, Croatia, p. 242.

32. BASTIANČIĆ, L., **N. ŠKVORC**, S. KUŽIR (2021): Morphological characteristics of lizard skin (Lacertilia, Squamata). Proceedings of the 2nd International Scientific and Professional Meeting on Reptiles and Exotic Animals “REPTILIA”, May 21-22, Zagreb, Croatia, pp. 37-41.

33. KUŽIR, S., L. BASTIANČIĆ, **N. ŠKVORC** (2021): Bone remains from archaeological sites in the Podravina area with traces of metallurgical activity. In: Interdisciplinary Research into Iron Metallurgy along the Drava River in Croatia: The TransFER Project. (Sekelj Ivančan, T., T. Karavidović, Eds.), Archaeopress, Oxford, pp. 227-232.
doi:10.2307/j.ctv20rsk2k.14

34. BUJANIĆ, M., **N. ŠKVORC**, F. MARTINKOVIĆ, D. KONJEVIĆ (2020): Hidatidoza divljih svinja (*Sus scrofa* L.) na području istočne Hrvatske. Hrv. vet. vjesn. 28, 36-41.

35. BUJANIĆ, M., **N. ŠKVORC**, B. ROKOŠ, L. MANOJLOVIĆ, Z. JANICKI, D. KONJEVIĆ (2019): Economic losses caused by disposal of skin and edible internal organs of the red deer – preliminary results. Book of Abstracts of 8th International Congress "Veterinary Science and Profession", October 10-12, Zagreb, Croatia, p. 123.

36. ŠOŠTARIĆ-ZUCKERMANN, I.-C., **N. ŠKVORC**, M. BUJANIĆ, D. KONJEVIĆ (2019): Fascioloidosis and fasciolosis in wild boar (*Sus scrofa* L.) on histological level. Proceedings of the International Symposium on Animal Science (ISAS) 2019, June 3-8, Herceg Novi, Montenegro, p. 31.

37. BUJANIĆ, M., F. MARTINKOVIĆ, I. ŠTIMAC, **N. ŠKVORC**, D. KONJEVIĆ (2019): Gastrointestinal parasites of wild badger (*Meles meles*) at Medvednica Nature Park – preliminary results. Proceedings of the International Symposium on Animal Science (ISAS) 2019, June 3-8, Herceg Novi, Montenegro, p. 30.

38. **ŠKVORC, N.**, M. BUJANIĆ, J. GRBAVAC, D. KONJEVIĆ (2018): Primjena inkrementnih linija u tvrdim zubnim tkivima u procjeni dobi srne obične (*Capreolus capreolus* L.). Hrv. vet. vjesn. 26, 5-6, 40-44.

39. KONJEVIĆ, D., M. BUJANIĆ, **N. ŠKVORC**, K. KRAPINEC, A. GUDAN-KURILJ (2018): Ovarian carcinoma in a roe deer (*Capreolus capreolus* L.). Proceedings of the 5th International Vet-Istanbul Group Congress and 8th International Scientific Meeting Days of Veterinary Medicine – 2018, September 23-27, Ohrid, R. of Macedonia, p. 98.

40. PERCAN, V., **N. ŠKVORC**, M. ŽIVKOVIĆ, A. GUDAN KURILJ, M. HOHŠTETER, B. ARTUKOVIĆ, L. MEDVEN ZAGRADIŠNIK, Ž. GRABAREVIĆ, I.-C. ŠOŠTARIĆ-ZUCKERMANN (2017): Anal sac apocrine adenocarcinoma of dogs – a histological, immunohistochemical and clinical characterization. Book of Abstracts of the 7th International Congress "Veterinary Science and Profession", October 5-7, Zagreb, Croatia, p. 85.